THE OPERATION AND PERFORMANCE OF A LARGE SCALE SEQUENTIAL CHROMATOGRAPHIC SEPARATOR

A Thesis submitted by D.M. Bell, B.Sc., to the Faculty of Engineering, University of Aston in Birmingham for the Degree of Doctor of Philosophy.

Department of Chemical Engineering
University of Aston in Birmingham
July, 1977.

218040
544.926 BEL
8 JUN 1978
(DC)

ACKNOWLEDGEMENTS

The Author is indebted to the following:

Professor G.V. Jeffreys and the Department of Chemical Engineering for making available the facilities for research.

Professor P.E. Barker, who supervised the work, for his help and guidance throughout this project.

Dr. R.E. Deeble, a joint supervisor, for his advice on both theoretical and practical aspects of the research topic.

Fellow members in the Separation and Purification Research Group, for many invaluable discussions.

Mr. N. Roberts and other members of the department technical staff.

The Science Research Council for provision of a scholarship.

Secretary Byrds Ltd., for the typing of this thesis.

The Operation and Performance of a Large Scale Sequential Chromatographic Separator

A Thesis submitted by Donald Michael Bell, B.Sc., to the Faculty of Engineering, University of Aston in Birmingham, for the degree of Doctor of Philosophy.

July, 1977.

A review is given of general chromatographic theory, the factors affecting the performance of chromatographic columns, and methods of improving column efficiency. Scale-up of the chromatographic process for preparative and production purposes is discussed.

The design of a sequential continuous chromatographic refining unit (SCCR1) for continuous gas/liquid chromatographic separations is reported. A novel feature of the unit is that counter-current operation is simulated by sequencing a system of inlet and outlet port functions around a closed symmetrical system of twelve fixed, 7.6 cm diameter columns.

The operating characteristics of the unit have been investigated using an equivolume feed mixture of 1,1,2-trichloro-1,2,2-trifluoro-ethane (Arklone.P), and 1,1,1-trichloro-ethane(Genklene.P.). The solvent phase was silicone oil DC 200/50 coated onto 500-355 μm particles of Chromosorb.P, with compressed air acting as the carrier fluid. Optimisation of the carrier gas flowrate and port function sequencing interval allowed the above chemical system to be separated into two product streams of purity >99.7%, at feedrates up to 1000 $cm^3 hr^{-1}$.

Investigations into the internal column temperature profile revealed extensive temperature differences with a minimum temperature of 26°C below ambient being recorded. Redesign of the solute feed vaporisation process reduced the temperature perturbations and allowed the maximum throughput of the unit to be increased to 1400 $cm^3.hr^{-1}$ for the system Arklone.P./ Genklene.P.

The ability of the unit to separate a second more difficult chemical system of Arklone.P., and dichloro-methane has also been demonstrated. Prior to any design changes this system had proved impossible to separate.

Theoretical treatments of the counter-current chromatographic process are reviewed, and a computer simulation of the SCCR1 based on the development of concentration,temperature and pressure profiles over a series of theoretical plates is presented. The accuracy of the model, methods to improve it, and applicability to other forms of continuous chromatography are discussed.

Key words :- Chromatography, continuous, sequential, production-scale.

CONTENTS

Abbreviations and Terminology used in this Thesis

Arklone.P	1,1,2-trifluoro- 1,2,2-trichloro-ethane
B.S.P.	British Standard Pipe fitting
c.p.m.	cycles per minute
d.c.m.	dichloro-methane
d.m.c.s.	dimethyl-dichloro-silane
F.I.D.	flame ionisation detector
F.F.A.P.	free fatty acid phase
Genklene.P.	1,1,1-trichloroethane
g.l.c.	gas-liquid chromatography
g.p.c.	gel-permeation chromatography
H.E.T.P.	height equivalent to a chromatographic theoretical plate
H.T.U.	height of a transfer unit.
Isolated or purge,column or section	Column into which purge gas enters to remove Product 2.
Mobile phase	gas phase
Product 1	The 'top' product which exits with the carrier gas
Product 2	The 'bottom' product which exits from the purge column
r.p.h.	revolutions per hour
stationary phase	liquid solvent phase
SCCR1	sequential continuous chromatographic refiner
S.T.P.	shake, turn, pressurise method of packing columns
TC1,TC2 etc.	thermocouple number 1,2 etc.

CHAPTER 1

INTRODUCTION

The origins of chromatography were founded in the work of Tswett (1,2) at the turn of the century. Martin and Synge (3) in 1941 introduced partition as the basis of separation and for this significant development were awarded the 1952 Nobel Prize in Chemistry. It wasn't until 1952 however, when the work of James and Martin (4-7) on the analysis of fatty acids was published, that gas chromatography began its unprecedented expansion. This paper plus the discussion of Van Deemter et al (8) provided the basic theory expressing the relationship between various chromatographic parameters and column performance. The theory was further refined in the following years by several researchers, in particular Giddings in conjunction with Eyring (9), who in 1958 produced the random walk theory of chromatography. Later developments by Giddings led in 1964 to the generalized non--equilibrium theory of chromatography (10,11), which to date has remained as the universally accepted description of chromatographic fundamentals.

As gas-liquid chromatography (g.l.c.) is a separation technique it is not surprising that the possibility of using the process for the separation of large amounts of highly pure substances has been considered since its conception. James and Martin (12) attempted to scale up their 0.4 cm diameter column to a diameter of 2.5 cm in order to be able to collect pure fractions. Using a horizontal 3 cm diameter column, Evans and Tatlow (13) obtained gram quantities of fluorinated hydrocarbons. Several industrial companies realising the potential of preparative chromatography began financing research projects and in 1957 the Du Pont company described a unit capable of separating a wide range of substances at high purity (14).

At this time the difficulty of preparing large diameter columns without loss of efficiency became apparent. This problem

is still of fundamental importance today and several approaches have been tried to combat it. The use of many small diameter parallel columns acting together was investigated by Carle and Johns (15) but the need for perfect matching of the column characteristics amongst other problems led to this idea being abandoned in favour of slightly larger diameter columns utilizing repetitive sample injection and product collection. Although throughputs are substantially improved by repetitive injection of feed samples, a limit is very soon reached above which the size and frequency of the injections cannot be increased without increase in the column diameter.

From purely theoretical considerations Golay (16) attributed the decrease in efficiency of large diameter columns to radial velocity fluctuations. Many workers have since upheld this hypothesis through experimental work (17,18). Methods of overcoming or minimizing the problem have taken the form of insertions into the column. Washers, baffles, coated discs and mixing devices (18-23), have all been tried with varying degrees of success.

Large diameter columns (30-120 cm) for production-scale g.l.c. have been developed by Abcor Ltd. (20) in the U.S.A. These columns fitted with baffles placed at regular intervals have evoked considerable interest but have presented severe economic problems. Continental Oil Co. (24), have reported the success of smaller units (30 cm diameter) in separating hydrocarbon mixtures of sample volumes up to 500 cm^3, whilst Valentin and co-workers (25) are known to have pilot plant equipment capable of producing 10 tons/year of very pure products, an example of which is the upgrading of n-pentane to a purity of 99.996%.

As already mentioned economic considerations must play a vital role in production chromatography and it is for these reasons that preparative g.l.c. is not as widespread as was originally envisaged. The production units mentioned above all utilize repetitive injection techniques and are therefore inherently batch processes. In the vast majority of chemical engineering processes batch operation is inferior to continuous operation both from a throughput standpoint and from economic considerations. Several workers have therefore attempted to develop process schemes based on continuous cross-current or counter--current operation.

With cross-current schemes the continuous separation of multi-component mixtures of high purity is possible, although practical problems have severely limited their use on a large scale. Very recent work by Wolf and Vermeulen (26) incorporating the concept of multiple layer beds appears encouraging in that throughputs have been increased between 2 and 30 times over the best single bed cross-flow units.

In counter-current schemes the mobile phase fluid and stationary phase fluid are moved counter-currently, whilst a continuous feed mixture is introduced at some point in the separating section. The feed components with the least affinity for the stationary phase fluid travel preferentially with the mobile fluid whilst the more strongly adsorbed components move in the opposite direction with the stationary phase. Consequently continuous product offtake is possible. Barker and co-workers (27-50) have, since the early 1960's, been at the forefront in developing counter-current chromatographic techniques. Many of the units now being operated by Barker and his group for both gas-liquid and gel-permeation chromatographic separations are based on a concept developed by Barker and Deeble (44), in which counter-current

movement is simulated by sequencing a system of inlet and outlet port functions around a closed loop of columns. In the first unit of this type called the Sequential Continuous Chromatographic Refiner, (SCCR1), the continuous fractionation of 1.1.2-trifluoro-1.2.2-trichloroethane (Arklone.P.) and 1.1.1-trichloroethane (Genklene.P.) was achieved at equivolume feedrates of up to 700 $cm^3 hr^{-1}$. The SCCR1 unit was constructed of 12 vertical volumns, 61 cm long and 7.6 cm diameter, packed with 500-355 μm particles of Chromosorb.P. The packing was coated with a solvent phase of silicone oil DC 200/50 (25% wt/wt).

The simulation of counter-current movement as outlined above is a new concept and the operation of continuous chromatographs based upon it varies greatly from conventional batch machines. Deeble (45), had obtained preliminary information concerning the operation of the SCCR1, and it was one of the aims of this thesis to continue this work to optimise operational parameters such as mobile phase flowrate length of the sequencing interval, and the solute feedrates.

The potential throughputs in a continuous machine may be far greater than for batch machines of the same column diameter, and it is likely therefore that the known temperature effects resulting from the passage of large amounts of solute will also be more pronounced in a continuous unit. The value of the solute partition coefficients upon which the initial flowrates are selected, are very susceptible to changes in temperature and therefore it was proposed to investigate the temperature profiles present in the continuous unit, and to determine the effect of these perturbations upon the separation.

The chromatographic separation factor for the system Arklone.P./Genklene.P. is approximately 2.6, and whilst the sytem

provides a convenient one for study it does not provide a severe test of the separating capabilities of the SCCR1. The possibility of separating a mixture of solutes of much lower separation factor was therefore to be investigated.

Concurrently with the experimental programme it was envisaged that development of a mathematical simulation would be carried out.

CHAPTER 2

Literature Survey

2.1 Scope

Following the work of James and Martin in 1951 (4), chromatography has developed into an accepted analytical and preparative technique. The swift growth of the subject has resulted in a great number of publications and it is necessary therefore to be restrictive in the summary of relevant literature. A definition of the basic terminology has been omitted as excellent reviews have previously been given (45,49).

The survey is concerned firstly with the development of theoretical models of the column chromatographic process. An introduction to the basic separation mechanism is given, followed by several independent theories designed to account for imperfections in the process.

Scale-up of the batch chromatographic process is next reviewed, with factors affecting the performance of such columns being discussed. Practical methods of improving column efficiencies are dealt with in detail, with optimisation techniques for production scale chromatography being reviewed.

The desire to obtain maximum column utilization by continuous operation has produced a number of novel schemes, and the development of the practice of continuous operation is followed. Finally the history of the developments leading to the construction of the SCCR 1 unit is traced through the work of Barker and co-workers (27-50).

2.2 Theory of Zone Spreading

2.2.1 Introduction

Chromatographic separations are governed by two criteria, thermodynamic equilibria and column dynamics. It is the latter which determines the width of the solute zones and which the theories of chromatography attempt to define.

The problem is to define the degree of broadening by a suitable number, to find out the factors upon which the broadening depends, and finally to produce quantitative relations linking the zone broadening with the factors which produce it.

2.2.2 The Theoretical Plate Concept

The theoretical plate model was introduced into chromatography by Martin and Synge (3) because of its effectiveness in describing distillation processes. Their early work has been subsequently, developed by James and Martin (4), Mayer and Tompkins (52), and Glueckauf (53).

The basic premiss is that the chromatographic column is divided into a number of zones or theoretical plates of such a length that within each plate complete equilibration of solute exists between the mobile and stationary phases. Further fundamental assumptions are made in that:

a) The solute exchange process is thermodynamically reversible such that instantaneous equilibrium is achieved.

b) The partition coefficient is constant throughout the column and therefore independent of concentration.

c) Longitudinal diffusion may be neglected.

d) The mobile phase flow is discontinuous, consisting of the stepwise additions of volumes of mobile phase equal to the mobile phase volume per plate.

By reducing the plate volume to an infinitessimal value, Gluekauf obtained a continuous model. The concentration profile showed a Poisson distribution which could if the number of plates, N, was large enough (>100), be approximated by a Gaussian distribution. The standard deviation (σ) of the Gaussian distribution (a direct measure of zone spreading) is given by

$$\sigma = (H.L_m)^{\frac{1}{2}} \qquad (2.1)$$

where H is the height equivalent to a theoretical plate (HETP) and L_m is the distance migrated. Equation (2.1) shows that H varies directly with σ^2, i.e. the variance of the distribution and an important statistical property of σ^2 is that it is the summation of independent contributions

$$\text{i.e.} \quad \sigma^2 = \sigma_1^2 + \sigma_2^2 + \sigma_3^2 + \ldots \qquad (2.2)$$

Hence the HETP can be expressed as

$$H = \Sigma_i \frac{\sigma_i^2}{L_m} \qquad (2.3)$$

Therefore contributions to the plate height may be determined independently and summed to give an overall value for H.

The most obvious conflict of the plate model with actual column processes lies in the assumption of plate wide equilibrium. In practice equilibrium is only achieved at the single point of the peak maximum. Giddings (54) attempts to overcome this inconsistency by redefining the plate height such that it is equivalent to the length of a cell whose mean concentration (not stationary phase concentration) is in equilibrium with its own effluent. Even overcoming this inconsistency the plate model still fails to give an adequate description of the chromatographic process as it is not designed to account for the basic effects of particle size, molecular diffusion, finite mass transfer effects and other factors giving rise to zone spreading. However the plate height is a useful and widely accepted parameter for the characterization of zone spreading and column efficiency.

2.2.3 Zone Broadening Rate Theories

2.2.3.1 Van Deemter Theory

Much theoretical work has been carried out to express the behaviour of a chromatographic column in terms of the H.E.T.P. Lapidus and Amundson (55) were the first to introduce mass transfer and diffusion terms into a model, and their theory was developed by Van Deemter, Zinderweg and Klinkenberg (56) who derived the following expression, relating the column parameters to the H.E.T.P.:

$$H = 2.\lambda d_p + \frac{2\gamma' D_M}{u} + \frac{8}{\pi^2} \frac{k' d_f^2}{(1+k')^2 D_s} u \qquad (2.4)$$

λ = packing characterization term for eddy diffusivity such that eddy diffusivity, E, $= \lambda . u . d_p$.

d_p = mean particle diameter

γ' = labyrinth factor to allow for the toruous flow path

D_M = Mobile phase molecular diffusivity

D_s = Stationary phase molecular diffusivity

d_f = thickness of stationary phase liquid film

u = interstitial gas phase velocity

k = $F_M/K.F_s$ = mass distribution coefficient

K = partition coefficient

F_M = Fractional volume of mobile phase

F_s = Fractional volume of stationary phase

In a shortened form Equation 2.4 is often expressed as

$$H = A + \frac{B}{u} + C_s u \qquad (2.5)$$

A, B and C_s are the 'eddy' diffusion, axial diffusion and stationary phase, mass transfer resistance terms respectively. Van Deemter (56) introduced a further term ($C_m.u$) to allow for resistance to mass transfer in the mobile phase.

Figure 2.1(a) represents graphically the Van Deemter Equation 2.4, showing how at low gas velocities the axial diffusion term is significant and therefore high molecular weight carrier gases are desirable to minimize H. At higher gas velocities the dependence of H on $(\frac{B}{u})$ disappears and the mass transfer resistance terms become controlling.

Figure 2.1(a)

Graphical Representation of the Van Deemter Equation

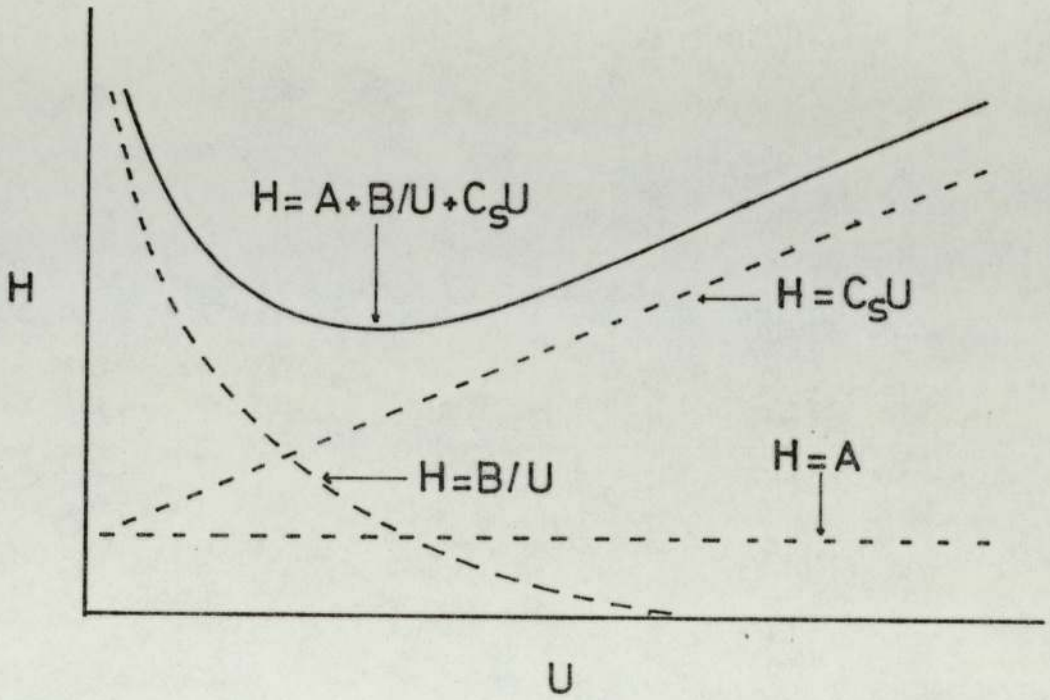

Figure 2.1(b)

Velocity Extremes in the Mobile Phase

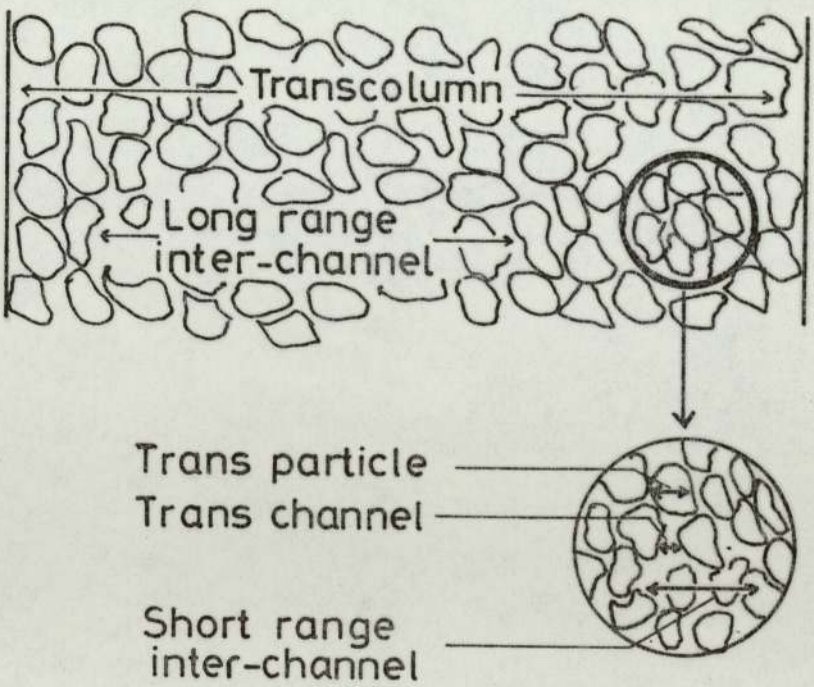

2.2.3.2 Random Walk

The original Van Deemter equation has been extended and modified by many workers (57-61). Giddings (11) in his standard text has carried out extensive theoretical studies into the mechanisms of zone broadening. Using the individual molecular processes occurring in a chromatographic column he developed a "random walk" model (11,62). The basic concept of this model is that the molecular movements of the solute, although random, have an equal chance of being forward or backward. If a large number of molecules start together on a random walk of many steps, the standard deviation (σ) of the resulting Gaussian concentration profile is simply

$$\sigma = \ell' . (n)^{\frac{1}{2}} \qquad (2.6)$$

where n is the number of steps taken and ℓ' is the average (root mean square) length of the actual displacement. Again it is convenient to write Equation 2.6 in terms of the variance σ^2 viz.

$$\sigma^2 = (\ell')^2 n \qquad (2.7)$$

and as each molecular process has its own value of ℓ' and n the whole may be summed to yield an equation the same as (2.2). Giddings evaluates the contribution to plate height from longitudinal mobile phase diffusion as:

$$H = \frac{2 \gamma' D_m}{u} \qquad (2.8)$$

By using the same Einsteinian relationship for diffusion (63) the stationary phase diffusion was calculated as

$$H = \frac{2\,\gamma_s . D_s}{u} \quad \frac{(1-R)}{R} \tag{2.9}$$

γ_s = obstructive factor within solid particles

R = retention ratio

Simple kinetic mechanisms describing the adsorption-desorption process can be formulated as a random walk and Giddings (11) obtained:

$$H = 2R.(1-R) \quad \frac{d_F^{\,2}.u}{D_s} \tag{2.10}$$

Diffusion in the mobile phase is more complicated than in the stationary phase because of the complex network of interconnected channels and void spaces, giving rise to velocity variations within the mobile phase. The mechanisms leading to this zone spreading within the mobile phase originate from

(i) Transparticle effects occurring through stagnant mobile phase trapped in the porous solid support particles

(ii) Transchannel effects caused by the higher velocity in the center of each interstitial flow channel

(iii) Short-range interchannel effects

(iv) Long-range interchannel effects

(v) Transcolumn effects

See for example Figure 2.1(b).

The final relationship for the mobile phase mass transfer term was obtained as:

$$H = \frac{w.d_p^2.u}{D_M} \tag{2.11}$$

$$w = \sum_i w_\alpha^2 . w_p^2/2 \tag{2.12}$$

w_α = (distance between velocity extremes)/d_p

w_β = (distance between extreme and average velocity)/u

Eddy diffusion is a consequence of the same velocity inequalities giving rise to the plate height term in Equation 2.11. Similarly separate eddy diffusion terms may be identified with each of the five categories of velocity inequalities yielding an eddy diffusion contribution of

$$H = 2.\lambda_i d_p \tag{2.13}$$

$$\lambda = \sum_i w_\beta^2 . w_\lambda/2 \tag{2.14}$$

w_λ = structural parameter

The separate contributions to plate height obtained from the random walk approach may be summed to give

$$H = 2\lambda d_p + \frac{2}{u}\left[\gamma' D_m + \gamma_s D_s \frac{(1-R)}{R}\right] + 2R.(1-R)\frac{d_f^2.u}{D_s} + \frac{w.d_p^2\,u}{D_M} \tag{2.15}$$

$$\text{or } H = A + \frac{B}{u} + C_s u + C_m u \tag{2.16}$$

As shown in Section 2.1 the successive additions of plate height contributions depends upon their independence from one another. Giddings (11) has shown that the eddy diffusion and mobile phase mass transfer terms are not independent and therefore their variances not

additive. Combining these two contributions in one term leads to the general equation

$$H = \frac{B}{u} + C_s u + \left(\frac{1}{A} + \frac{1}{C_m u}\right)^{-1} \qquad (2.17)$$

As seen from Figure 2.2(a) the value of the coupled term in Equation 2.17 is always less than either of the component parts. In relating practical results to theoretical preductions the results of Hammond and Harper (64) are most accurately described by the coupling theory.

A major criticism of the random walk model is that it is based on a fixed number of steps for all participating molecules, while in reality particularly in reference to sorption-desorption kinetics a variable number of steps are taken. De Clerk and Buys (65) attempt to overcome this deficiency by recognising that the integrals derived by Aris (66) may be interpreted in terms of a random walk mechanism. The Aris integrals describe the resistance to mass-transfer contributions to the effective diffusion coefficient arising from non-equilibrium in the mobile and stationary phases. Giddings (62) also recognised the limitation of the random walk approach and developed the generalized non-equilibrium theory of zone broadening (10,67) to describe the mass transfer terms in Equation 2.16. Although these terms constitute only part of the total plate height expression they are for practical chromatographic purposes the most significant.

2.2.3.3 Generalized non equilibrium theory

The non-equilibrium theory is based on the fact that sorption/desorption processes require a finite amount of time to occur. A schematic diagram of the non-equilibrium process is illustrated in

Figure 2.2(a)

Classical and Coupled Equations for Plate Height

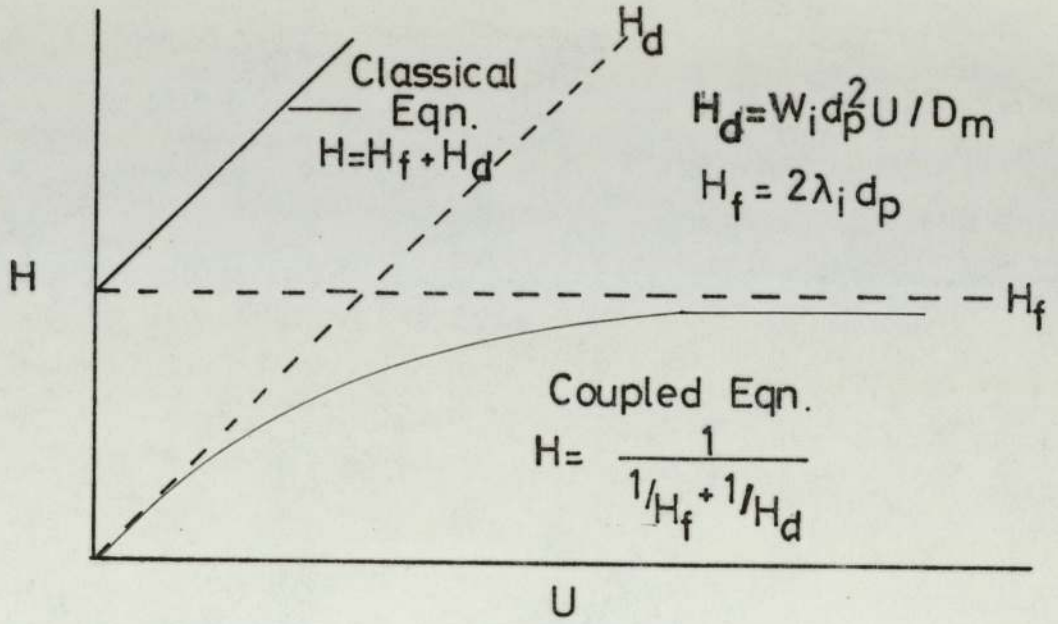

Figure 2.2(b)

Actual and Equilibrium Component Zone Concentration Profiles

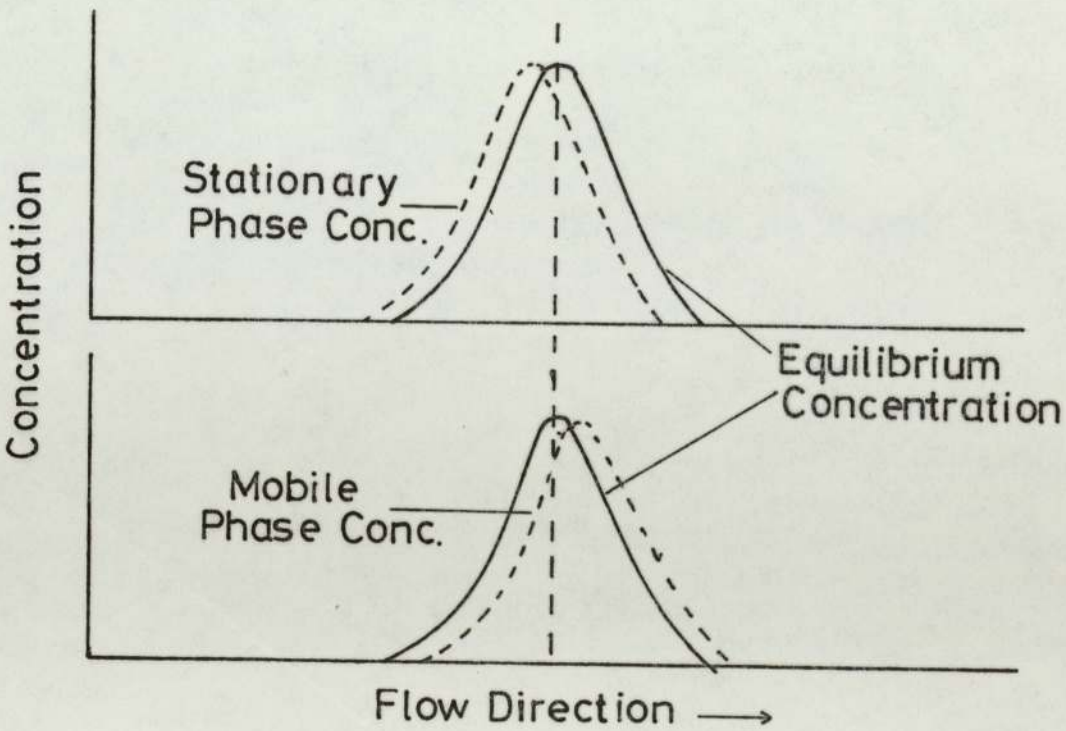

Figure 2.2(b), and shows that the stationary phase concentration has a lag in its equilibrium value whilst the mobile phase concentration will always be ahead of its equilibrium concentration. The degree of non-equilibrium, indicated by the gap between the related curves of Figure 2.2(b), is a function of the rate of mass transfer between the phases and can be minimised by having the zone migrating slowly thus preventing rapid concentration changes.

The advantages of using the non-equilibrium approach is that it replaces the single molecular events of the random walk method by the gross processes of mass transfer, and includes terms to account for packing geometries. Giddings (11) evaluates the term to account for diffusion in the stationary phase as

$$H = q' R \frac{(1-R).d^2.u}{D_s} \qquad (2.18)$$

q' = configuration factor

This gives a more exact representation of the stationary phase term obtained from random walk theory, Equation 2.10. The mobile phase diffusion expression is again a function of the five mechanisms discussed in the random walk theory and if several simplifying assumptions are made Equation 2.11 is again produced. The final relationship for H derived from non-equilibrium theory becomes:

$$H = \frac{2\gamma'.D_M}{u} + q'R(1-R)\frac{d_f^2.u}{D_s} + \left[\frac{1}{2\lambda d_p} + \frac{D_M}{w.d_p^2 u}\right]^{-1} \qquad (2.19)$$

The relative significance of the individual terms of Equation 2.19 determines whether or not simplifying assumptions to the mobile phase diffusion expression are valid or not.

The preceding models whilst giving a detailed account of the mechanisms involved in zone dispersion, do not include contributions to the plate height equation relating to the sample size, the shape and size of the column etc. A theoretical treatment of these factors will be discussed in the following section.

2.3 Scale Up of the Batch Chromatographic Process

2.3.1 Further Mechanisms Leading to Zone Broadening

2.3.1.1 Flow Dynamics in Packed Columns

Giddings (11) has postulated five mechanisms by which velocity inequalities may occur in packed columns, (Section 2.2.3.2). In large diameter columns the 'transcolumn' term is of particular importance owing to the large velocity differences which often occur across the column cross-section. Additional zone spreading resulting from unevenness in flow velocity have lead to a further term, H_c, being added to the Van Deemter plate height equation:

$$H = (A + \frac{B}{u} + C_m u + C_s u) + H_c \qquad (2.20)$$

The exact form of the velocity profile and therefore H_c has remained a matter for debate but it is generally accepted that with column diameters greater than 2 to 5 cm, H_c is usually the dominant term.

Giddings (68) has proposed a velocity profile convex to the direction of flow. This approach is based on the lower resistance to flow being found at the column wall. Using the non-equilibrium theory Giddings (68) found the plate height contribution to be:

$$H_c = G_2 \left(\frac{r_c^2 u}{96.\gamma'.D_m}\right) \qquad (2.21)$$

G_2 = constant

This correlation was found to give good agreement with experimental results obtained from 0.6 cm and 5.1 cm-diameter columns (69). The proposed convex flow profile was observed in a 7.5 cm diameter column

by Huyten et al. (17), with similar observations being made by Friscone (18). A similar expression to Equation 2.21 was therefore obtained by Huyten et al (17) Higgins and Smith (70) and Rijinders (71).

In contrast to these proposals Hupe et al (72) and Volkov (73) have observed maximum zone velocities at the centre of their packed columns, attributing this to the fact that the higher packed density in the central sections of a column lead to faster mass transfer rates. Bayer, Hupe and Mack (19) based their derivations on this observation and obtained an expression for H_c as:

$$H_c = 2.83 \frac{r_c^{0.58}}{u^{1.886}} \qquad (2.22)$$

which gave good experimental agreement for columns between 1.3 cm and 10.2 cm diameter.

The band spreading resulting from the non uniform velocity profile will be reduced by lateral diffusion. Littlewood (74) and Sie and Rijinders (75) describe the lateral diffusion in terms of a molecular diffusion expression ($\gamma' D_m$) and a convective diffusion term ($\alpha' . d_p . u$). Combining these with the longitudinal diffusion terms they obtained.

$$H_c = \frac{0.5\ I' . d_c^2 . u}{\gamma' D_m + \alpha' d_p . u} \qquad (2.23)$$

α' = packing geometry factor

I' = complicated double definite integral of the velocity profile gradient. (c.f. Aris integrals (66), Section 2.2.3.2).

The preceding expressions for H_c all predict the decrease of efficiency with increase in column diameter. Pretorius and De Clerk (76) doubted this prediction and considered the 'wall effect' and the 'particle to column diameter ratio', d_{pc}, to be of fundamental importance in determining the velocity profile. The resultant profile they developed was of a 'W' shape with the maximum velocity being experienced several particle diameters into the bed. The semi-empirical expression to allow for this contribution to plate height was:

$$H_c = \frac{M' d_c^2 u}{2 D_r . d_p} \qquad (2.24)$$

where $$M' = \left(\frac{1}{100}\right) \exp\left(-\frac{d_c}{10 d_p}\right) \qquad (2.25)$$

According to this study, the plate height first increases with d_c at constant $\frac{d_p}{d_c}$, reaches a maximum at $\frac{d_p}{d_c} = 0.05$ and then decreases with increasing d_c. The results of Spencer and Kucharski (77) and Knox (78) give support to the above hypothesis, Spencer et al (77) observed a fall in H.E.T.P. above column diameters of 6.4 cm, whilst Bayer et al (19) record a lessening of the rate of increase in H.E.T.P. as the column diameter is increased from 1 cm to 50 cm. Giddings (68,69) proposes that this effect could be due to the fact that if radial equilibrium is not achieved in large diameter columns then plate height becomes independent of diameter. The deleterious wall effects can be overcome by having a column of sufficient diameter so that the sample is eluted before it has time to diffuse to the wall, as proposed by Knox and Parcher (79). The authors also suggest a technique whereby only the central portion of the eluted solute band is removed. The feasibility of such a proposal is somewhat questionable owing to the very poor column utilisation.

As shown above, differences of opinion exist as to the effect of column diameter, although the body of opinion indicates a loss of efficiency when columns are scaled up to the production level, because of increasing radial velocity variations. Dixmier, Roz, and Guiochon (80) however, doubt whether any explanation is fully correct and point to the paradoxical results of Huyten et al (17) who found that increased radial variation in velocity was accompanied by improved efficiency.

2.3.1.2 Temperature Effects in Packed Columns

In the derivation of the plate height equation isothermal operating conditions were assumed. This cannot be true in practice because of the combined effects of the heat of solution of the larger samples and the finite rate of heat transfer across large diameter columns. The non-isothermal operation of 10 cm columns has been demonstrated by Hupe et al (72) and in 2.5 cm columns by Peters and Euston (81), and Rose et al (82). Scott (83) has studied the temperature effects resulting from the passage of a solute through a theoretical plate and concludes that the excess heat generation increases with:-

a) Increasing flow rate

b) Increasing sample size

c) Decreasing partition coefficient values.

The first two factors are of significance in preparative and production chromatography and the results of Rose et al (82) indicate that heat transfer properties could be of primary importance in the design of preparative and production columns. Giddings (68) noting that the solute zone migration velocity was dependent upon the local column temperature introduced a further plate height term (H_t), to allow for thermal fluctuations across the column:

$$H_t = \alpha_t . (\Delta T) \frac{r_c^2 . u}{900 . D_M} \qquad (2.26)$$

α_t = constant of value approximately 0.004

ΔT = temperature difference between the centre and wall.

The temperature lag between the centre and wall of the column, attributable to the resistance to heat transfer is also of importance when temperature programming is used. Giddings (68) concluded that an additional term to describe the contribution to plate height caused by the thermal lag could be described by:

$$H_{tp} = \frac{\alpha_t . \beta^2 . u . r_c^6}{14400 . K^2 . D_M} \qquad (2.27)$$

H_{tp} = contribution to plate height from temperature programming

β = heating rate

2.3.1.3 Finite Concentration Effects

Feed band width and feed concentration are closely linked parameters and an increase in either leads to a marked reduction of the column efficiency in terms of the number of theoretical plates (84,85). For the case of a linear adsorption isotherm the fundamental retention equation for a chromatographic system is:

$$V_R = V_M + KV_s \qquad (2.28)$$

V_R = retention volume of component

V_M = column mobile phase volume

V_s = column stationary phase volume

K = equilibrium partition coefficient

However if the partition coefficient is a function of solute concentration, i.e. non-linear isotherm, then the elution volume is given by (86)

$$V_R = V_M + V_s \cdot \left(\frac{\partial q}{\partial c}\right)_c \qquad (2.29)$$

q = solute concentration in stationary phase

c = solute concentration in mobile phase

Figure 2.3 shows the effect of the three commonest types of isotherm on the shape of the solute peak. For a Langmuir type isotherm, Figure 2.3(b), the retention volume and associated partition coefficient, K = q/c, decrease with increasing concentration. The resulting solute peak has a sharpened leading edge and a diffuse trailing edge. Similarly, the anti-Langmuir isotherm, Figure 2.3(c), exhibits a diffuse leading edge and sharpened trailing edge. The vast majority of chromatographic systems exhibit non-linear isotherms resulting in an increased band width and therefore a longer column is necessary to obtain the same degree of separation. However, the gain in throughput obtained by operating at high solute concentrations in many cases outweighs the detrimental effects of peak skewing.

2.3.2 Practical Methods of Improving Column Efficiency

2.3.2.1 Column Packing Techniques

From a purely theoretical standpoint, differences in H.E.T.P. values between large and small diameter columns should not exist.

Figure 2.3

The Relationship between the Solute Zone Boundary Concentration Profile and the Type of Partion Isotherm

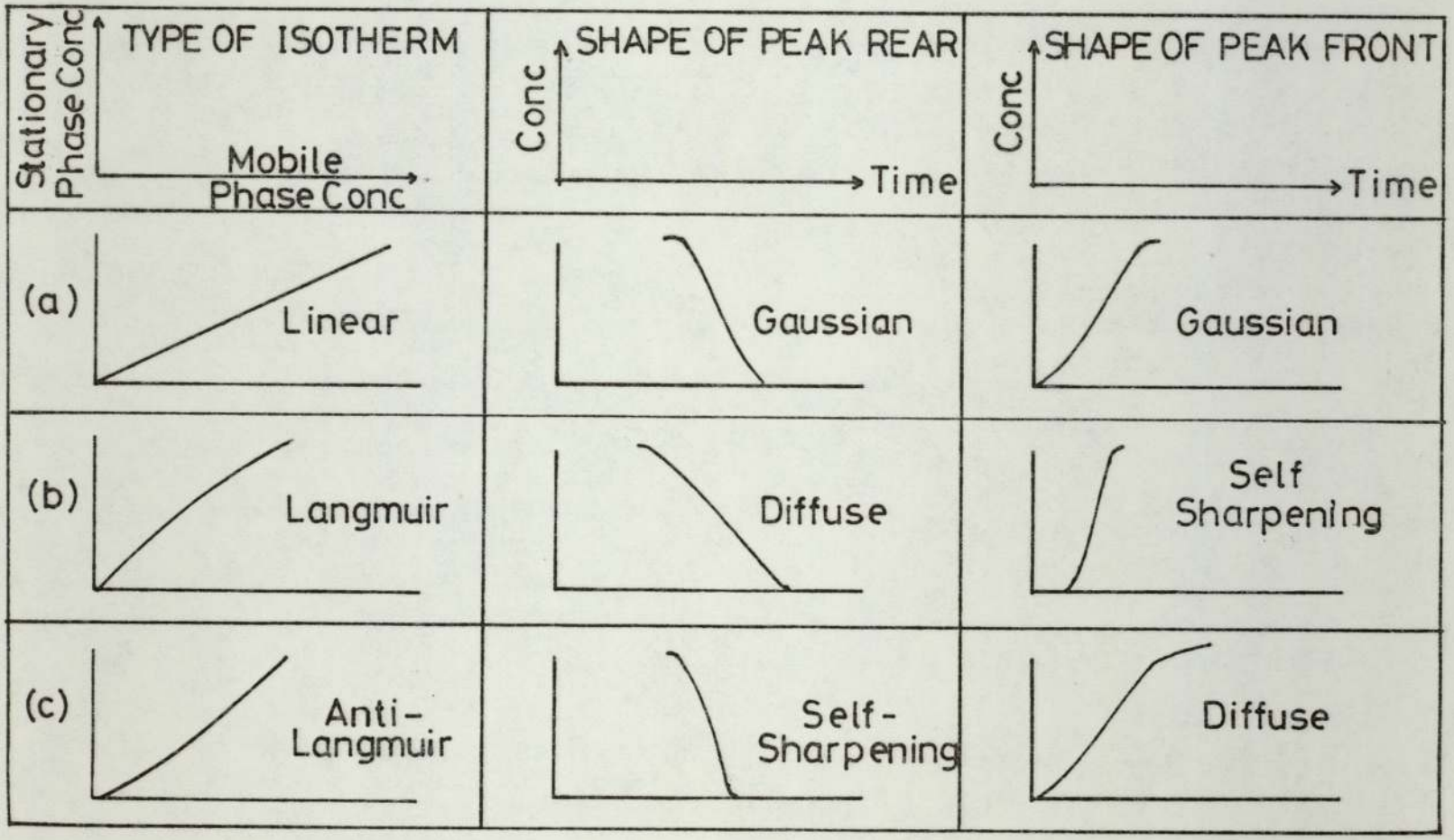

The fact that large diameter columns exhibit comparatively low efficiencies is due in the main to the method of packing, hence many workers have sought to achieve a packing technique giving both high and reproducible column efficiencies.

The simplest method of packing is pouring small amounts of support into the column which is being bounced and tapped on the side. This method having been used by Giddings and Jensen (69) and Hargrove and Sawyer (87) has been shown by Huyten et al (17) to give cross-sectional non uniformity in the packed bed. Higgins and Smith (70) described several methods of packing such as "bulk", "snow", and "mountain" packing. In the first method the entire column packing is poured in at once. In the second, the packing is allowed to trickle in slowly while the column is being vibrated. The "mountain" technique allows the support to flow through an orifice positioned just above the level of packing in the column, so that a small cone is always formed on top of the settled bed. This method was reported as giving the best results, with H.E.T.P's in the order of 1 mm being obtained. Guillemin (88-90) used a fluidisation technique, which although giving high initial efficiencies never achieved universal acceptance as the packed beds so produced were prone to collapse owing to the low packed densities inherent in the method. Bayer et al (19) advocated mechanical tapping and vibration to improve efficiencies whilst Hupe et al (72) have used a conical plunger to achieve better packing. In this latter method the conical plunger is rested on the packing inside the column whilst tapping takes place. The idea is to increase density in the peripheral regions of the column. Verzele (91) introduced a new method known as the "shake-turn-pressurise", or S.T.P. method. In this the column is shaken in the radial

direction and is rotated along its own axis whilst being packed and periodically pressurised. In all the above methods the H.E.T.P.'s measured were of 0.1 cm and above, reproducibility in some cases being very poor. Recently a novel packing method developed by Reese and Grushka (92) giving highly stable columns, has achieved efficiencies equivalent to those in analytical columns. The technique consists simply of drawing the support upwards into the column by means of a vacuum, homogenizing the bed, turning the column over, and tapping it. Reproducible H.E.T.P's in the order of (0.05-0.07 cm) have been obtained by this method for columns of 3.3 cm diameter.

2.3.2.2 Changing the Column Shape

The vast majority of preparative, and all production columns, are of the standard circular cross section. However, in an attempt to increase the efficiency of columns alternate forms are used to avoid particle segregation, and improve heat transfer into the bed.

Studies on oval columns (93,94), annular columns (95,96, 97), and "shamrock" type columns (98), have been conducted as well as the introduction of fins (99,100) and internal rods (80). A major criticism of the above types of columns is that with the exception of Reiser's hexagonal finned column (100), the rest were of an equivalent diameter of under 3 cm, and although improved efficiencies were noted, the difficulty and expense of fabrication limits their application to the preparative scale.

The use of a multidiameter columns has been investigated by Friscone (18) and Walker (102). The latter linking columns of between 0.3 and 0.9 cm, with the object of compensating for sample overloading at the inlet. Pirogova et al (103) attempted to correct for the

expansion of the carrier gas as it progresses through a packed bed by joining columns of 2.6, 1.2 and 0.6 cm diameter. The variation in linear carrier gas velocity was thereby reduced with the corresponding increase in efficiency.

A novel approach to maintaining column efficiency during scale up is to use a matrix of small parallel columns to produce an effective large column diameter (104,105). The detrimental effects of large diameter columns are thus avoided without any loss in capacity, however, for the system to be a success the retention characteristics and solute velocities in each column must be identical to prevent peak overlap at the outlet. Difficulties also encountered in the distribution of solute and carrier gas have meant that parallel column systems have not yet found acceptance for production purposes.

2.3.2.3 The Use of Flow Distributors and Mixing Devices

2.3.2.3.1 Inlet/Outlet Cones

To ensure uniform distribution of carrier gas over the column cross-section, packed inlet cones (19,101) have received universal acceptance. Musser and Sparks (106) investigated the performance of inlet cones and their results were in agreement with Huyten et al (17) in that wide angle cones (60-90^{o}) packed to about 80% of their volume provide the most efficient means of distribution. Albrecht and Verzele (107) packed the inlet cone of a 7.5 cm diameter column with glass spheres and reported improved efficiency. It is generally accepted that the column outlet cone should be completely packed (17,107).

2.3.2.3.2 Homogenizers

Apart from improved packing techniques the adverse effects of the solute profile may be overcome by remixing the solute stream at intervals along the column. The thin mixing chambers developed by Carel and Perkins (108,109,110) have proved the most popular devices to date. Consisting of a sintered disc either side of a plate with a single central hole. The device is inserted into the column at the point where the flow profile has become clearly developed (111). The sintered discs provide redistribution whilst the 'doughnut' plate serves to remix the gaseous stream. Plate heights of 2 mm in a 10 cm diameter column have been reported (108). Using a similar device Verzele (112) has reported in a private communication with Pescar (113) H.E.T.P.'s in the order of 0.3 cm in 7.6 cm diameter columns. The spacing of homogenizers as reported by Pescar (113) is not critical, although contrary to this opinion, Golay (16) suggests that too many mixing devices may actually contribute to zone broadening and that the law of diminishing returns applies. With n_1 mixing devices the plate height, H_{CN} is given by Mir (114) as,

$$\frac{H_{CN} - H'}{H_C' - H'} = \frac{1}{n_1} \qquad (2.30)$$

H' = Intrinsic plate height for packing as measured on an analytical column

H_C' = Plate height for the same large diameter column without mixing devices.

2.3.2.3.2 Baffles and Washers

Baffles as a means of flow distribution have found universal acceptance in many chemical engineering processes and it is not surprising that this type of method has been incorporated into large scale gas chromatographs (20). Abcor Inc., Massachusetts (21,22), rely on the 'disc and doughnut' type of system, in which the discs of smaller diameter than the column, force the gas flow to the walls, after which the flow strikes the 'doughnut' and is redirected to the centre. Efficiencies of 10 cm diameter columns utilizing 'discs and doughnuts' are reported to be comparable with 0.64 cm diameter analytical columns operating under the same conditions (21).

Systems incorporating only the 'doughnut' form have been used by Bayer et al (19) and Amy and coworkers (23). Friscone (18) used filter paper washers coated with stationary phase to retard the normally advanced solute profile near the column wall. Utilizing restricting devices in a similar manner Verzele (115) obtained no beneficial effect, and therefore the benefits of such chemical washers are somewhat uncertain. However in conclusion, the incorporation of packed end cones, and some form of baffling to promote radial mixing, have greatly enhanced the viability of production scale gas chromatographs.

2.3.2.4 The Use of Repeated Feed Injections

In the normal elution mode of operation of an analytical chromatograph, the solute sample is injected and the resolved components collected before any further sample is injected. As the solute bands only occupy a small part of the available column packing at any one time, column utilization is poor, and unacceptable for

preparative and production purposes.

To increase utilization, subsequent injections are made before the previous injection has emerged from the column, hence many injections may be separated in the column at the same time. The rate of injection is a critical factor to avoid excessive overlap. In practice, two modes of operation exist. The first where the eluted profiles are completely resolved and successive injections do not overlap, and a second technique in which the solute bands are allowed to overlap and the central impure portion is 'cut-out' and recycled. Pretorious and de Clerk (76) have expressed the production rate of a component eluted by the first mode of operation as:

$$E_p = \frac{(m_i - \Delta m_i).u}{W_{to}(1+K_i)} \qquad (2.31)$$

E_p = production rate of given component

Δm_i = mass of component in sample

m_i = mass of component recycled during fraction cutting

W_{to} = chromatogram width per sample at the column outlet

To ensure that samples do not overlap the distance between samples is taken as being twice the distance between the two peaks within the sample, and therefore to separate the peaks by six standard deviations the parameter W_{to} is fixed as:

$$W_{to} = 12.R_s.\sigma_{to} \qquad (2.32)$$

σ_{to} = standard deviation at column outlet within the column

Pretorious and de Clerk (76) maintain that operation in such a manner would lead to an impurity of 0.15% for a two component mixture.

Gordon et al (116-120) maintain that the 'heart cutting' technique leads to higher throughputs where product purity is a controlling factor, but that only minimal gains are obtained when lower purities are permissable. Therefore the cost of sophisticated equipment required by chromatographs employing a 'heart-cutting' method must be carefully weighed against any increase in production. Conder (121,122) has reported that it is always preferable to overlap the component bands rather than to avoid the need for cutting by increasing column length and resolution, and that an optimum recovery value exists at 60% of the injected sample. The remaining contaminated 40% being recycled (122).

2.3.3 Performance Optimisation for Production Scale Chromatography

2.3.3.1 Performance Criteria

Several criteria for evaluating the performance of production and preparative chromatographs have been proposed (22,123-127). The best single criterion which describes the overall performance of a production chromatograph is the reciprocal of the total separation cost per unit mass of product (127,128) i.e. q_r/G_{TC} where q_r is the throughput and G_{TC} includes all capital and running costs.

Before any optimisation procedure can take place the total cost, G_{TC}, must be broken down into its component parts and related to chromatographic parameters, this has been achieved by Conder (129) who obtained

$$G_{TC} = A'+B' \left| d_c \frac{(n.u.h_o.f')^{0.4}}{(\alpha-1)^{0.8}} \right| + C' \frac{d_c^{2.5} n.u.h_o.f}{(\alpha-1)^2} \qquad (2.33)$$

α = relative volatility of key solute components

f' = factor to allow for the effect on column length of increasing the mole fraction of solute in the liquid phase.

n = normalised value of the number of theoretical plates in the column.

h_o = reference value of H.E.T.P. as defined by:

$$h_o = \frac{10.h}{u} \left(\frac{4}{d_c}\right)^{0.5} \qquad (2.34)$$

A,B,C = constants independent of column dimensions, nature of the solutes and carrier gas velocity.

To determine A, B,C in Equation 2.33 requires cost data based on construction and operating experience with production chromatographs. Ryan and Dienes (130,131) obtained such data whilst employed by 'Abcor Incorporated, Massachusetts' in the separation of α- and β-pinenes, fitting their data to the equation:

$$G = 27800 + 9400\, d_c + 1800\, d_c^{2.5} \qquad (2.35)$$

Conder (194) further defined the throughput, q_r, to be:

$$q_r = \frac{r.n_f}{n} \left(\frac{a.t_r}{6.t_c}\right) \frac{M_f.\rho_f}{R_g.T} \cdot \frac{\pi d_c^2 \varepsilon.u}{4} \qquad (2.36)$$

r = recovery ratio after fraction cutting

ε = void fraction of packed bed

t_R = retention time for solute in column

T = temperature

t_c = cycle time between repetitive injections

R_g = gas constant

M_f = molecular weight of feed component

p_f = partial pressure of feed component

n = normalised value of $N = N_a^2/36$

n_f = normalised value of $N = N_a/6$

N = number of theoretical plates in column

N_f = number of theoretical plates occupied by feed band

a = constant defined by:

$$a = 2\left(\frac{\alpha-1}{\alpha+1}\right)\left(\frac{K}{1+K}\right) \tag{2.37}$$

By combination of Equations 2.34 to 2.36 a relationship is obtained by which it is possible to compare the economic performance of a chromatograph with various design parameters

$$\frac{q_r}{G} + \frac{r.n_f.d_c^2.\beta'}{n\left[27800 + \frac{1590.d_c(n.u.h_o.f)^{0.4}}{(\alpha-1)^{0.8}} + \frac{21.5.d_c^{2.5}.n.u.h_o.f}{(\alpha-1)^2}\right]} \tag{2.38}$$

where $\beta' = \frac{a.t_R}{6.t_c}\ \frac{M_f.p_f}{R_g.T}\ \frac{\pi.\varepsilon.u}{4}$ (2.39)

2.3.3.2 Optimisation of Variables

2.3.3.2.1 Feed band width (n_f), column length (n), and recovery ratio, (r)

The above three parameters are independent from any other terms in Equation 2.38 they are however dependent upon each other and may be optimised together. Conder (129) suggests it is preferable to regard the feed band width amd recovery ratio as the independent variables to be optimised separately and then to choose a column length to give the desired purity. Experimental evidence (121) suggests that the optimum values for recovery ratio and feed band width are 0.6 and 2.0 respectively.

2.3.3.2.2 Mobile Phase Velocity (u)

Increase in carrier gas velocity has been shown to have four principal effects (129)

(i) H.E.T.P. is increased, (c.f. Figure 2.1(A)), which increases the column length required and therefore the cycle time.

(ii) The amount of feed which can be injected in each batch is increased in direct proportion to the increase in H.E.T.P., for a constant feed band width.

(iii) The cycle time is reduced in proportion to u.

(iv) The pressure drop in the column increases.

The effects of (i) and (ii) on throughput cancel out so that throughput is controlled by (iii) and is therefore directly proportional to carrier gas velocity. The combined effects of (i)-(iv) upon the parameter q_r/G are more complicated, but in general it is desirable to use the highest possible velocity in order to maximise q_r/G. Although this necessitates a larger column, the increased cost is offset by increased throughput.

2.3.3.2.3 Column Temperature (T)

Throughput (q_r) is inversely proportional to temperature and also affected by the dependence of relative volatility (α) and the vapour pressure (p_f) upon temperature. The result of combining these factors has been shown to give rise to an optimum temperature around the boiling point for thermally stable compounds (132).

The column temperature principally affects the parameter (G), through its influence upon (f), where (f) measures the effect of band broadening upon column length arising from finite concentration effects. It has been shown by Valentin et al (25) that band broadening caused by finite concentration effects is minimised when the column temperature is close to the solute boiling point.

In a recent paper, Roz et al (133) propose that the optimum temperature is the lowest of the three values

(i) maximum temperature for the stationary phase

(ii) maximum temperature for sample stability

(iii) 'Valentin temperature' at the highest possible outlet pressure

where the 'Valentin temperature' is defined such that

$$P^{o}_{A} = P_{O}\,\frac{3}{4}\,\frac{(P_{IO}^{4}-1)}{(P_{IO}^{3}-1)}\,\frac{1}{\gamma_{A}^{\infty}}\,\left(1-\frac{\gamma'^{\infty}_{A}}{\gamma^{\infty}_{A}}\right) \qquad (2.40)$$

P^{o}_{A} = vapour pressure of component

P_{O} = column outlet pressure

P = inlet to outlet pressure ratio

γ_{A}^{∞} = activity coefficient at infinite dilution

γ'^{∞}_{A} = activity coefficient correction to allow for non-ideality

2.3.3.2.4 Feed Concentration

Conder (132) maintains that the concentration of solute in both stationary and mobile phases should be as high as possible and that the feed vapour should have unit mole fraction in the vapour phase. Contrary to this Roz et al (133) maintain that when the 'Valentin' equation, (2.40), is satisfied and the optimum temperature determined, the maximum value of solute concentration in the gas phase is 0.3 mole fraction and that to increase the solute concentration may lead to a non optimum column temperature being used.

2.4 Continuous Chromatography

2.4.1 Introduction

The main advantage in choosing a continuous scheme over a batch type operation is that it allows the whole of the chromatographic column to be utilized for separation purposes, as illustrated by Figure 2.4(a,b). Greater throughputs, higher purities and lower costs are normally found in continuous mass transfer processes when compared with equivalent batch processes and consequently many workers have sought to design and perfect chromatographic systems capable of operation in a continuous mode. These schemes may conveniently be classified as fixed bed, moving bed, and simulated moving bed.

2.4.2 Fixed Bed Systems

2.4.2.1 Non-Cyclically Operated

Tiley and co-workers (134) investigated a counter-current fixed bed system using a 2.5 cm diameter column. In this the stationary phase of dinonyl-phthalate flowed downwards over the packing element of "knitmesh", against the carrier gas flow. The separation of a 1:1 mixture of di-ethyl ether and dichloromethane at a rate of 5 $cm^3.hr^{-1}$ was achieved, product purities being in excess of 99%. Column efficiencies expressed in terms of H.E.T.P.'s were however much lower than those obtained from columns in which the packing was flowing (135,136).

Kuhn et al (137,138) also utilized a flowing liquid phase. By superimposing a temperature gradient onto the column they used to their advantage the temperature dependence of the partition coefficients to separate multicomponent mixtures at different specific places along the column. Continuous separation of the ternary mixture of propionic,

Figure 2.4(a)
Repeated Batch Co-current Operation

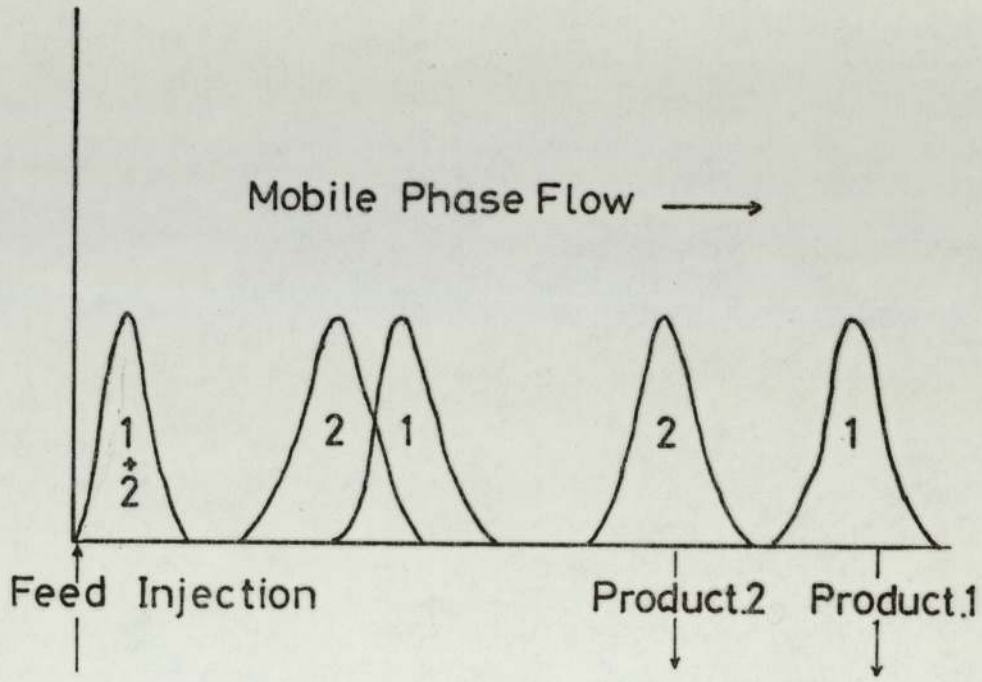

Figure 2.4(b)
Continuous Counter-current Operation

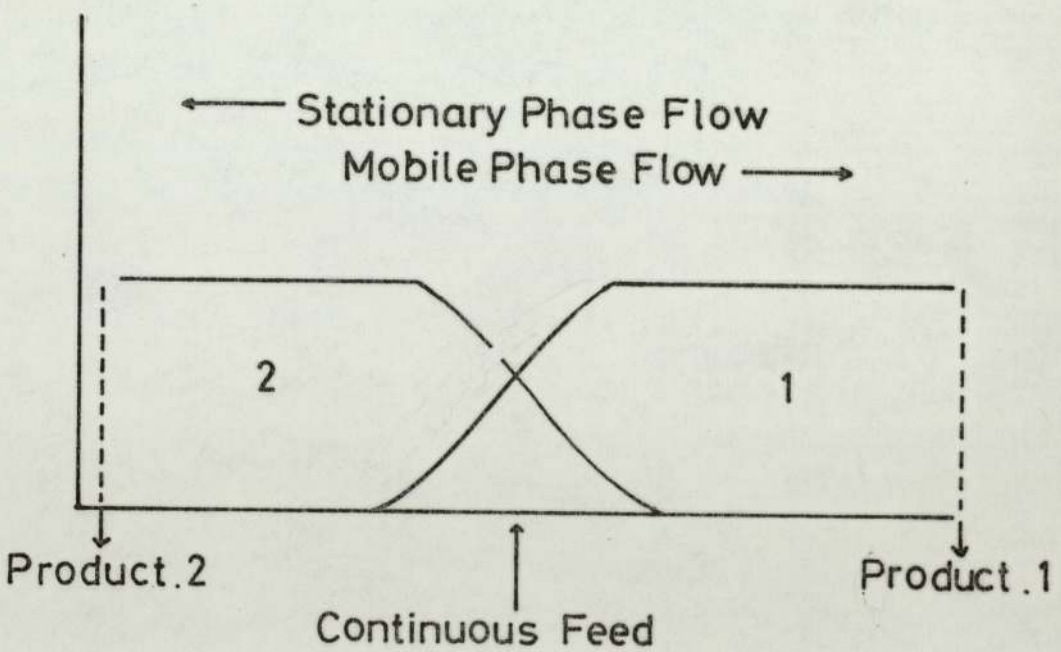

n-butyric, and n-valeric acids was achieved using paraffin oil containing 10% stearic acid as the flowing liquid phase. Purities in the order of 95% were quoted.

Cross-current operation in a fixed bed was obtained by Turina et al (139), by using two parallel glass plates 1 mm apart containing the inert support, Figure 2.5(a). The carrier gas enters along one vertical edge and exits at the opposite edge through a series of outlet ports. Stationary phase enters the top edge travelling down through the bed to exit from the base. A continuous feed mixture enters at the corner between the two fluid inlets and the individual components travel at different angles through the bed due to their different retention times in the stationary phase.

The advantage in using this type of system is that it lends itself to the separation of multicomponent mixtures. However, in common with Tiley and Kuhn's schemes low efficiencies and throughputs were obtained, due in part to the low diffusion rates caused by the relatively thick liquid film. Maldistribution of the liquid film upon the packed column or plate will also lead to a loss in efficiency as a much lower surface area/unit volume ratio will be obtained than when solid supports are used.

2.4.2.2 Cyclically Operated (Parametric Pumping)

In recent years it has been found that operation of separation processes in a cyclic manner so that they never achieve a steady state can greatly increase the separating power and efficiency of the process. Cyclic operation may involve flows of various phases which are intermittent or which vary sinusoidally with time, or a variable such as temperature, pressure, or concentration can be made to change cyclically.

Figure 2.5(a)
Scheme of Turina et al (139)

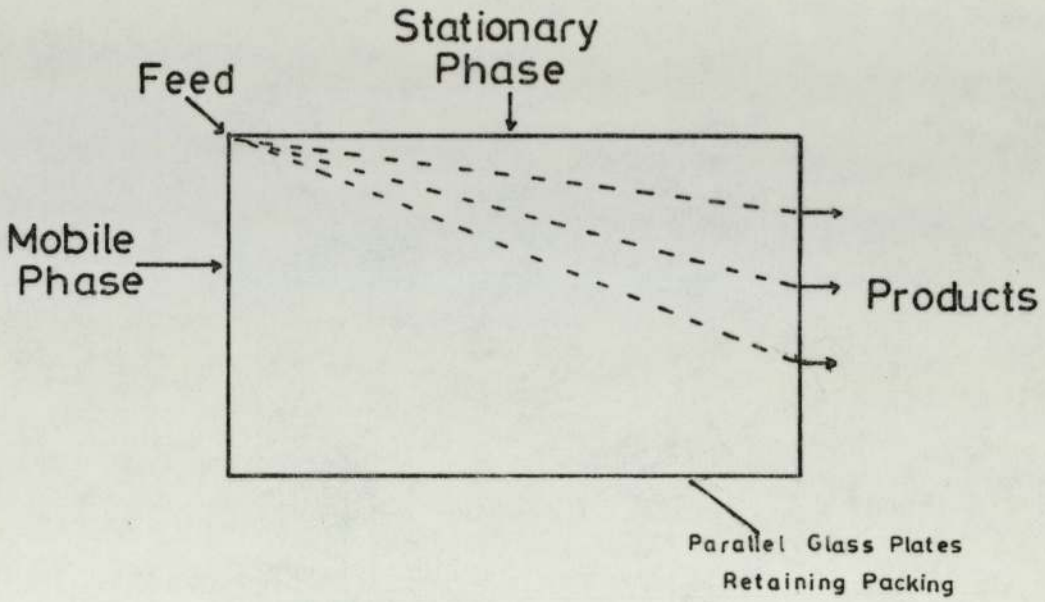

Figure 2.5(b)
Scheme of Tuthill (146)

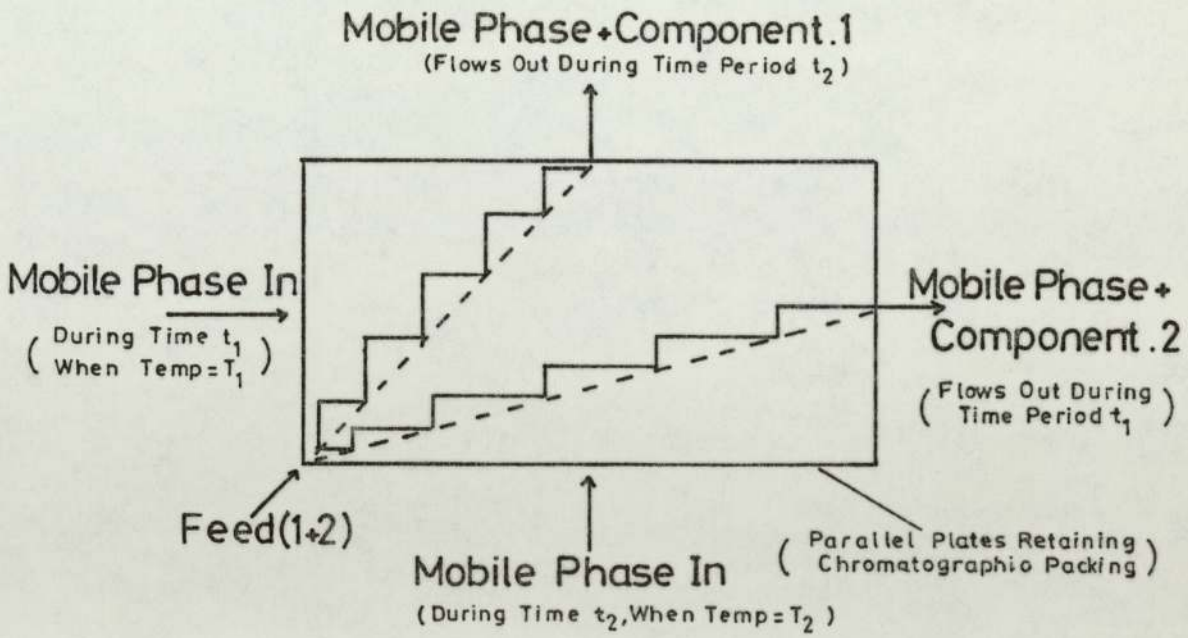

The process of parametric pumping was demonstrated by Wilhelm et al (140-143). Mobile phase flow is pumped alternately up and down a column packed with solid adsorbent particles. Heat is added to the column during the downward part of the cycle to utilize the temperature dependence of the partition coefficients. Coupling of the concentration changes caused by the flow and temperature gradient produces a separation of the components in the mobile phase. Although successfully operated in the batch mode, continuous feeding and product removal, resulted in a great loss of efficiency in the scheme.

Pigford and coworkers (144,145) demonstrated a process in which the flow of the mobile phase passing through the fixed bed of adsorbent is steady rather than cyclic. The temperature of the bed is then changed cyclically either by means of a heating jacket or by means of switching the mobile phase flow alternately between a heater and cooler prior to entry into the bed. Due to the temperature dependence of the partition coefficients the effluent concentration cycles between being rich and poor in the solute to be separated.

Improved separations can be obtained by passing the mobile phase continuously through additional columns with alternate columns being heated and cooled out of phase with one another.

Tuthill (146) combined the idea of parametric pumping using a temperature cycle, with the scheme previously described by Turina (139). The feed mixture is introduced continuously into one corner of a rectangular chromatographic slab whilst the entry of the mobile phase alternates between the two sides of the slab adjacent to the feed entry point. The temperature of the system is cycled in phase with the direction of flow of mobile phase, with the result that the

vectorial flow paths of the various components in the feed are deflected across the adsorbent bed and thereby resolved into individual product streams, Figure 2.5(b).

Using a single column Thompson (147,148) developed a co-current semi-continuous chromatographic separation in which the inlet stream varied from 100% carrier gas to 100% feed mixture. By adjustment of the frequency and flow rates through the column, individual component waves left the column out of phase by virtue once again of their different affinity for the stationary phase. Using benzyl ether as a stationary phase and carbon dioxide for a carrier gas, Thompson separated a 1:1 mixture of ethane and propane into products of 70% and 74% respectively, at a total feed rate of 82 $cm^3.min^{-1}$ and frequency of 40 c.p.m.

Further systems involving parametric pumping have been extensively reviewed by Wankat (149) who has also applied the technique to the separation of multicomponent mixtures using a single column (150).

2.4.3 Moving Bed Systems

2.4.3.1 Cross-Current Flow Processes

In cross-flow systems the chromatographic bed moves perpendicular to the direction of mobile phase flow within the bed. Development of this principle has taken two distinct forms, helical flow through annular columns and radial flow between parallel discs.

2.4.3.1.1 Helical Flow Systems

First proposed by Martin (151) for the continuous separation of a multicomponent mixture, the helical flow type column is illustrated

in Figure 2.6(a). The column was formed by packing an annular space between two concentric cylinders. The feed and mobile phase enter at the top and follow a helical path through the column with the feed components thus leaving the column at specific points around the circumference of the base.

Dinelli, Taramasso and co-workers (152,153) replaced the packed annulus by 100 packed columns 6 mm in diameter and 1.2 m long. The composite column is rotated at speeds up to 50 r.p.h. past fixed inlet and outlet ports, Figure 2.6(b). For the separation of cyclohexane/benzene on tricreysyl phosphate at 80°C, product purities greater than 99.9% were obtained for a maximum feed rate of 200 $cm^3.hr^{-1}$. Under optimum operating conditions the theoretical maximum was predicted to be 220 $cm^3\ hr^{-1}$ (154). An enlarged unit using 36 tubes of 2.4 m length has been used to separate isomers and close boiling mixtures (155-157). The matching of individual column characteristics, the physical movement of a large column bundle and the necessity of reliable seals between the individual columns and the traps make it unlikely that this type of machine can be scaled up to a production size unit.

A final method in this section combines chromatography with electrophoresis and is termed ELECTROCHROMATOGRAPHY (159,160). Different degrees of absorption cause the feed components to move at different net velocities down an annular chromatographic bed, whilst different electrical mobilities cause the components to move at different net velocities horizontally in response to the transverse electrical field, Figure 2.6(c). The overall result is a series of curved paths for the feed components so that they appear in the column effluent at different positions in a manner similar to Martin (151).

Figure 2.6(a)
Principle of Helical Flow

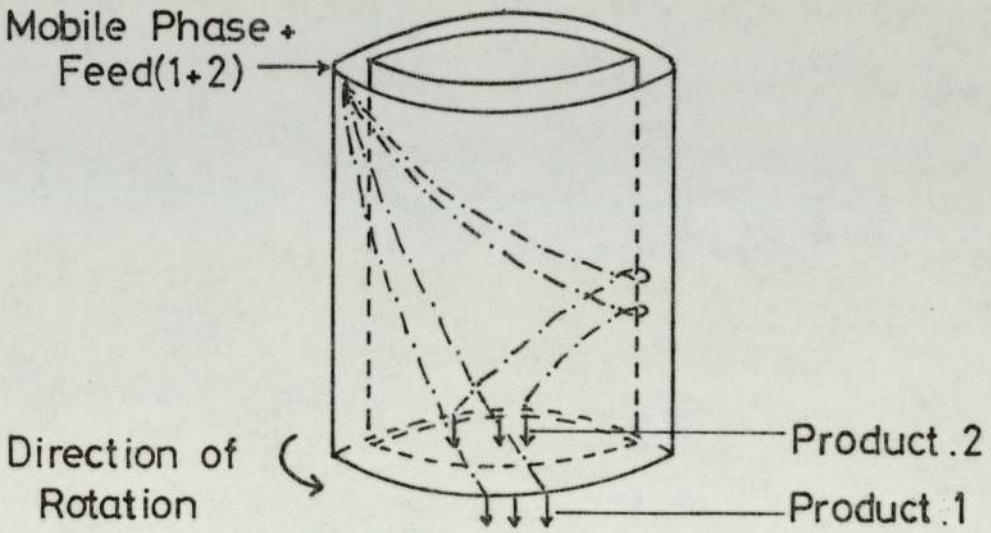

Figure 2.6(b)
Scheme of Taramasso(152)

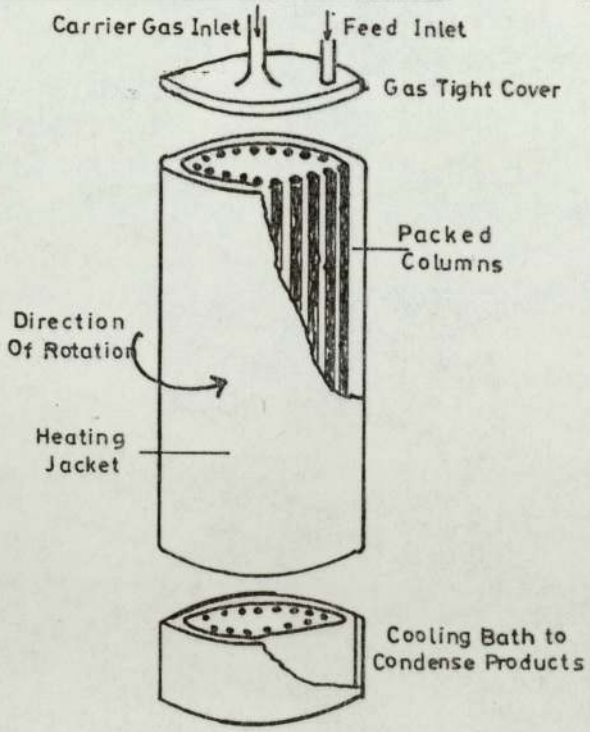

Figure 2.6(c)
Scheme of Hybarger et al(159)

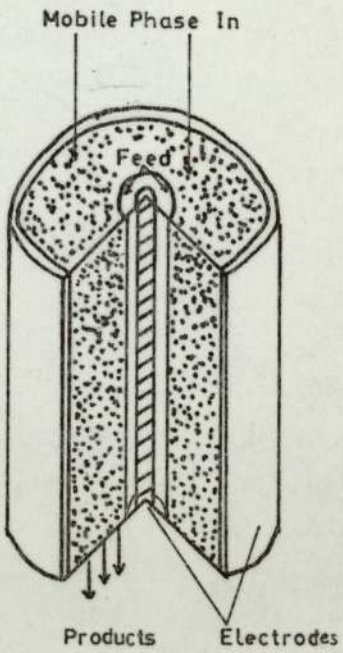

2.4.3.1.2 Radial Flow

An annular packed column in which the component paths are radial has been patented by Mosier (158) and is shown in Figures 2.7(a,b). The best way of operating the unit is to rotate the packing around the fixed feed injection and product collection ports, so that feed enters at the centre of the annulus and travels towards the circumference where products are removed from the base of the unit.

Other radial cross-flow units have been developed by Sussman et al (161-164) in which the packing has been replaced by annular discs coated with a stationary phase and separated by a gap of no more than 150 μm, Figure 2.7(c). This close spacing of the coated surfaces produces small H.E.T.P.'s so that a relatively compact machine of 30.4 cm diameter can achieve separation. Throughputs of 18 $cm^3.min^{-1}$ have been reported for the separation of the 3-component mixture of methane, propylene, and butane, and theoretical studies by the authors have led them to claim that throughputs of 50 $cm^3\ min^{-1}$ are possible (163,164).

A major shortcoming of the radial-flow units is that their resolution capabilities are inherently less than that of conventional long column chromatographs. Further scale up of Sussmans' unit may also be difficult owing to the high degree of precison engineering required.

2.4.3.2 Counter-current Flow Processes

2.4.3.2.1 Moving Packing

Counter-current movement in a chromatographic column can be achieved simply by having the packing flowing downwards under gravity against the mobile phase. Barker and co-workers (27-34) have

Figure 2.7(a)
Principle of Radial Flow

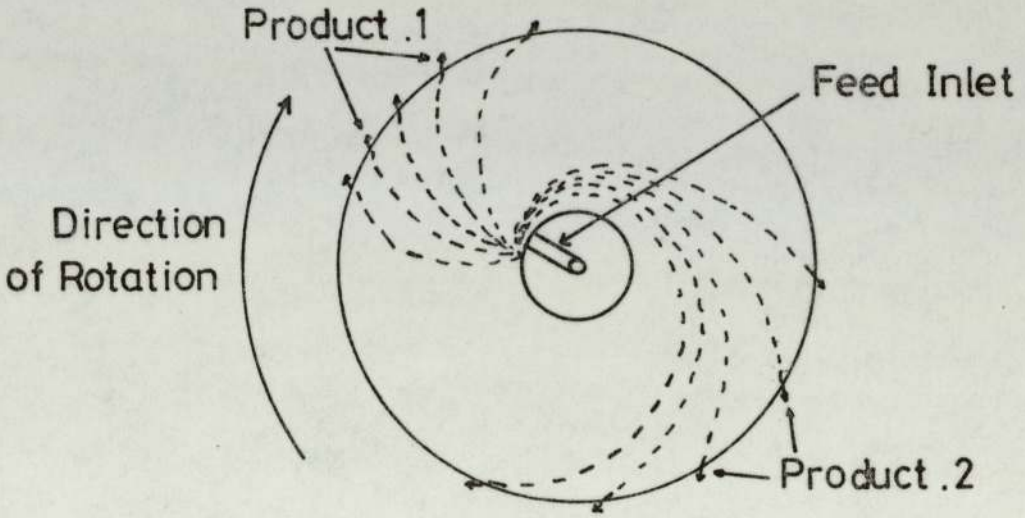

Figure 2.7(b)
Scheme of Mosier (158)

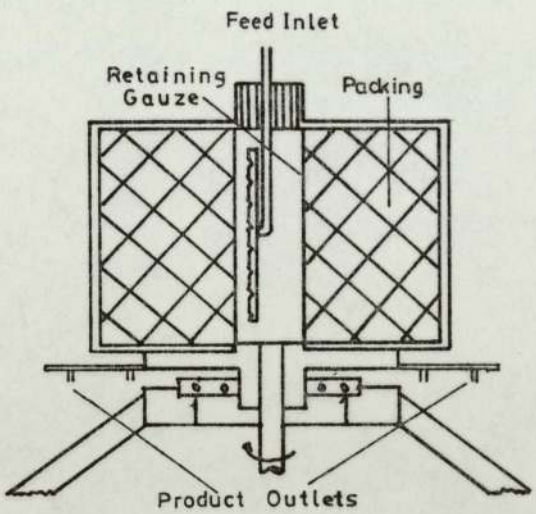

Figure 2.7(c)
Scheme of Sussman (161)

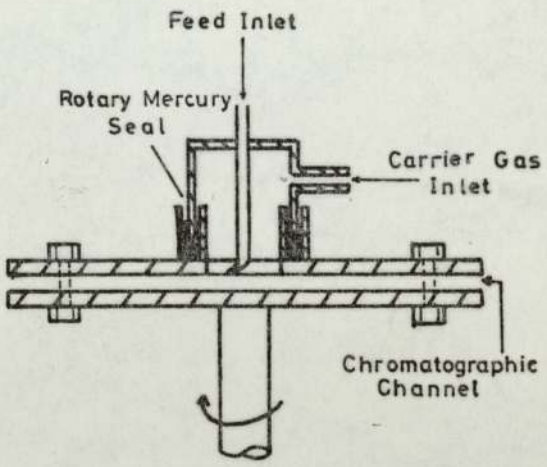

pioneered and extensively studied this principle and developed the column shown in Figure 2.8. Control of the solids flow rate is by a rotating table at the column base whereupon the solids are airlifted back to the hopper. Vibration of the column wall ensures a steady flow of packing. The more strongly adsorbed feed component is carrier with the packing into the heated stripping section and thereby removed at the Product.2 offtake. Travelling preferentially with the mobile phase will be the least strongly adsorbed component which exits at the Product.1 port. Components being recovered from their respective product streams by cold traps. Using air as carrier gas and a chromatographic packing of polyoxyethylene 400 diricinoleate coated onto C22 Sil.O.Cel Firebrick the binary hydrocarbon mixture of cyclohexane and methylcyclohexane was separated at feedrates of up to 30 cm^3 hr^{-1}. Later modifications to the unit (31,34) allowed the separation of ternary mixtures possible by the addition of a side-arm, Figure 2.8. For the separation of an equivolume mixture of cyclohexane, methylcyclohexane and benzene at 12.6 cm^3 hr^{-1}, product purities of 99.5% were obtained for the top and bottom products (cyclohexane, benzene) and 78.6% for the sidestream of methylcyclohexane (32,33).

Tiley and co-workers (135,136), Scott (165) and Schultz (166) using similar moving packing principles have reported successful separations on small diameter units. Clayer et al (167,168) using a 2 cm diameter column of length 1.9 m, with silicagel as the flowing packing, and either helium or nitrogen as a carrier gas, separated the isotopes of hydrogen. For the separation of a 65% protium, 35% deuterium feed mixture at 150 $cm^3.min^{-1}$, the authors claim a top product purity of 99.99% protium and a bottom product of 96% deuterium. In a similar column using dinonyl phthalate on C22 firebrick for the separation of isobutane/butane 2, the authors claim purities of greater

Figure 2.8

Counter-current G.L.C. with Flowing Packing (27)

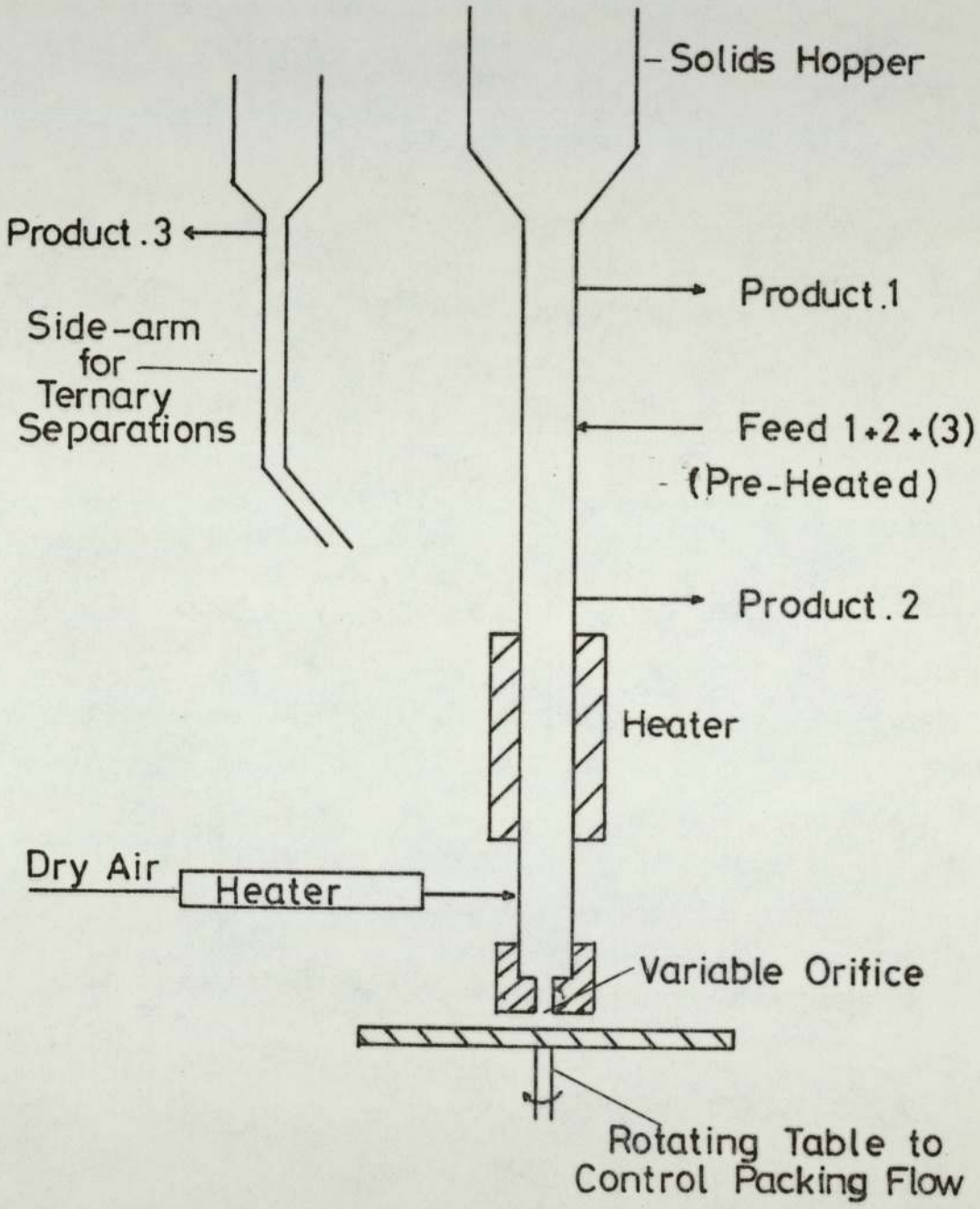

than 99.99% for feed flowrates up to 375 $cm^3.min^{-1}$. The Phillips Petroleum Co.(169) report having constructed a unit 15 cm diameter and 2.5 m long for the separation of a 30% cyclohexane/70% benzene mixture at 225 $cm^3.min^{-1}$.

The Union Oil Company, California, USA., (170) have developed the technique on an industrial scale using activated carbon adsorbent flowing down through a stream of hydrocarbon gases. A 16 million cubic feet/day unit was built by the Dow Chemical Company, Michigan, U.S.A., but proved uneconomic. Apart from economic considerations other factors have also led to the abandonment of the technique. Low, uneven packed densities are produced and accurate control of the solids flow is therefore difficult to achieve. Attrition of the friable packing occurs, necessitating regular sieving and replenishment, and finally the gas velocity within the column must not exceed that of minimum fluidisation. Schemes to overcome these problems have led researchers to develop units based on the rotation of a circular column past fixed inlet and outlet ports.

2.4.3.2.2 Moving Columns

Maintaining counter-current operation in a moving column system is achieved by having the mobile phase flowing in the opposite direction to the rotation of the columns, Figure 2.9. In the designs of Pichler (171), Gulf Research and Development Corporation (172), Luft (173), and Glasser (174) the flow of carrier gas within the column is controlled by pressure drop. Barker (35) improved the utilization of the column length by using cam-operated locks between the carrier gas inlet and Product.1 outlet. As the gas travels only in one direction the length of the column that can be used for

Figure 2.9
Moving Column Schemes for Continuous G.L.C

(a) Pichler & Schultz(171)

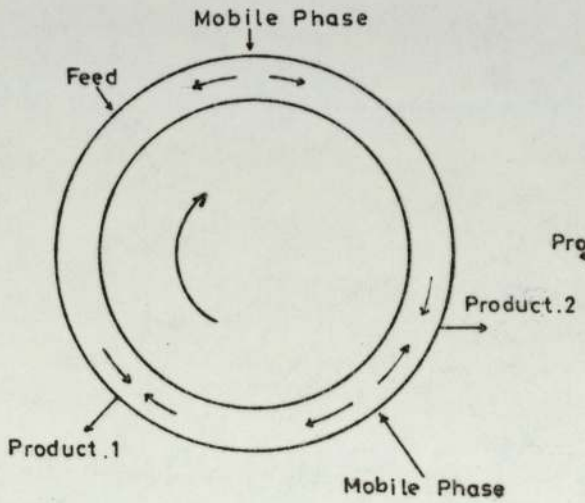

(b) Luft(173)

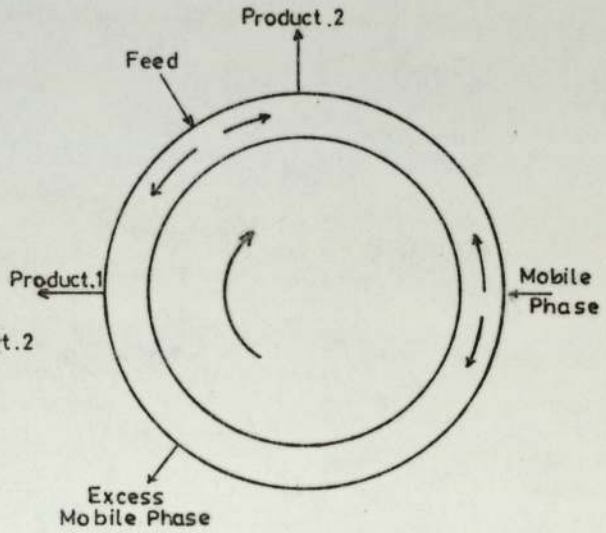

(c) Glasser(174)

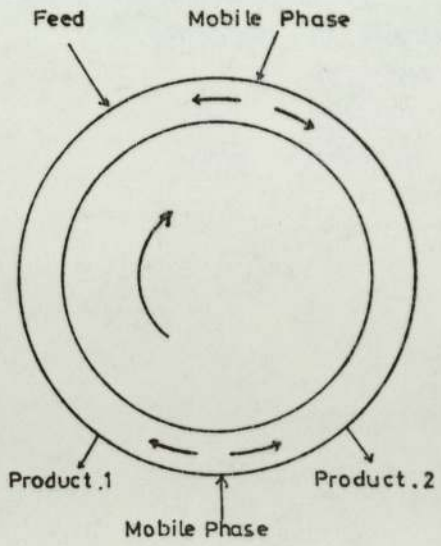

(d) Barker(35)

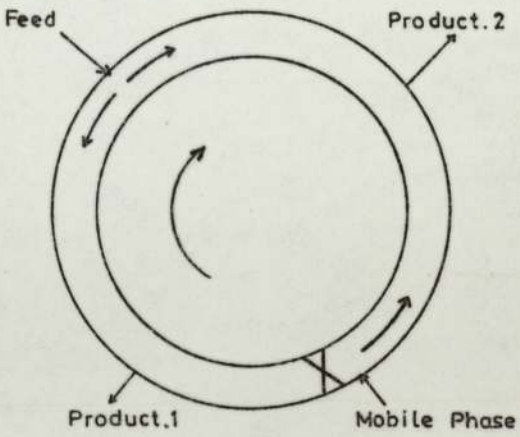

separation purposes is only limited by the amount required for the short stripping section and to provide a gas seal.

Based on this scheme Barker and Huntington (33,36,37) constructed the unit shown in Figure 2.10(a), consisting essentially of eight 3.8 cm square cross-section chambers linked through external valves to form a circle of diameter 1.5 m, which rotated at speeds between 1 and 10 revolutions per hour. To permit gas flow into and out of the column, 180 gas passages were equally spaced over the chamber face, automatic self-sealing valves controlling the inlet/outlet ports. Sealing between the ports and the rotating column was obtained by having 'O' rings set in the torroid face. The performance of the unit in separating a wide range of chemical systems including azeotropic and close-boiling mixtures has been reported (33,36,38).

One of the main deficiencies of the unit was the limited separating power resulting from the effective column length only being 2.75 m. To increase the separating length of the unit would require the construction of a larger more cumbersome machine. Barker (35) overcame the difficulty of compactness by forming a closed-loop cylindrical nest of 44 straight tubes, 2.5 cm in diameter and 22.8 cm long, Figure 2.10(b). The tube bundle rotated at speeds between 0.2 and 2 r.p.h. past fixed inlet/outlet ports, whilst transfer of fluid between the tubes was automatically controlled by cam operated "poppet" valves. A considerable improvement in purities were obtained from the unit relative to the 1.5 cm circular chromatograph (38-41), although throughputs were reduced by a factor of 3, due to the decrease in cross-sectional area of the compact unit. Operational difficulties were encountered with the unreliable nature of the 'poppet' valves and the necessity for a reliable face seal between the fixed inlet/outlet

Figure 2.10(a)
Moving Column Chromatograph (38)

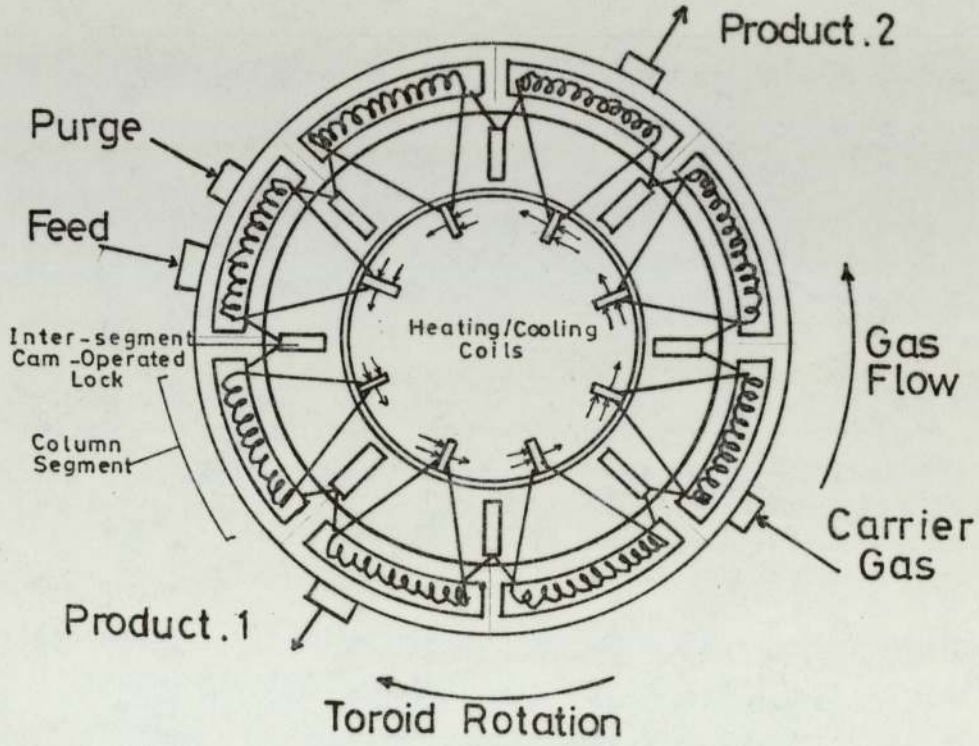

Figure 2.10(b)
Compact Moving Column Chromatograph (35)

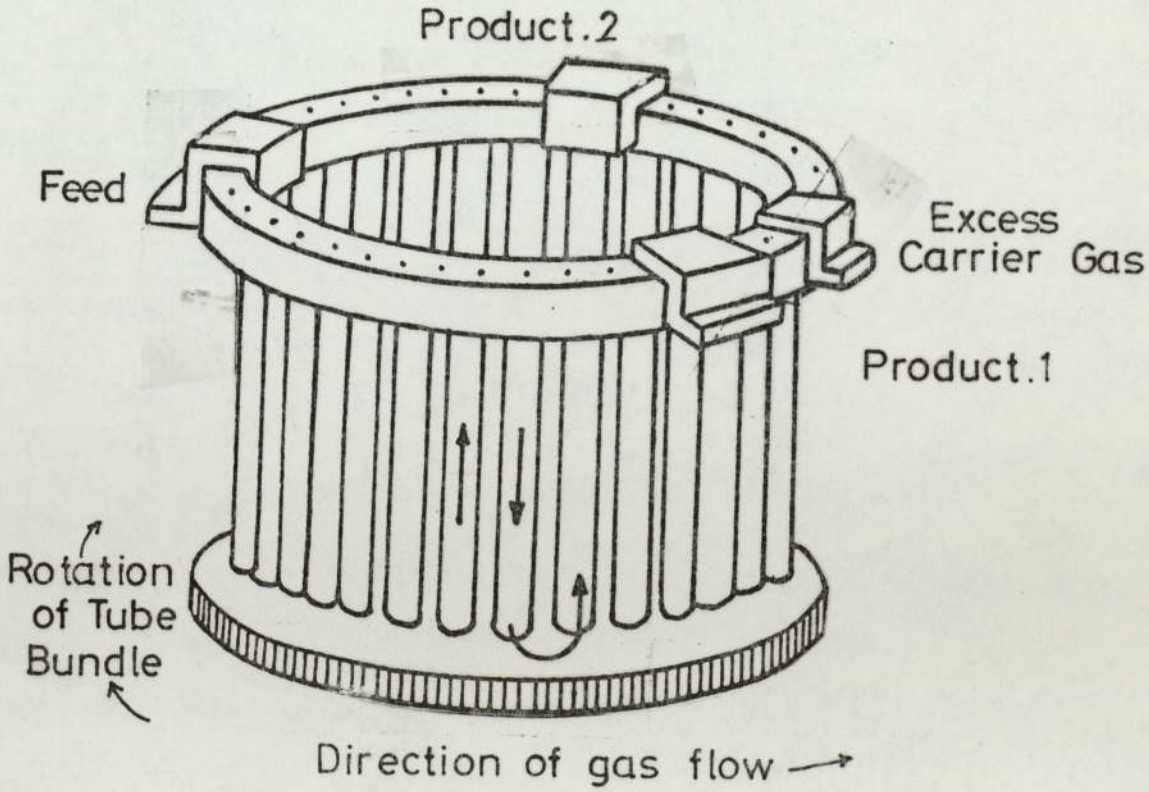

ports and the top ring supporting the columns. Further increase in throughputs was not limited therefore by the separating power of the machine but by mechanical weaknesses associated with its design.

2.4.4 Pseudo Moving Bed Counter-Current Systems

To overcome the sealing problems and the difficulties and expense of rotating large tube bundles, several workers have devised methods of simulating column movement by rotation of the inlet and outlet ports.

Szepesy et al (175) have used a rotary valve to move the inlet and outlet ports relative to a series of stationary columns. The system, shown schematically in Figure 2.11(a) can handle flowrates up to 330 $cm^3.min^{-1}$, which the authors claim would be suitable for use with column diameters up to 3 cm. Recently, Chizhkov (183) has published a theoretical treatment to enable columns incorporated into circulation systems (175), to be compared with normal columns of equivalent length and performance.

Industrially the Universal Oil Products Co., (176,177) have employed a rotary valve system for a variety of separations. In the "MOLEX" process for the separation of paraffins from other hydrocarbons using molecular sieves, the inlet/outlet ports to a single column are indexed to simulate counter-current movement of the packing, Figure 2.11(b). In the purification of p-xylene, purities of 99.5% have been reported (177) obtained from a feed of 14.3% p-xylene in a mixture of C_8 aromatic isomers.

Barker and Deeble (42-46) progressed from moving column units to design a scheme utilizing fixed columns, and the programmed sequencing of solenoid valves to simulate counter-current movement of

Figure 2.11(a)
Scheme of Szepesy et al(175)

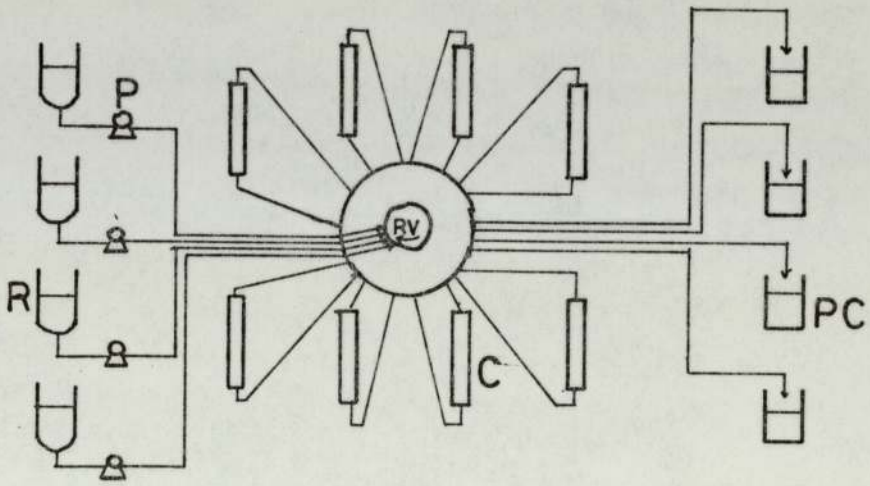

C - columns P - pumps R - reservoirs
RV - rotary valves PC - product collection

Figure 2.11(b)
"Molex" Process (176)

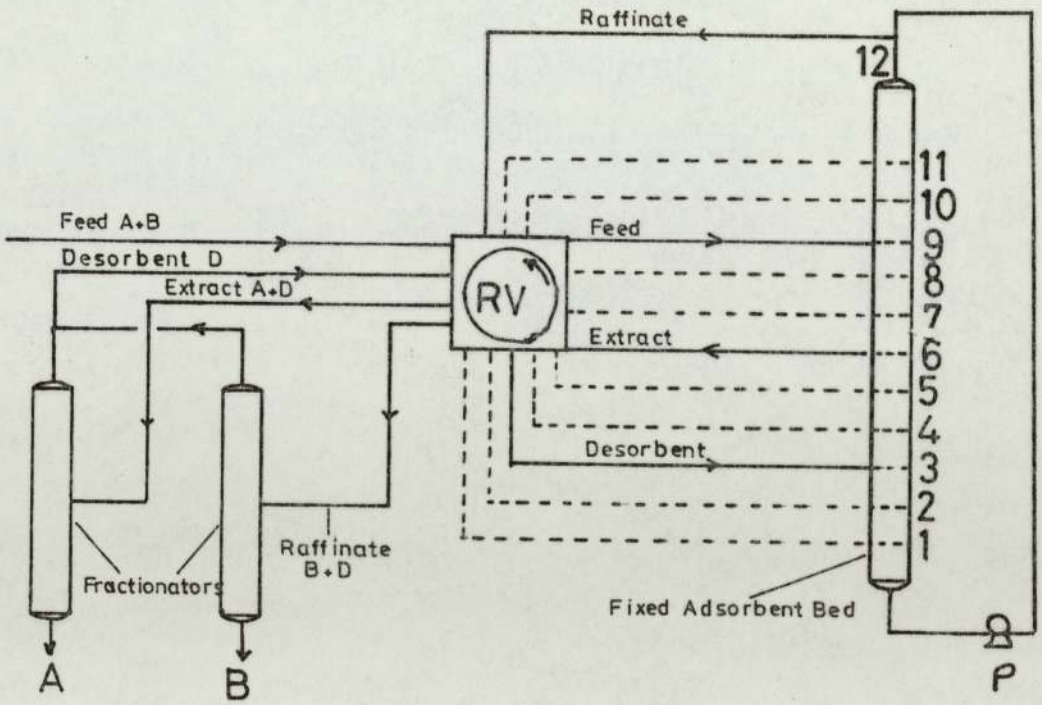

packing and carrier gas. Twelve columns of diameter 76 cm arranged vertically in a circular form gave a total length for separation purposes of 6.7 m. Deeble (45) obtained purities in excess of 99.7% for the separation of a 1:1 mixture of trichloroethane and trichloro-trifluoroethane at feed rates up to 700 $cm^3.hr^{-1}$. The main success of the unit is perhaps its reliability, all moving parts having been eliminated the unit has been operated without failure for over 4000 hrs. Further studies with the sequential chromatograph are the subject of this thesis.

A similar unit constructed from 2.5 cm diameter stainless steel tubes is also in operation in the Chemical Engineering Department at the University of Aston in Birmingham. Replacing the solenoid valves by pneumatically operated valves permits temperatures up to 200°C to be used for gas-liquid chromatographic separations. Liodakis (47) has obtained 99.9% purities for the separation of 80 $cm^3.hr^{-1}$. of Ethyl-lactate and Methyl chloroacetate and is presently engaged on the recovery of γ-methyl Linolenate from 'Primrose Oil', the separation of which is both difficult and expensive by means other than chromatography.

Simulated moving-bed units are by no means limited to gas-liquid chromatographic separations. Barker et al (48) report the design and operation of a unit for the continuous fractionation of a dextran polymer by gel-permeation chromatography. Using 10 columns of 5.1 cm diameter, and 70 cm in length, the removal of both high and low molecular weight ends of a polymer feed distribution, to produce products meeting commercial specifications, has been achieved (49).

CHAPTER 3

THE DESIGN AND OPERATION OF THE CHROMATOGRAPHIC SEPARATOR

3.1 Principle of Operation

Figure 3.1(a) shows the distribution of a pair of components after injection into a chromatographic column. The gradual separation of the two species is brought about by virtue of their differing affinities for the solvent laden stationary phase.

Consider now the situation illustrated in Figure 3.1(b) where the two ends of column AB are joined together to form a closed loop. If, instead of the feed entering with the carrier gas, it enters at point F, then the solutes will distribute themselves as shown. A discrete section of the closed loop is isolated by locks T_1 and T_2, these locks advancing co-currently with the carrier gas. The speed of rotation of the locks can be judiciously selected so that the more strongly absorbed species is continually removed between locks T_1 and T_2, whilst the less strongly absorbed component exits with the carrier gas. A separate gas supply is required to desorb the slower moving species, and thereby regenerate the section of stationary phase packing between locks T_1 and T_2.

To allow the gas locks to advance over discrete sections, the closed loop is broken into individual compartments connected by transfer lines.

Figure 3.1(c), shows the next stage of the cycle where the locks T_1 and T_2 have advanced to the next compartment thereby isolating it from the rest of the closed loop. The position of the feed is advanced by the same distance around the loop so that it is still diametrically opposite the isolated compartment.

Figure 3.1
Principle of Operation

(a)

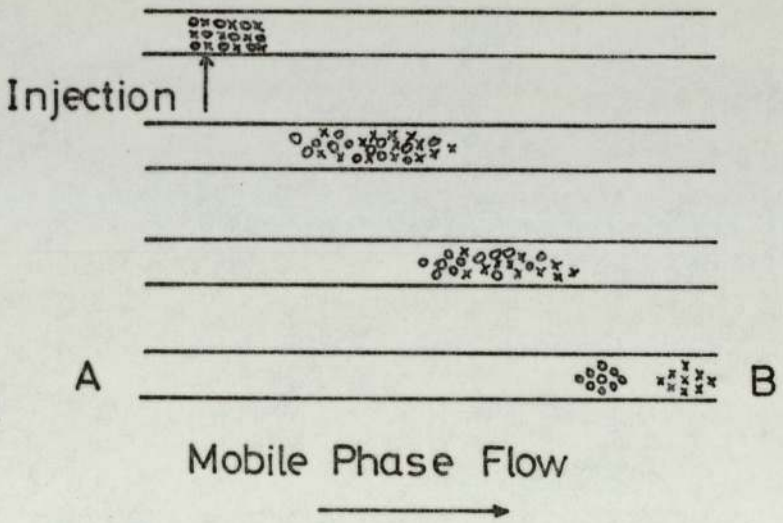

(b)

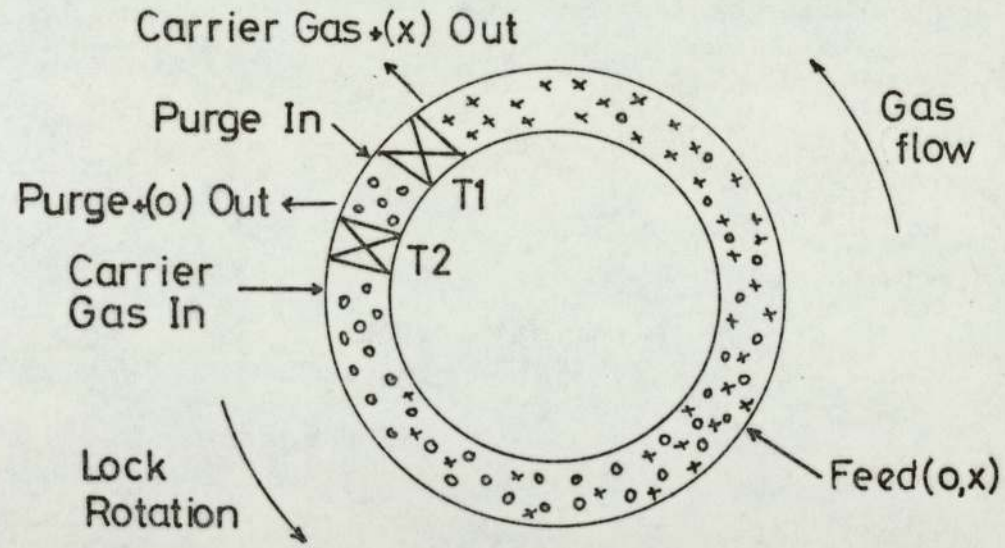

(c)

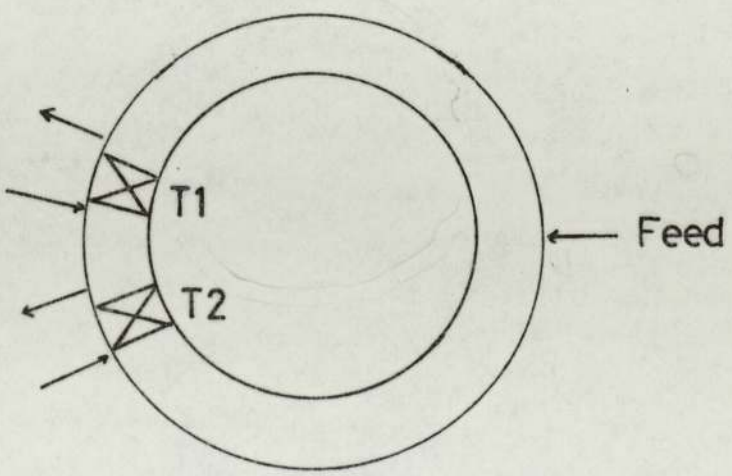

3.2 Mode of Operation

To achieve the above principle the compartments into which the closed loop was broken, were provided for by having 12 vertical chromatographic columns on a circular pitch of diameter 90 cm. Adjacent columns were linked together alternatively top and bottom by transfer lines. Normally open solenoid valves were positioned in the transfer lines between columns so that when any two consecutive valves were energised the column situated between them was effectively isolated from the remaining unit.

The input/output functions necessary for the entry and exit of the carrier and purge gases are provided by normally closed solenoid valves. These valves were positioned on the end cones of each column. By continual advancement of the input/output functions at a speed which is less than the velocity of the less strongly sorbed component, but faster than that of the more strongly sorbed component, it is possible to separate in a continuous manner, a feedstock into two products.

Normally closed solenoid valves also provided the inlet ports for the liquid feed and were mounted at the mid-point of the columns, Figure 3.2.

All the input/output functions were connected to a central distribution network via a pipe network. Pressure regulators on the inlet side, and rotameters on the outlet side, controlled the pressures and flowrates of the process fluids.

Figure 3.2
Schematic Diagram Showing Relative Positions of Solenoid Valves

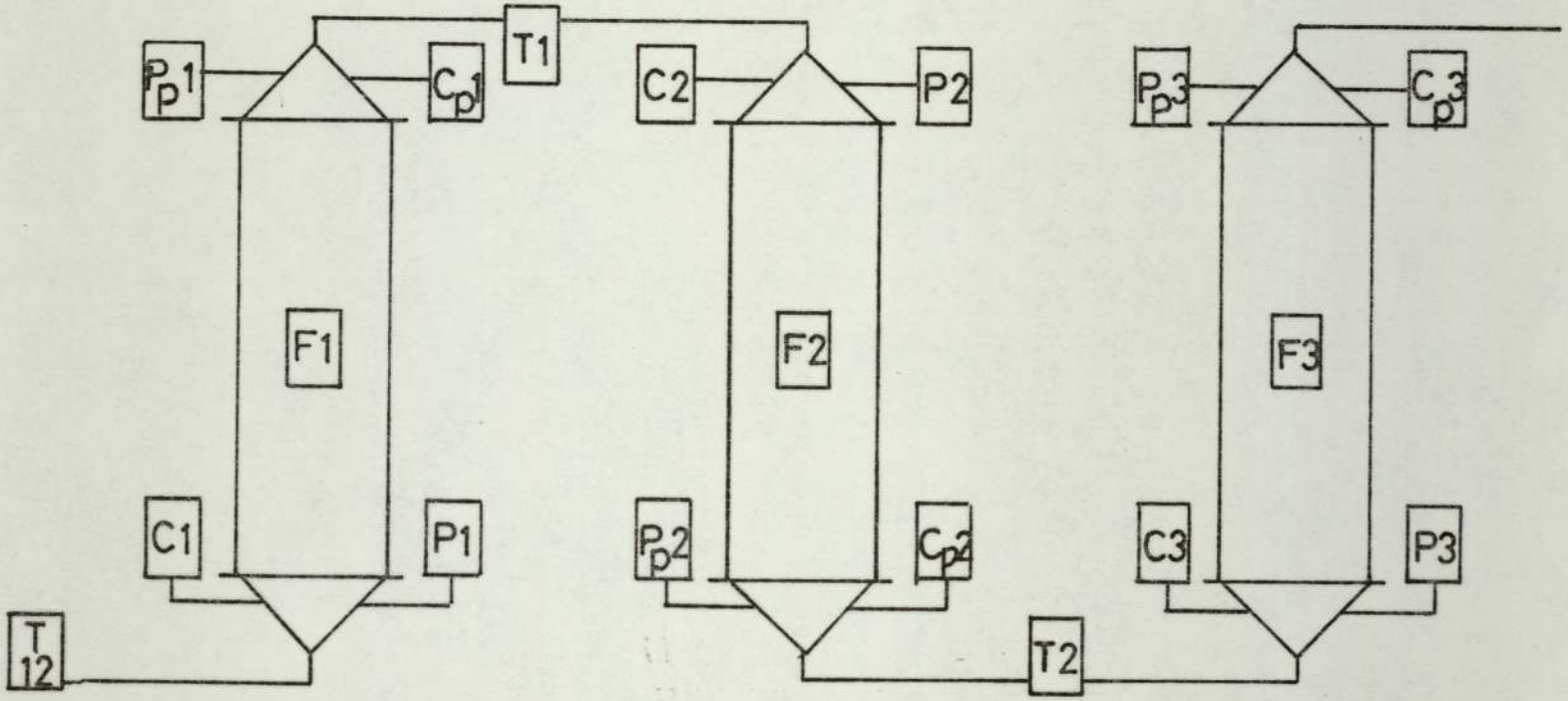

T= Transfer Valve
C_p=Carrier Outlet(Product.1)
P_p = Purge Outlet(Product.2)

F=Feed Valve
C=Carrier Gas Inlet Valve
P=Purge Gas Valve

3.3 Principal Features of the Chromatograph

Full design specifications of the chromatograph are given by Deeble (45) and in the patent by Barker and Deeble (44). The following description is a precis of the above specifications highlighting the major characteristics of the sequential continuous chromatographic refining unit, SCCR1.

3.3.1 The Columns

Twelve copper-columns of 7.6 cm (3 in.) diameter were constructed from standard 3 inch i.d. copper tubing. The length of the columns was 61 cm (24 in.), this being in keeping with a length/diameter ratio of 8:1 used in the unit constructed by Universal Fisher (35,38-40). The columns were evenly spaced on a pitch circle diameter of 90 cm. This gave a distance between column centres of 21.6 cm.

1.3 cm (½ in.) mild steel flanges were silver soldered to either end of the tube, with four, 9.6 cm (⅜ in.), bolt holes evenly spaced on a pitch circle diameter of 10.2 cm (4 in.). Support for the packing inside the column was provided by a copper gauze of 150 μm aperture size, silver soldered onto an annular brass ring of 8.9 cm (3.5 in.) i.d. The column end cones (cone angle 60°), were fashioned out of 1.6 mm copper sheet, Figure 3.3. The cones were truncated at a point where a 1.6 cm (⅝ in.) B.S.P. female stud coupling could be soldered onto the apex. This gave them a height of 5.1 cm (2 in.). A 1.6 cm o.d. (⅝ in.) copper transfer line could then connect the column with its isolating solenoid valve and the adjacent column.

Two 9.5 mm (⅜ in.), gas inlet/outlet lines from the central distribution network were positioned in the cones, the ends of these

Figure 3.3
Column End Cone Design

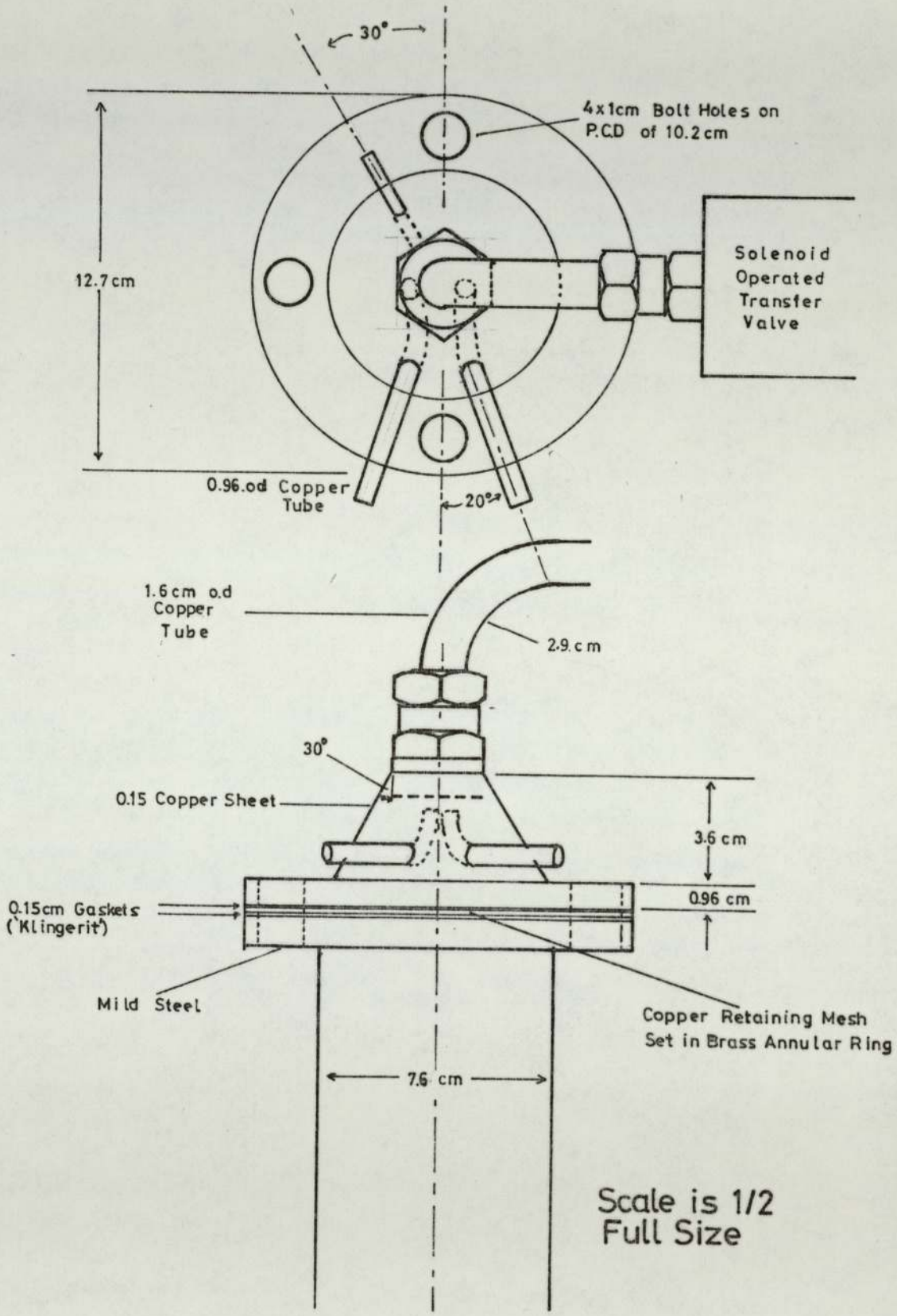

lines being turned through 90°, so they were parallel to the gas flow in the cone.

Midway down the column, and facing towards the central distributors, a 3.2 mm (⅛ in.) brass stud coupling was soldered onto the column wall. The feed solenoid valve could then be attached onto the column. Similar stud couplings were soldered onto the opposite side of the columns to act as sample points. Eight columns were fitted with two sample points, equidistant between the feed point and column inlet/outlet. In the remaining four columns, sample points were positioned at 7.6 cm (3 in.) intervals down the whole length of the column.

As the unit was to be operated at pressures of several atmospheres, sealing was of prime importance. Sealing between the columns, flanges and retaining gauzes was provided by inserting 2.4 mm, (3/32 in.) gaskets of 'Klingerit' coated with a pipe jointing compound. Gas tight sealing of the sample points was achieved by inserting silicone rubber septa into the 3.2 mm nut heads prior to screwing them onto the stud couplings. Where there was a likelihood of liquid feed contacting the silicone rubber septa, they were replaced by 'Viton' rubber septa.

3.3.2 The Packing

3.3.2.1 The Solid Support and Stationary Phase

For a support material Deeble (45) selected untreated 'Chromosorb P', the selection being made mainly from an economic standpoint as over 20 Kg of support were required to fill the columns. After sieving, over 90% by weight of the packing fell in the size range 355-500 μm, (30-44 B.S. mesh). The major disadvantage of Chromosorb.P. as a support material is the availability of active

sites for adsorption of the solutes, leading to severe tailing of the components. To overcome this problem a solvent loading at 25% of the total weight was found desirable, this being the highest attainable without the packing losing its free flowing properties. The solvent phase selected was Silicone Fluid D.C. 200/50.

Much work has been conducted into the most suitable method for packing preparative columns (18,70,89,90) and the following method, recommended by Hupe (72) and Verzele (91) was adopted by Deeble.

Approximately 50 gm samples of the coated support were added to the copper column, and a 3.0 kg concave metal cone placed on top of the packing. The column was then beaten a specific number of times. This vibration, plus the presence of the metal cone, resulted in an increase in the packing density in the peripheral region of the column, thereby promoting a plug flow type of velocity profile and negating the detrimental effects of a parabolic profile. Successive 50 gm samples were added to the column and treated in the above manner until the mid-point of the column was reached, whereupon the feed distributor was centrally positioned.

Packing was then continued in the upper half of the column until the tube was full, the copper retaining gauze and end cone then being secured in position.

3.3.2.2 Comparison of the Packed Columns

Comparisons of the individual column characteristics using the conventional packed column term of the 'Height Equivalent to a Theoretical Plate', were made by Deeble (45), Table 3.1.

Table 3.1
Comparison of Individual Column Characteristics

Column Inlet Pressure = 232.6 kN m^{-2}

Volumetric Gas Flowrate = 610 $cm^{-3}s^{-1}$

Assigned Column Number	Pressure Drop across the Column	Weight of Packing	Interparticle Volume	Volume of Packing	$\bar{U}$	H
	kN m^{-2}	g	cm^3	cm^3	cm s^{-1}	mm
1	6.7	1635	1915	867	8.6	4.9
2	6.9	1650	2007	774	8.2	8.4
3	5.9	1650	1977	804	8.4	9.5
4	6.1	1635	1820	962	9.1	5.1
5	6.7	1650	1861	921	8.9	7.2
6	7.3	1650	1893	890	8.8	7.0
7	7.6	1635	1862	920	8.9	7.2
8	6.7	1650	1896	886	8.8	5.9
9	6.9	1650	2017	765	8.2	10.0
10	7.1	1635	1826	955	8.9	4.6
11	8.5	1650	2014	767	8 3	8.8
12	6.5	1650	1900	881	8.7	9.5
Average	6.9	1645	1917	849	8.7	7.4

These results were high when compared with the results reported for a 7.6 cm diameter column, by Albrecht and Verzele (107) in which H.E.T.P's were in the order of 1.2 mm. Considerable column to column variation was also registered.

It was correctly concluded that even with these large column to column variations the separation of Arklone.P. and Genklene.P. would not be adversely affected. At any one time eleven columns are linked to form the separating section and, because of the cyclic nature of operation of the unit, the variation in the total number of plates within the separating section will be a factor of 10 less than for individual columns.

However, if a more difficult separation were to be attempted, this variation in the total number of plates within the separating section may have a noticeable effect upon the degree of success of that separation.

3.3.3 The Solenoid Valves

In the design of the sequential chromatograph, two distinct types of solenoid operated valves were required.

For the transfer valves, 13 mm orifice, (⅝ in.) B.S.P. port, normally open, servo-acting solenoids were selected, being constructed of brass bodies with 'Viton' seats.

To successfully seat this type of valve it was necessary to supply an independent gas stream to the valve at a pressure in excess of the maximum process stream pressure. This was achieved by linking in series each of the twelve transfer valves to an external high pressure air supply.

The valves required to control the carrier and purge gas inlet and outlet functions were 6 mm orifice, (¼ in.) B.S.P. port, normally closed, direct acting solenoid valves. Being direct acting valves no independent air supply was required to aid the sealing of their 'Viton' seats. Smaller direct acting valves, ⅛ in. B.S.P. port, 3 mm orifice, were inset as input valves for the feed network.

Sealing of the direct acting valves in the de-energised state is of prime importance for the successful operation of the chromatographic separator, and therefore the valves were tested for leakage at back pressures far in excess of those likely to be met in normal operation of the unit.

3.3.4 The Air Distribution Network

Figure 3.4, a schematic diagram for the gas lines, shows the distribution of the inlet air and outlet product streams around the chromatograph.

Mains air from a low pressure air compressor was supplied at 700 $kN.m^{-2}$ to a 0.125 m^3 surge tank. Preliminary filtering of the air was accomplished by a 5 μm 'Norgren' filter. A 6.3 mm i.d. pressure tube of p.v.c. led from the surge tank to an isolating solenoid valve, so that in the event of an emergency the chromatograph could be quickly disconnected from the air supply. After passing through the solenoid valve, the air which still may contain moisture was passed through silica gel drying beds, the design of which was similar to the main copper columns, with the exception of their being 90 cm in length. As a final treatment the air was passed through a 'Norgren Ultraire' filter to remove final traces of oil. Being of a sintered brass type

Figure 3.4

Flow Diagram for SCCR1 System

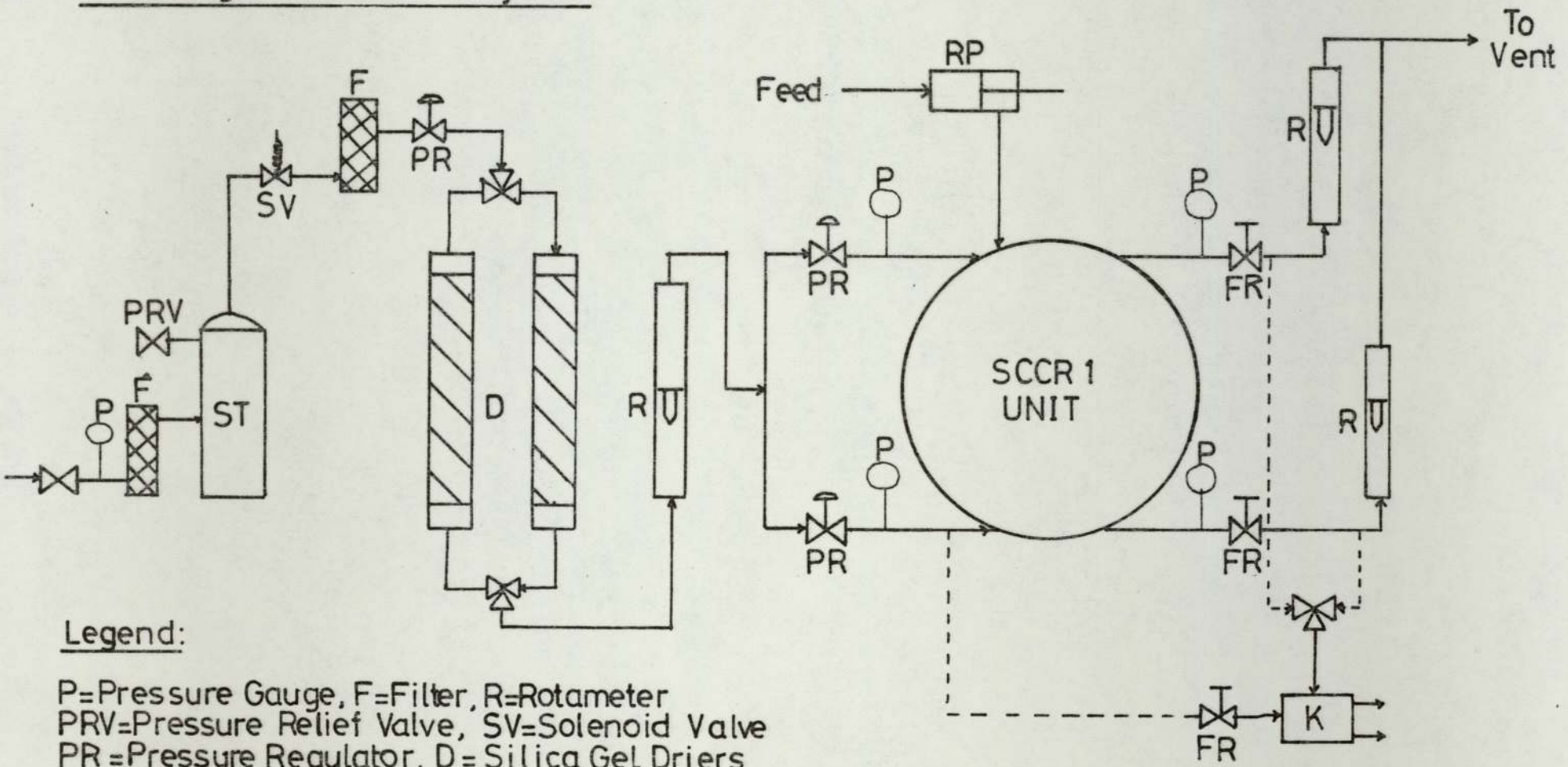

Legend:

P=Pressure Gauge, F=Filter, R=Rotameter
PRV=Pressure Relief Valve, SV=Solenoid Valve
PR=Pressure Regulator, D=Silica Gel Driers
FR=Flow Regulator, RP=Reciprocating Pump
K=Katharometer

of filter, pressure drops of up to 50 $kN.m^{-2}$ were measured across it. For this reason, at a later stage of the research it was necessary to remove this final filter. Fortunately, the central air compressor had by then been replaced by a 'Broomwade' low pressure compressor, the gas from which was both oil and moisture free.

Two independent air supplies were required for carrier and purge streams. Therefore the inlet air supply was divided, precision 'Norgren' pressure regulators being inserted into each line to control the air inlet pressure. The carrier and purge gases then pass to separate distributors situated at the centre of the twelve columns.

From Figure 3.2, it can be seen that, because of the symmetrical nature of the cyclic unit, the position of the four inlet/outlet gas ports alternated between the top and bottom of adjacent columns. Therefore, for each gas inlet or product outlet line two distributors were required, each supplying six columns. The eight central distributors required were arranged as in Figure 3.5. 9.6 mm copper tubing linked the distributors to their relevant inlet/outlet ports.

The flowrate of the two product streams was controlled by diaphragm-type flow regulators. Measurement of these flowrates was by 18K and 14K rotameters for the bottom and top products respectively. Calibration charts for the rotameters are shown in (Figures A.1.1 and A.1.2, Appendix 1).

Reclamation of the product streams proved impractical, as an expensive two stage refrigeration cycle would be required.

3.3.5 The Feed Network

Feed enters the chromatographic unit through solenoid valves positioned at the column mid-points, 6.5 mm (¼ in.) i.d., polypropylene tubing connected these solenoids to a central feed distributor, Figure 3.5. The distributor was supplied by a positive displacement reciprocating type pump, the size of pump head used being in keeping with the flowrate desired. Both the pump and the 10 dm^3 glass feed reservoir were placed for safety in a fume cupboard and linked to the distributor with 6.3 mm tubing.

Monitoring of the feed flowrate was achieved by having a 3-way tap inserted in the line between the reservoir and the pump. A 100 cm^3 burette was connected to the third arm to allow measured volumes of feed to be timed entering the unit.

Distribution of the liquid feed within the columns was accomplished by dividing the feed line into four arms set at right angles to one another, Figure 3.6. From the ends of each arm, a 1.6 mm o.d. copper tube projected some 4 cm, being turned in the direction of gas flow. Such a system provided four feed injection points within the 7.6 cm column, set on a circular pitch of diameter 4 cm.

3.3.6 The Electrical Circuitry

Figure 3.2 provides the clearest means by which the operation of the solenoid valves can be shown. Assuming column.2 is to be isolated, then transfer valves T_1 and T_2 are energised to close. Purge inlet valve P_2, and purge product valve P_{p2} are opened to allow the bottom product to be removed from column.2. Fresh carrier gas enters column.3 through valve C_3 and exits carrying with it the 'top'

Figure 3.5
Arrangment of Central Distributors

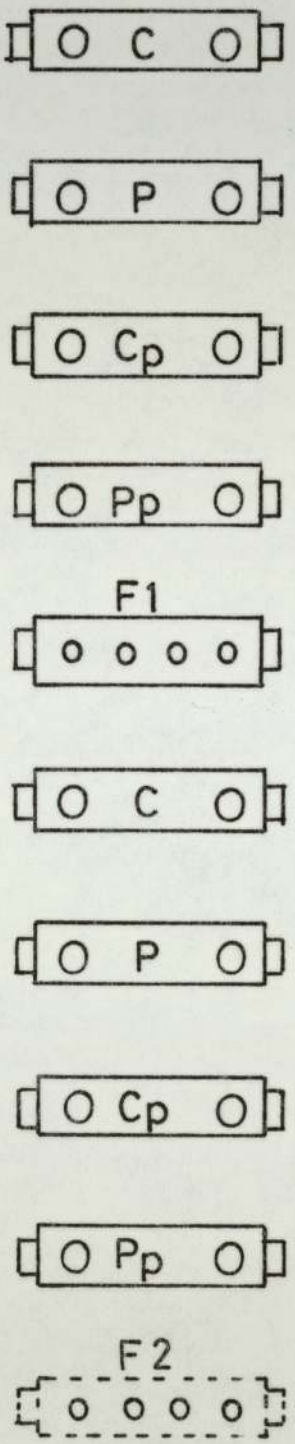

C = Carrier

Cp = Carrier Product.1

P = Purge

Pp = Purge Product.2

F1 = Feed

F2 = Repositioned Feed(Chapter7)

Figure 3.6
Internal Feed Distributor

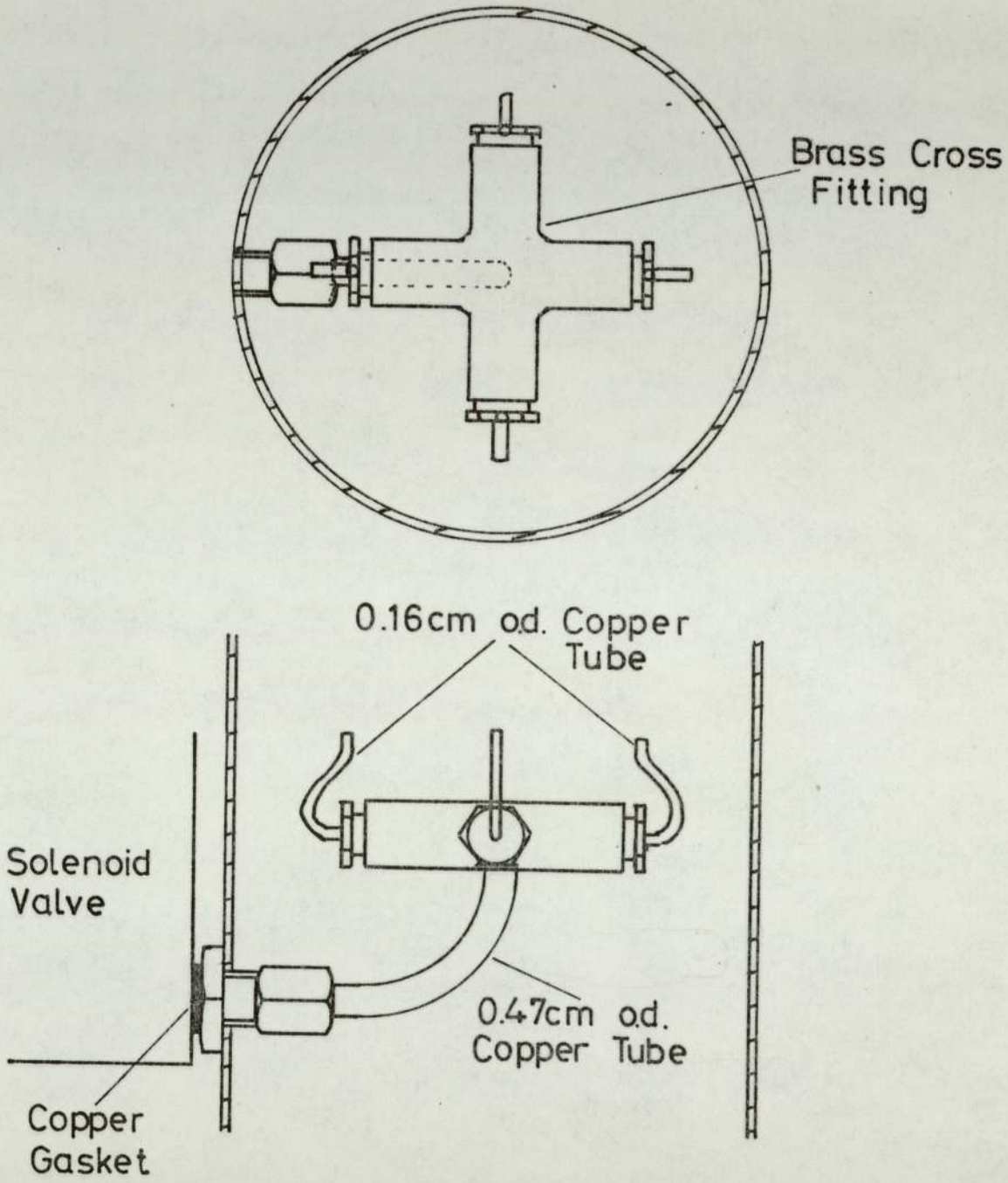

Scale is Full Size

product from column 1, via valve C_{p1}, feed meanwhile enters column.8 through F_8.

After a predetermined time switching of the valves occurs, whereby column.3 then becomes isolated. Valves P_2, P_{p2}, C_3, C_{p1}, F_8 and T_3 close, and P_3, P_{p3}, C_4, C_{p2}, F_9 and T_1 open.

Table 3.2 shows the energisation sequence of the solenoid valves, and it can be seen that at any instant during the operation of the sequential chromatograph it is required that five inlet/outlet solenoids and two transfer solenoids be energised. This is accomplished by linking together the relevant valves through a network of relay banks, the circuit diagrams for which are given by Deeble (45).

An automatic timing device was incorporated into the circuit to govern the sequencing rate of the solenoid valves. Scaling of this timing circuit gave a range of 1-10 minutes, with the calibration chart given in (Figure A.1.5, Appendix 1).

Table 32

Solenoid Valve Energisation Pattern

Column Isolated	1	2	3	4	5	6	7	8	9	10	11	12
Terminals Energised in Rail W_{xx}	W12 W1	W1 W2	W2 W3	W3 W4	W4 W5	W5 W6	W6 W7	W7 W8	W8 W9	W9 W10	W10 W11	W11 W12
Transfer Valves Energised	T12 T1	T1 T2	T2 T3	T3 T4	T4 T5	T5 T6	T6 T7	T7 T8	T8 T9	T9 T10	T10 T11	T11 T12
Terminals Energised in Rail V_x	V1	V2	V3	V4	V5	V6	V7	V8	V9	V10	V11	V12
Inlet / Outlet Valves Energised	C2 Cp12 P1 Pp1 F7	C3 Cp1 P2 Pp2 F8	C4 Cp2 P3 Pp3 F9	C5 Cp3 P4 Pp4 F10	C6 Cp4 P5 Pp5 F11	C7 Cp5 P6 Pp6 F12	C8 Cp6 P7 Pp7 F1	C9 Cp7 P8 Pp8 F2	C10 Cp8 P9 Pp9 F3	C11 Cp9 P10 Pp10 F4	C12 Cp10 P11 Pp11 F5	C1 Cp11 P12 Pp12 F6

Figure 3.7 Front Panel of SCCR 1

A	Isolating Switch
B	Sequencing/Timer Unit
C	Katharometer Control
D	Thermocouple Switch
E	Digital Voltmeter
F	Purge Rotameter
G	Carrier Rotameter
H	Inlet Pressure Gauge
I	Transfer Valve
J	Packed Column

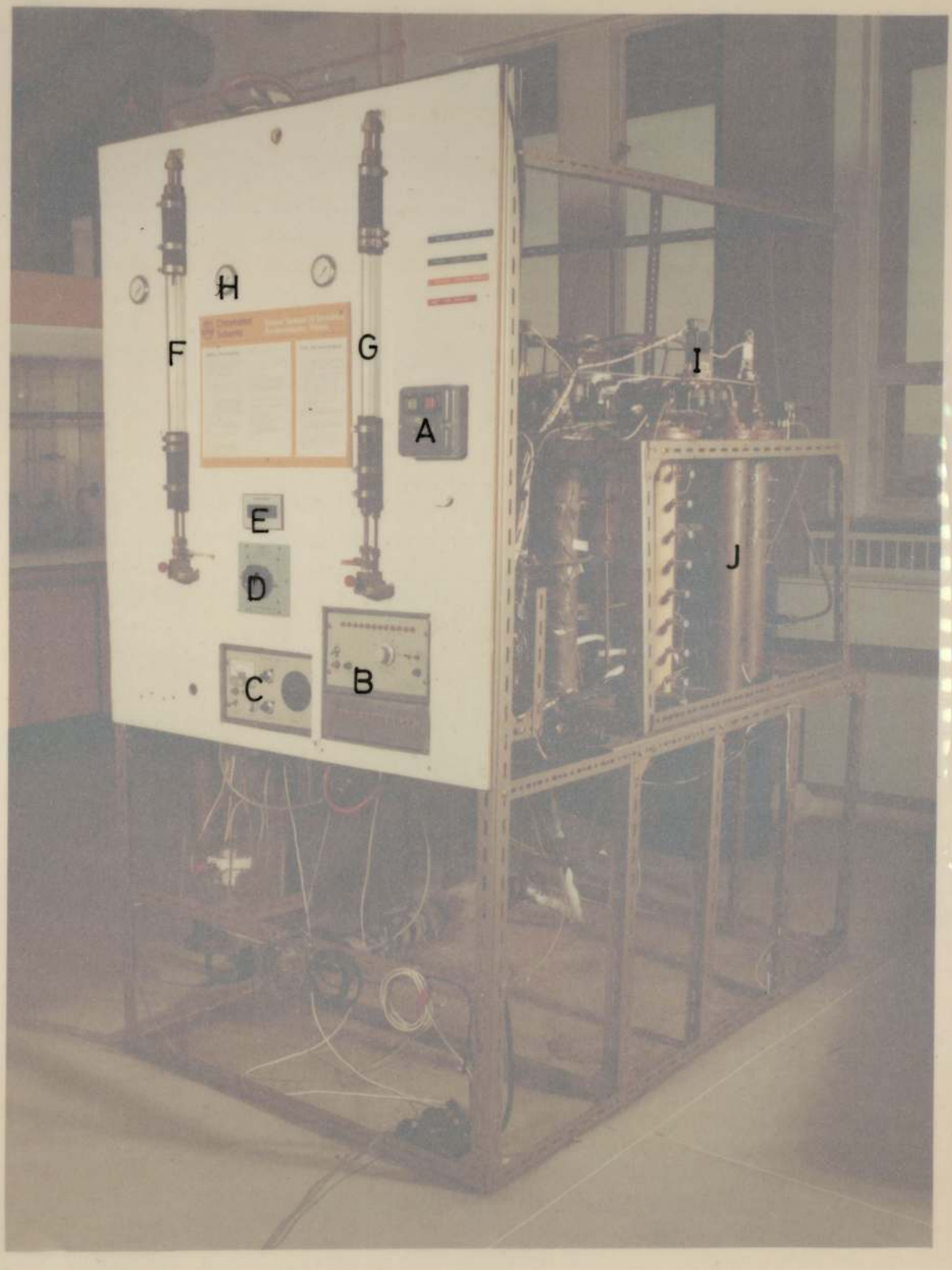
H
F
G
I
A
E
D
J
C
B

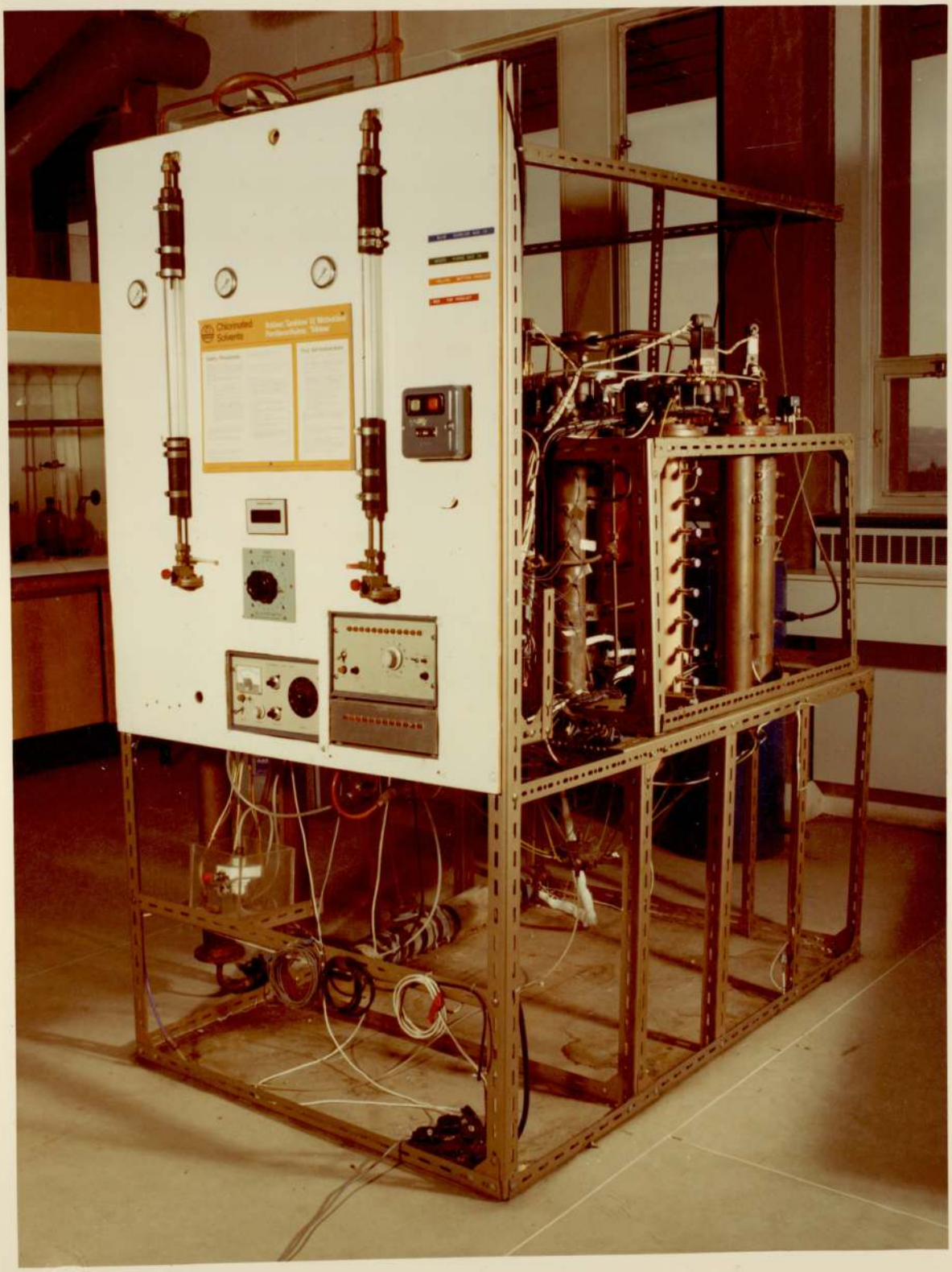
Chromatest
Solvents

Figure 3.8 SCCR 1

A Transfer Valve

B Feed Valve

C Inlet/Outlet Gas Valve

D Glass Column

E Column. 1

F Thermocouples

G Central Distributor

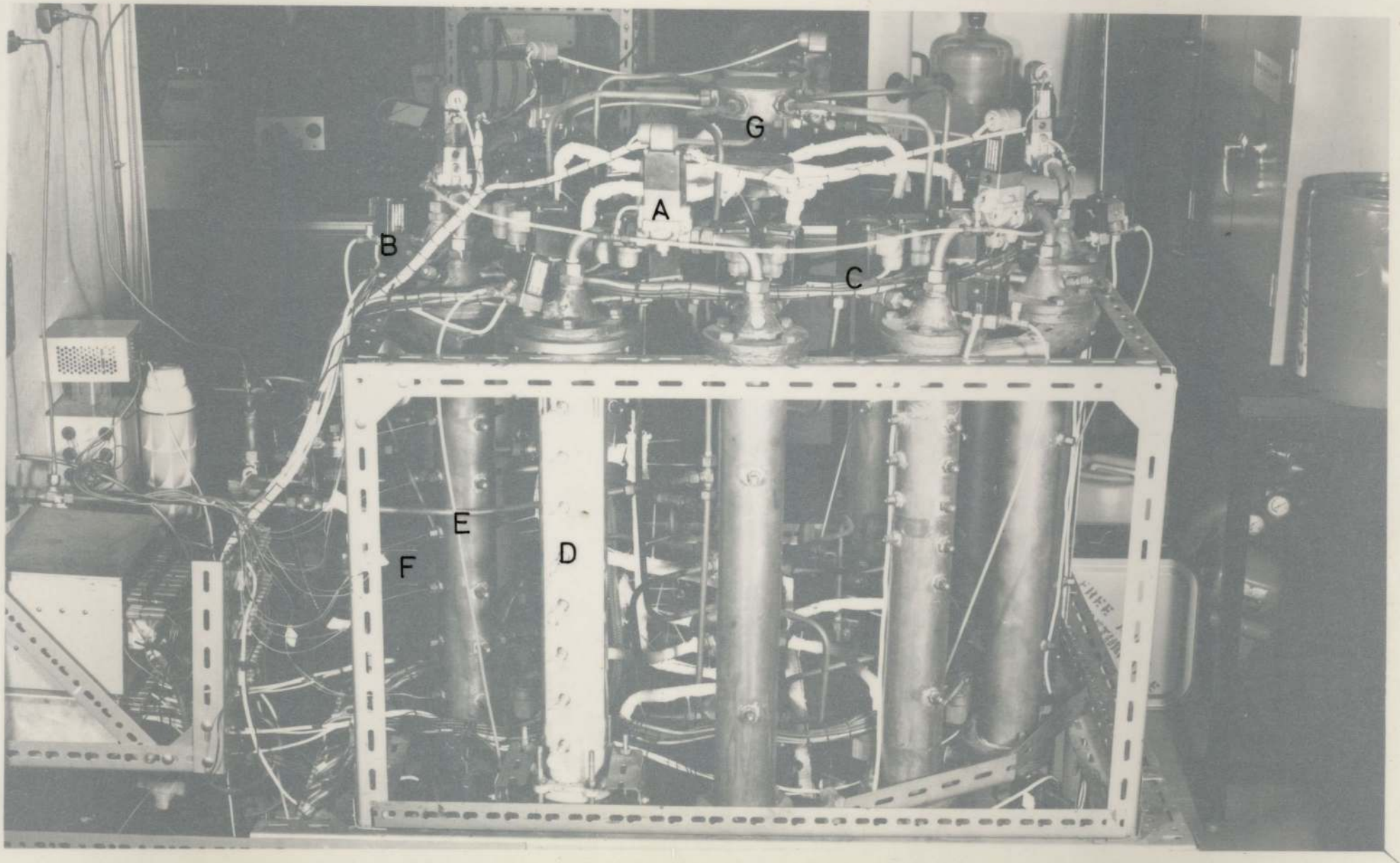
G
A
B
C
E
D
F

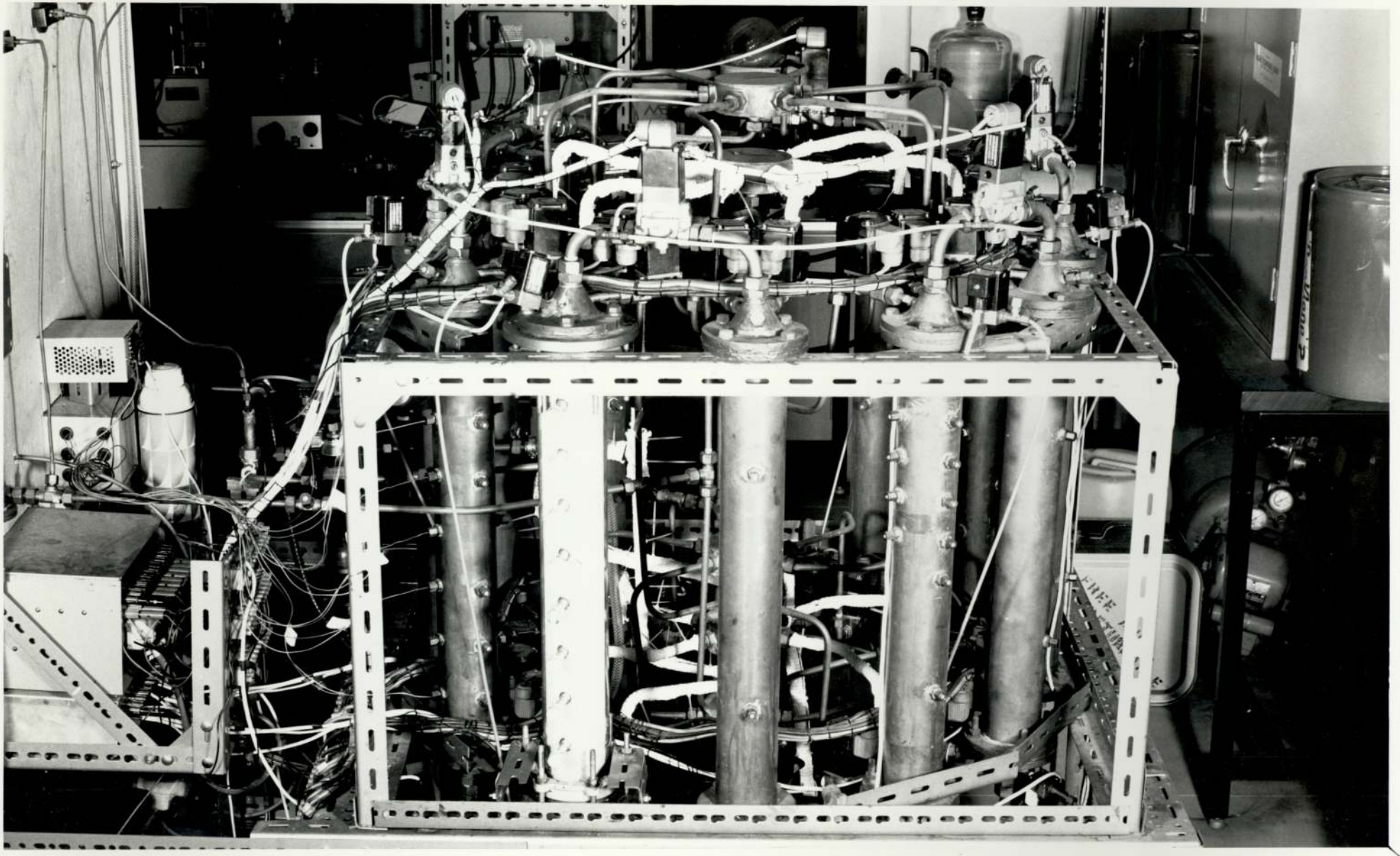

CHAPTER 4

EXPERIMENTAL TECHNIQUES AND ANALYSIS

4.1 Selection of Chemical Systems for Investigation

In the selection of suitable feed components for investigation factors such as cost, safety aspects, and thermodynamic compatibility of feed components with the stationary phase, play a vital role. Deeble (45) used the two halocarbons 1,1,1-trichloro-ethane and 1,1,2-trichlo--1,2,2 trifluoro-ethane during his research. Both solvents exhibit high volatility at room temperature, relatively low toxicity, and are totally non-flammable in any percentage of oxygen.

Whilst it was envisaged that a majority of the research programme could be carried out using the above two solutes a second binary feed system would be required to investigate the sequential chromatographs performance in separating a more difficult system. The'degree of difficulty' of a system is related to the separation factor of the feed components, which is determined from the value of the partition coefficients with respect to the silicone oil stationary phase. In the case of the Arklone.P./Genklene.P. system the separation factor for the binary system is approximately 2.6 and for a second system components exhibiting a separation factor of around 1.5 was sought.

The use of air as a carrier gas, coupled with the non-sparkproof solenoid valves necessitates the choice of systems having no explosive or flammable tendencies, and whilst a number of systems with separation factors of 1.5 were available, all had to be rejected on the grounds of safety. The only possible system fulfilling the strict safety regulations was again a pair of halocarbons; 1,1,2 trifluoro-1,2,2 trichloroethane and dichloromethane. Unfortunately, this system possessed a separation factor of 1.17, (measured at infinite dilution and 20^{o}C), and therefore by the

constrictions imposed by Equation 5.18, complete separation of the system into two relatively pure product streams is unlikely.

For the practical operation of the chromatograph and the subsequent mathematical modelling, accurate thermodynamic data is essential. If, as is generally the case this data is not available, a long and tedious programme must be implemented for its experimental determination. Sunal (50) working with the aforementioned halocarbons has tabulated the vast majority of the thermodynamic data required, and therefore whilst from an experimental point of view halocarbon systems may not be ideal, safety aspects and the availability of data led to their selection for study.

The three organic fluids required were all available in bulk from I.C.I. Ltd., their general use being for industrial and domestic cleaning. Product specifications gave the total impurity concentration as less than 1% for all three chemicals, and the relevant physical properties are given in Table 4.1.

Table 4.1

Physical Properties of Feed Components

Trade Name	Arklone.P.	Genklene.P.	Methylene Chloride	
Chemical Name	1.1.2-trichloro-1,2,2-trifluro-ethane.	1.1.1 trichloro-ethane	Dichloro-methane	
Density g cm^{-3}	1.57	1.34	1.34	a
Boiling Point °C	47.6	74.1	40.1	a
Melting Point °C	-35.0	-32.5	-96.7	a
Vapour Pressure @ 20°C kN m^{-2}	35.9	13.3	47.9	a
Toxicity ppm	1000	350	500	b
Partition Coefficient on DC 200/50 (20°C)	141	411	120	c
$\bar{h}^{s}$ cal/g.mole	6599·0	7240.5	6359.0	d
$\bar{h}^{e}$ cal/g.mole	511.5	311.8	1216.5	d
ΔH_v cal/g.mole	7110.5	7552.3	7575.5	d

References: a) 181
b) 203
c) 45
d) 50

4.2 Start Up/Shut Down Procedure

For reasons of safety and good experimental technique the following 'start up' procedure was adopted.

(a) A servicing of the chromatograph was carried out, with all worn septa being replaced. The packed air dryers were checked and if necessary were replenished with regenerated silica gel. The oil and dust filters were similarly checked and cleaned.

(b) All feedstock remaining in the feed reservoir from previous runs was rejected and a fresh 50:50 by volume mixture made up. Rejection of feedstock remaining from previous runs became necessary when it was found that over a period of days the preferential evaporation by one of the feed components could substantially alter the 50:50 volume ratio. All taps on the feed system and the feed pump were lubricated using a 'Manitol' based grease, the powerful degreasing properties of the feedstock quickly dissolving any other form of grease.

(c) The main electrical isolating switch was turned on and the electronic sequencing/timer unit energised. Air was circulated around the chromatograph after opening the inlet carrier and purge gas regulators, and the mains inlet air valve.

(d) Testing of the solenoids was carried out by manually 'skipping' the sequencing/timer unit. Any malfunction was quickly registered by the outlet flow regulators and appropriate action taken.

(e) Pressure testing of the unit was carried out in two stages. The carrier and purge gas outlet flow regulators were closed, and any leakage was registered by a discrepancy between the inlet and outlet pressure gauges. Large leaks could be detected audibly and were generally associated with loose couplings in the air distribution network. Smaller leaks had to be detected by the use of soap solution and could nearly always be attributed to a faulty septum.

The second form of pressure testing was to detect any fault in the sealing of the solenoids. The inlet carrier gas pressure regulator was closed so that only the isolated column was subject to gas pressure. If the outlet purge gas flow regulator was then closed, one column in the unit would then be at high pressure and the other eleven at ambient pressure. Any depressurisation of the column, indicated a leak through a closed solenoid valve. Once again manually 'skipping' the sequencing/timer unit ensured all solenoid valves were checked. The selected carrier and purge gas rates could then be set by adjustment of the outlet flow regulators.

(f) Having checked that the unit was operating correctly the procedure for feed introduction could be implemented.

The chosen feedrate was set by reference to the calibration chart (Figure A.1.4, Appendix 1), and adjustment of the feed pump micrometer. With the feed pump started, pressurisation of the feed network commenced, with any air or vapour trapped in the system being released from the 'tee' junctions connected to the feed solenoids. Whilst the pressurisation process was taking place the feed solenoids

were connected into the sequencing/timer unit. The common negative lead for the twelve feed solenoid valves was connected to the appropriate socket in the sequencing/timer unit. Eleven separate live lead connections were then made between the feed valves and the single energised socket terminal rail. The twelfth and final connection was not made until the pressure in the feed network was equal to that of the column due to receive the solute feed. Failure to adhere to this procedure would result in either a 'blow-back' of carrier gas into the feed network or a surge of feed into the column.

Correct functioning of the feed solenoid valves was observed during the first cycle of operation of the chromatograph with any malfunction being registered immediately after the sequencing action as an increase in pressure in the feed network.

With certain parts of the equipment being subject to air pressures of 700 $kN.m^{-2}$, toxic chemicals at 250 $kN.m^{-2}$, and complex electric and electronic circuitry, it was essential that the above procedure however tedious be rigidly adhered to.

During the time required by the unit to reach equilibrium, procedures such as the calibration of the flame-ionisation detector (Section 4.4.2.4), and the setting up of the katharometer (Section 4.4.1) were carried out.

The 'shut-down' procedure was basically the reverse of the 'start-up' technique, namely:

a) Switching off the feed pump

b) Removing all twelve connections between the feed solenoid valves and the energised socket terminal rail, and disconnecting the common negative lead.

c) Although at this stage feedstock was no longer entering the unit, solute present in the chromatograph would continue to circulate for many cycles. To remove all traces of solute the carrier gas inlet flow regulator was closed thereby preventing any movement of solute, the purge gas flow rate could then be increased and the isolated column switched around the unit until all twelve columns had been purged of the two feed solutes.

d) The mains air inlet valve was closed and the pressure surge tank emptied.

e) Finally all remaining electrical functions were terminated by switching off the main isolating switch.

4.3 Safety

Several safety devices were built into the chromatograph including a pressure relief valve positioned in the mains air surge tank. This valve was set to blow at approximately 800 $kN.m^{-2}$, a pressure well below the safe working pressure of the tank. In the construction of the unit the selection of the thickness of all metal tube and plate wall under pressure, was greatly in excess of that required by British Standards 1500 and 2871.

Between the surge tank and the inlet flow regulators a solenoid valve of the type used for the inlet/outlet gas ports was positioned. De-energisation of this valve provided instantaneous isolation of the chromatograph from the mains air supply. Electrical connections to this valve together with leads to the sequencing/timer unit, Katharometer and digital voltmeter were fed to an A.C. contactor--starter. This fused switch incorporated a relay system to prevent restart when power was restored after failure.

Care was needed when handling the chemical feedstock with skin contact to be avoided. Transfer of fluid to and from the feed reservoir had to be carried out in a fume cupboard to avoid inhalation of the toxic fumes.

4.4 Analytical Equipment

4.4.1 The Katharometer

Continual monitoring of the solute concentration levels in the product streams is an essential requirement for the successful operation of the sequential chromatograph. To this end a 'Gow-Mac' hot wire detector, coupled to a 'Servoscribe' potentiometric recorder was employed.

In the hot wire detector or Katharometer, an electrically heated wire is supported in the gas stream. Heat losses from the wire are determined mainly by the thermal conductivity, specific heat and flow rate, of the gas surrounding it. As the sample passes through the detector, these factors change and result in a different wire temperature. This is detected as a resistance change from which an indication is obtained of the amount of sample passing through. Four hot wires are connected in a Wheatstone's bridge circuit, two of the wires being suspended in the sample stream and two in a similar reference stream of air. The incorporation of a reference channel minimizes the effect of temperature changes of the block that contains the wires, and provides a base line for comparative purposes. Flowrates through the Katharometer were in accordance with those recommended by Gow-Mac (178) and in the order of 12.5 $cm^3.s^{-1}$ for each stream, measurement being carried out by a soap bubble meter.

The signal from the Katharometer, although being a function of the level of concentration in the sample stream, gives no indication of the composition of that stream. The Katharometer cannot therefore be used for quantitative analysis. Monitoring of the product streams is however useful for observing the onset of pseudo-equilibrium within the sequential chromatography, this being the point after which

reproducible results may be safely taken. Also, any malfunction of the feed solenoids or the feed pump would be clearly indicated on the Katharometer trace. And finally, by monitoring the bottom product stream, the effectiveness or otherwise of the purging operation can be determined. See for example Figure 4.1.

4.4.2 The Flame Ionisation Detector (F.I.D.)

4.4.2.1 Mechanism

Quantitative analysis to obtain the concentration profile in the sequential unit was carried out using a Perkin Elmer F11 gas chromatograph, linked to a Hewlett Packard 3373B integrator.

The flame ionisation detector comprises a hydrogen flame into which the output of the column flows. The detector output signal is produced by changes in the electrical conductivity of the flame. The conductivity of a pure hydrogen flame is negligible, but sample components entering the flame produce ions that will conduct a current. A potential difference is applied across the flame to collect the ions produced, and a small current is generated, the size of which is proportional to the rate at which the sample enters the flame. An ionisation amplifier converts this current into a millivolt signal, compatible with the input to a potentiometric recorder or integrator.

4.4.2.2 Analytical Columns

For analysis of the Arklone.P./Genklene.P. system the column chosen was a 2.97 m, 0.3 cm, o.d. annealed stainless steel tube, packed with 10.187 gm of 355-500 μm (B.S.mesh 30-44), Chromosorb.P. support. This packing was coated with 25% by weight silicone oil.

Figure 4.1

Example of Katharometer Traces + Errors

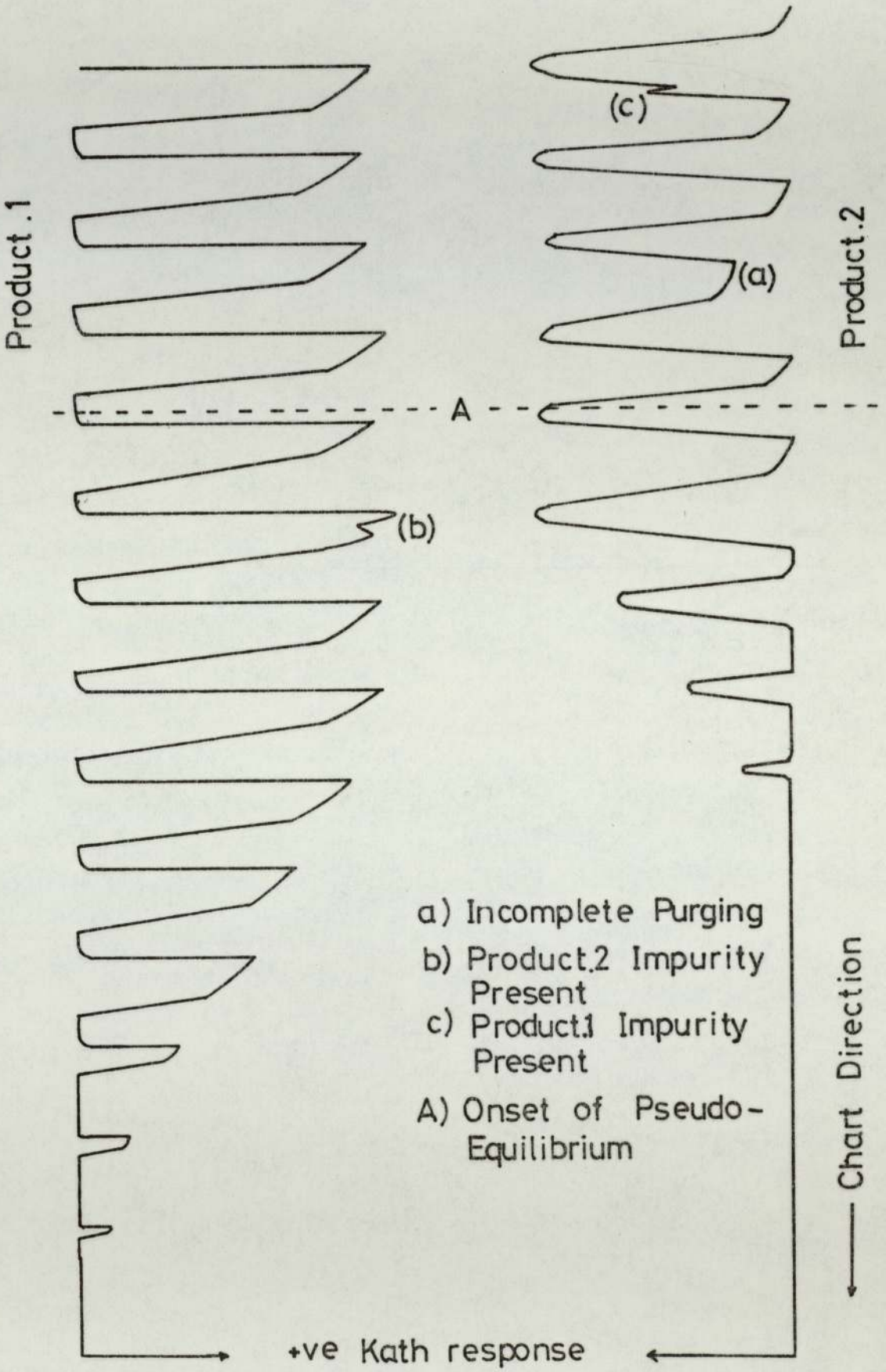

DC 200/50. To prevent 'tailing' by adsorption onto active sites, the column was treated with 100 mm^3 injections of dimethyl-dichlorosilane (D.M.C.S.), at an oven temperature of 180°C. Normal oven temperature during analysis was set at 60.0°C.

The above column proved inadequate for the second system used, that of Arklone.P./dichloromethane. With a separation factor of approximately 1.17 resolution of the two components was incomplete, hence another analytical column was required. After experimentation the column decided upon was a 1.10 m, 0.3 cm o.d. stainless steel tube, packed with 3.569 gm of 252-500 µm (B.S.mesh 30-60), Chromosorb.W. support. The column having previously been acid washed and D.M.C.S. treated required no further conditioning. The liquid phase coated onto the support was 16.67% by weight Free Fatty Acid Phase (F.F.A.P.)

4.4.2.3 Optimisation of Gas Flowrates

Three gases are required by the F.I.D.; hydrogen and oxygen to produce a flame, and oxygen free nitrogen for a carrier gas.

The F.I.D. instruction manual (179), gives the criteria for setting up the oxygen flowrate as being the highest oxygen pressure to the flame consistent with a stable base line, this was found to be 275 $kN.m^{-2}$. The regulator attached to the gas cylinder proved adequate to maintain this pressure as any slight fluctuations in the oxygen inlet pressure do not affect the sensitivity of the F.I.D.

Greater control is however required in the nitrogen line, as the detector response is a function of the carrier gas flowrate. Therefore a 'Brooks' self contained, differential flow regulator was inserted into the carrier gas line to maintain a constant flowrate.

The flowrate decided upon was 2.732 $cm^3.s^{-1}$, thereby giving a resolution of the sampled components in under 90 seconds. This seemingly 'fast' analysis time was necessary as more than one sample may have to be analysed within a sequencing interval of the semi-continuous chromatograph. Finally to optimise the hydrogen flowrate, the inlet pressure was adjusted until maximum response was obtained from the detector. This occurred at a pressure of 158.0 $kN.m^{-2}$.

4.4.2.4 Calibration of the Detector

Calibration of the detector involved relating the weight of a component in a gas sample of known concentration, to the number of integrator units produced upon integration of the eluted peak of that sample.

For the Arklone.P./Genklene.P. system, 50 mm^3 liquid samples of both components were injected into a sealed 1 dm^3 flask, the exact volume of which was known. After sufficient time had elapsed to allow the liquid samples to evaporate and diffuse throughout the flask, gaseous samples were withdrawn through a side arm in the flask and injected into the F.I.D. For this purpose a 1.0 cm^3 'Pressure Lok' gas syringe was employed. Reproducibility of the gas sample volumes was essential and achieved by using brass spacers on the syringe plunger. By withdrawing gas samples of various known volumes in this manner, and recording the integrated area of their eluted peaks, a calibration chart such as Figure 4.2 could be obtained.

The integrator count was such that values in excess of 40000 units could be recorded whilst operation was still in the linear range of the detector. This simplifies the operation of the

Figure 4.2

F.I.D Calibration for Arklone.P and Genklene.P.

(Amplifier Attenuation = 1×10^4)

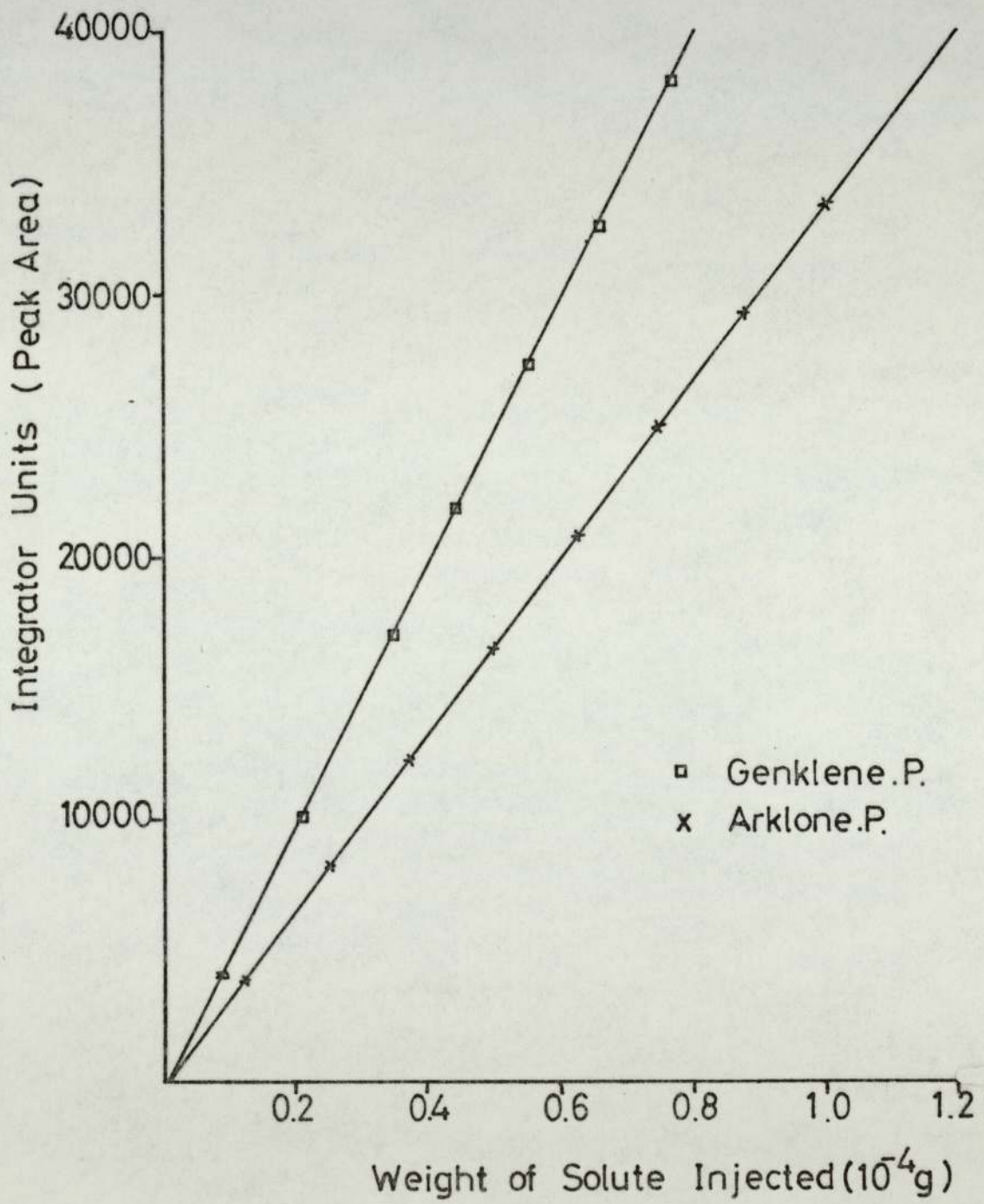

F.I.D. as adjustments to the attenuation of the ionisation amplifier need not be made to compensate for samples of widely different concentrations.

4.4.3 The Thermocouple Network

4.4.3.1 Selection of Thermocouples

Of all available temperature transducers a thermocouple network was chosen to investigate the non-isothermal behaviour of the sequential chromatograph. Some principal advantages are, cost, simplicity, flexibility, fast response time, and the fact that thermocouples are not subject to self heating problems.

In the selection of a particular type of thermocouple certain considerations have to be made.

(a) Response:- A thermocouple may be suited for a special application because its thermal properties permit an optimised design for good response. The response, is rated in terms of how rapidly the thermocouple temperature rises to a certain fraction of the temperature medium to which it is suddenly exposed, usually 63%.

(b) Accuracy:- Thermocouple accuracy is the total error in measuring a given temperature, expressed as a percentage of that temperature. At best, accuracy is such that temperatures can only be measured to $\pm$ 0.2^{o}K under strict laboratory conditions. Even to achieve this standard many calibration points need to be determined and correlated with computational curve fitting procedures.

(c) Reproducibility:- For the type of work to be undertaken by the thermocouples, repeatability of results is perhaps the most important factor in the selection of a suitable couple. The effects of instability,drift and hysteresis, all of which lead to poor

reproducibility need to be minimised.

Using the above principles as guidelines, the following thermocouples were selected to be specially manufactured, Figure 4.3(a).

Conductor metal:- 18/8/1 Chromium-Nickel-Titanium stabilised steel.

Response time:- 0.24 seconds

Cable nominal diameter: 1.5 mm

Route length:- 15 cm

Overall length:- 100 cm

Insulated hot junctions were stipulated on all thermocouples to prevent earthing, although this type of hot junction does result in a longer response time. With thermocouples bonded on the extreme tip of the probe, e.m.f. errors may be introduced if a number of probes are to be connected to multipoint instrumentation having single pole switching.

4.4.3.2 Calibration of the Thermocouples

The calibration of a thermocouple consists of the determination of its electro-motive force at a sufficient number of known temperatures so that, with some accepted means of interpolation, its e.m.f. will be known over the entire temperature range in which it is to be used. The process requires a standard thermometer to indicate temperatures on a standard scale, a means for measuring the e.m.f. of the thermocouple, and a controlled environment in which the thermocouple and the standard can be brought to the same temperature.

A thermocouple circuit is by its nature a differential measuring device, producing an e.m.f. which is a function of the temperatures of its two junctions. The reference junction is held

at $0^{\circ}C$ in a Dewar flask containing a well stirred mixture of ice and water, whilst the measuring junction is inserted into a stirred liquid bath. The liquid bath provides the best medium for establishing a controlled environment up to $100^{\circ}C$.

Calibration charts for the various thermocouples are given in Figure A.1.6. Appendix 1.

4.4.3.3 Experimental Circuit

One of the problems associated with a network of thermocouples is the continual monitoring of their output e.m.f's. Ideally a multipoint potentiometric recorder or data logger should be used, but in their absence the thermocouples were connected to a multipoint selector switch, Figure 4.3(b). The single pole output from this selector switch was fed to a high performance operational digital panel meter, which displayed in a digital form the thermocouple e.m.f. to an accuracy of ± 1 microvolt.

Figure 4.3(a)
Thermocouple Design

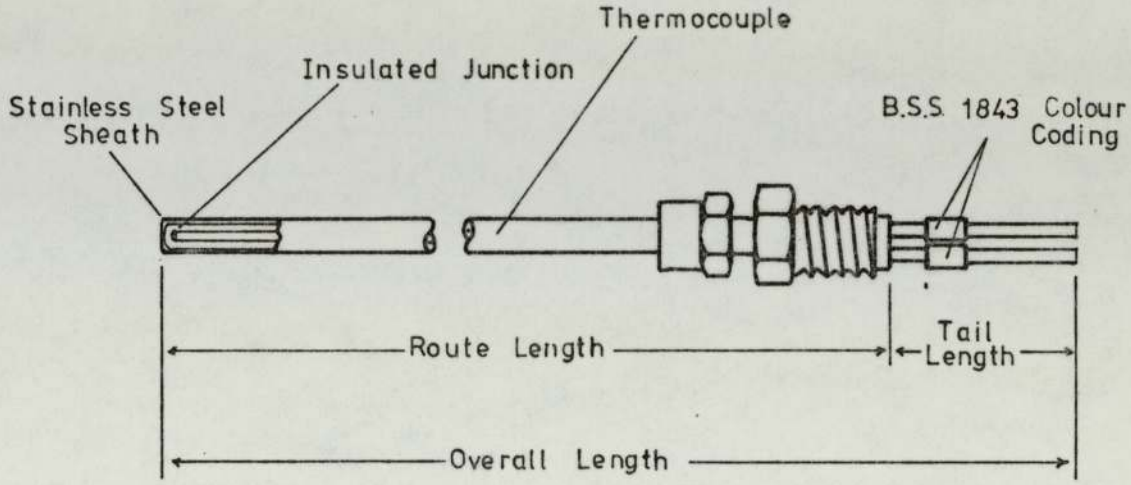

Figure 4.3(b)
Experimental Circuit

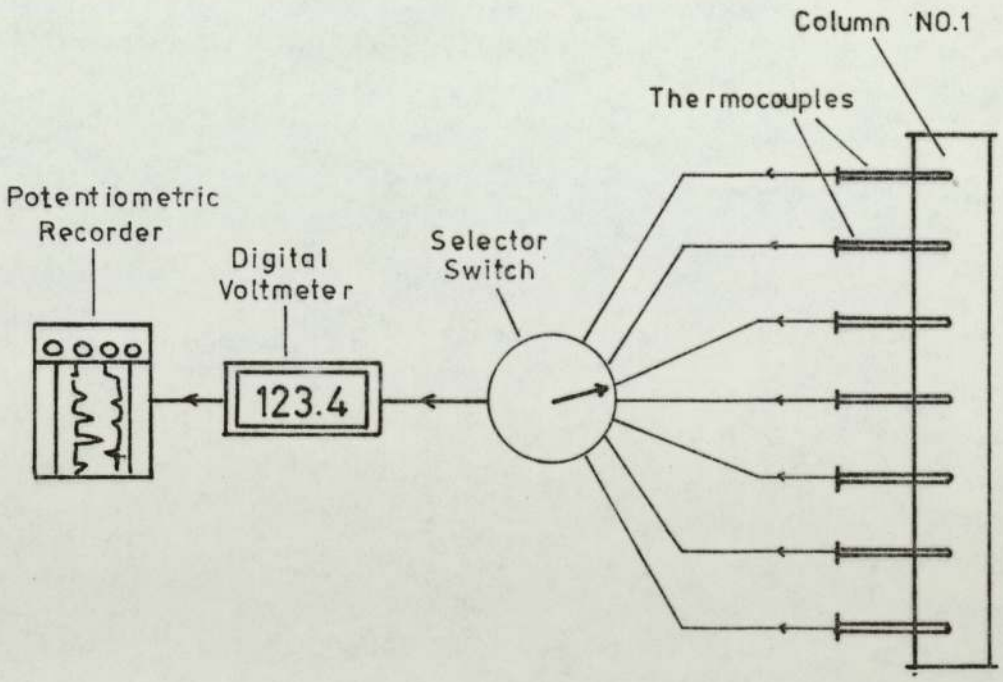

CHAPTER 5

THEORY OF CHROMATOGRAPHIC SEPARATIONS

5.1 The Selection of Experimental Operating Conditions

5.1.1 Introduction

Sections 2.2 and 2.3 dealt with the mechanisms governing chromatographic separations, which gave rise to differences in the relative migration rates of components as they passed through a batch chromatographic column. If, as with the SCCR1, the packing is moved counter-currently to the mobile phase flow, then by correct setting of the rate of packing movement the slowest moving component can be made to travel with the packing, whilst the faster moving component travels with the mobile phase. Figure 5.1, illustrates schematically the operating conditions of the SCCR1 unit, where the packing movement is simulated by the valve sequencing action. The faster moving component will exit with the mobile phase at the Product 1 outlet, and the slower moving component with the greater affinity for the stationary phase will be preferentially carried with the packing and exit with the purge gas at the Product 2 outlet.

To achieve separation in the above manner requires theoretical equations or models to predict the correct operating conditions for the desired separation.

5.1.2 The Idealized Case

If, with respect to Figure 5.1 a material balance is taken on component i at the feed point, then

$$f_i = G.c_i + L\, q_i \qquad (5.1)$$

f_i = feedrate of component i

c_i = concentration of component i in the mobile phase

Figure 5.1
Schematic Diagram of the SCCR1 Unit

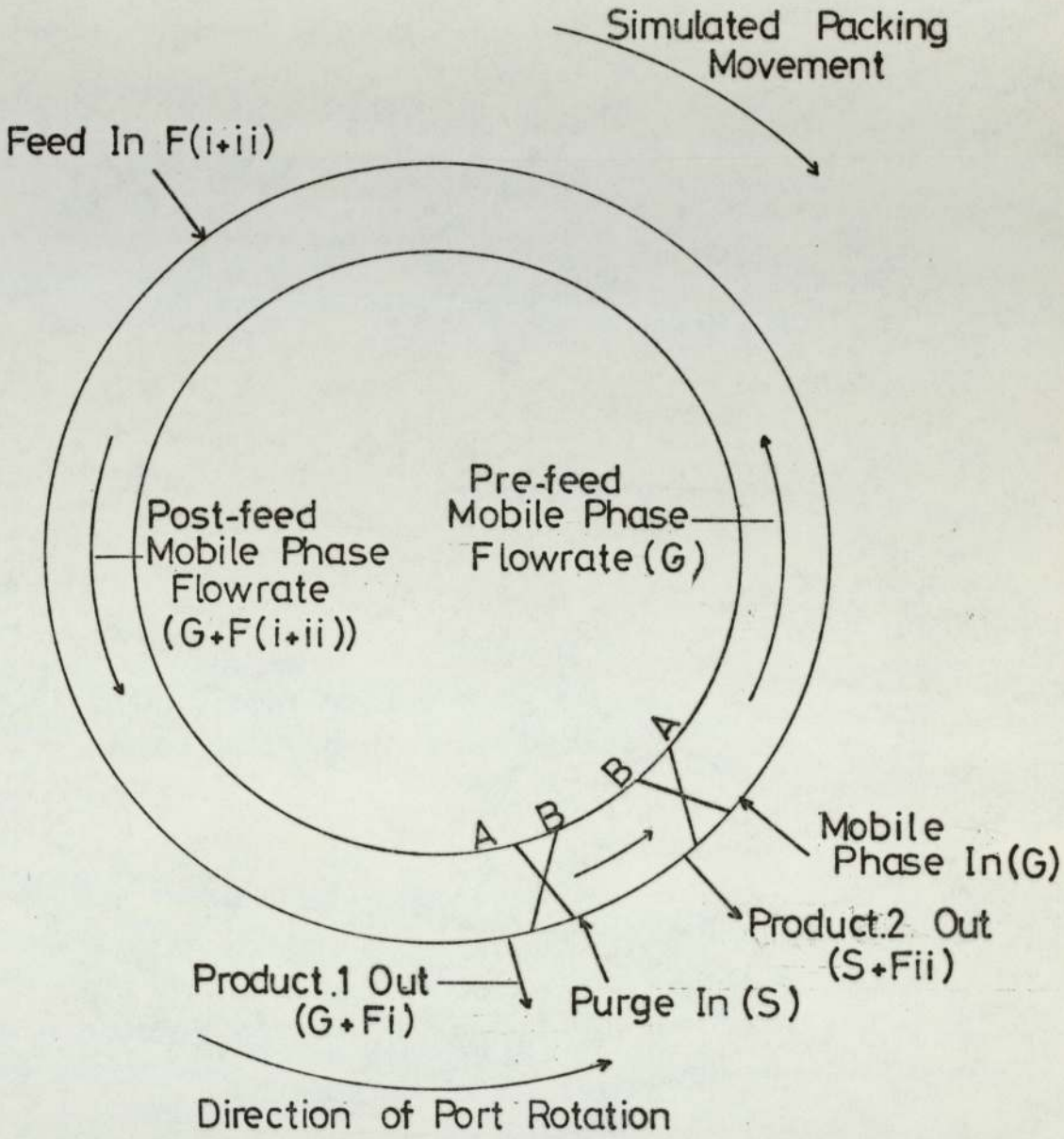

A-A Separating Section
B-B Purge Section

q_i = concentration of component i in the stationary phase,

and for the preferential movement of component i with the mobile phase we must have the condition where

$$G.c_i > L\, q_i \tag{5.2}$$

$$\text{i.e.} \quad \frac{G}{L} > \frac{q_i}{c_i} \tag{5.3}$$

$$\text{or} \quad \frac{G}{L} > K_i \tag{5.4}$$

Similarly for component ii to travel preferentially with the stationary phase,

$$\frac{G}{L} < K_{ii} \tag{5.5}$$

If the ratio of volumetric mobile phase flow rate to the apparent liquid phase flow rate (G/L) is set so that it lies between the two values of the partition coefficient K_i and K_{ii} then the two components i and ii will travel in opposing directions and theoretically a separation will be achieved.

$$K_i < \frac{G}{L} < K_{ii} \tag{5.6}$$

Also component ii will be completely purged from the isolated column if:

$$\frac{S}{L} > K_{ii} \tag{5.7}$$

Where S is the volumetric gas flowrate in the purge section of the chromatograph.

5.1.3 The Practical Situation

The criteria for a counter-current separation defined by Equations 5.6 and 5.7 provides a basis for the selection of operating conditions, however, several factors can impose restrictions upon the above equations namely,

(i) Chromatographic zone broadening

(ii) The sequential nature of operation

(iii) Finite column length

(iv) Finite concentration effects

(v) Finite feed flowrate

(vi) Mobile phase compressibility

(vii) The effect of temperature fluctuations.

5.1.3.1 Zone Broadening

Chromatographic zone broadening has previously been discussed in Section 2.2. The net effect is for a component with a partition coefficient of value K_i to be eluted from a chromatographic column over a range of K values, from $K_i - \delta_i$ to $K_i + \delta_i$, where $2\delta_i$ is the total baseline peak width in K_i units. Hence the $\frac{G}{L}$ value must be maintained within narrower limits to maintain a successful separation

$$(K_i + \delta_i) < \frac{G}{L} < (K_{ii} - \delta_{ii}) \qquad (5.8)$$

Similarly in the isolated section, the purge gas flowrate has to be increased so that,

$$\frac{S}{L} > K_{ii} + \delta_{ii} \qquad (5.9)$$

5.1.3.2 The Sequential Nature of Operation

As previously mentioned (Section 3.2), the counter-current movement of the stationary phase relative to the mobile phase in the SCCR1 unit is achieved by the sequencing of solenoid valves. Thus the counter-current movement of packing occurs as a step movement of one column length of packing every sequencing interval. During the switching interval the unit then operates as a co-current 'frontal-elution' system. At the end of a sequencing interval the whole of the material in a column is transported in the direction of the packing movement in a discontinuous manner and therefore the range over which G/L may be selected is further reduced.

$$(K_i + \delta_i + \delta'_i) < \frac{G}{L'} < (K_{ii} - \delta_{ii} - \delta'_{ii}) \qquad (5.10)$$

where: L' = the apparent volumetric liquid phase flowrate

$$= \frac{\text{total volume of liquid phase in column}}{\text{cycle time}}$$

δ'_i & δ''_{ii} factors to allow for the reduction in the limits of $\frac{G}{L'}$ attributable to the sequencing action.

δ'_i δ'_{ii} are functions of the number of columns used, and can be reduced by increasing the number of columns. The length of the sequencing interval will also affect δ'_i & δ''_{ii} as the degree of discontinuity is a function of the sequencing time.

5.1.3.3 The Effect of a Finite Column Length

The length of column is of paramount importance in determining whether a successful separation will be achieved for a given set of operating flow conditions. The closer together the values of K_i and K_{ii}, the closer they both are to the value of $\frac{G}{L'}$, and therefore the greater is the reluctance of the components to move in opposing directions. Therefore as K_i and K_{ii} approach each other a longer column is required to achieve the same degree of separation, but for a finite column length this has the effect of further reducing the range over which $\frac{G}{L'}$ may be selected to give complete separation.

$$(K_i + \delta_i + \delta_i' + \delta_i'') < \frac{G}{L'} < (K_{ii} - \delta_{ii} - \delta_{ii}' - \delta_{ii}'') \qquad (5.11)$$

where δ_i'' and δ_{ii}'' are functions of the number of theoretical plates for the system.

5.1.3.4 Finite Feed Flowrate

The volume of the vaporised feed although small compared with the carrier gas flow never the less occupies a finite volume which at high feed rates can approach 10% of the mobile phase flow. Consequently as shown by Figure 5.1 the mobile phase flow rate has two values within the separating section of the SCCR1 unit. The pre-feed value is taken as G, whilst the post-feed section has a value of G + F (i+ii) = G'. For most practical cases G >> F(i+ii) and hence F(i+ii) the feed flow effect, may be ignored. When F(i+ii) does become significant a further reduction in the range of $\frac{G}{L'}$ criterion occurs.

$$(K_i + \delta_i + \delta_i' + \delta_i'') < \frac{G}{L'} < \frac{G'}{L'} < (K_{ii} - \delta_{ii} - \delta_{ii}' - \delta_{ii}'') \qquad (5.12)$$

5.1.3.5 The Effect of Mobile Phase Compressibility

The pressure drop associated with the flow of gas through a packed bed results in a continual change in the volumetric gas flowrate. Consequently at the column inlet, G will have a minimum value and as the pressure falls a maximum value of G will occur at the column outlet.

Of all the restrictions imposed upon Equation 5.6, the change in G caused by gas expansion is the most severe, and for typical separation runs performed by the SCCR1 unit (45), there can be a 100% change in the volumetric gas flowrate. In practical terms this means that should both solute molecules be present in the region close to the carrier gas inlet, the rate of migration will be reduced, with the solute molecules which should be travelling preferentially with the carrier gas eventually being retarded enough so that they cause contamination of the Product 2. i.e. component i contaminating component ii.

At the other end of the separating section the opposite effect is experienced with the rates of migration greatly accelerated. Any component ii molecules present near to the outlet will have a resultant velocity in the direction of mobile phase flow and produce a long leading edge to the concentration profile with the eventual contamination of the Product.1 stream.

Introducing the effects of changing volumetric flowrate into Equation 5.12 leads to

$$(K_i+\delta_i+\delta'_i+\delta''_i) < \frac{G_{min}}{L'} < \frac{G'_{min}}{L'} < \frac{G_{max}}{L'} < \frac{G'_{max}}{L'} < (K_{ii}-\delta_{ii}-\delta'_{ii}-\delta''_{ii}) \qquad (5.13)$$

where G_{min} and G_{max} are the respective volumetric flowrates at the separating section inlet and outlet.

In the isolated section the purge flowrate must be further increased to ensure complete removal of Product.2, so that,

$$\frac{S_{min}}{L'} > K_{ii} + \delta_{ii} + \delta'_{ii} + \delta''_{ii} \qquad (5.14)$$

where S_{min} is the volumetric flowrate of the purge stream as it enters the isolated column.

5.1.3.6 Finite Concentration Effects

Section 2.3.1.3 dealt with concentration effects and the influence they have upon the partition coefficients. For a non-linear partition isotherm the distribution coefficient, K, changes with solute concentration. With increasing concentration, K decreases for a Langmuir isotherm while for an anti-Langmuir isotherm K increases, with all K values being referenced to K^{∞}, the value of the partition coefficient at infinite dilution. Therefore the effective K value of a solute at a finite concentration may be expressed in terms of its infinite dilution value and the change of K, ΔK, which may be positive or negative, occurring at this concentration.

$$K = K^{\infty} + \Delta K \qquad (5.15)$$

Therefore for complete separation of components i and ii we now have:

$$(K_i^{\infty} + \Delta K_i + \delta_i + \delta'_i + \delta''_i) < \frac{G_{min}}{L'} < \frac{G'_{min}}{L'} < \frac{G_{max}}{L'} < \frac{G'_{max}}{L'}$$

$$< (K_{ii}^{\infty} + \Delta K_{ii} - \delta_{ii} - \delta'_{ii} - \delta''_{ii}) \qquad (5.16)$$

and for the purge section:

$$\frac{S_{min}}{L'} > K^{\infty}_{ii} + \Delta K_{ii} + \delta_{ii} + \delta'_{ii} + \delta''_{ii} \qquad (5.17)$$

As well as influencing the value of the partition coefficients, finite concentration effects will also lead to an increase in zone broadening with the resulting effect of increasing the values of δ_i and δ_{ii} in Equations 5.16 and 5.17.

5.1.3.7 The Influence of Temperature Perturbations

It is probable that some of the band velocity profile phenomena discussed in Section 2.3.1 are due to transient heat of solution effects in the chromatographic bed. In general, absorption is exothermic and desorption endothermic, hence a temperature profile will travel with the solute zone. The height of the temperature wave is dependent upon the solute feed rate and gas phase concentration. The presence of temperature fluctuations in chromatographic columns has been demonstrated by several researchers (17,70,72,81,82,83) and attempts have been made to describe the change in temperature of a solute as it passes through a theoretical plate (83).

In practice any temperature variations accompanying the solute band will be relaxed by heat conduction through the column packing and column wall. An axial temperature gradient will however still exist in which the leading edge of the solute band will be at a higher than ambient temperature giving an increased solute migration rate, whilst the trailing edge of the solute band will be retarded due to the lower temperature being experienced.

Radial gradients will give rise to non-uniform cross-column solute migration rates, and also contribute to band velocity profile differences. The effect of the radial temperature gradient upon the solute migration rate is still a matter for conjecture with Hupe and coworkers (72) maintaining that the centre of the band will be advanced relative to the column wall. Conversely Huyten et al (17) believe that the band centre is retarded relative to the column wall. It is possible that both bodies of opinion may be correct. In investigating temperature profiles in chromatographic columns, diameters ranging from 0.1 to 10 cm have been used and whilst it is questionable to compare results from columns of differing diameters, a general trend may be that as the column diameter increases the column tends towards an adiabatic situation, whereas analytical columns can be regarded as being isothermal.

The complex temperature profile will add contributions to both the solute band broadening factors δ_i and δ_{ii} and to the partition coefficients K_i and K_{ii} and the final criterion for a successful separation may be expressed as:

$$(K_i^{\infty} + \Delta K_i + \Delta K_i' + \delta_i + \delta_i' + \delta_i'') < \frac{G_{min}}{L'} < \frac{G'_{min}}{L'} < \frac{G_{max}}{L'} < \frac{G'_{max}}{L'}$$

$$< (K_{ii}^{\infty} + \Delta K_{ii} + \Delta K_{ii}' - \delta_{ii} - \delta_{ii}' - \delta_{ii}'') \qquad (5.18)$$

and for the purge section

$$\frac{S_{min}}{L'} > (K_{ii}^{\infty} + \Delta K_{ii} + \Delta K_{ii}' + \delta_{ii} + \delta_{ii}' + \delta_{ii}'') \qquad (5.19)$$

where $\Delta K'$ is the correction to K^{∞} to allow for temperature changes.

5.1.4 Prediction of Operating Conditions

Equation 5.18 provides the limits for comlete separation of components i and ii. Use of the equation requires a detailed knowledge of all the parameters involved, which in turn necessitates a detailed practical and theoretical study. It will be apparent from Sections 5.1.3.1 to 5.1.3.7 that many of the parameters in Equation 5.18 are interactive with one another and therefore definitions based purely upon experimental data would be impossible. A theoretical model proposed in Chapter 9, may allow the study of the individual factors in isolation, with operational data from the SCCR1 unit, Chapters 6 and 8, being used to prove the validity of the model.

Allowing for the fact that it is not possible to give numerical values to some of the parameters from Equation 5.18, accurate determination of K^{∞}, ΔK and $\Delta K'$ is possible.

5.1.4.1 Determination of the Partition Coefficient K

5.1.4.1.1 Infinite Dilution K^{∞}

From basic chromatographic theory the partition coefficient at infinite dilution can be defined as:

$$K^{\infty} = \frac{F \left(\frac{T_c}{T_a}\right) \cdot \left(\frac{P_o}{P_a}\right) \cdot j \cdot (t_R - t_m)}{V_L} \qquad (5.20)$$

where F = Carrier gas flowrate measured at ambient conditions

T_c = Column temperature

T_a = Ambient temperature

P_o = Column outlet temperature

P_a = Ambient pressure

t_R = Retention time for component

t_m = Retention time for unabsorbed component

V_L = Volume of the liquid phase impregnated on the solid support

j = James and Martin (4) compressibility factor

$$= 1.5 \, (P_{io}^2 - 1) \, / \, (P_{io}^3 - 1) \qquad (5.21)$$

and P_{io} = ratio of inlet to outlet column pressures.

Restrictions upon the accurate application of Equation 5.20 are that,

(a) The partition coefficient must be independent of concentration.

(b) The volume of the solute in the gas phase must not make a significant contribution to the retention volume

(c) Gas phase ideality is assumed

(d) No adsorption of the solute onto the solid support surface.

Measurement of the partition coefficient at infinite dilution has been carried out by Sunal (50) and Deeble (45), using 4.8 mm o.d. analytical columns. The small sample sizes used satisfied restrictions (a) and (b) above, whilst treatment of the analytical columns to saturate any active sites overcame restrictions (c) and (d).

In summarizing the results of Deeble (45), the partition coefficients for three halocarbons were determined over the temperature range 20-100^{o}C, the solvent phase used in the analytical columns being the same as that used by the SCCR1 unit namely silicone fluid DC 200/50.

As predicted by thermodynamic theory (180) the plot of Log K_i^{∞} against reciprocal of absolute temperature gave a straight line Figure 5.2, from which a 'least squares' fit to the data gave the

Figure 5.2
Plot of Log K^{∞} against 1/T for Arklone.P, Genklene.P, Dichloromethane on Silicone Fluid DC 200/50 Phase

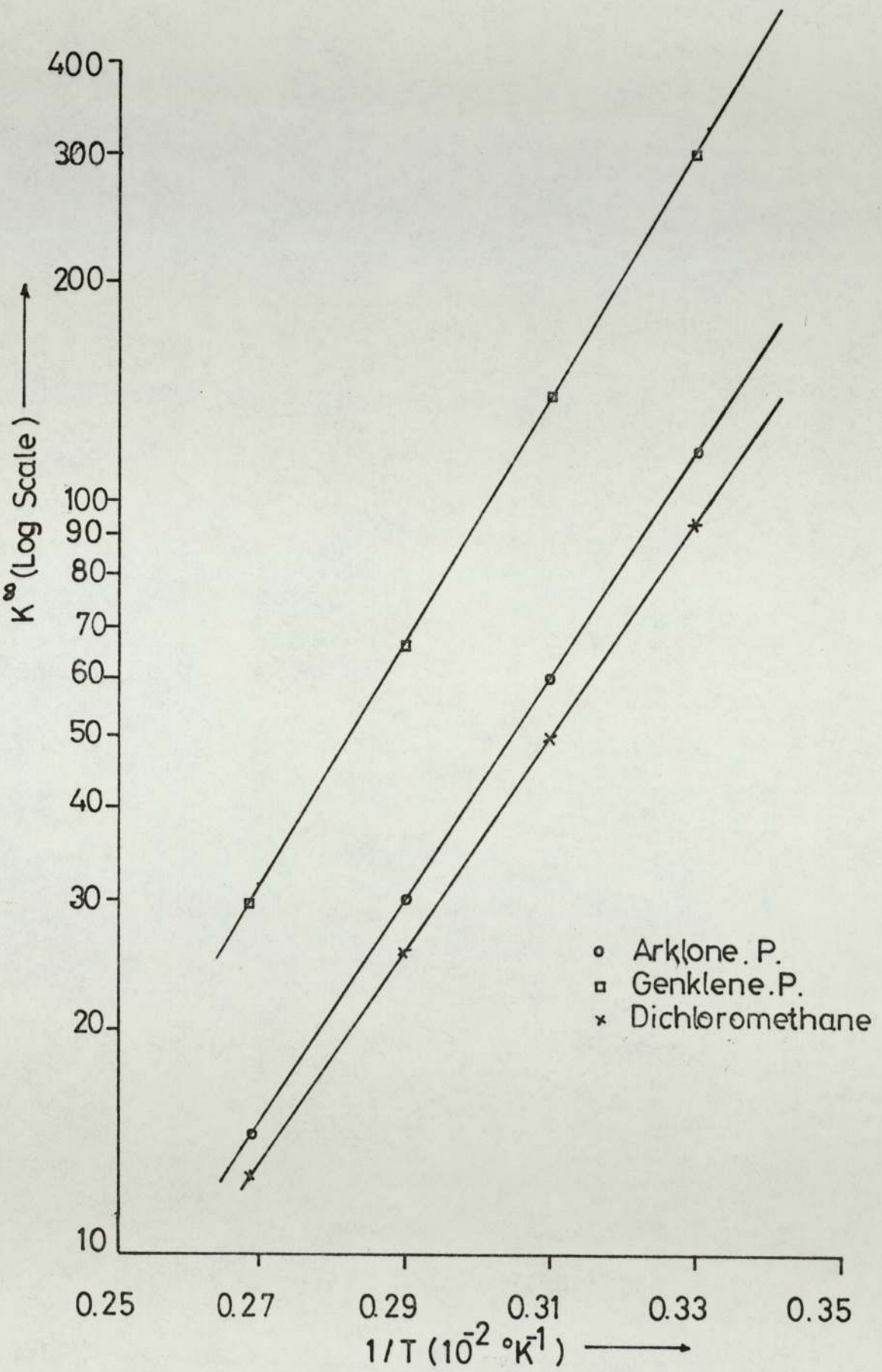

following correlations relating the partition coefficient to absolute temperature.

Dichloromethane: $\text{Log}_{10} K_{D.C.M.} = 1311.2/T - 2.3909$

Arklone.P. : $\text{Log}_{10} K^{\infty}_{AP} = 1363.3/T - 2.4993$

Genklene.P. : $\text{Log}_{10} K^{\infty}_{GP} = 1528.3/T - 2.5976$

5.1.4.1.2 Finite Concentrations

The partition coefficient at a finite concentration may be expressed as

$$K_i = \frac{q_i}{c_i} = \frac{\frac{m_i(L)}{V_L}}{\frac{m_i(G)}{V_m}} \qquad (5.22)$$

$m_i(L)$ = mass of solute in liquid phase

$m_i(G)$ = mass of solute in gas phase

V_L = volume of liquid phase

V_m = volume of gas phase

The mole fraction of the solute in the liquid phase (x_i) may be expressed as,

$$x_i = \frac{\frac{m_i(L)}{M_i}}{\frac{m_i(L)}{M_i} + \frac{m_L}{M_L}} \qquad (5.23)$$

where m_L = mass of solvent

M_i = molecular weight of solute

M_L = molecular weight of solvent

Similarly the mole fraction in the gas phase (y_i) can be written as,

$$y_i = \frac{\frac{m_i(G)}{M_i}}{\frac{P.V_G}{R_g.T}} \qquad (5.24)$$

where P = total pressure

R_g = gas constant

T = absolute temperature

Having defined the gas and liquid phase mole fractions allows the substitution of $m_i(L)$ and $m_i(G)$ in Equation 5.22, so that,

$$K_i = \frac{x_i.R_g.T}{y_i.P.V_L} \left(\frac{m_i(L)}{M_i} + \frac{m_L}{M_L}\right) \qquad (5.25)$$

The relationship between x_i and y_i is given by Raoult's Law as

$$\frac{x_i}{y_i} = \frac{P}{\gamma_i(L).P_i^o} \qquad (5.26)$$

where $\gamma_i(L)$ = activity coefficient for component i in the liquid phase

P_i^o = saturated vapour pressure

Hence

$$K_i = \frac{R_g.T}{P_i^o.\gamma_i(L)\ V_L} \cdot \left(\frac{m_i(L)}{M_i} + \frac{m_L}{M_L}\right) \qquad (5.27)$$

and by rearrangement

$$K_i = \frac{R_g . T . \rho_L}{P_i^o . M_L . x_L} \cdot \frac{}{\gamma_i(L)} \qquad (5.28)$$

where x_L = mole fraction of solute in the liquid phase

$= 1 - x_i$

ρ_L = density of solvent phase

The activity coefficient $\gamma_i(L)$ is itself dependent upon solute concentration, and therefore to calculate K_i a correlation must be found relating $\gamma_i(L)$ and x_i.

Sunal (50) using activity coefficients calculated from true K values (i.e. $K^{\infty} + \Delta K$) has correlated these activity coefficients with the solute mole fraction in the liquid phase. The equation used was of the Flory-Huggins type viz:

$$\gamma_i(L) = \frac{\tau_i}{\tau_i . x_i + x_L} \exp\left[\frac{x_L (1-\tau_i)}{\tau_i x_i + x_L} + \psi_i \left(\frac{x_L}{\tau_i x_i + x_L} \right)^2 \right] \qquad (5.29)$$

where τ_i = fitted experimental constant

= 0.008101 for dichloromethane

= 0.015984 for Arklone.P.

= 0.008536 for Genklene.P.

ψ_i = fitted experimental constant

= 0.9547 for dichloromethane

= 0.43764 for Arklone.P.

= 0.93041 for Genklene.P.

The vapour pressures of the solutes was calculated from an equation of the form

$$\text{Log}_{10} P_i^o = (-0.2185\ A''/T) + B \qquad (5.30)$$

where A'' = molar heat of vaporisation

B = constant

The values of A" and B used were those computed by Sunal (50) from the data given in several references (181,182).

Obtaining the value of K_i for a specific x_i value allowed the concentration c_i to be then calculated from

$$c_i = \frac{x_i . \rho_L . M_i}{K_i . x_L . M_L} \qquad (5.31)$$

Figure 5.3 gives a flowchart for a FORTRAN program to obtain the relationship between partition coefficients and gas phase concentration of solute, for temperatures between 270.2 and 303.2 ^oK at intervals of 0.5^oK. The full program listing is given in Appendix 2, Figure A.2.1.

A graphical portrayal of the results is given in Figure 5.4 where it is shown that a plot of activity coefficient against solute concentration for a series of temperature yields a group of parallel curves for each individual solute.

Whilst reference is made to the results shown in Figure 5.4 for determining the operating conditions in the SCCR1 unit, the main use of the relationship between K_i, C_i and T is in the mathematical modelling of the unit. For this purpose the most convenient form of expressing the results is by describing them as 2nd, 3rd or 4th order

Figure 5.3
Flow Chart for the Computation of K_i/C_i for a Series of Temperatures

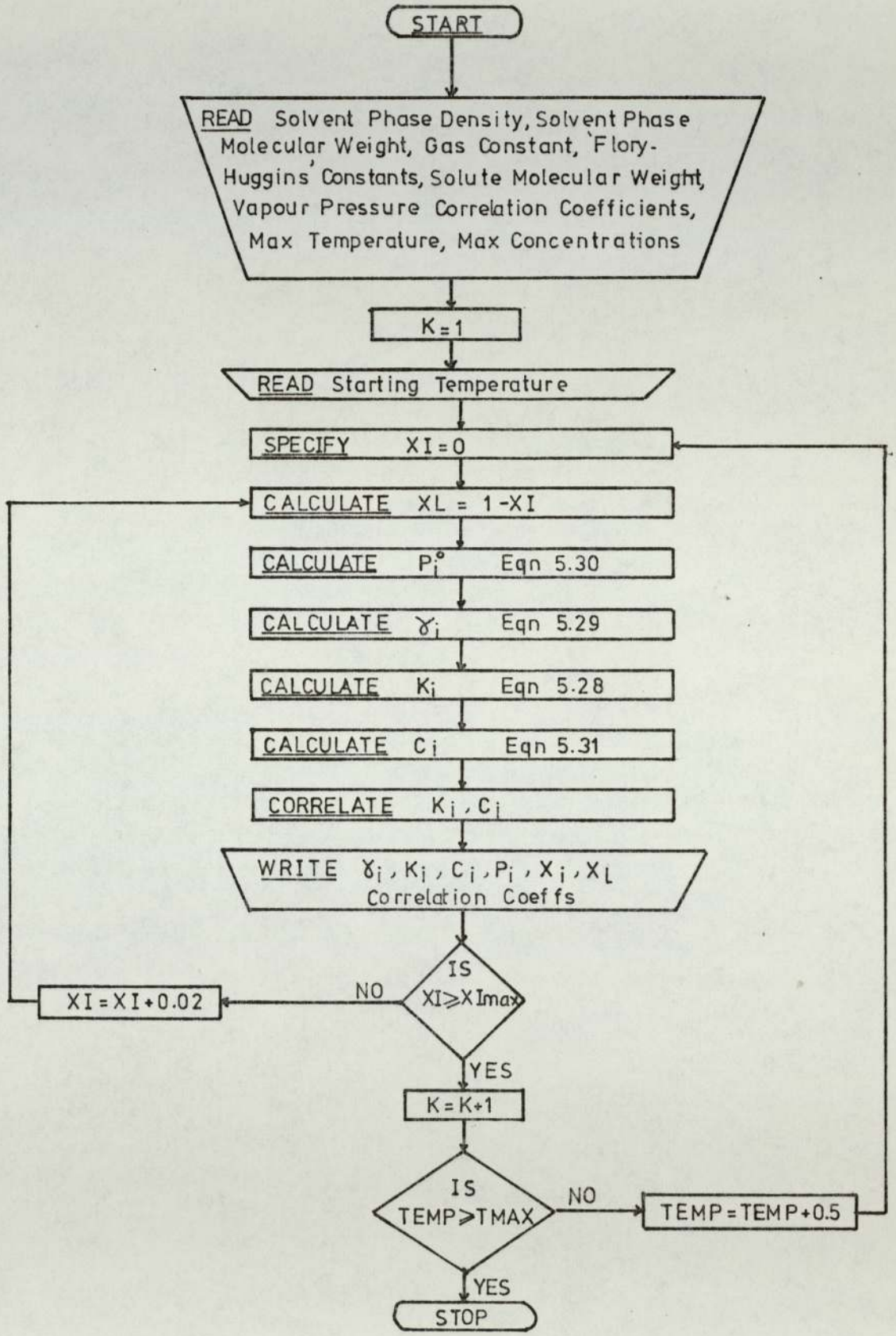

polynomials relating K_i to C_i for a fixed temperature.

The polynomial coefficients for Arklone.P., Genklene P. and dichloromethane for temperatures ranging between 270.2 and 303.2^{o}K are given in Appendix 3.

5.1.4.2 Determination of the Apparent Gas to Liquid Ratio

Equation 5.18 provides the limits between which $\frac{G}{L'}$, must be selected to provide a separation. For the case of two solutes with a high separation factor, the range over which $\frac{G}{L'}$, can be chosen may itself be large, and as a practical guide $\frac{G}{L'}$, was generally chosen to lie midway between the partition coefficient values measured at infinite dilution and 20^{o}C

As shown in Section 5.1.3.5, as the carrier gas expands during its passage through the chromatograph, so $\frac{G}{L'}$, changes between $\frac{G_{min}}{L'}$ and $\frac{G_{max}}{L'}$. Therefore it is desirable to arrange for $\frac{G_{min}}{L'}$ and $\frac{G_{max}}{L'}$ to be equidistant from the mid-point of the two partition coefficients. This is attained be redefining the $\frac{G}{L'}$, ratio so that G becomes the gas flowrate at mean column pressure, G_{mc}, and by using the James and Martin compressibility factor:-

$$\frac{G_{mc}}{L'} = \frac{G_a \times \frac{P_a}{P_o} \times j}{L'} \qquad (5.32)$$

Where G_a is the gas outlet flowrate measured at atmospheric pressure. The setting of a mean column gas flowrate by adjustment of the inlet pressure and outlet flowrate requires a trial and error procedure and to assist in this procedure the experimentally determined relationship between G_{mc} and the height of the outlet gas rotameter for a series of

inlet pressures was recorded, Appendix 1, Figures A.1.2 and A.1.3.

An example of the calculation of $\frac{G_{m.c.}}{L'}$ is given in Appendix 4.

Figure 5.4
Partition Coefficient(K_i) against Gas Phase Solute Concentration C_i

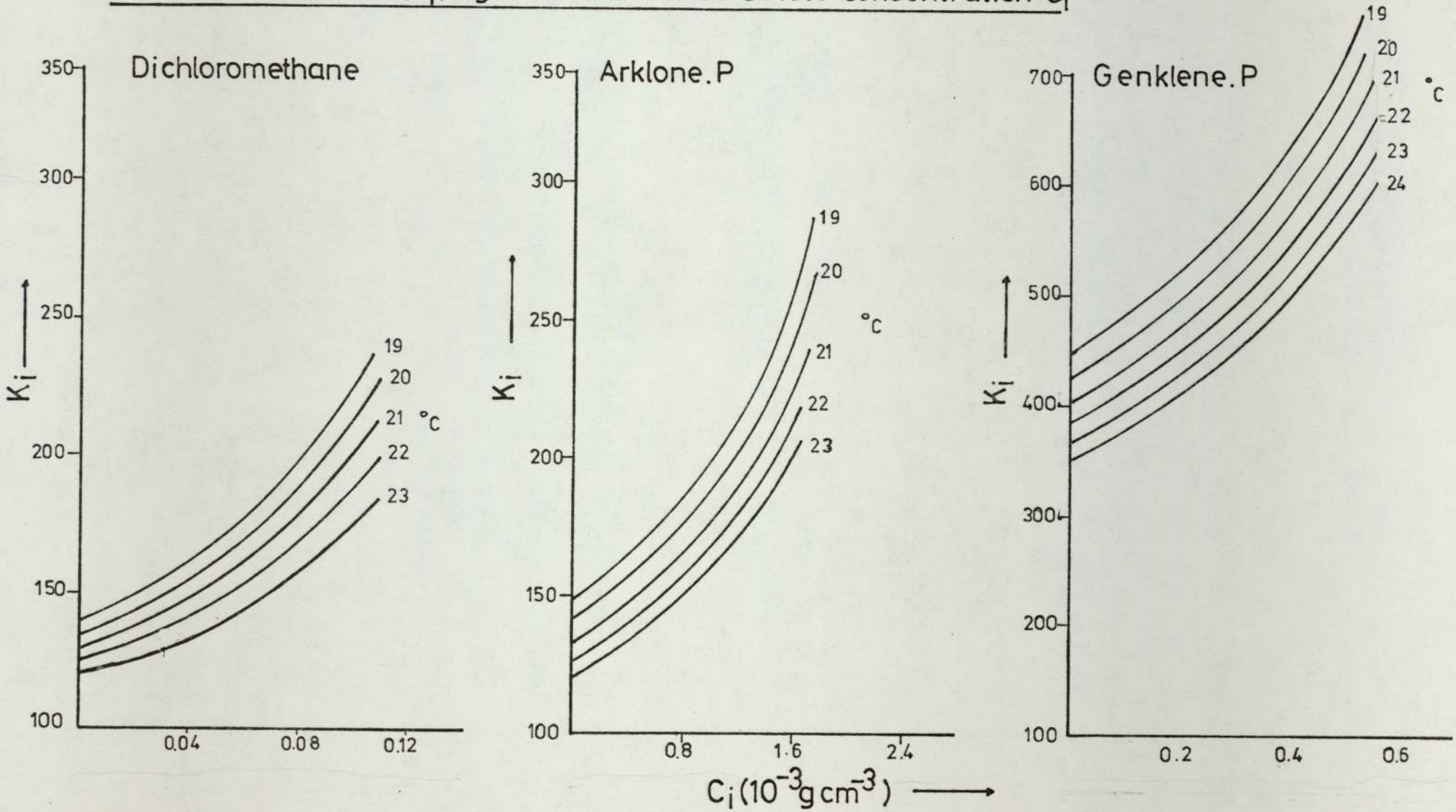

CHAPTER 6

INITIAL STUDIES WITH THE SCCR1 FOR THE SYSTEM ARKLONE.P./GENKLENE.P.

6.1 Introduction

In defining objectives for the separation studies particular attention was made to the conclusions and recommendations recorded by Deeble (45).

As the SCCR1 unit is essentially a production scale unit, the optimisation of throughput was of primary importance. Possible ways of achieving this were by increasing the carrier gas flowrate, and by operating at an ambient temperature closer to the solute boiling points. Isolating two columns for purging, to increase the time available for regeneration also warranted further study.

As well as providing improvements to the practical operation of the SCCR1 a fuller understanding of the factors affecting any separation was required. As previously mentioned any experimental studies would have to be limited to three halocarbons on the grounds of safety, and therefore it was essential that an accurate mathematical model of the unit be developed to allow the computer simulation of systems for which practical investigation is unsafe using air as a carrier gas and non sparkproof solenoid values.

In all the runs performed, the feedstock was maintained as an equivolume mixture of two solutes. These 50-50 mixtures provided the most difficult feed ratios to separate into two pure product fractions. Although facilities were available for introducing the feedstock at any point within the unit, the feed inlet was always positioned at the mid-point of the separating section.

For consistency in comparison of experimental results certain operating parameters must be held constant, and therefore if a parameter such as the 'apparent gas to liquid rate', G_{mc}/L', is to remain constant throughout the experimental programme it is essential that the numerical

value selected be optimised. Deeble (45) studied the effect of varying G_{mc}/L' between the limits of K^{∞}_{AP} and $K^{\infty}_{G.P}$. Not surprisingly he found that the optimum range lay approximately midway between K^{∞}_{AP} and K^{∞}_{GP}. The nearer the value of G_{mc}/L' approached the partition coefficient for Arklone.P., the greater was the tendency for both solutes to travel in the direction of the packing, with the resultant contamination of Product.2. Similarly as G_{mc}/L' approached the value of $K^{\infty}_{G.P.}$ the solutes were preferentially carried with the mobile phase and consequently Product.1 purity was lost. As a guideline for separation runs, the value of G_{mc}/L' was designated as 265.

The results and discussions pertaining to the experimental programme have been set out in three chapters. This first chapter gives details of data recording, the investigations into the sequencing interval and feed rate, and the temperature profiles experienced in the SCCR1. Based on the results outlined in this chapter, modifications to the chromatograph were required. These design changes and their success or otherwise are described in Chapter 7. Further studies into feedrate and temperature profiles for the system Arklone.P./Genklene.P. are given in Chapter 8, along with the studies into the separation of Arklone.P./dichloromethane.

6.2 Data Recording and Analysis

6.2.1 Column to Column Concentration Profile

The plotting of concentration profiles and the comparing of results requires that these results are reproducible and therefore obtained when the SCCR1 has attained equilibrium. Although the column to column profile changes with time during a sequencing interval, a point is eventually reached where the dynamic profile for the unit is reproduced form one cycle (twelve sequences) to another. This onset of 'pseudo steady-state' is observed clearly on the Katharometer traces as Point A in Figure 4.1. In general the unit is allowed to function for a further two complete cycles after equilibrium has been reached before any samples are removed.

Gas sampling was achieved by inserting a 1 cm^3 'Pressure-Lok' syringe through a septum in one of the columns and withdrawing the sample. Reproducibility of sample volume was again achieved by using grooved spacer rods. For a complete cycle, sampling was carried out at a fixed point in the unit, at a set time after each sequencing of the port functions. The resultant profile from this method of sampling was equivalent to sampling all twelve columns at the same instant. Sampling for more than one cycle in this manner confirmed that the unit had reached and remained in a steady state of operation.

Although each sample volume taken was identical, the sample pressure changed, and therefore for each sample removed the pressure at the point of sampling was recorded using a 0-400 $kN.m^{-2}$ 'Norgren' pressure gauge attached to a hypodermic needle and inserted into the column. Injection of the sample into the flame ionisation detector produced a peak area expressed in integrator units, and from the appropriate calibration charts the injected solute mass was calculated.

The concentration of the sample may be expressed in two ways:- a) on-column concentration, b) standardised concentration. A standardised concentration is where the gas phase solute concentration is expressed as the solute mass divided by the sample volume corrected to atmospheric pressure. The standardised concentration has been adopted for comparison of experimental results.

Each successful run is characterised with a unique title in the following way. For example Run 300-275-400-A signifies a nominal feedrate of 300 $cm^3.hr.^{-1}$, a nominal G_{mc}/L' ratio of 275, a nominal sequencing interval of 400 seconds respectively, with the final character namely 'A' denoting that the run was the first to be performed under the above operating conditions. Subsequent runs under identical conditions being denoted B, C, D, etc.

Tables 6.1 and 6.2 give an example of the results taken during a separation run of the SCCR1, with Table 6.3 giving a list of results computed from the experimental readings. A flow diagram for this computer program is given in Figure 6.1, the full program listing being given in Appendix 2, Figure A.22. Experimental and computed results for all the runs discussed in the following chapter are given in Appendix 5.

6.2.2 Reproducibility of the Concentration Profile and Experimental Error

The concentration profile analysis technique in which samples are removed from a fixed point in the unit at a set time after sequencing, assumes that all the columns have perfectly matching characteristics. Experimentally determined results (45), show there to be a large

Table 6.1

Example of Data Recorded for Run 300-265-400-A

Feedrate 325 $cm^3 hr^{-1}$
Sequencing Time 399 s
Ambient Temperature 16.5 °C
Ambient Pressure 101.0 $kN\ m^{-2}$

Isolated Column Number	Separating Section			Purge Section		
	P in	P out	14K. RT	P in	P out	18K. RT
	$kN.m^{-2}$	$kN.m^{-2}$	cm	$kN.m^{-2}$	$kN.m^{-2}$	cm
1	378	190	15.5	232	197	14.0
2	378	190	15.4	232	197	14.0
3	378	180	15.6	232	194	13.5
4	378	180	15.5	232	197	14.0
5	378	180	15.5	232	197	14.0
6	378	187	15.4	232	197	14.0
7	378	190	15.5	232	197	14.0
8	378	187	15.5	232	197	14.0
9	378	190	15.5	228	194	13.5
10	378	190	15.5	228	194	13.5
11	378	190	15.5	232	197	14.0
12	378	187	15.5	232	197	14.0
Average	378	186	15.5	232	196	13.9

Table 6.2
Example of Data Recorded for Run 300-265-400-A

Concentration Profile Analysis Data:
Samples Taken 15cm from Column 1 Outlet
Syringe Sample Volume 0.100 cm^3

Isolated Column Number	Time After Switch	Sample Point Pressure	F.I.D. Attenuation	Peak Area	
				Arklone	Genklene
	s	kNm^{-2}			
1	100	207	2×10^2	2243	38080
1	300	204	"	1022	1471
2	100	194	"	145700	715
2	300	197	"	223000	1233
3	100	211	"	225200	1579
3	300	211	"	315000	1323
4	100	235	"	261200	1350
4	300	245	"	287000	2603
5	100	245	"	265000	2302
5	300	259	"	286700	224
6	100	266	"	288600	828
6	300	273	"	273500	1133
7	100	290	"	297300	18360
7	300	290	"	253800	144100
8	100	304	"	195800	334000
8	300	307	"	8780	365100
9	100	321	"	3131	480100
9	300	321	"	1403	351400
10	100	338	"	2729	567000
10	300	338	"	1121	592500
11	100	359	"	371	520200
11	300	359	"	714	514600
12	100	376	"	1400	311900
12	300	376	"	7100	439500

Table 6.3

Computed Data for Run 300-265-400-A

Actual $G_{m.c} / L' = 284$

Concentrations $< 1.0 \times 10^{-6}$ g cm^{-3} are not recorded

Distance of Sample Point from Carrier Gas Inlet	Time After Sequencing	Sample Volume Corrected to P_{std}	Concentration at Column Pressure		Standardised Concentration	
			Arklone	Genklene	Arklone	Genklene
cm	s	cm^3	10^{-3} g cm^{-3}	10^{-3} g cm^{-3}	10^{-3} g cm^{-3}	10^{-3} g cm^{-3}
717	100	0.205	0.002	0.014	0.001	0.007
717	300	0.202	0	0	0	0
656	100	0.192	0.083	0	0.043	0
656	300	0.195	0.129	0	0.066	0
595	100	0.209	0.127	0	0.061	0
595	300	0.209	0.180	0	0.086	0
534	100	0.230	0.152	0	0.066	0
534	300	0.233	0.151	0	0.065	0
473	100	0.243	0.163	0	0.067	0
473	300	0.256	0.164	0	0 064	0
412	100	0.263	0.163	0	0 067	0
412	300	0.270	0.157	0	0 058	0
351	100	0.287	0.166	0.005	0 058	0.002
351	300	0.287	0.144	0.049	0 050	0.017
290	100	0.301	0.111	0.114	0 037	0.038
290	300	0.304	0.006	0.128	0 002	0.042
229	100	0.318	0.003	0.165	0 001	0.052
229	300	0.318	0.001	0.121	0	0.038
168	100	0.335	0	0.198	0	0.059
168	300	0.335	0	0.208	0	0.062
107	100	0.356	0	0.181	0	0.051
107	300	0.356	0	0.181	0	0.051
45	100	0.372	0	0.108	0	0.029
45	300	0.372	0.004	0.153	0001	0.041

Figure 6.1

Flow Diagram for Computation of Concentration Profile Results

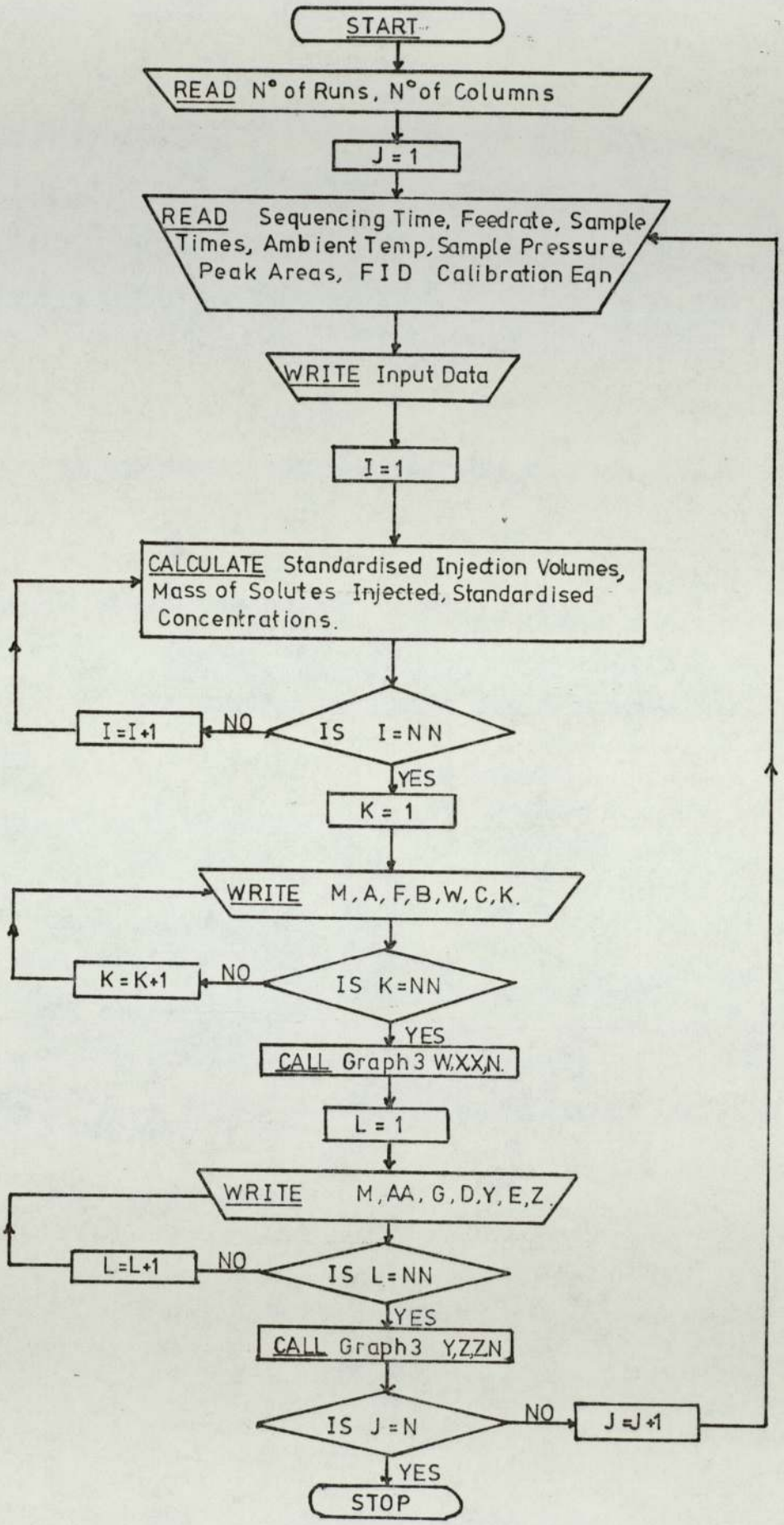

variation in the individual column H.E.T.P's. However as eleven columns are always linked together to form the separating section in the SCCR1, the assumption of matching columns remains acceptable, with any variation in the profile analysis only likely to be noticed in the results from the single isolated column.

Confirmation of a reproducible concentration profile is shown in Figures 6.2 and 6.3. The profiles for successive cycles of operation at 600 $cm^3.hr^{-1}$ are illustrated in Figure 6.2, giving very close agreement. Samples for these two cycles were all taken from a point 15 cm from the top of column No.2. Comparison of profiles obtained from sample points at opposite sides of the unit is given in Figure 6.3, in which the samples for Run 600-265-262-B1 were taken from 15 cm down column No.2 and for Run 600-265-262-B5 the samples were removed from a point 15 cm down column No.8. Also shown on Figure 6.3 is a third concentration profile for Run 600-265-262-C1 in which sampling was performed from a point 45 cm down column No.1, and despite the known individual column variation in efficiency, very similar point concentration values were obtained.

Inherent in the concentration profile analysis will be errors resulting from the F.I.D. calibration, pressure, and the time of sampling. Including a contribution for the syringe volume, the calibration of the F.I.D. will give an error of no more than ± 2%. The error relating to the recording of the sample point pressure from the calibrated pressure gauge was assumed to be within ± 1%. The maximum error therefore in the standardised concentration was ± 3%.

The sample withdrawal was timed with an accurate stopwatch and whilst any error in the stopwatch is assumed to be negligible,

Figure 6.2 Reproducibility of Concentration Profile for Runs 600-265-262-B1 & 600-265-262-B3

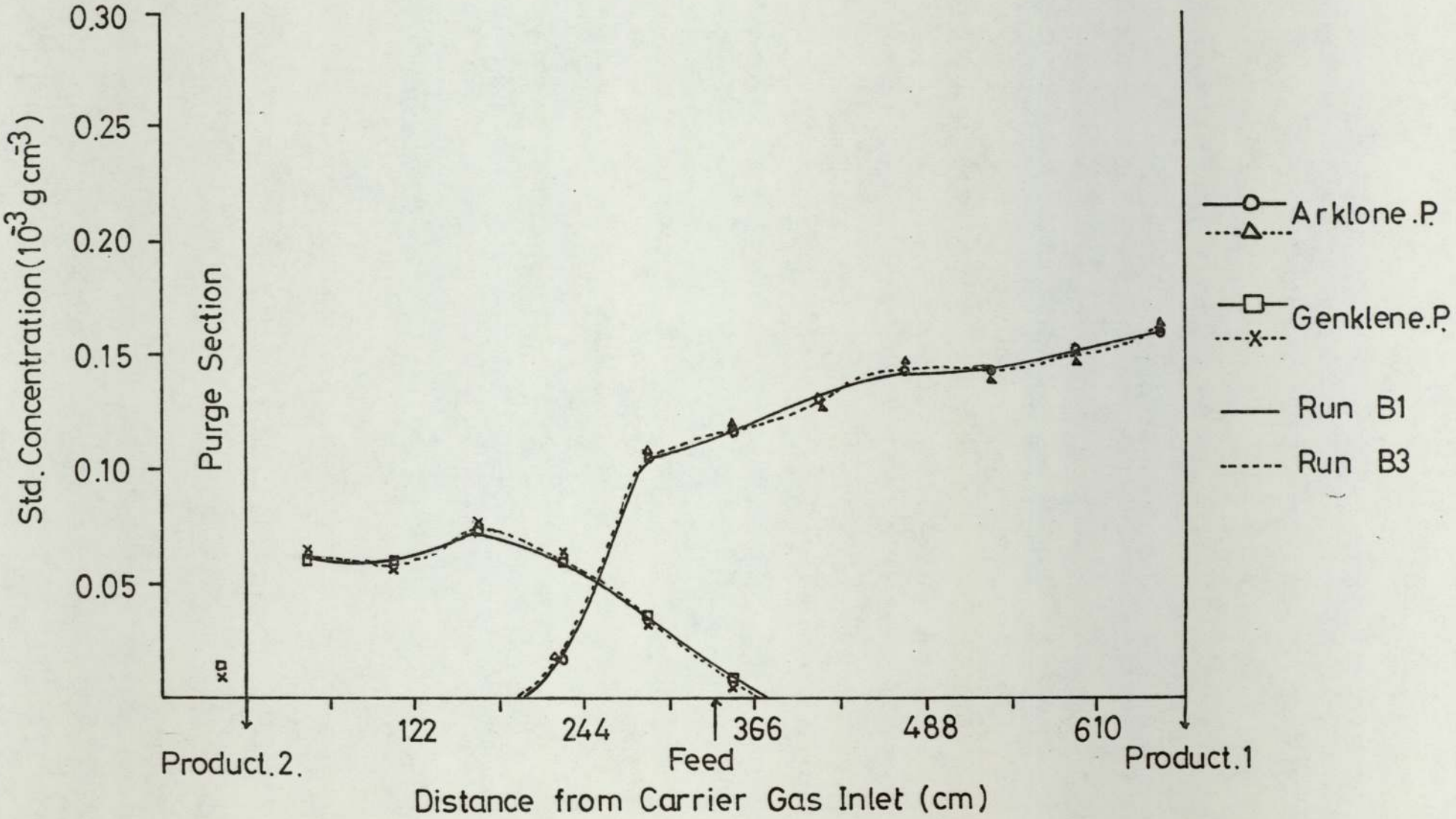

Figure 6.3 Reproducibility of Concentration Profile for Runs 600-265-262-B1, 600-265-262-B5 & 600-265-262-C1

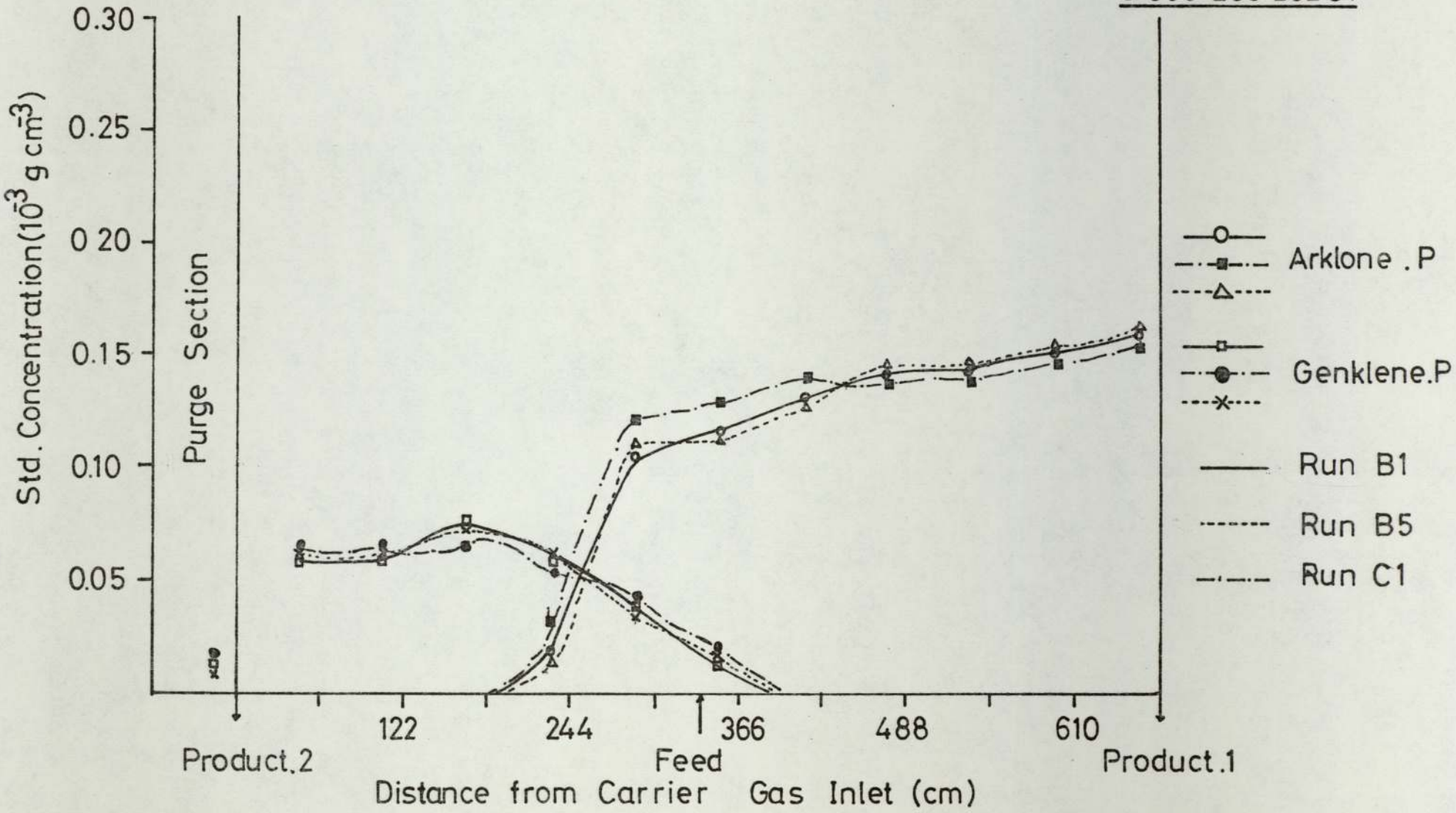

the manual operation of sampling requires a finite time which may vary by a second or more. The effect of any such error will be small unless at the time of sampling the concentration was changing rapidly in which case a significant error could be incurred.

Errors in the values of G_{mc} and S_{mc} will arise through fluctuations in the outlet column pressures. The inlet pressures to the separating and purge sections of the unit were accurately controlled, but outlet pressures could vary as much as ± 5 k.N m^{-2}. Combining this error together with the inherent rotameter calibration error, a possible total error of ± 2% in $G_{m.c}$ and $S_{m.c}$ may be possible.

No significant error was thought to result from the determination of L', as the sequencing time was accurately measured with a 10 second sweep stopwatch, and the weight of liquid phase in the unit had also been accurately determined. However, as results presented in Chapter 7 show, the weight of liquid phase within the SCCR1 unit had decreased from an initial 4.935 kg (25% loading) to 4.535 (23% loading), owing to the leaching effect of the liquid solutes. Consequently for the results presented in this chapter there may be a significant error in the calculation of $G_{m.c}/L'$ in the order of ± 8%.

6.3 The Investigation of Carrier Gas Flowrate and Sequencing Time

6.3.1 Results

The proposed experimental programme for this study had to be curtailed owing to mechanical limitations, with only three runs being able to be performed.

The calculated value of G_{mc}/L' ranged from 251 to 284 and although G_{mc}/L' should have remained constant at 265, this somewhat large deviation of G_{mc}/L' was not thought to have any effect upon the general conclusions drawn from the discussion in Section 6.3.2.

Sequencing times of 400, 300 and 250 seconds were selected and in keeping with an experimental G_{mc}/L' value of 265, the outlet carrier gas flowrates were maintained at 875, 1150 and 1275 $cm^3.s^{-1}$ respectively.

The criteria for selection of the purge gas rate was such that S_{mc}/L' always remained higher than the partition coefficient at infinite dilution of Genklene.P, thereby ensuring complete regeneration of the isolated column.

Computed results included values of the partition coefficients at the maximum recorded on-column concentration, along with maximum, and minimum values for G/L', and S/L'. The product purities quoted are simply a chromagraphically measured ratio of the two feed components, as sampled from the product exit lines. Sampling from the Product.1 stream was taken close to the end of a sequencing interval, whilst Product,2 was sampled soon after sequencing had occurred. Samples taken in this way will not only correspond to the maximum level of solute concentration in the respective streams, but also correspond to the maximum percentage of impurity.

A summary of experimental and computed results is shown in Table 6.4, with the respective concentration profiles given in Figure 6.4 to 6.6. These results are tabulated in more detail in Appendix 5, Figures A.5.1 to A.5.3.

6.3.2 Discussion

During a sequencing interval the main separating section operates as a conventional frontal elution chromatographic system. Plotting the concentration profile for two sampling times within that interval allows the progress of the respective profiles to be followed.

Both solutes travel in the direction of the Product.1 exit during a sequencing interval, with the advancement of the Arklone.P. profile being greater than that for Genklene.P., in keeping with their respective partition coefficients. Reproducibility of profiles during a sequencing interval should therefore be high, however, it is only from Run 300-265-250-A that the dynamic profile for the unit can be seen clearly to be advancing in a reproducible manner. The length of column in which both solutes are present, (i.e. length required for separation), increases from 122 cm for Run 300-265-250-A, to 183 cm for Run 300-265-400-A.

Purely from experimental observations it was apparent that increased efficiency was achieved at lower sequencing rates and that further runs in which the switching time was reduced below 250 seconds were required. To maintain a constant $G_{m.c}/L'$ ratio, a corresponding increase in carrier gas flow rate is required, as the sequencing interval is shortened, similarly the purge gas flow rate must also be increased. For Run 300-265-250-A the combined flow rates of purge and carrier gas were in excess of 12000 litres per hour and further increase in the total air supply was not permissable due to limitations on the capacity of the mains air compressor.

From a theoretical standpoint it seems logical to assume that an optimum sequencing interval exists. In Section 2.2.3.1 it was shown that an optimum carrier gas flowrate occurs giving a minimum value for H.E.T.P. and it would be a relatively simple matter to determine this flowrate and therefore the switching time required to achieve it. In practice however factors such as pressure drop and dilution of products influence the choice of carrier gas flowrate and only very rarely are chromatographs operated at the flowrate giving minimum H.E.T.P.(11).

In a similar practical investigation Liodakis (47) working at sequencing times of under 100 seconds for a 2.5 cm i.d. sequential unit has found that increased separating efficiency was achieved by increasing the sequencing interval and reducing the carrier gas flowrate. These results working at low sequencing times would tend to confirm that a parabolic relationship exists between separating efficiency and switching interval, although the minimum of this relationship may not correspond to minimum H.E.T.P.

In conclusion it can be said that with regard to the SCCR1 unit, improved separations will occur at lower sequencing intervals although mechanical limitations do not allow the unit to be operated at the optimum value switching time, I_s.

Table 6.4
The Study of the Sequencing Interval(I_s) at Constant $G_{m.c.}/L'$

Experimental Settings

Run Title	Solute Feed Rate	I_s	L'	P_a	T_a	Separating Section				Purge Section			
						G_a	P_{in}	P_{out}	G_{mc}/L'	S_a	P_{in}	P_{out}	S_{mc}/L'
	$cm^3 hr^{-1}$	s	$cm^3.s^{-1}$	$kN.m^{-2}$	°C	$cm^3.s^{-1}$	$kN.m^{-2}$	$kN.m^{-2}$		$cm^3.s^{-1}$	$kN.m^{-2}$	$kN.m^{-2}$	
300-265-400-A	325	399	1.063	101.0	16.5	875	378	186	284	1600	232	196	709
300-265-300-A	304	300	1.414	101.0	21.0	1150	403	187	267	2187	256	229	644
300 265 250 A	297	250	1.697	101.0	21.0	1275	406	168	251	2187	256	222	544

Computed Results

Run Title	K+ K_{max}		Sep^n Sect'		Purge Sect'		% Product Purity		Conc' Analysis Results in Appendix	Conc' Profile in Figure
	A.P	G.P	$\frac{G_{min}}{L'}$	$\frac{G_{max}}{L'}$	$\frac{S_{min}}{L'}$	$\frac{S_{max}}{L'}$	A.P	G.P		
300-275-400-A	165	488	221	447	655	776	>99.8	>99.7	A.5.1	6.4
300-275-300-A	139	397	204	439	610	682	>99.0	>99.9	A.5.2	6.5
300 275 250 A	136	397	187	452	508	587	>99.9	>99.9	A.5.3	6.6

Figure 6.4 Standardised Concentration Profile for Run 300-265-400-A

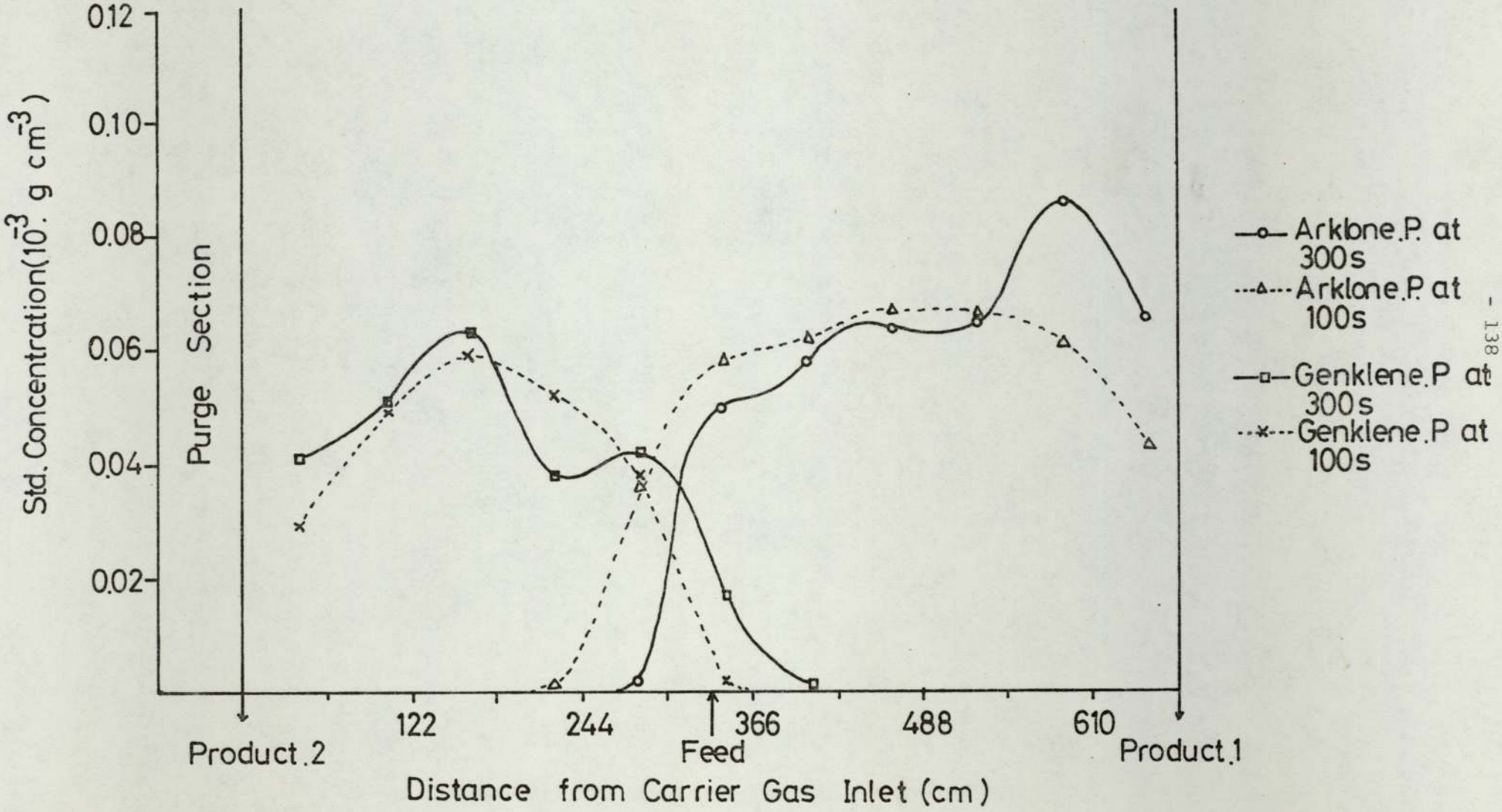

Figure 6.5 Standardised Concentration Profile for Run 300-265-300-A

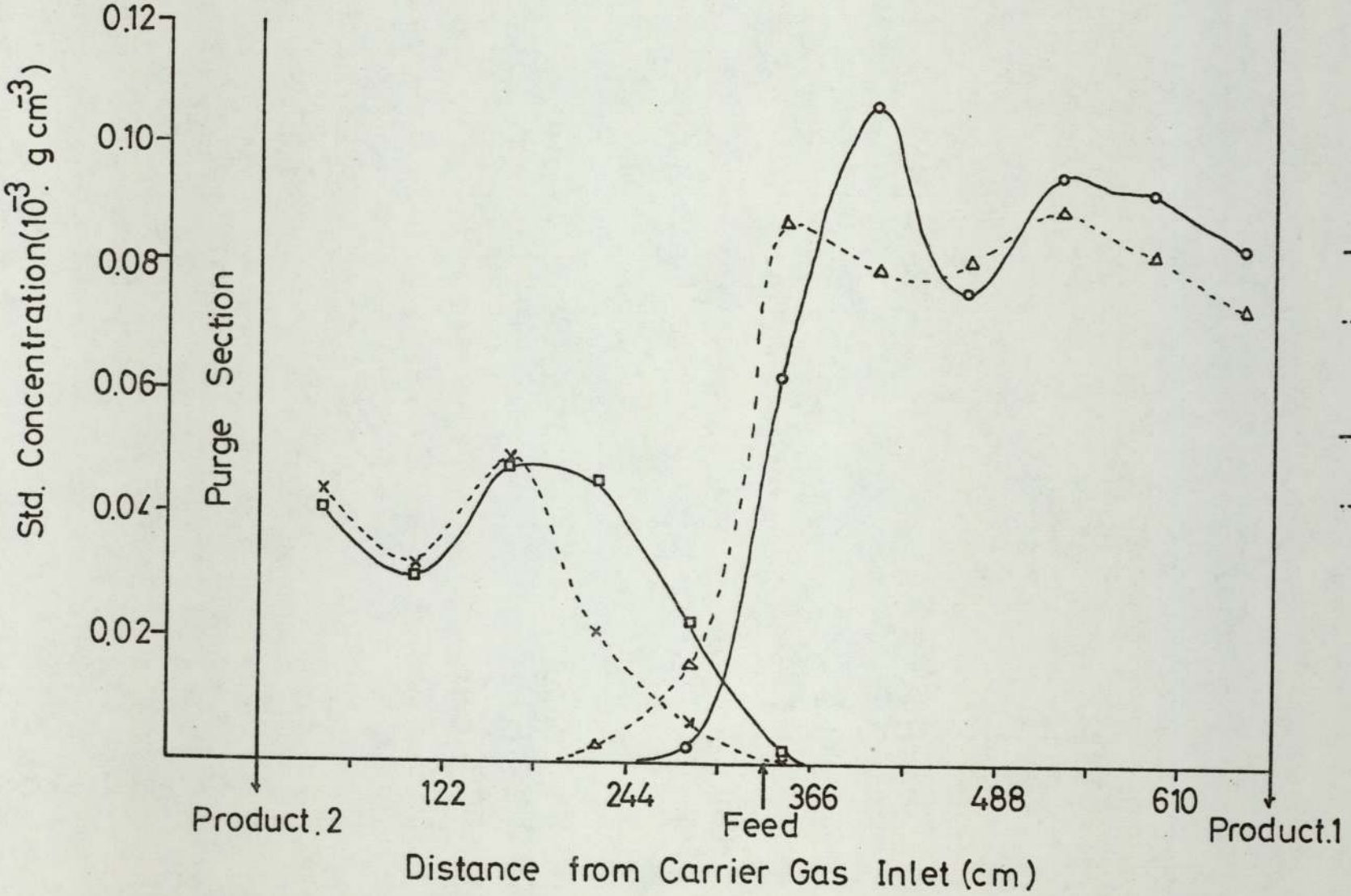

Figure 6.6 Standardised Concentration Profile for Run 300-265-250-A

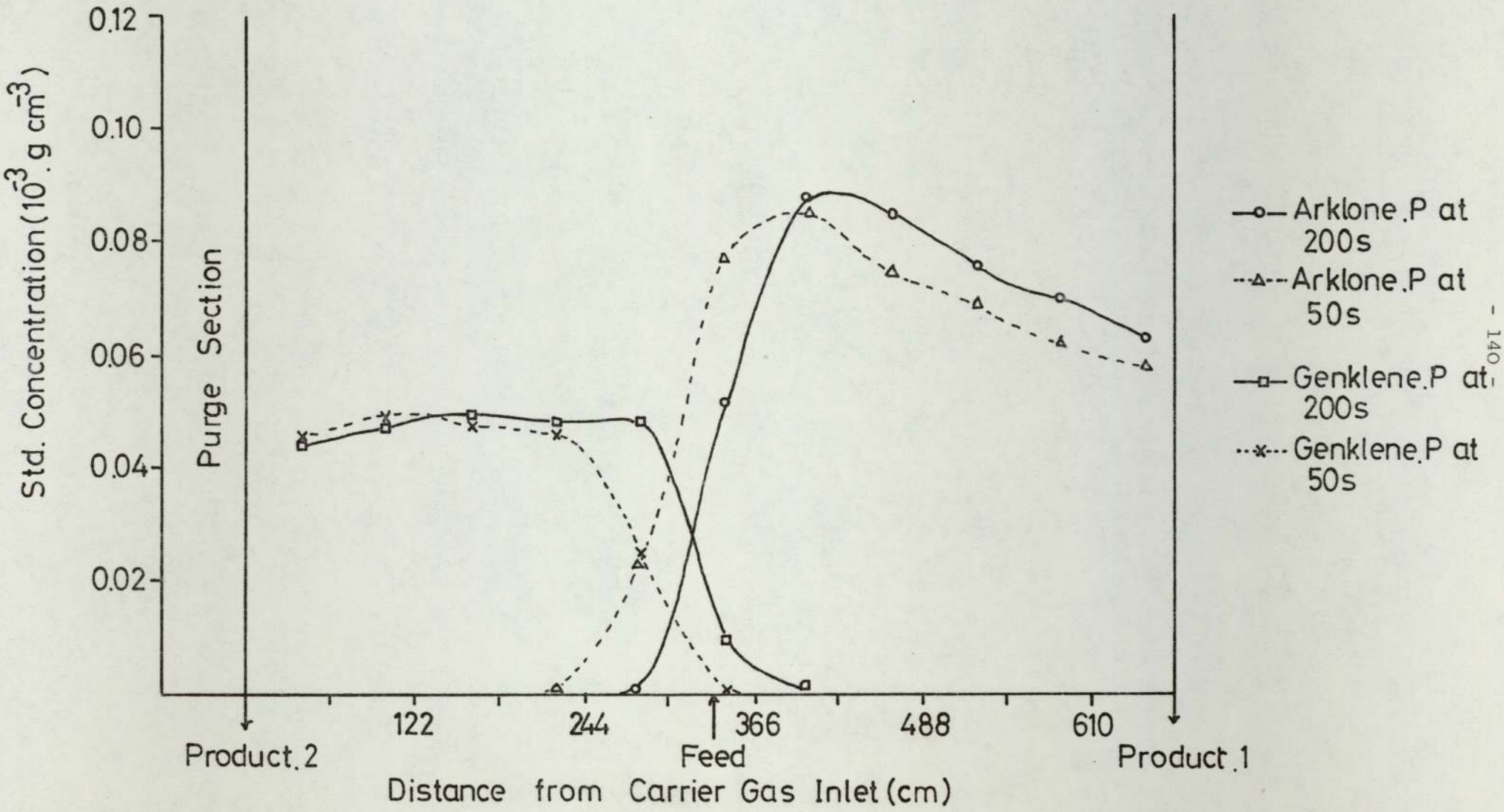

6.4 The Investigation of Feed Throughput

6.4.1 Results

Following the conclusions from the study of sequencing intervals it was decided to operate the chromatograph at as small a sequencing time as was practically possible. An interval of 262 seconds was selected, slightly above the minimum possible value, to allow for any fluctuations in the mains air supply.

The $G_{m.c}/L'$ ratio was again selected at 265 for all the feedrate investigations, and therefore to maintain $G_{m.c}/L'$ at 265 with a sequencing interval of 262 seconds, the carrier gas flowrate was set at 1275 $cm^3.s^{-1}$.

Starting at a feedrate of 400 $cm^3.hr^{-1}$ the feed throughput was increased at 100 $cm^3\ hr^{-1}$ intervals to a maximum of 1000 $cm^3.hr^{-1}$, after which point severe contamination of products occurred. Analytical samples were taken at times of 50 and 200 seconds after sequencing. Reproducibility of the profiles during a sequencing interval was good, with the only inconsistency being apparent in the samples taken from the bed prior to the isolated column. Samples taken in this bed at 50 seconds are of a lower concentration than those at 200 seconds owing to the fact that the advancing Arklone.P. profile has not had sufficient time to become fully developed. For clarity the concentration profile was plotted for one sample time only, that of 200 seconds.

Discussion will be limited to runs of 400,600,800,1000 $cm^3.hr^{-1}$, with the relevant data for these runs being given in Table 6.5, and the concentration profiles in Figures 6.7 to 6.10. The complete tabulated data for these runs along with data pertaining to intermediate runs of 500 and 700 $cm^3.hr^{-1}$, are given in Appendix 5, Figures A.5.4 to A.5.9.

6.4.2 Discussion

Comparison of the concentration profiles in Figures 6.7 to 6.10, show several well defined trends.

As the feedrate is increased from 400 to 1000 $cm^3.hr^{-1}$, the general level of the gas phase concentration for Arklone.P. rises accordingly. The trailing edge of the Arklone P. profile gradually extends in the direction of the isolated column, until in Run 1000-265--262-A the Arklone.P. begins to contaminate the Product.2 stream. The tendency for the Arklone.P. profile to move towards the isolated column is consistent with an anti-Langmuir adsorption isotherm, for which the preference of the solute for the solvent phase increases with increasing concentration.

A description of the Genklene.P. profile is somewhat more difficult. In all the feedrate runs the profile did not extend more than 61 cm; i.e. one column length, in front of the feed point. This observation should have indicated that Product.1 purity would be very high for all of the runs. Although Product.1 purity was in excess of 99.9% for Runs 400-265-262-A and 600-265-262-A, it had dropped to 99.9% for Run 1000-265-262-A, and for an unrecorded run at a feedrate of 1100 $cm^3.hr^{-1}$ indications were that Product.1 purity was below 95%. The conclusions drawn from these observations was that the purging process was not being successful at high feedrates even though the purge gas flowrate was at least 50% higher than the flowrate needed to obey the inequality $S_{min}/L' > (k^{\infty} + \Delta K_{max})_{G.p.}$ This relationship theoretically guaranteeing total removal of products from the isolated column.

The level of concentration of the Genklene.P. profile is of particular interest. Averaging 0.05 x 10^{-3} $g.cm^{-3}$ for Run 400-265-262-A, the gas phase concentration does not change appreciably for any run up to and including Run 1000-265-262-A, at which point the feedrate is 250% higher. It is to be expected that the general level of Genklene.P. concentration will be lower than that of Arklone.P. owing to the Genklene.P. having a higher partition coefficient, but the general level of Genklene.P. gas phase concentration was expected to rise with increasing feedrate, as was the case with the Arklone.P. profile.

In attempting to explain this paradoxical situation where the gas phase concentration for Genklene.P. appeared to be independent of its own feedrate the possibility that all of the Genklene.P. liquid feed stock was not being evaporated was investigated. Once the partial pressure of Genklene.P. approaches the saturated vapour pressure value, further increase in the level of gas phase concentration is impossible. Calculations of the partial pressures of Genklene.P. (see for example Appendix 4, Figure A.4.2), for various positions in the chromatograph, appeared to be well below the value for the saturated vapour pressure (s.v.p.) of Genklene.P. measured at ambient temperature. However, if the air passing through the feed zone was cooled sufficiently the s.v.p. would be reduced accordingly so that the maximum permissible gas phase concentration may not be large enough to ensure that all the Genklene.P. entering the unit as liquid was evaporated.

If it could be shown that the air temperature was low enough to prevent total evaporation of the feedstock the unexpected results concerning the Genklene.P. concentration profile could be better interpreted in that firstly the apparent independence of gas phase

was in fact saturated with Genklene.P. due to the low temperature. Secondly, advancement of the Genklene.P. profile in the direction of carrier gas flow would be unlikely as the partition coefficient would be significantly increased because of its inverse relationship with the absolute temperature. Finally the failure of the purging process at high feedrates could be explained in that not only would the Genklene.P. adsorped in the liquid solvent phase have to be removed, but also an amount of unvaporised feed. Evaporation and desorption both being endothermic thermodynamic processes would tend to cool the purge bed, and if the temperature drop was sufficient then the partition coefficient value of Genklene.P. may increase so that $(K^{\infty} + \Delta K_{max})_{G.P.}$ becomes greater than S_{min}/L' and hence complete purging becomes impossible.

Unevaporated Arklone.P. is also a possibility, and it may be that the advancement of the Arklone.P. profile in the direction of the isolated column is not only due to the effect of an anti-Langmuir absorption isotherm but also to liquid Arklone.P. being transferred in that direction after every sequencing interval of the unit. The presence of any unevaporated feed within the unit will contain a much higher proportion of Genklene.P., as Arklone.P. has a higher s.v.p. and will therefore preferentially evaporate.

Concluding this part of the study on changes in feedrate, a maximum throughput of 1000 $cm^3.hr^{-1}$ was achieved, but this limit was not thought to be controlled by any chromatographic limitations of the SCCR1 unit, but more to the combined effects of temperature and non evaporation of the liquid feedstock.

Table 6.5

The Study of Feedrate

Experimental Settings

Run Title	Solute Feed Rate	I_s	L'	P_a	T_a	Separating Section				Purge Section			
						G_a	P_{in}	P_{out}	G_{mc}/L	S_a	P_{in}	P_{out}	S_{mc}/L
	$cm^3 hr^{-1}$	s	$cm^3 s^{-1}$	$kN m^{-2}$	°C	$cm^3 s^{-1}$	$kN m^{-2}$	$kN m^{-2}$		$cm^3 s^{-1}$	$kN m^{-2}$	$kN m^{-2}$	
400-265-262-A	402	256	1.657	100.0	20.5	1275	407	152.5	260	2300	259	225	579
600-265-262-A	596	262	1.619	100.0	21.4	1275	407	152.5	266	2300	259	225	592
800-265-262-A	808	262	1.619	101.0	23.0	1275	407	152.5	266	2600	259	232	660
1000-265-262-A	1015	262	1.619	101.0	22.0	1275	407	152.5	267	2850	259	232	723

Computed Results

Run Title	$K^{\infty} \div K_{max}$		Sepn' Sect'		Purge Sect'		% Product Purity		Conc' Analysis Results in Appendix	Conc' Profile in Figure
	A.P	G.P	$\frac{G_{min}}{L'}$	$\frac{G_{max}}{L'}$	$\frac{S_{min}}{L'}$	$\frac{S_{max}}{L'}$	A.P	G.P		
400-265-262-A	139	414	189	504	540	617	>99.9	>99.8	A.5.4	6.7
600-265-262-A	131	399	193	516	549	632	>99.9	>99.7	A.5.6	6.8
800-265-262-A	126	375	195	527	626	699	>99.8	>99.8	A.5.8	6.9
1000 265 262 A	131	382	196	521	686	766	>99.6	>99.6	A.5.9	6.10

Figure 6.7 Standardised Concentration Profile for Run 400-265-262-A

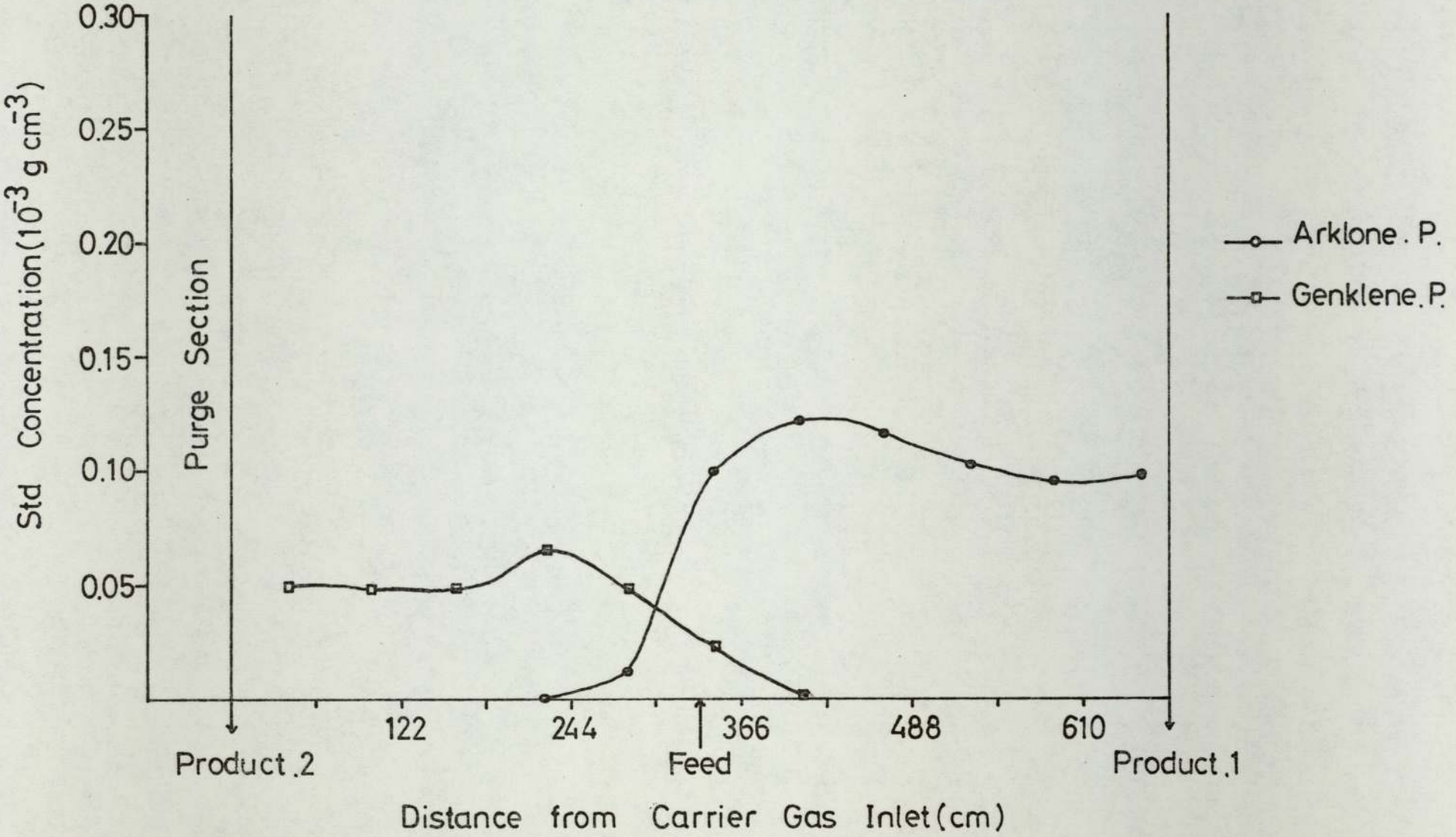

Figure 6.8 Standardised Concentration Profile for Run 600-265-262-A

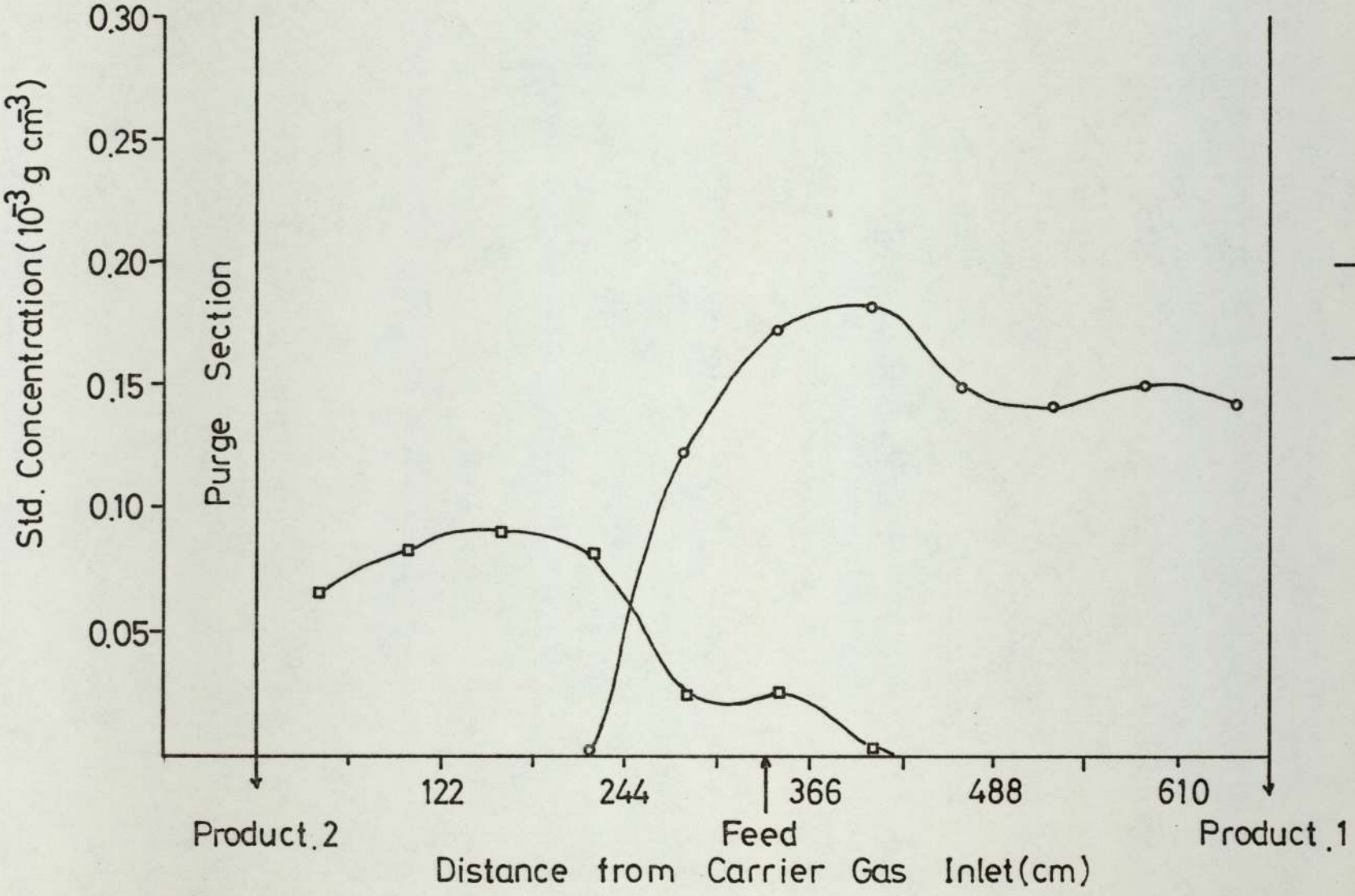

Figure 6.9 Standardised Concentration Profile for Run 800-265-262-A

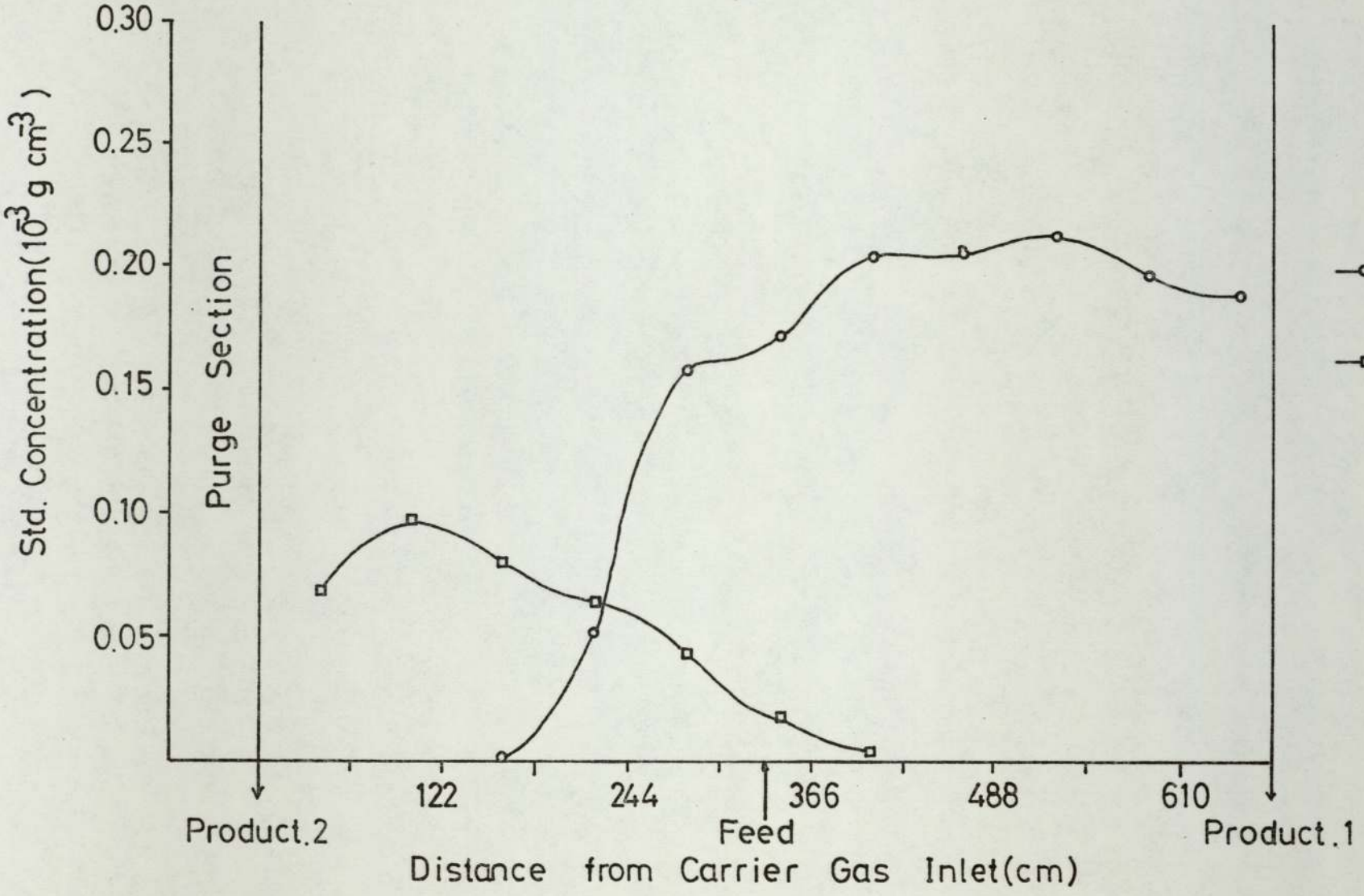

Figure 6.10 Standardised Concentration Profile for Run 1000-265-262-A

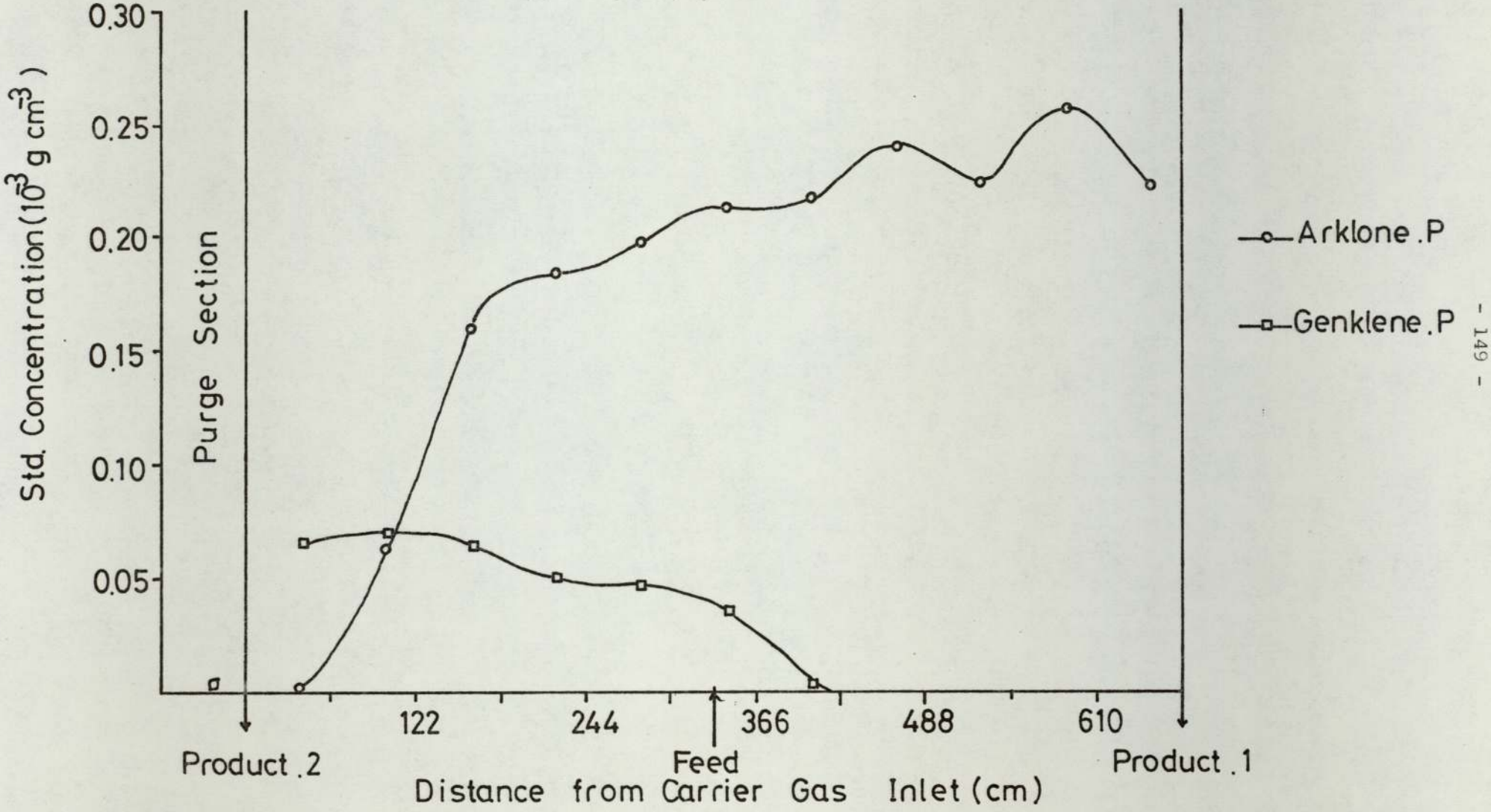

6.5 Investigation of the Temperature Distribution

6.5.1 Column to Column Temperature Profile

The construction of a temperature profile is similar to the production of a concentration profile in that the temperature is recorded at a fixed point in the unit, at a set time after each sequencing of the port functions. Again, this method of recording is equivalent to recording the temperature in all twelve columns at the same instant. If several thermocouples are positioned in the column and their temperatures recorded at the same instant a composite picture of the radial and axial temperature gradients can be built up. At any one time it was only possible to record from eight thermocouples. As two of these were continually monitoring the inlet gas and ambient temperature the temperature within the bed was followed by the remaining six thermocouples.

More than six positions within the column were required to obtain the composite profiles and therefore after a particular cycle of operation in which recordings were taken, the six thermocouples would be moved to other locations within the bed and a further set of results tabulated during the next cycle of operation. This procedure was repeated until an equivalent of 49 locations had been scanned within the bed.

The validity of the experimental method depended upon reproducibility of the temperature profile, not only between successive cycles of operation but also between successive runs. During operation of the SCCR1, gas samples were continually analysed and if the concentration profiles were perfectly matched it was assumed that the temperature profile also matched.

6.5.2 Definition of Ambient Temperature

To study the temperature distribution within the chromatograph arising from the effects of absorption, desorption and evaporation, it was necessary to eliminate any thermal effects resulting from changes in temperature of the inlet carrier and purge gases, along with fluctuations in the ambient temperature.

The inlet gas temperatures were closely related to ambient temperature as the mains air passed through a large surge tank prior to entry into the SCCR1. A pseudo ambient temperature was defined simply as being the arithmetic mean of the ambient and inlet gas temperatures, and all measurements recorded within the bed were made relative to this pseudo-ambient temperature, hence the effects of changes in temperature of the ambient atmosphere or inlet gas temperatures were minimised.

Two further sources of error may be that the expansion of the carrier gas as it passes around the unit could lead to cooling. Secondly the electrically operated solenoid valves become heated and may transfer a significant amount of heat to the gas. The effects of the above two possibilities were investigated by running the unit under operational gas flow rates but without the introduction of any feedstock. Figure 6.11 gives a graphical portrayal of the results. A cyclic pattern is noticeable with the carrier gas always leaving the column cooler than it enters. In passing through the transfer lines between columns it can be seen that the gas absorbs heat and warms slightly. After passing through all eleven columns the carrier gas has cooled approximately $0.3^{\circ}K$. Although the cyclic effect is a real effect, the temperature changes are only fractions of one degree centigrade, and therefore the phenomena giving rise to these perturbations will

have no significant effect upon the temperature profile when the halocarbon solutes are present.

6.5.3 Estimation of Experimental Error

Prior to presenting and discussing the results obtained from the study of temperature, they must first be put into perspective by an estimation of their accuracy.

At best under strict laboratory conditions temperatures recorded by thermocouples can only be measured to ± 0.2°K. Further recording errors incurred by the digital volt meter will be small as it is quoted as being accurate to within 1 microvolt at 20°C which for the scale of operation during these studies is equivalent to ± 0.03°K

More serious errors are however inherent in the experimental method. The perturbations occurring as pure carrier gas flows around the unit, Section 6.5.2, can lead to errors of ± 0.3°K. Another source of fluctuation will arise from the changing of inlet carrier gas and ambient air temperatures, but correction of the experimental results by the definition of a pseudo-ambient temperature will greatly reduce this error.

The assumption of a reproducible temperature profile between each cycle may lead to errors when results taken from different cycles of operation are combined together on one profile. Finally results are taken at a specific time after the sequencing action and if the temperature was changing rapidly at the time of recording, a significant error could occur.

Considering the actual temperature recorded by the thermocouple an error of no more than ± 0.3°K will be incurred. Transposing the results into a profile that can be readily interpreted leads to far greater errors as outlined above, and the graphical results can only

be quoted to an accuracy of ± 1.5°K.

6.5.4 Temperature and Feedrate for Arklone.P. and Genklene.P.

6.5.4.1 Results

The positions of the thermocouples are referenced to the top of column No.1. As the number of sample points per column varied, Section 3.3.1, the column possessing the greatest number of access points was chosen, (No.1), for the insertion of the thermocouples. Longitudinally the thermocouples could be positioned at distances of 7.6; 15.2; 22.9; 30.5; 38.1; 45.7 and 53.3 cm from the top of the column, whilst radially distances of 3.8; 2.5; 1.3 and 0.0 cm from the inside column wall, were used. 3.8 cm from the column wall corresponding to the column axis.

As results could be taken from different cycles of operation of the same run, a further digit was required in the 'run title' for uniqueness, signifying from which cycle after equilibrium the results were taken.

A $G_{m.c}/L'$ ratio of 265 was maintained for all runs along with a sequencing interval of 262 seconds. Equivolume mixtures of Arklone.P. and Genklene.P. were again used for study at combined throughputs of 400, 600 and 800 $cm^3.hr^{-1}$. Summaries of the results required to build up a temperature profile for the above feedrates are given in Tables 6.6 to 6.8. Experimentally measured millivoltages and corrected temperatures corresponding to the above runs are given in Appendix 5, Figures A.5.10 to A.5.24.

6.5.4.2 Discussion

The most striking observation from the investigation was the scale of temperature fluctuations. Studying of temperature profiles in a continuous chromatograph has not been attempted previously and hence the literature available appertains to the work done with batch columns. Hupe et al (72) have recorded deviations of up to $7^{o}K$ below ambient, and it was to be expected that continuous operation would in certain cases lead to greater changes. Temperatures greater than $15^{o}K$ below ambient were regularly recorded in the SCCR1, and in one case for Run 800-265-262-E1 a temperature of $26.3^{o}K$ below ambient was recorded for the purge column. It is interesting to note that at this latter temperature the K^{∞} values for Arklone.P. and Genklene.P. are 1150 and 360 respectively, values three times greater than at ambient temperature. Under these conditions it is hardly surprising that complete purging of the isolated column was proving difficult.

Figures 6.12 to 6.15, give the temperature profiles for a feedrate of 400 $cm^{3}.hr^{-1}$, at sample times 200 seconds after sequencing. All the major depressions in temperature, with one exception occur behind the feed bed, the exception being the Product.1. outlet column. The minimum temperatures in the separating section were always recorded in the region around the feed distributor, though not at the column axis. The fact that minimum temperatures are found at distances between 1.3 and 2.6 cm from the column wall can be understood with consideration of the feed distributor design. Figure 3.6 shows that liquid feed is injected at four points within the column, approximately 2.0 cm from the wall.

Major depressions in temperatures ($>-8^{o}K$) extend for three columns behind the feed column (i.e. 122-305 cm), indicating the

probability that liquid feed is present in at least two of these columns. Total evaporation of the feed appears to be accomplished in the 3rd or 4th column behind the feed when the temperature returns to ambient.

A further sharp drop in temperature was recorded in the first column of the separating section (i.e. 0-61 cm). This drop is unrelated in any way to evaporation and is the result of the trailing edge of the Genklene.P. concentration profile travelling through the column.

The isolated column, (671-732 cm), also shows a region of low temperature. The net thermodynamic process in the purge bed is one of desorption and therefore a large negative heat flow is to be expected.

Columns in front of the feed column, (366-671 cm), exhibit comparatively small fluctuations in temperature as they are unable to experience any vaporisation effects. The level of Arklone.P. concentration remains stable throughout these columns and therefore any heat effects resulting from absorption and desorption of the advancing profile will cancel out. A small column to column fluctuation is recorded but this may be attributed to the gas expansion and solenoid value heating effects described in Section 6.5.2.

The last column in the separating section (610-671 cm), does however show a sharp fall in temperature. The reason for this is that in the previous sequencing interval this column in question was the isolated bed undergoing the endothermic desorption process. A finite time is required for the column to regain ambient temperature and therefore the column will remain 'cold' for a certain time after sequencing.

In common with the concentration profile, the temperature profile resulting purely from absorption and desorption should advance through the column during a sequencing interval. Figure 6.16 shows the temperature profile for the thermocouples positioned at the column axis, recorded 50 seconds after sequencing, and can be compared with Figure 6.12, for the same thermocouples recorded at 200 seconds after sequencing. The region of negative temperature in the isolated column is shown clearly to be advancing through the column. After 50 seconds the column receiving feed, (305-366 cm), has not yet begun to experience any cooling through evaporation and this only becomes apparent on the readings at 200 seconds.

The most striking comparison is that in the three columns behind the feed bed, (122-305 cm),the regions of extreme 'cold' do not change position, always remaining around the feed points, indicating a none chromatographic process which can only be attributed to the effects of vaporisation in the aforementioned columns.

The temperature profiles for feed rates of 600 and 800 $cm^3.hr^{-1}$ are given in Figures 6.17 to 6.26. The minimum recorded temperatures for the above runs are again centered around the feed points, although these minimum temperatures do not noticably increase with increasing feed rate. This probably indicates that even at feedrates as low as 400 $cm^3 hr^{-1}$ the carrier gas is saturated and therefore the rate of evaporation is constant for all feed rates above 400 $cm^3\ hr^{-1}$. Hence lower temperatures would not be expected even though the feedrate is increased. For the profiles relevant to 400 $cm^3\ hr^{-1}$ the regions of 'low' temperature extend for three columns behind the feed bed. However for solute feedrates of 600 and 800 $cm^3.hr^{-1}$, it can be seen

that the depressions in temperature are experienced in all columns behind the feed bed, (0-305 cm), indicating that unvaporised liquid is present in all these beds. Further evidence that 'free liquid' is present up to and including the isolated column can be seen from Figure 6.23, the profile for thermocouples positioned at 2.6 cm from the column wall with a feedrate of 800 $cm^3 hr^{-1}$. Minimum temperatures in the separating section where vaporisation is taking place are approximately -14 to $-18^{\circ}K$. In the isolated column the temperature drops to $-26^{\circ}K$, Figure 6.23, at certain positions. This sudden drop may be attributed to the fact that the purge gas flowrate is over twice the carrier flowrate and therefore the rate of vaporisation of any remaining liquid feed within the purge column will be higher than for any position within the separating section, with the resultant further reduction in temperature.

In obtaining Figures 6.12 to 6.26 the results from the equivalent of 49 thermocouple positions in the column were recorded. This number of different locations allows the construction of an isothermal diagram. Figure 6.27 show for a feedrate of 600 $cm^3 hr^{-1}$ the distribution of temperature within the columns when the SCCR1 unit is operating under equilibrium conditions. Very noticable is the length of the unit that is operating below $-5^{\circ}K$, with eight columns continuously experiencing temperatures below $-10^{\circ}K$. The very poor thermal conductivity of the packing giving rise to low radial heat conduction is shown clearly in column No.6, (244-305 cm), where at a position two thirds of the way down the column a constant temperature different of $20^{\circ}K$ exists between the column wall and a position 2.6 cm from the wall.

Table 6.6 Summary of Results for the Temperature Profile, at a Feedrate of 400 $cm^3 hr^{-1}$

Run Title	Solute Feed Rate	I_s	$G_{m.c}/L'$	T_{amb}	Inlet Gas Temp	Position of Thermocouples															
						TC1		TC2		TC3		TC4		TC5		TC6		TC7		TC8	
						A	R	A	R	A	R	A	R	A	R	A	R	A	R	A	R
	$cm^3 hr^{-1}$	s		°C	°C	cm	cm	cm	cm	cm	cm	cm	cm	cm	cm	cm	cm	cm	cm	cm	cm
400-265-262-B1	402	261	262	23.6	24.9	30.5	0.0	Carrier Inlet		Purge Outlet		45.7	3.8	53.3	0.0	53.3	1.3	Ambient		\	
400-265-262-C1	408	262	266	22.0	22.1	30.5	1.3	38.1	1.3	38.1	0.0	45.7	2.5	53.3	2.5	53.3	3.8	Carrier Inlet		Ambient	
400-265-262-C3	408	262	266	22.0	21.8	22.9	1.3	30.5	2.5	38.1	3.8	38.1	2.5	45.7	0.0	45.7	1.3	"		"	
400-265-262-D1	405	262	267	23.2	23.4	7.6	1.3	7.6	0.0	15.2	0.0	22.9	3.8	22.9	2.5	30.5	3.8	"		"	
400 265 262 D3	405	262	267	23.4	23.3	7.6	3.8	7.6	2.5	15.2	3.8	15.2	2.5	15.2	1.3	22.9	0.0	"		"	

TC1, TC2 ... = Thermocouple N° 1, 2 ... etc

A = Axial Distance from Top of Column

R = Radial Distance from Column Wall

Table 6.7 Summary of Results for the Temperature Profile at a Feedrate of 600 $cm^3 hr^{-1}$

Run Title	Solute Feed Rate	I_s	$G_{m.c}/L'$	T_{amb}	Inlet Gas Temp	Position of Thermocouples															
						TC1		TC2		TC3		TC4		TC5		TC6		TC7		TC8	
						A	R	A	R	A	R	A	R	A	R	A	R	A	R	A	R
	$cm^3 hr^{-1}$	s		°C	°C	cm	cm	cm	cm	cm	cm	cm	cm	cm	cm	cm	cm	cm	cm	cm	cm
600-265-262-B1	601	262	269	23.5	23.6	7.6	3.8	7.6	2.5	15.2	3.8	15.2	2.5	15.2	1.3	22.9	0.0	Carrier Inlet		Ambient	
600-265-262-B3	600	262	269	23.5	23.6	7.6	1.3	7.6	0.0	15.2	0.0	22.9	3.8	22.9	2.5	30.5	3.8	"		"	
600-265-262-B5	602	262	265	23.4	23.5	22.9	1.3	30.5	2.5	38.1	3.8	38.1	2.5	45.7	0.0	45.7	1.3	"		"	
600-265-262-C1	598	262	267	21.5	21.5	30.5	1.3	38.1	1.3	38.1	0.0	45.7	2.5	53.3	2.5	53.3	3.8	"		"	
600-265-262-C3	598	262	268	21.3	24.4	30.5	0.0	Carrier Inlet		Carrier Outlet		45.7	3.8	53.3	0.0	53.3	1.3	"		"	

TC1, TC2... = Thermocouple N° 1, 2... etc

A = Axial Distance from Top of Column

R = Radial Distance from Column Wall

Table 6.8 Summary of Results for the Temperature Profile at a Feedrate of 800 $cm^3 hr^{-1}$

Run Title	Solute Feed Rate	I_s	$\frac{G_{mc}}{L'}$	T_{amb}	Inlet Gas Temp	Position of Thermocouples															
						TC1		TC2		TC3		TC4		TC5		TC6		TC7		TC8	
						A	R	A	R	A	R	A	R	A	R	A	R	A	R	A	R
	$cm^3 hr^{-1}$	s		°C	°C	cm	cm	cm	cm	cm	cm	cm	cm	cm	cm	cm	cm	cm	cm	cm	cm
800-265-262-B1	795	262	264	23.6	24.3	7.6	3.8	7.6	2.5	15.2	3.8	15.2	2.5	15.2	1.3	22.9	0.0	Carrier Inlet		Ambient	
800-265-262-C1	790	261	265	21.1	21.1	7.6	1.3	7.6	0.0	15.2	0.0	22.9	3.8	22.9	2.5	30.5	3.8	"		"	
800-265-262-D1	807	263	268	22.1	23.9	22.9	1.3	30.5	2.5	38.1	3.8	38.1	2.5	45.7	0.0	45.7	1.3	"		"	
800-265-262-E1	804	262	266	23.4	25.2	30.5	1.3	38.1	1.3	38.1	0.0	45.7	2.5	53.3	2.5	53.3	3.8	"		"	
800-265-262-E3	802	262	266	24.4	25.1	30.5	0.0	Carrier Inlet		Ambient		45.7	3.8	53.3	0.0	53.3	1.3	\		\	

TC1, TC2... = Thermocouple N° 1, 2...etc

A = Axial Distance from Top of Column

R = Radial Distance from Column Wall

Figure 6.11 Temperature Profile in the Absence of any Feed Solutes

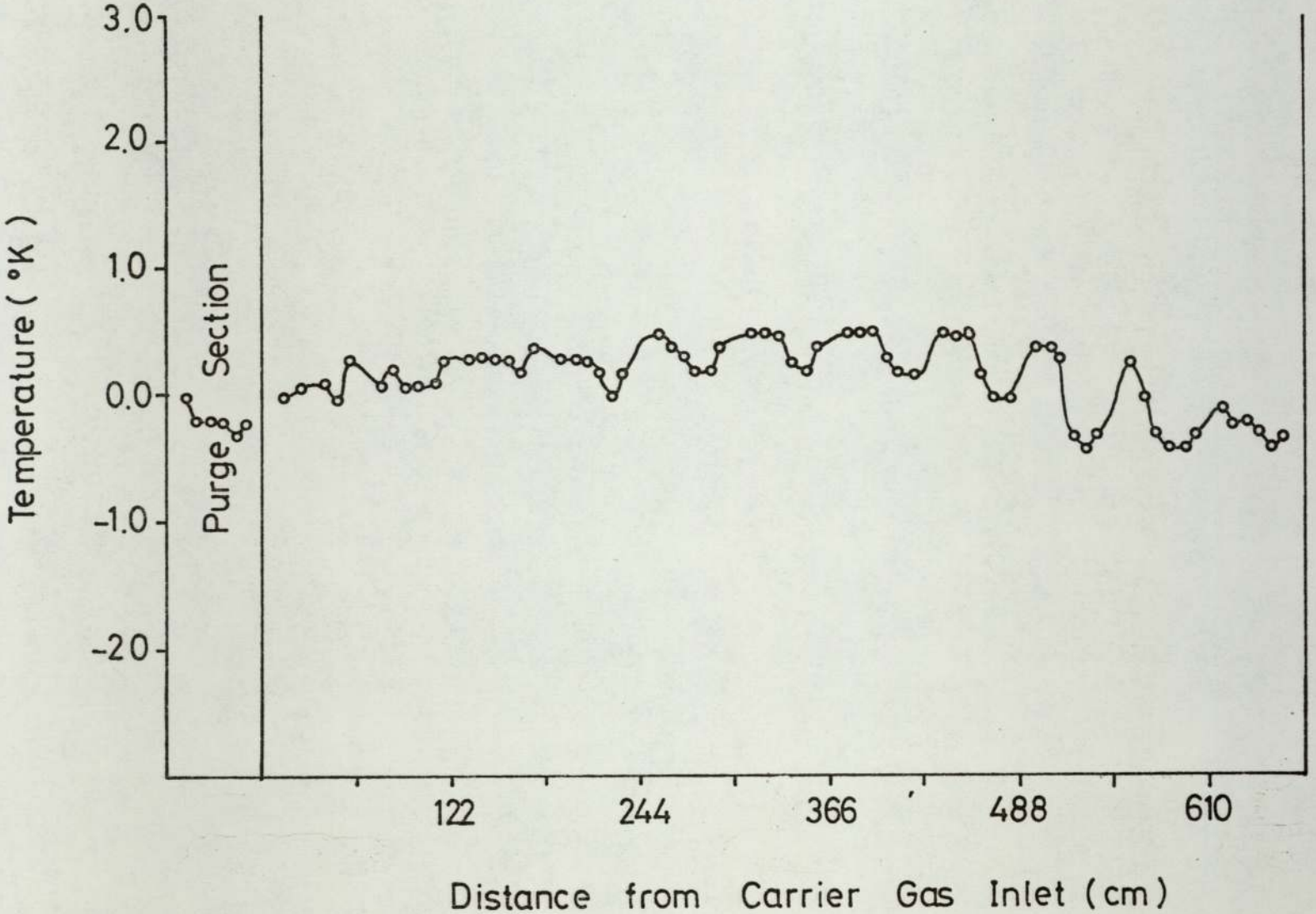

Figure 6.12 Temperature Profile for a Feedrate of 400cm^{3}hr^{-1} (TC's 3.8cm into Column)

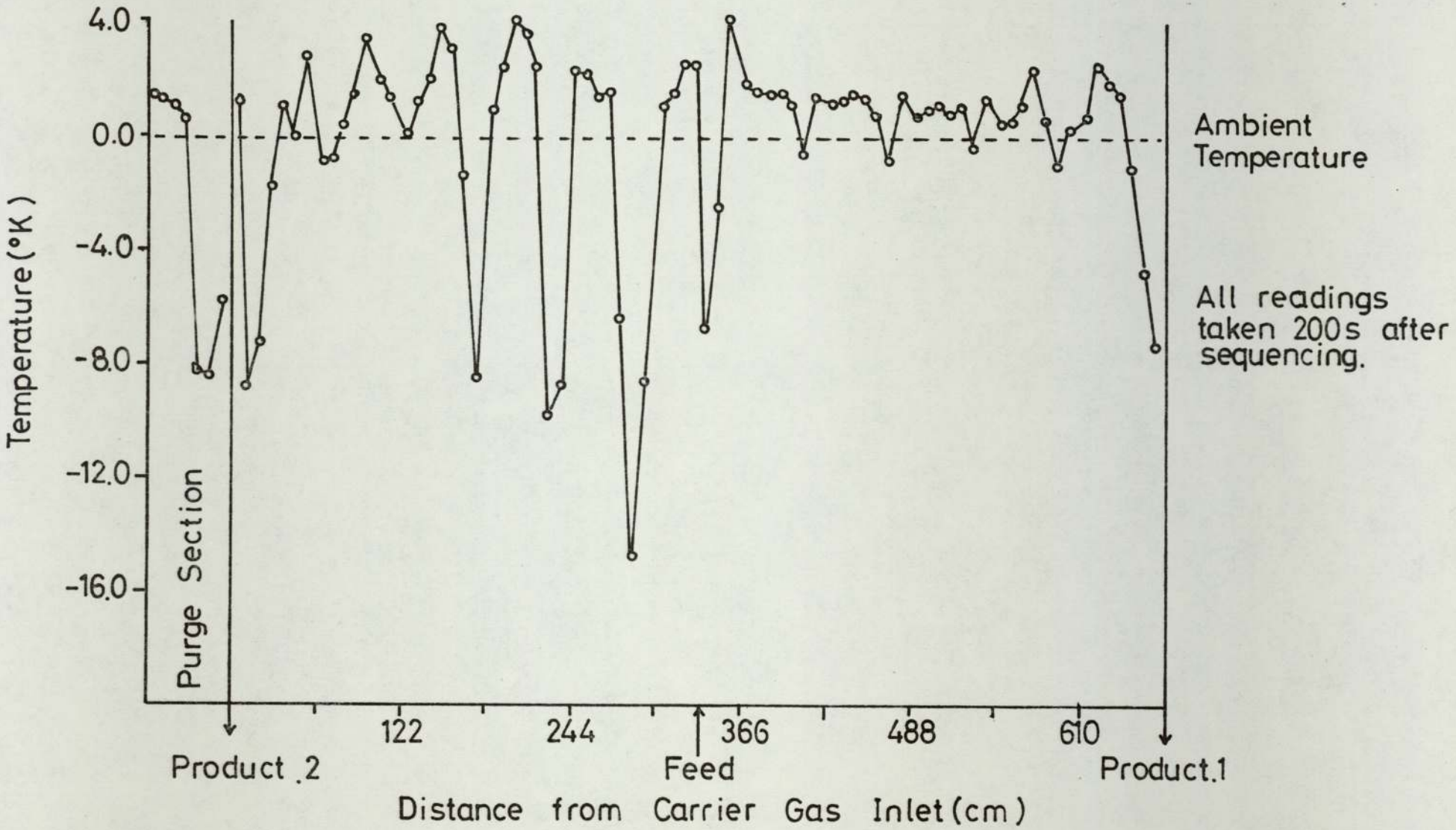

Figure 6.13 Temperature Profile for a Feedrate of 400 $cm^3 hr^{-1}$ (TC's 2.5 cm into Column)

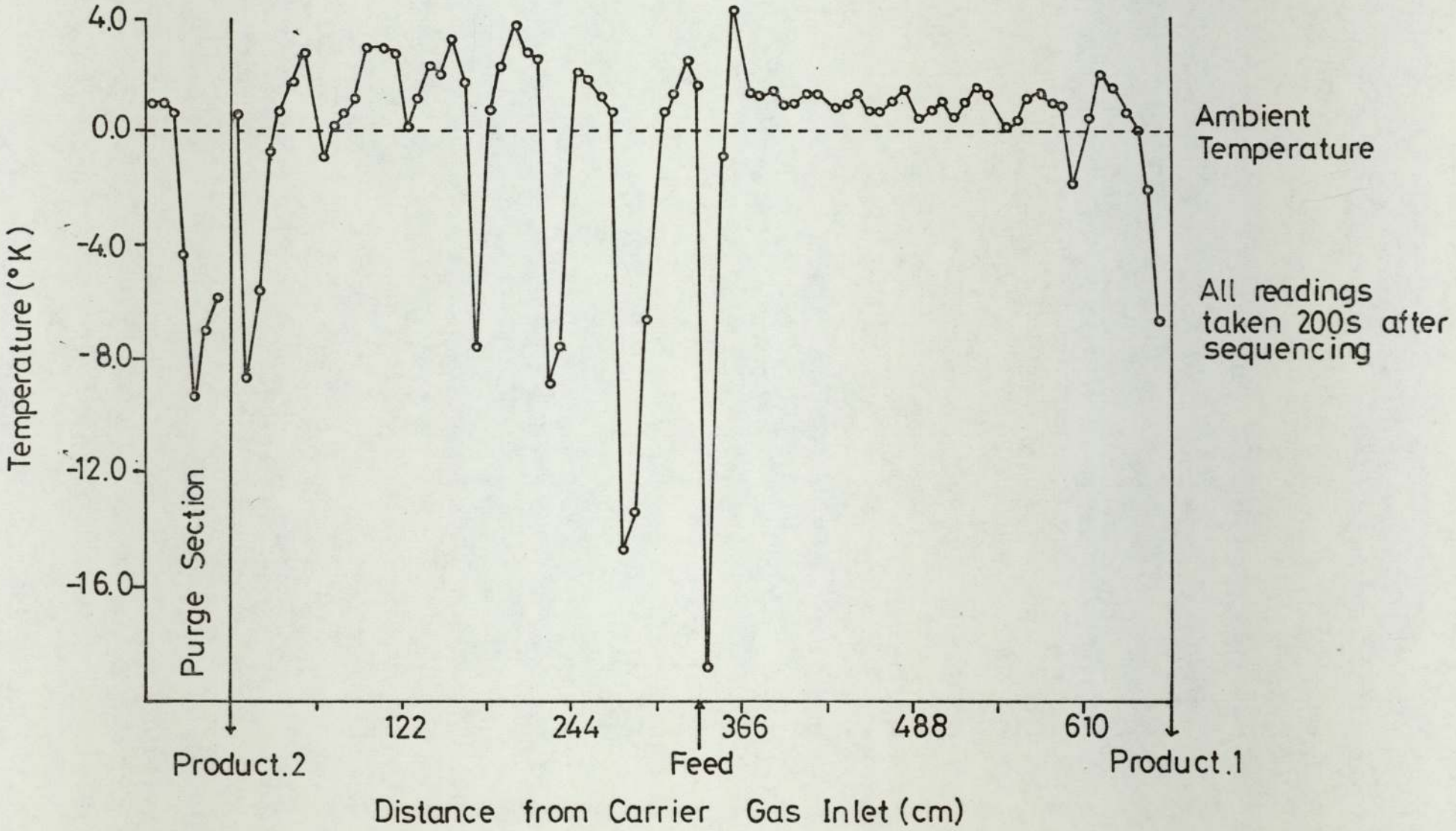

Figure 6.14 Temperature Profile for a Feedrate of 400 $cm^3 hr^{-1}$ (TC's 1.3 cm into Column)

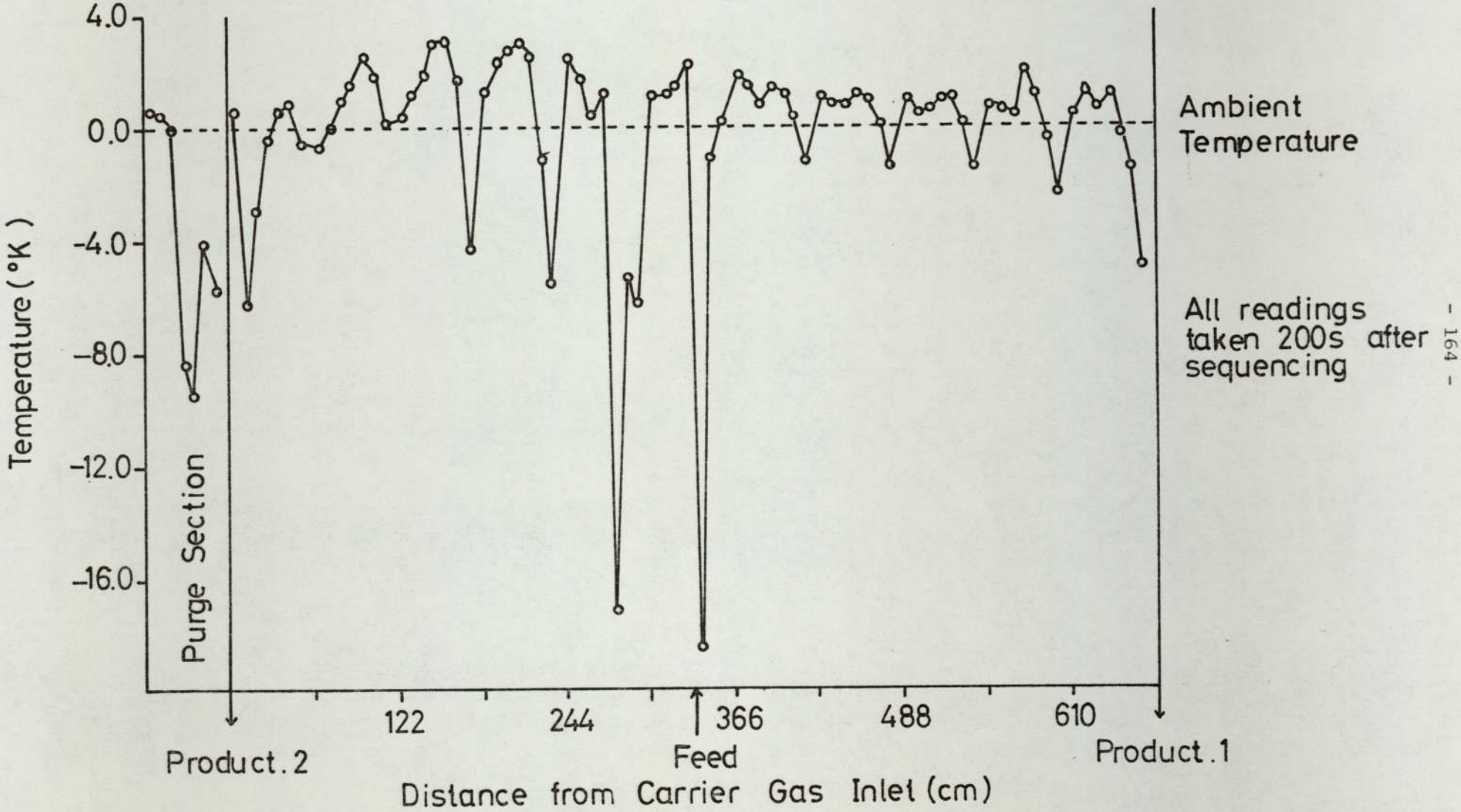

Figure 6.15 Temperature Profile for a Feedrate of 400 $cm^3 hr^{-1}$ (TC's at Column Wall)

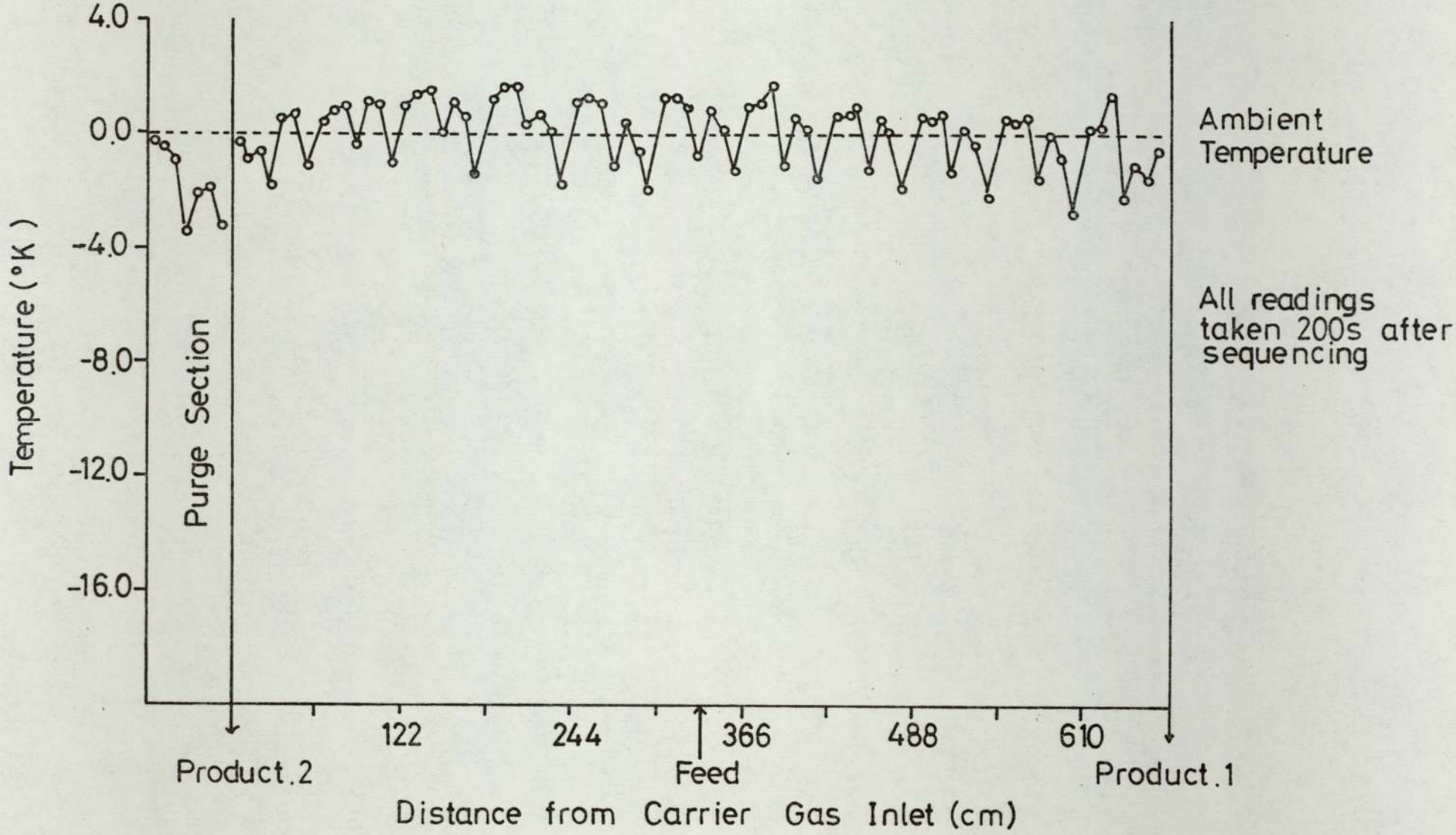

Figure 6.16 Temperature Profile for a Feedrate of 400 cm^3 hr^{-1} (TC's at 3.6 cm into Column)

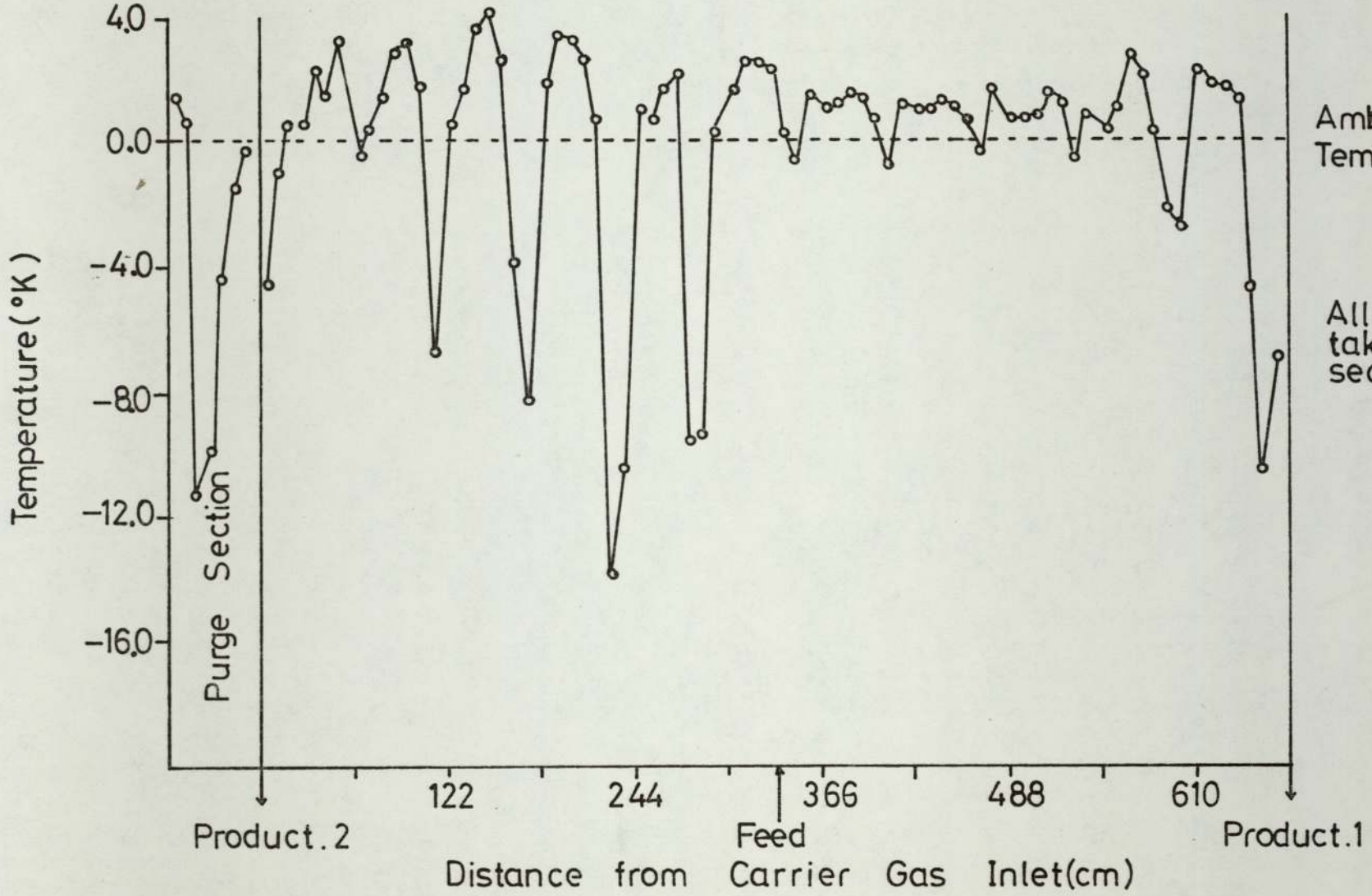

Figure 6.17 Temperature Profile for a Feedrate of 600cm^{3}hr^{-1}(TC's 3.6cm into Column)

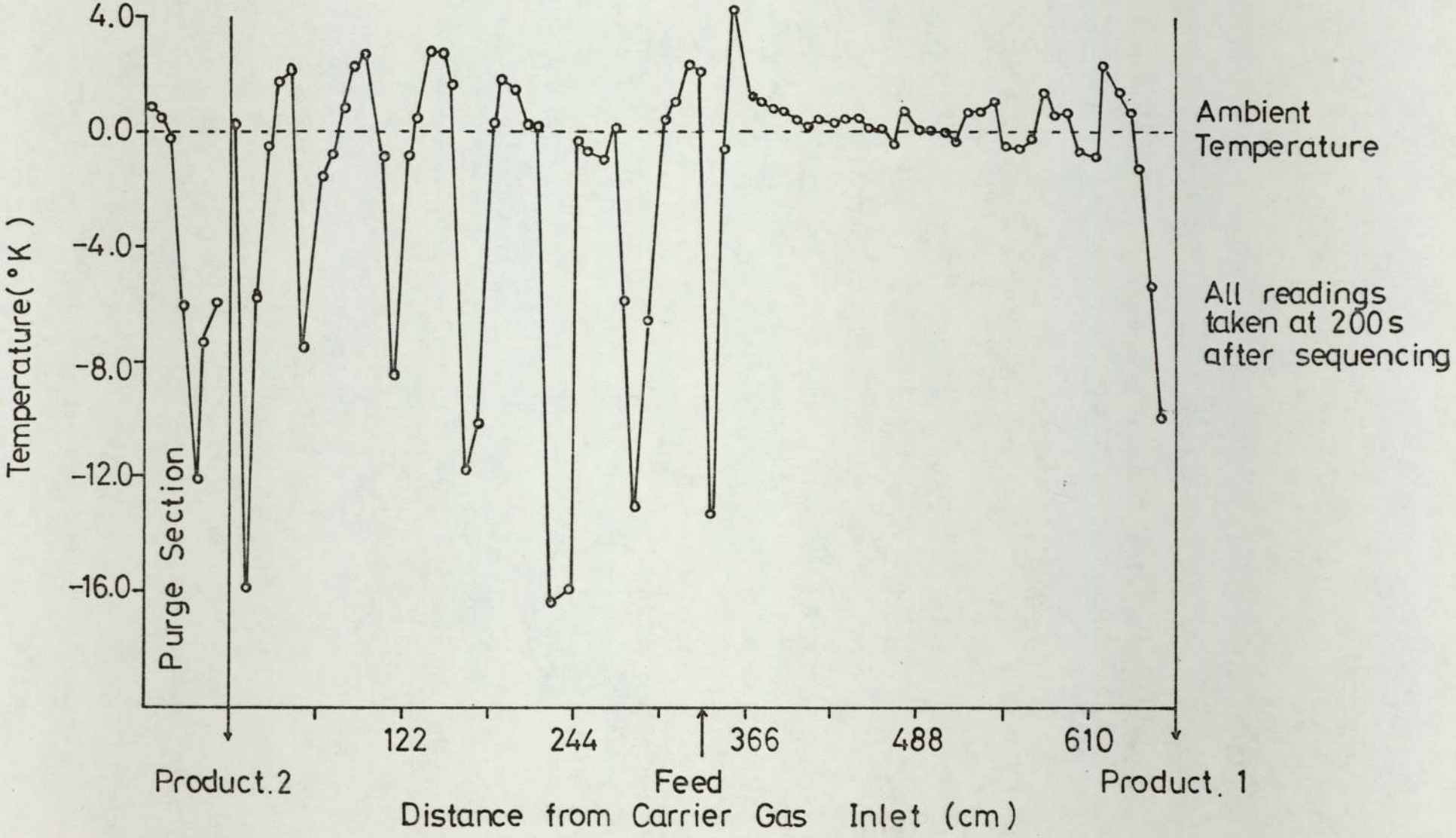

Figure 6.18 Temperature Profile for a Feedrate of 600cm^{3}hr^{-1} (TC's 2.5cm into Column)

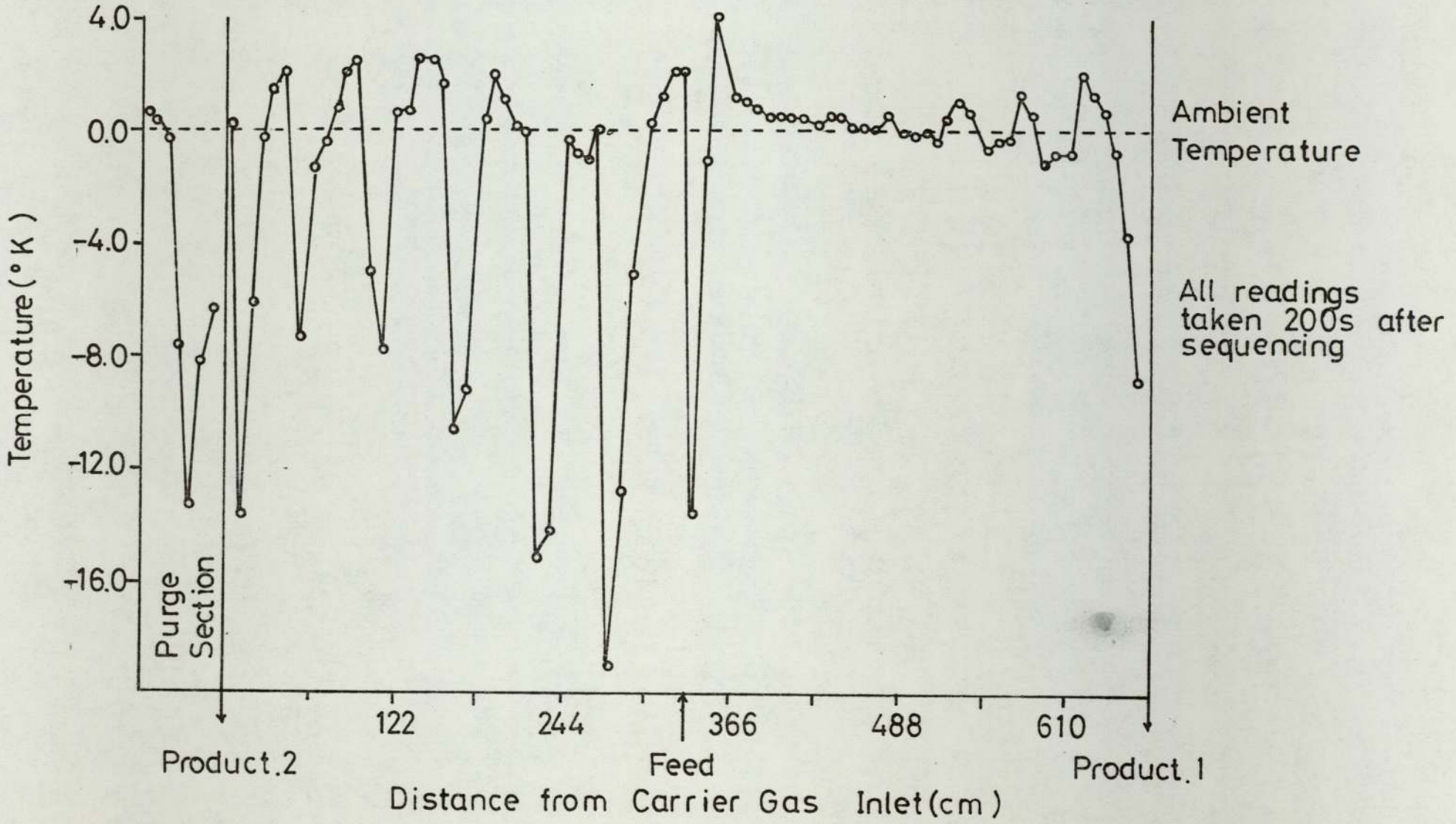

Figure 6.19 Temperature Profile for a Feedrate of 600 $cm^3 hr^{-1}$ (TC's 1.3 cm into Column)

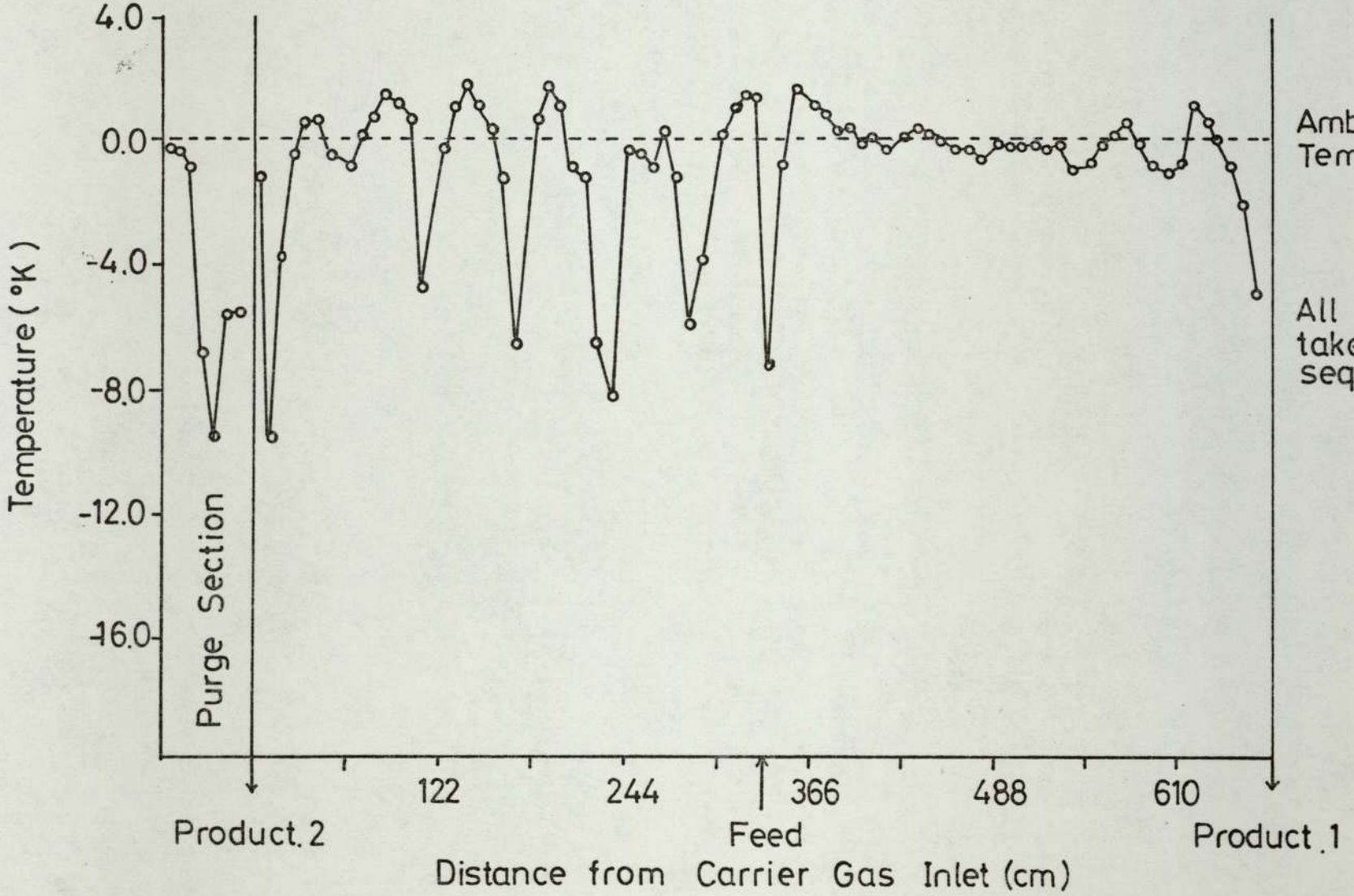

Figure 6.20 Temperature Profile for a Feedrate of 600 $cm^3 hr^{-1}$ (TC's at Column Wall)

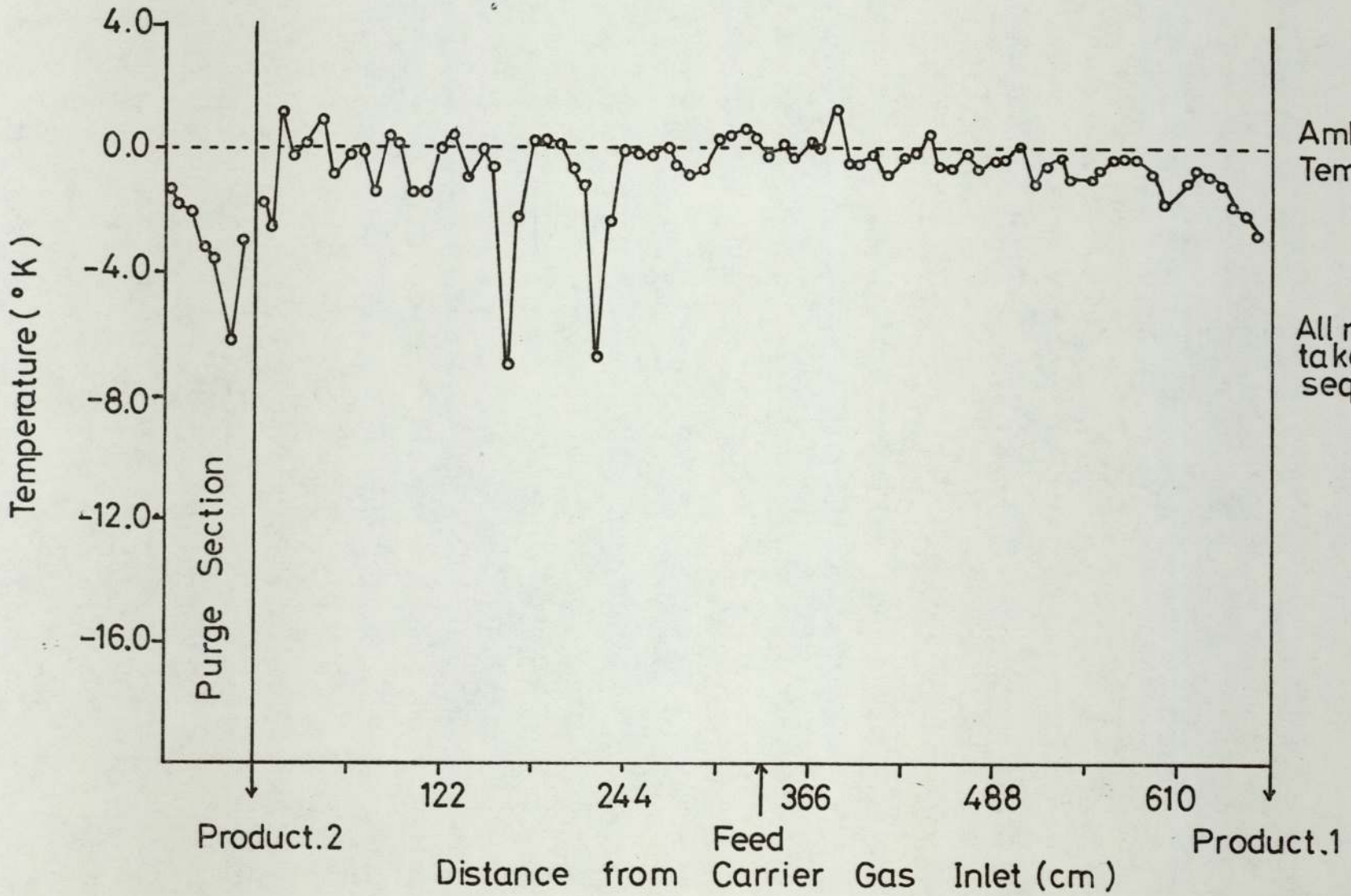

Figure 6.21 Temperature Profile for a Feedrate of 600cm^{3}hr^{-1} (TC's 3.8cm into Column)

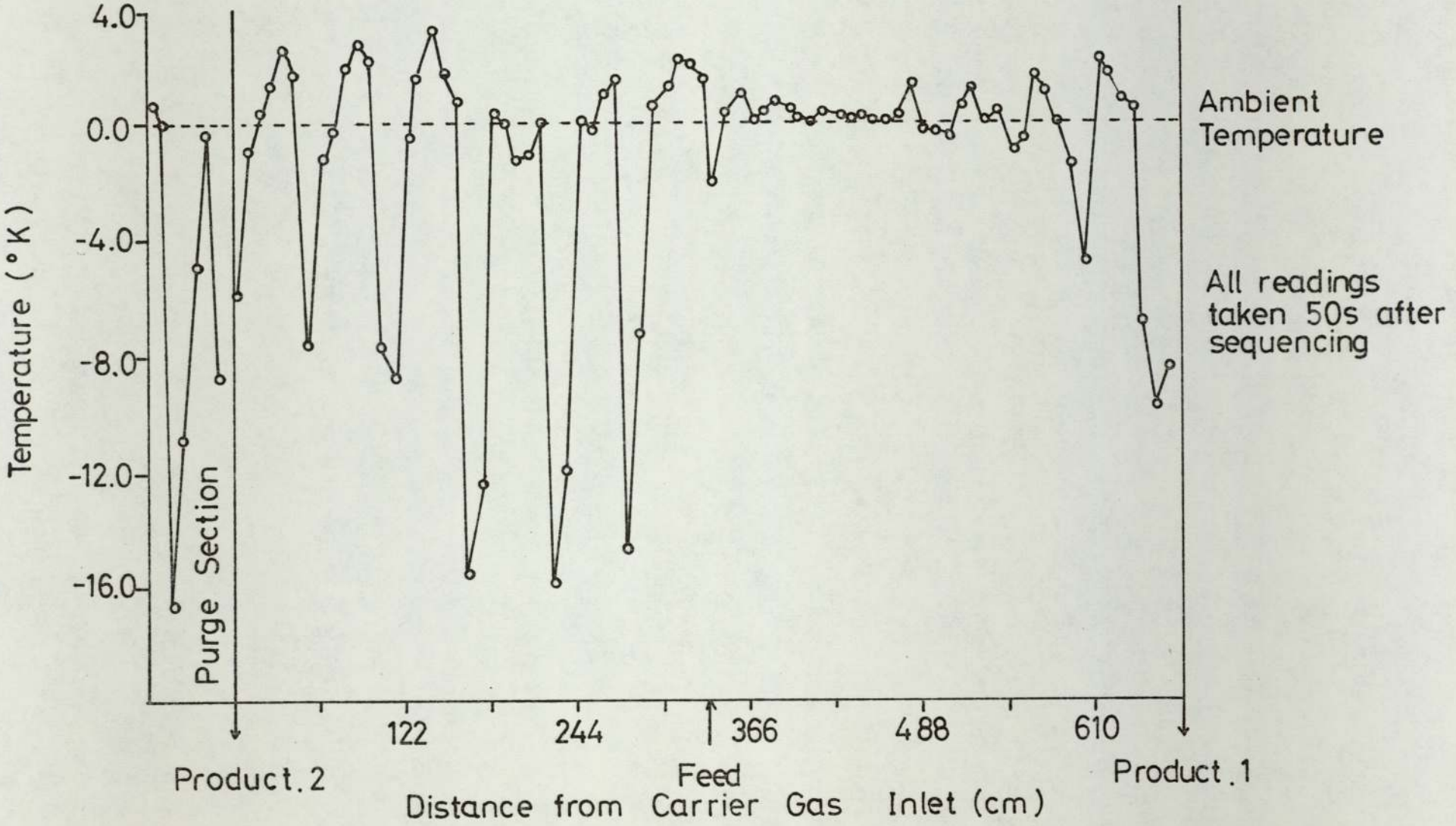

Figure 6.22 Temperature Profile for a Feedrate of 800cm^{3}hr^{-1} (TC's 3.8cm into Column)

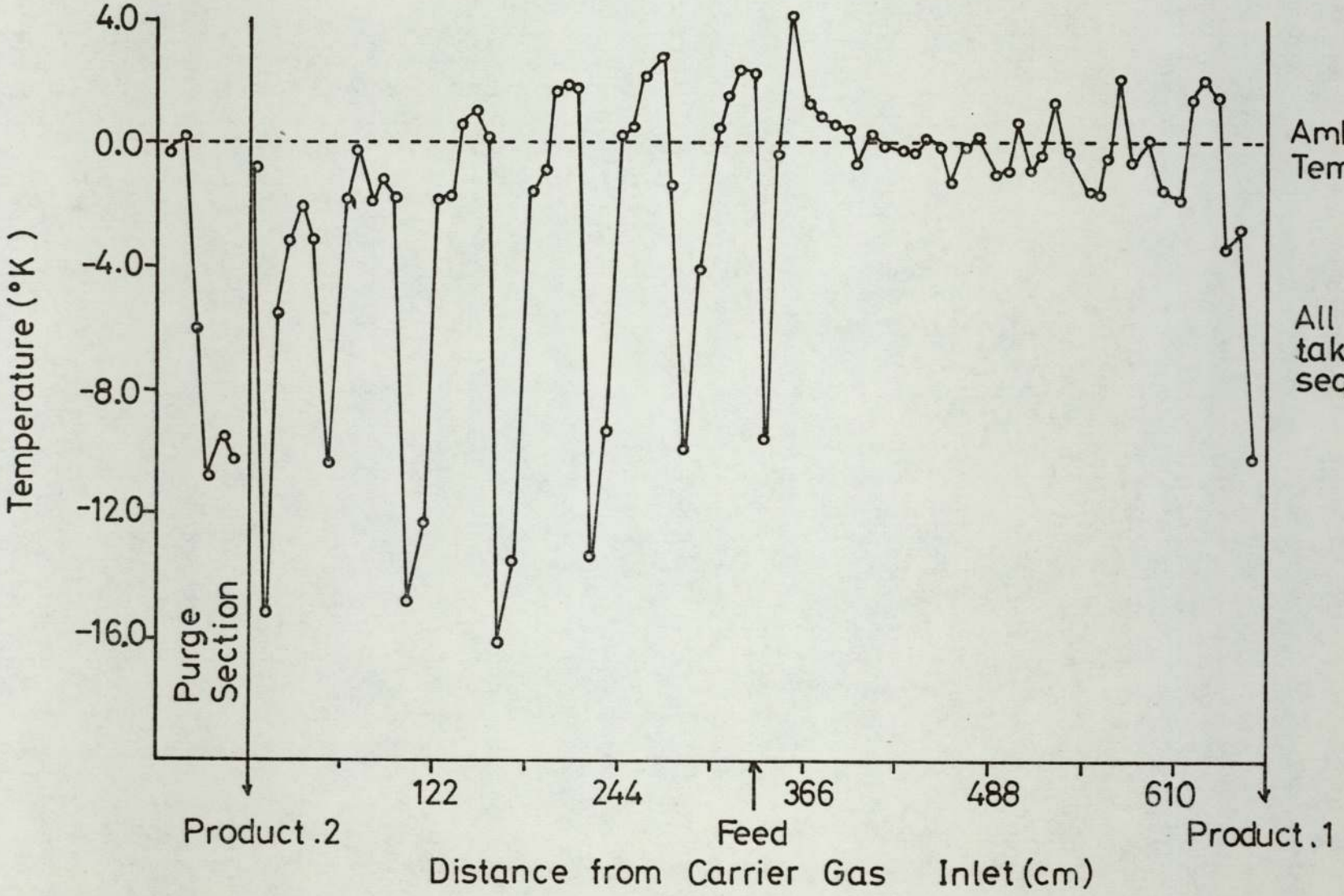

Figure 6.23 Temperature Profile for a Feedrate of 800cm^{3}hr^{-1}(TC's 2.5cm into Column)

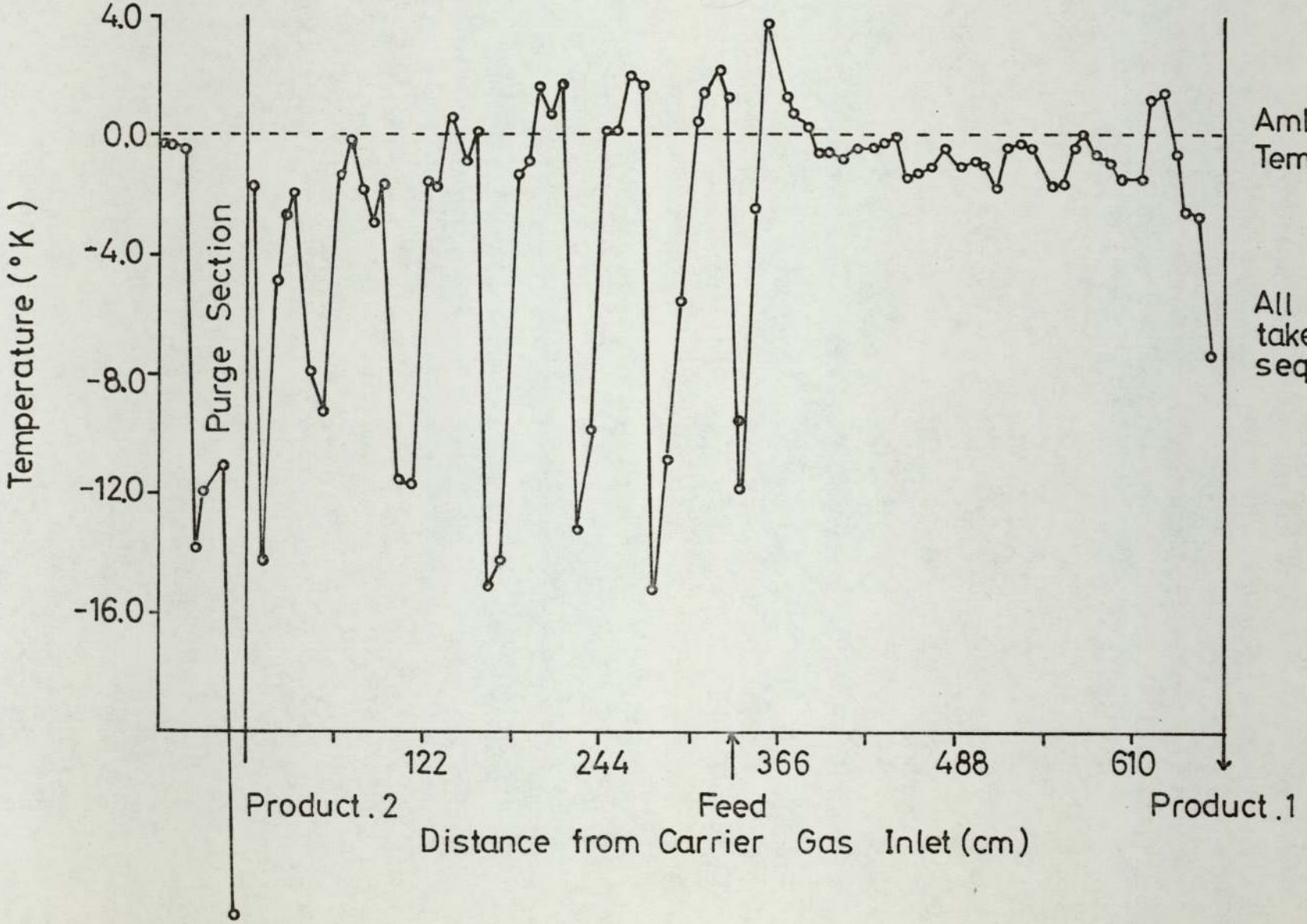

Figure 6.24 Temperature Profile for a Feedrate of 800cm^3 hr^{-1} (TC's 1.3cm into Column)

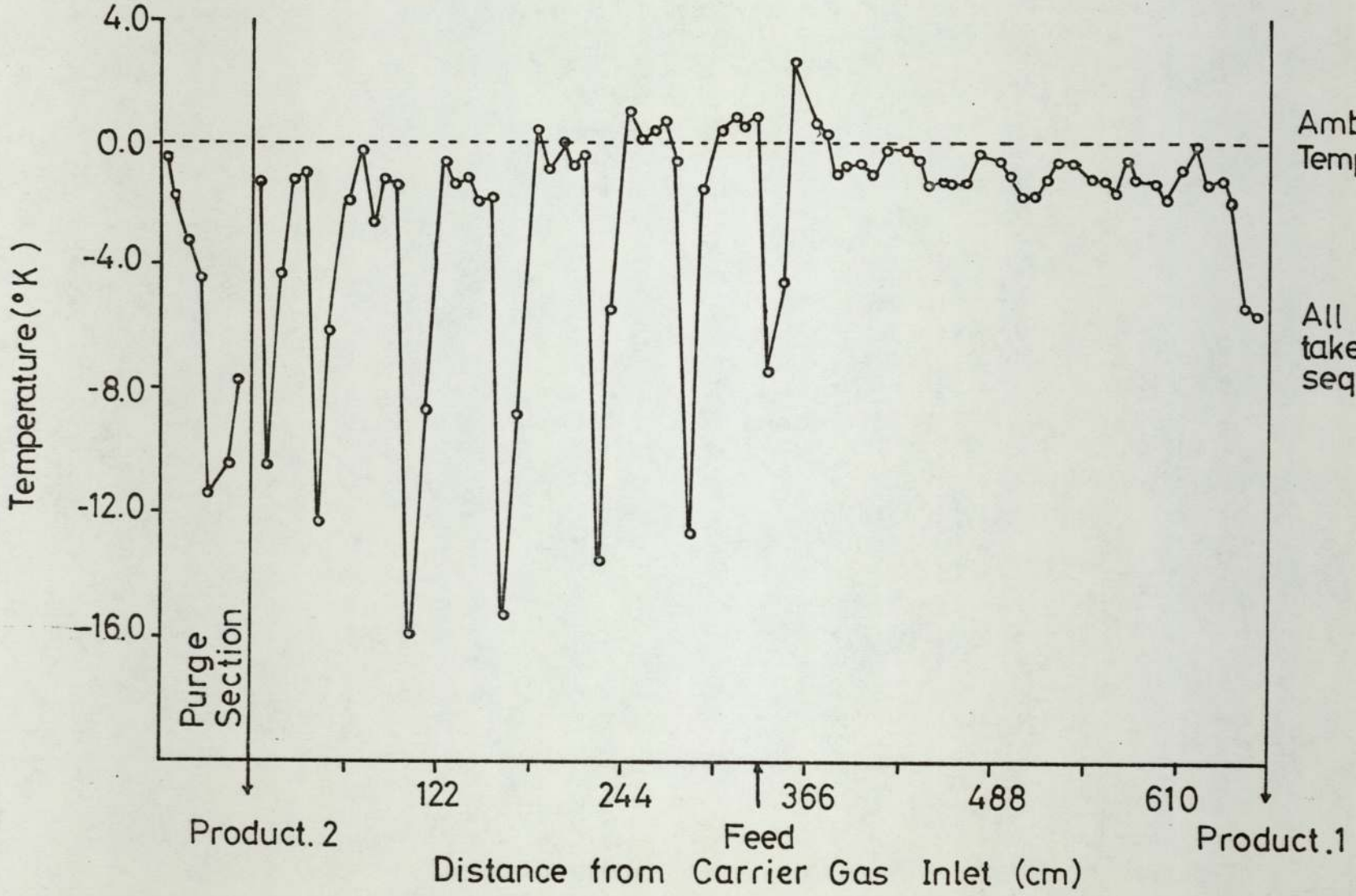

Figure 6.25 Temperature Profile for a Feedrate of 800 $cm^3 hr^{-1}$ (TC's at Column Wall)

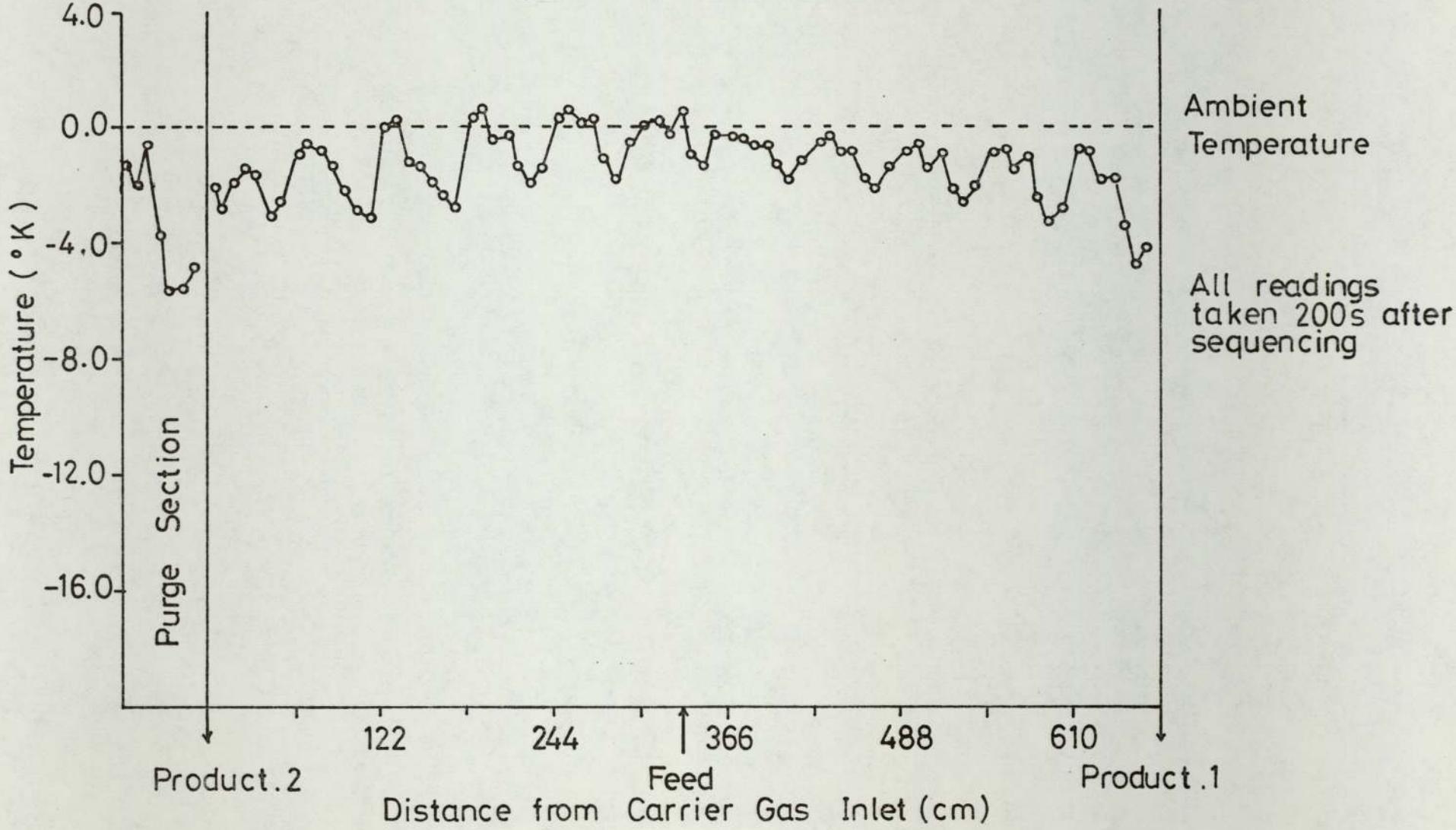

Figure 6.26 Temperature Profile for a Feedrate of 800cm^3 hr^{-1} (TC's 3.6cm into Column)

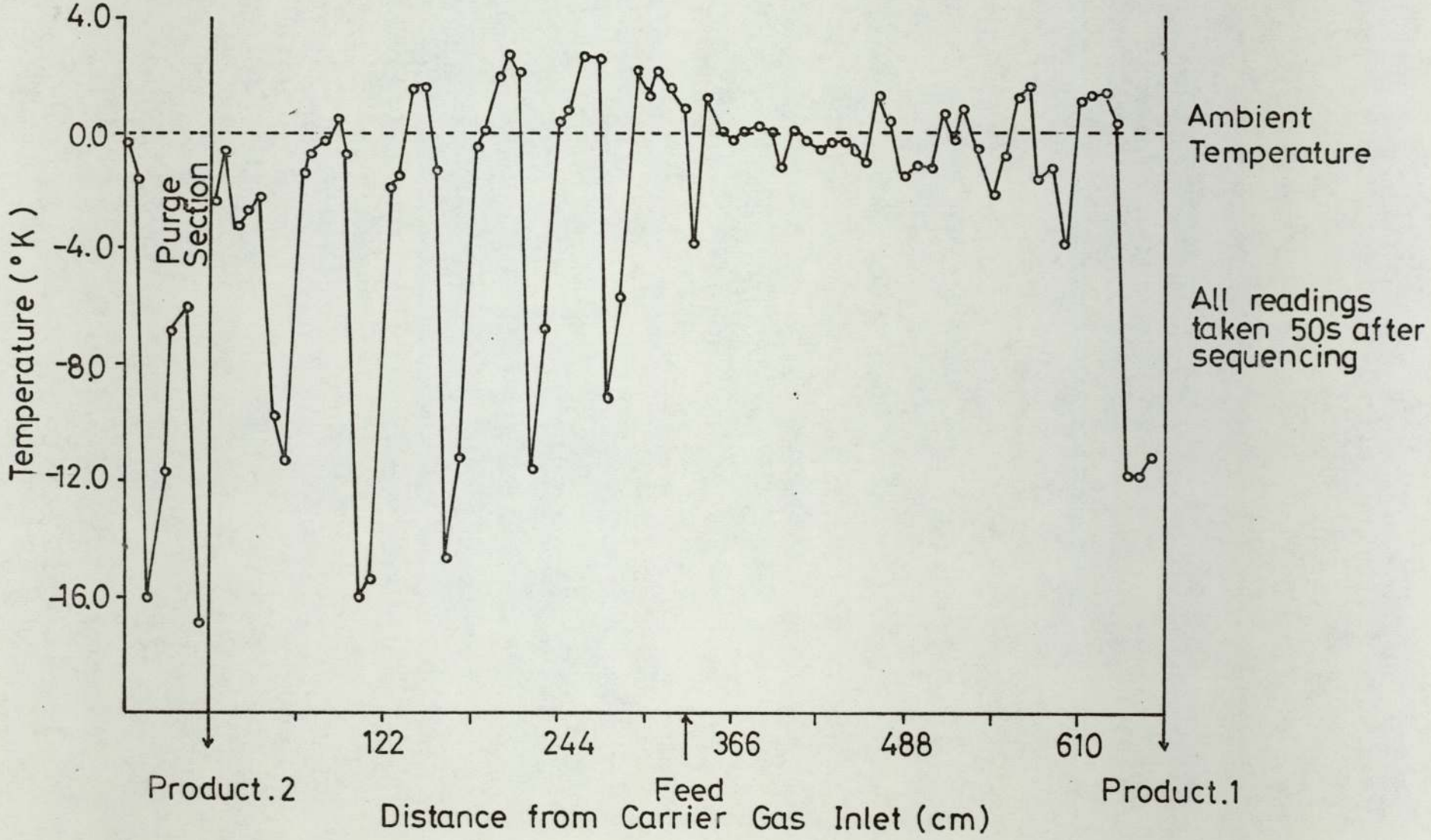

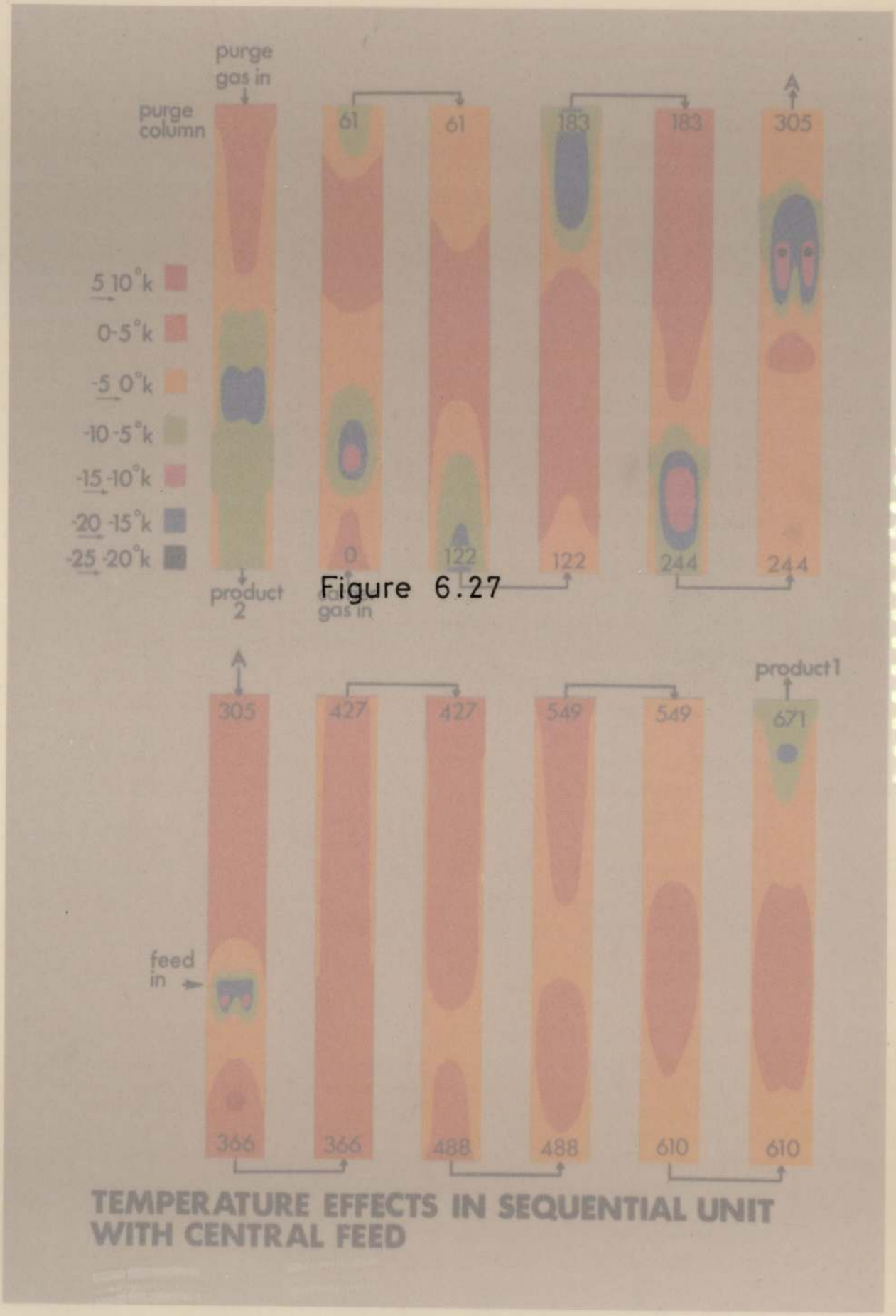

Figure 6.27

TEMPERATURE EFFECTS IN SEQUENTIAL UNIT WITH CENTRAL FEED

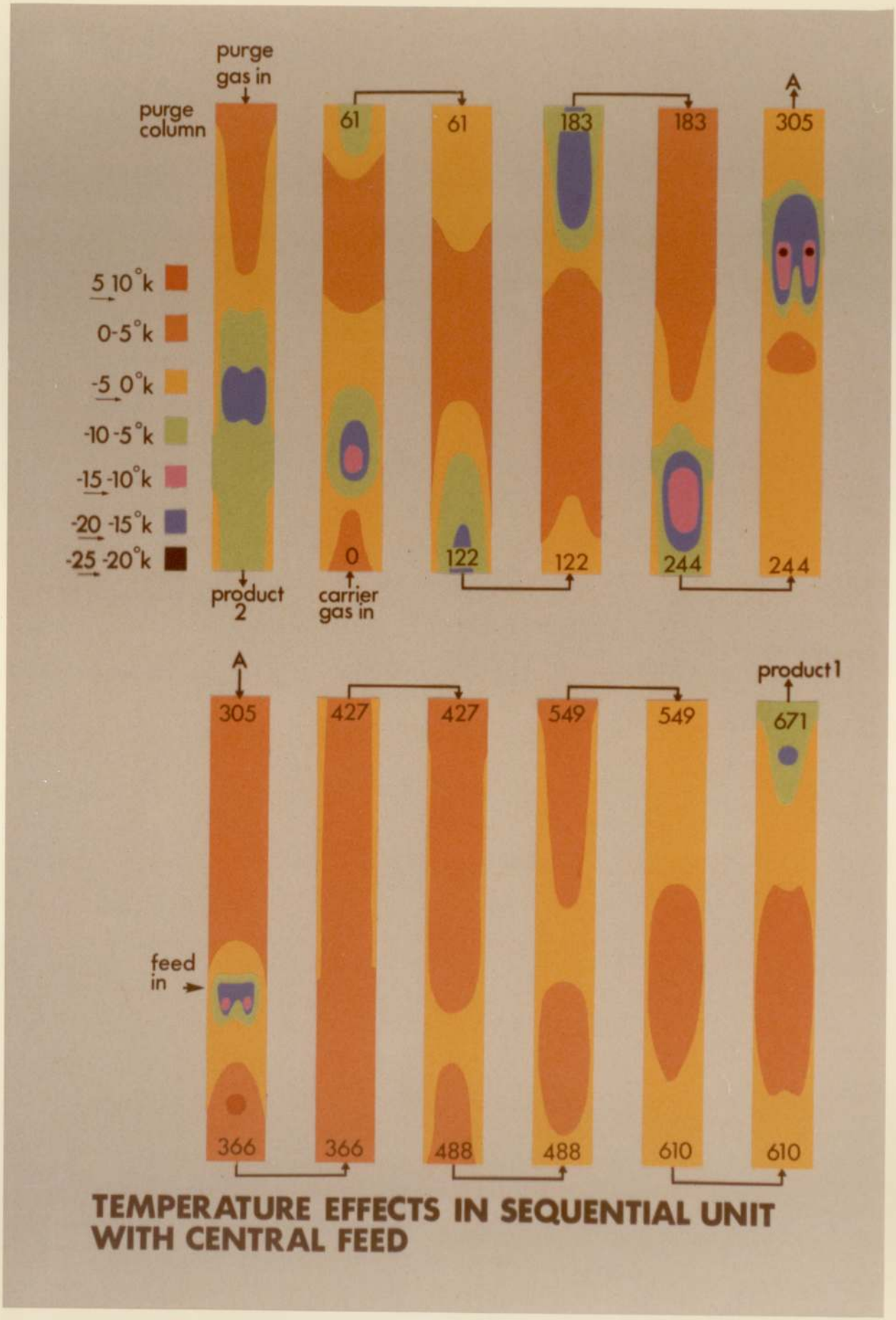

TEMPERATURE EFFECTS IN SEQUENTIAL UNIT WITH CENTRAL FEED

CHAPTER 7

COLUMN PACKING ANALYSIS AND MECHANICAL DESIGN CHANGES

7.1 Determination of the 'On-Column' Liquid Phase Loadings

Results presented in Chapter 6 had shown conclusively that above a feedrate of 600 $cm^3 hr^{-1}$ a certain percentage of feedstock was remaining in the liquid state until it was purged out in the isolated section.

Apart from the detrimental effects this was having upon the chromatographic operation of the SCCR1, there was also the strong possibility that this free liquid would be leaching the silicone oil from the firebrick solid support. Loss of liquid phase will also have occurred because it possesses a finite vapour pressure at ambient temperature, albeit very small.

The solid support in the SCCR1 was originally coated with liquid phase to give a 25% loading. After over 2000 hours of operation it was probable that the 25% loading upon which the $G_{m.c}/L'$ ratio is based, had changed and that for future accurate predictions of $G_{m.c}/L'$ the 'on-column' liquid phase loading should be determined.

Columns 1 and 2 were removed from the symmetrical configuration and carefully unpacked in sections of approximately 200 gm, so that for each column eight discrete batches were available for sampling.

The technique for determining the liquid phase loading is similar to that for determining the partition coefficient at infinite dilution.

The relationship of the partition coefficient, K, to the elution chromatogram is given by,

$$K = \frac{V_R^o - V_G}{V_L} \qquad (7.1)$$

where: V_G = corrected gas 'hold-up' in the column and associated fittings

$= j\ V_m$

V_L = volume of stationary liquid phase

V_R^o = corrected retention volume

V_m = volume of unabsorbed component

The corrected retention volume may be calculated from

$$V_R^o = F \cdot \frac{T_C}{T_a} \cdot \frac{P_o}{P_a} \cdot j \cdot t_R \qquad (7.2)$$

where F = flowrate measured at ambient conditions

T_C = column temperature

T_a = ambient temperature

P_o = column outlet temperature

P_a = ambient pressure

t_R = 'elution' or retention time for a component

j = James and Martin compressibility factor

Rearrangement of Equations 7.1, 7.2 gives an expression for the volume of liquid stationary phase as,

$$V_L = ((F. \frac{T_c}{T_a} \cdot \frac{P_o}{P_a} \cdot j\ t_R) - V_G))/K \qquad (7.3)$$

$$= F. \frac{T_c}{T_a} \cdot \frac{P_o}{P_a} \cdot j\ (t_a - t_m)/K \qquad (7.4)$$

t_m = retention time for unabsorped component

The eight sections of packing from each column were coned and quartered and from each batch a 2.4m, 4.8 mm o.d. analytical column was packed. The coiled column was then connected to the injection head of the Perkin-Elmer F.I.D. and treated with di-methyl chlorosilane to remove any active sites. After treatment the column outlet was connected to the detector head, the oven was set at 60.5°C, and the nitrogen carrier gas flowrate set at approximately 1.9 $cm^3 s^{-1}$ with a soap bubble meter.

The measurement of the column gas hold up V_m was determined by the measurement of the retention time of an unabsorped solute, for which methane was used. Following this a series of 0.1 mm^3 injections of Arklone.P. were introduced and the retention time recorded with an accurate stop watch. The calculation of the volume of liquid phase requires a knowledge of the partition coefficient of Arklone.P. at 60.5°C, and this had previously been experimentally determined as 40.79.

An example of the determination of the percentage liquid phase loading is given in Appendix A.4.3 and the results of the study are given in Table 7.1.

The total weight of liquid phase in columns 1 and 2 was 371.4 and 384.5 gm respectively and if these columns are taken as being representative of the other columns in the unit then the total liquid phase remaining in the SCCR1 was 4535.4 g, i.e. (4675.7 cm^3). This figure represents a loss of 400 gm of liquid phase since the commissioning of the SCCR1, as initially 4935 gm of silicone oil were present in the unit. In future determinations of $G_{m.c}/L'$ the new value of 4.676 dm^3 for the total volume of solvent phase will be used.

One other feature of the analysis of the column packing was the distribution of liquid phase within the column. In the region

of the feed distributors (i.e. batch 6 for column 1, batch 3 for column 2), the percentage liquid loading is the lowest for the whole column indicating the 'washing off' of the liquid phase by the feedstock. Some of liquid phase removed in this manner appears to be redeposited on the solid support farther along the column in the direction of carrier gas flow. For both column 1 and 2 the highest recorded stationary phase loadings are at the column exits, where the loadings were 25.13% and 26.01%. These values are both above the original value of 25%.

Having determined the loss of stationary phase within the SCCR1, the columns could be repacked and connected back into the chromatograph. A glass column was designed to replace one of the copper columns in the unit, in the hope that visual evidence of the partial vaporisation of feedstock may be obtained.

Table 7.1
Liquid Phase Loadings

Column N°.1

Batch N°	Approx Position of Batch	Weight of Batch	% Liquid Loading	Weight of Liquid Phase
	cm	gm		gm
1	52-61	227.4	23.13	52.6
2	45-52	180.5	22.74	41.0
3	36-45	234.1	23.87	55.9
4	29.5-36	172.4	22.8	39.3
5	23.5-29.5	166.5	22.0	36.6
6	17.5-23.5	160.4	19.9	31.9
7	11-17.5	171.3	23.3	39.9
8	0-11	295.2	25.13	74.2
Total		1607.8		371.4

Column N°.2

Batch N°	Approx Position of Batch	Weight of Batch	% Liquid Loading	Weight of Liquid Phase
	cm	gm		gm
1	51-61	275.5	22.45	61.8
2	43-51	215.5	22.88	49.3
3	37-43	152.2	22.08	33.6
4	29-37	201.5	23.30	46.9
5	22.5-29	177.0	23.6	41.8
6	16-22.5	177.5	24.15	42.9
7	8-16	203.5	25.89	52.7
8	0-8	213.3	26.01	55.5
Total		1616.0		384.5

7.2 The Glass Column

The column used was of the standard 'QVF' type, of length 61 cm and diameter 7.6 cm. Screw threaded glass sample points were fused into the side of the column at 6.8 cm intervals down its whole length. At a point 30 cm down the column, opposite to a sample point, a 1 cm diameter hole was drilled through the glass. This permitted the feed distributor and associated solenoid valve to be fixed onto the column, 'Viton' rubber gaskets providing an airtight seal.

To secure the copper end cones onto the glass column, annular brass plates first had to be bolted onto the column. The bolt heads were countersunk into the brass plate so that when the end cones were attached they were flush with the brass plates. The seals between the tube, the brass plate and the end cone flange were provided by 2.4 mm thick gaskets of 'Klingerite' coated with a pipe sealing compound.

In view of the dangers of using pressurised gases in glass vessels, the column underwent stringent pressure testing. Static, mobile and shock tests were conducted at three times the expected normal operating pressure.

To maintain continuity in the experimental results the analysed solid support was repacked into the glass column batch by batch with as little mixing as possible. The 'shake-turn-pressure' method of packing was employed (91), this being the method used when the columns had originally been constructed. Upon completion of the repacking the column was again pressure tested before being connected back as part of the chromatographic unit. As a further safety measure the whole of the SCCR1 unit was enclosed with reinforced perspex sheets.

Observations made with the glass column are shown in Figure 7.1. For this example shown, the binary halocarbon feed enters the column at points X,Y, in a manner described in Section 3.3.5. For demonstration purposes the feedrate was 1700 $cm^3.hr^{-1}$,with the carrier gas flowing in an upward direction at a rate of 1100 $cm^3.hr^{-1}$.

Figure 7.1(a), shows the situation 200 seconds into the 300 second sequencing interval. The solid support moistened by the unvaporised feed is clearly visible in the region around the sample ports.

After 250 seconds of continuous feeding into the columns, Figure 7.1(b), the area of wetted packing had considerably increased and formed a band at the column wall some 15 cm in length and 3 to 4 cm in width. Three similar bands were observed around the circumference of the column, offset by 90° from the one shown in Figure 7.1. All four bands being produced by virtue of the shape of the feed distributor, Figure 3.6.

Figure 7.1(c) taken at 300 seconds, i.e. the end of the feeding cycle, shows that approximately half of the solid support visible at the wall had been wetted. An indication of the low temperature being experienced inside the column can be seen by the appearance of condensed water vapour on the outside of the column.

A further 300 seconds after feeding had terminated shows the wetted packing still clearly visible although the wetted area is decreasing as evaporation of the feed continues to take place inside the column, Figure 7.1(d).

The remaining two Figures 7.1(e) and 7.1(f) were taken 900 and 1500 seconds after feeding had stopped. In Figure 7.1(f) it can be seen that all the free liquid previously visible at the wall had evaporated, although it is still probable that liquid is present in the bulk of the packed column.

Figure 7.1 Liquid Wetting

A	200s into feeding sequence
B	250s " " "
C	End of 300s feeding sequence
D	300s after end of feeding sequence
E	900s " " " "
F	1500s " " " "

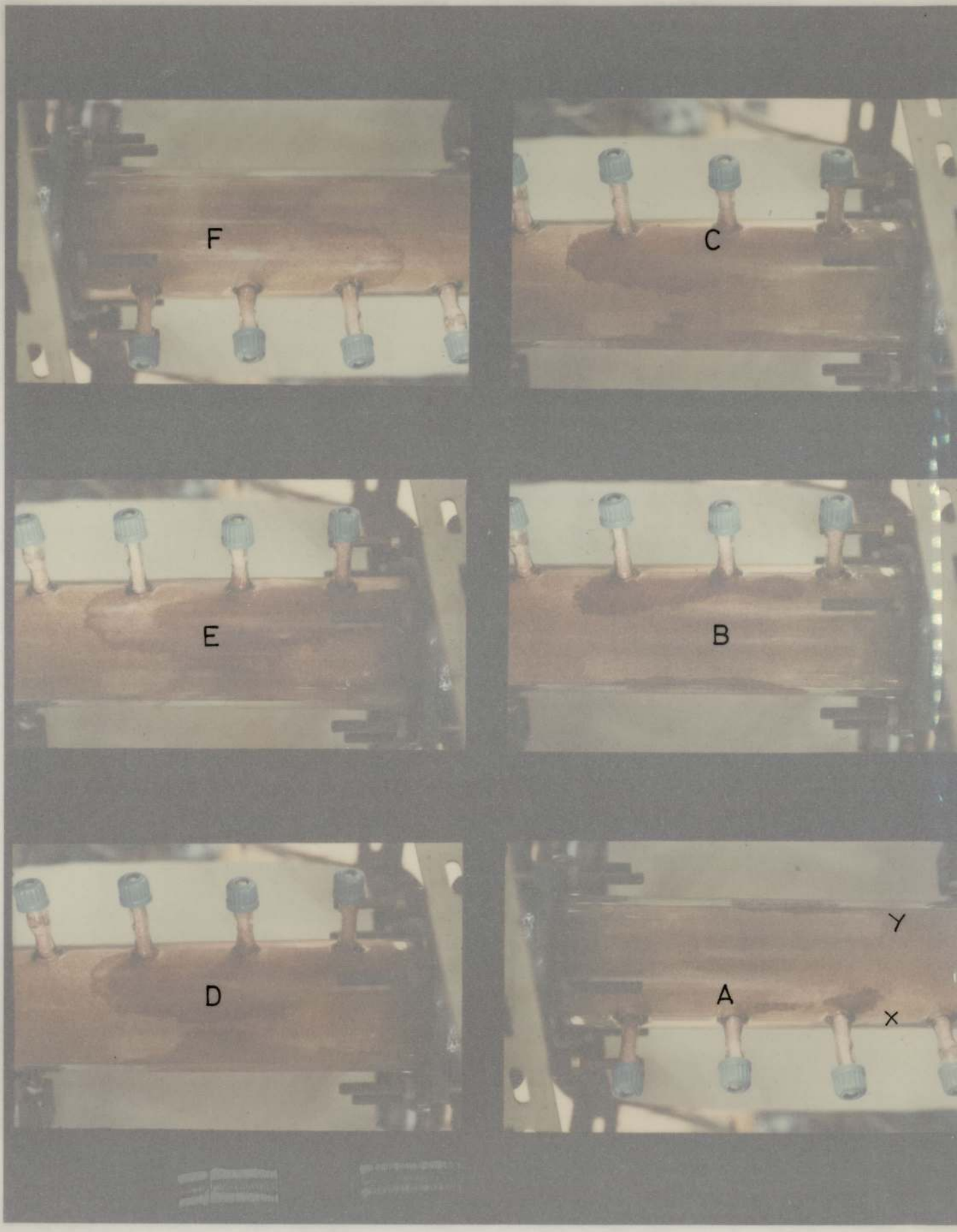
F
C
E
B
D
A
Y
X

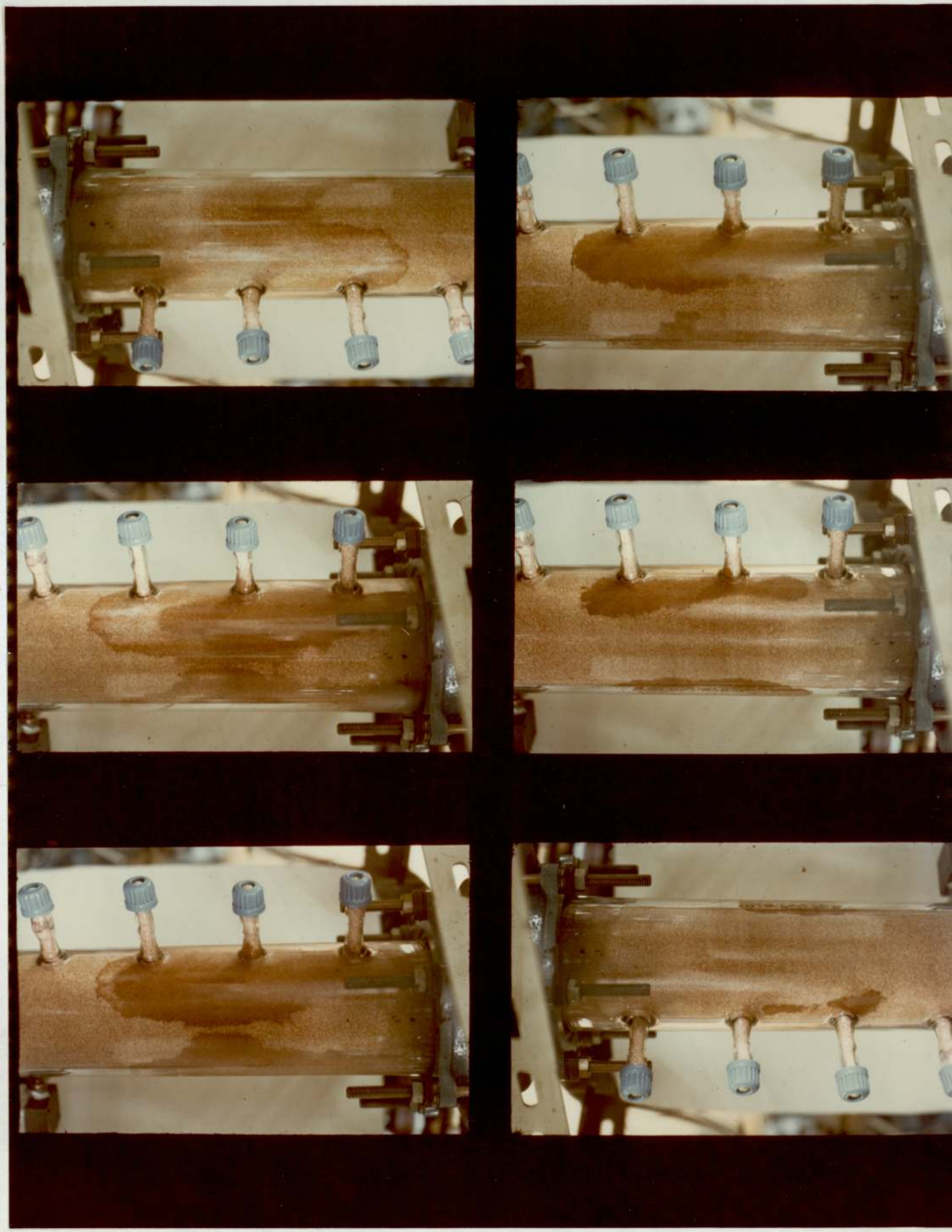

7.3 Redesign of Feed Distribution Network

7.3.1 Repositioning of the Feed Valves

One of the conclusions to be drawn from the experimental results in Chapter 6 was the need for repositioning the feed valves, and their associated feed distributors.

Liquid feeding anywhere within the packed columns would lead to the problems highlighted previously in Chapter 6 and therefore the only remaining point at which feed could be practically injected was in the column end cones. The feed distributors were originally situated at the column mid-points because of the physical difficulty of siting their solenoid valves on the end cones, along with the other inlet/outlet valves. This problem was overcome by feeding through the sample tube positioned in the end cones, and assembling the solenoid valve onto the outlet of the sample tube with a 0.95 cm male to male brass stud coupling, Figure 3.3.

After introducing the feed into the end cone some means was required to distribute and vaporise it. Advantage was taken of the shape of the cone in that it tapered down to a throat of less than 1.3 cm diameter. Gas velocities in excess of 250 $cm.s^{-1}$ could be expected in this region and therefore if a stream of liquid could be injected into the throat, a pseudo-venturi atomiser could be created(184).

A 0.8 mm o.d. 0.4 mm i.d. copper capilliary tube was sealed onto the outlet from the solenoid valve, and then inserted through the sample tube into the cone. Bending the capilliary tube through 90 degrees brought it up into the throat of the end cone, parallel with the gas flow. Upon energisation of the solenoid valve, liquid feedstock issued from the tube, co-current to the high velocity gas stream and was quickly brokeninto small droplets thereby greatly

enhancing the vaporisation process.

New feed distributors were fitted to the outlet cones on all twelve columns, so that the feed entry point alternated from top to bottom between adjacent columns.

Repositioning of the feed valves in this manner caused the feed entry point on six of the columns to be lower than the central feed distributor, Figure 3.5. Under these conditions it became possible to create an air or vapour lock in the feed distribution line, hence the central feed distributor had to be repositioned in such a manner so that it was below the lowest feed injection point as shown in Figure 3.5.

7.3.2 Testing of the New Method of Feed Distribution

In gauging the degree of improvement in the new feed distribution network, the rates of evaporation before and after repositioning the valves, needed to be compared. Measurement of these rates of vaporisation were conducted in the following manner.

For the situation where the feed valves were sited at the mid-point of the columns, the SCCR1 unit was operated under the usual conditions of $G_{m.c}/L'$, 265, and with a sequencing time of 262 seconds, but without any feedstock being present. For one sequencing interval only, Arklone.P. and Genklene.P. were fed into one column in the unit and the gas phase concentration exiting from this column monitored until all the solute had passed through. Recording the level of concentration with respect to time gave an indication of the rate of evaporation from within the packed column. A correction needed to be made to the recorded time to allow for the chromatographic movement of the solutes between the feed entry point and the sampling point, (i.e. half a column length).

When the feed valves had been transferred to the column end cones a similar procedure was adopted to measure the evaporation rate in the end cones. The solute feed being introduced into the cone for one sequencing interval only, and the gas phase concentration of the vaporising liquid being monitored with respect to time. As the cones were not packed with chromatographic support material no correction to the measured time was necessary.

The results from runs in which the feedrate was increased from 400 to 1000 $cm^3.hr^{-1}$ are shown in Figures 7.2 to 7.5, and in Appendix 6, Figures A.6.1 to A.6.4. The time taken for the feed to be vaporised in the end cones, is very clearly shown to be considerably less than for feeding into the centre of the packed column. In practical operation the time required for the total evaporation of the feedstock will be longer than shown on Figures 7.2 to 7.5. The carrier gas passing over the liquid feed either in the column or the end cone was solute free, whereas in practice the mobile phase entering the feed zone will always contain Arklone.P. and Genklene.P. and will not therefore be able to absorb as much vaporising feedstock as would solute free air.

When feeding into the middle of the bed, the total vaporisation times for Arklone.P. and Genklene.P. increase greatly with increasing feedrate, with some of the Genklene.P. above a rate of 400 cm^3hr^{-1} remaining as liquid until being removed as the purged product. (Seen on Figures 7.3 to 7.5 as a peak at 1550 seconds). Conversely with feeding into the cone even at feed rates of 1000 cm^3hr^{-1} all the Genklene.P. has been evaporated after 700 seconds with the Arklone.P. requiring some 150 seconds less for total vaporisation.

The improved results for feeding into the end cones not only occurred because of the change in design of the feed distributor but

also from the improved heat transfer within the cone. It was anticipated therefore that as well as improving the maximum throughput of the SCCR1 the detrimental cooling effects from feed vaporisation would be reduced.

Figure 7.2 Comparison of Evaporation Rates for Bed & Cone Feeding ($400 cm^3 hr^{-1}$)

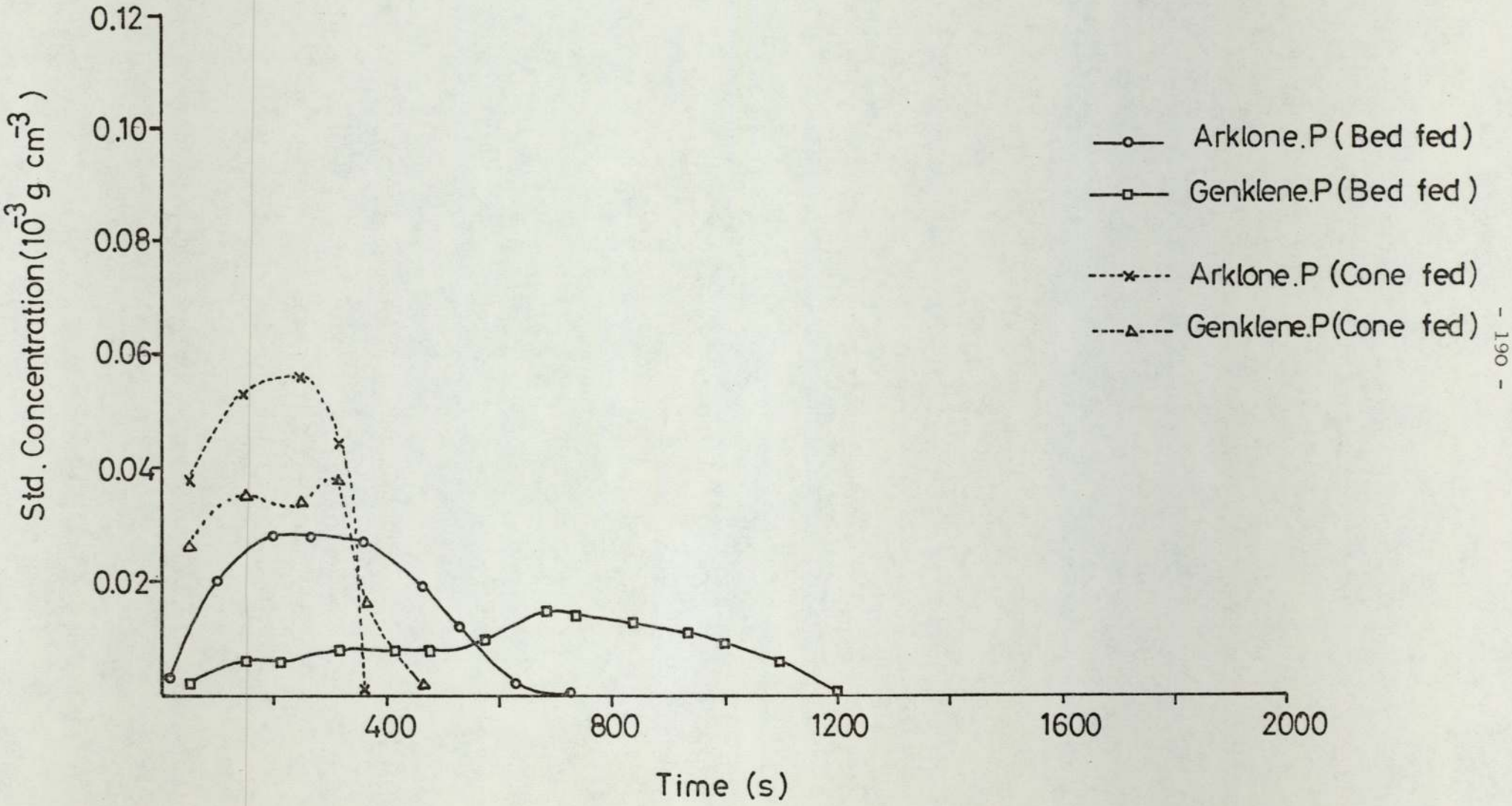

Figure 7.3 Comparison of Evaporation Rates for Bed & Cone Feeding ($600\ cm^3 hr^{-1}$)

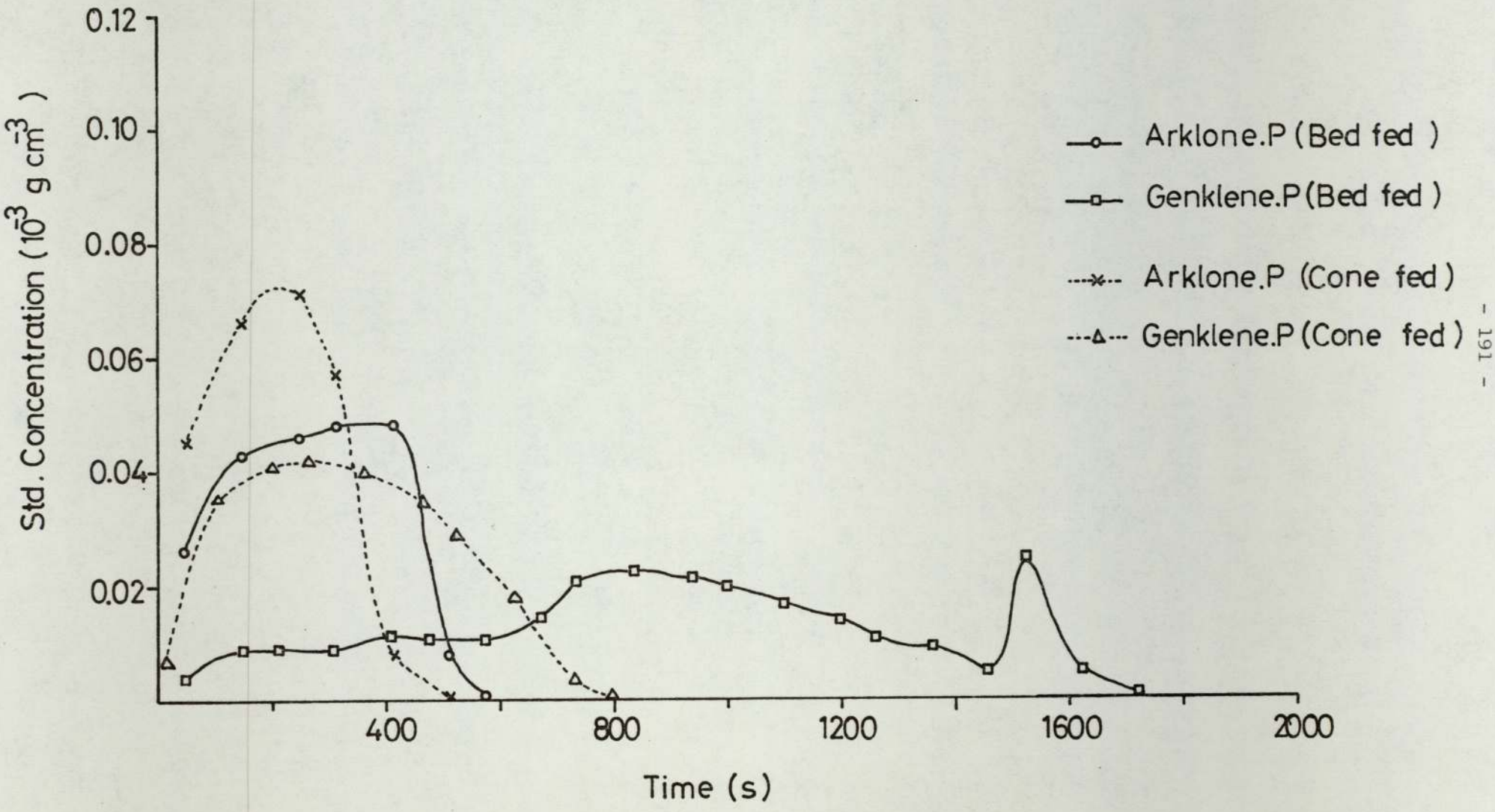

Figure 7.4 Comparison of Evaporation Rates for Bed & Cone Feeding (800 $cm^3 hr^{-1}$)

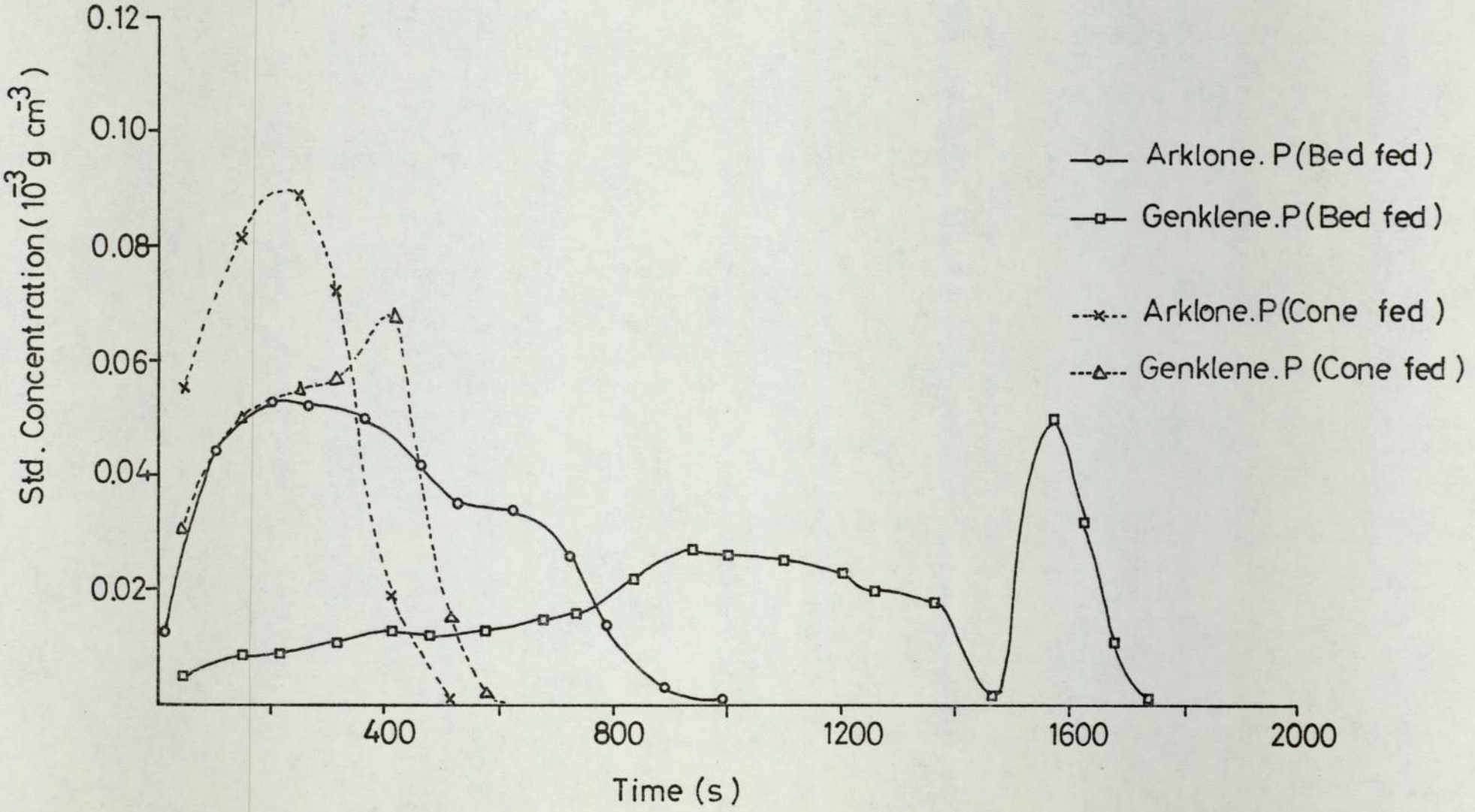

Figure 7.5 Comparison of Evaporation Rates for Bed & Cone Feeding (1000 $cm^3 hr^{-1}$)

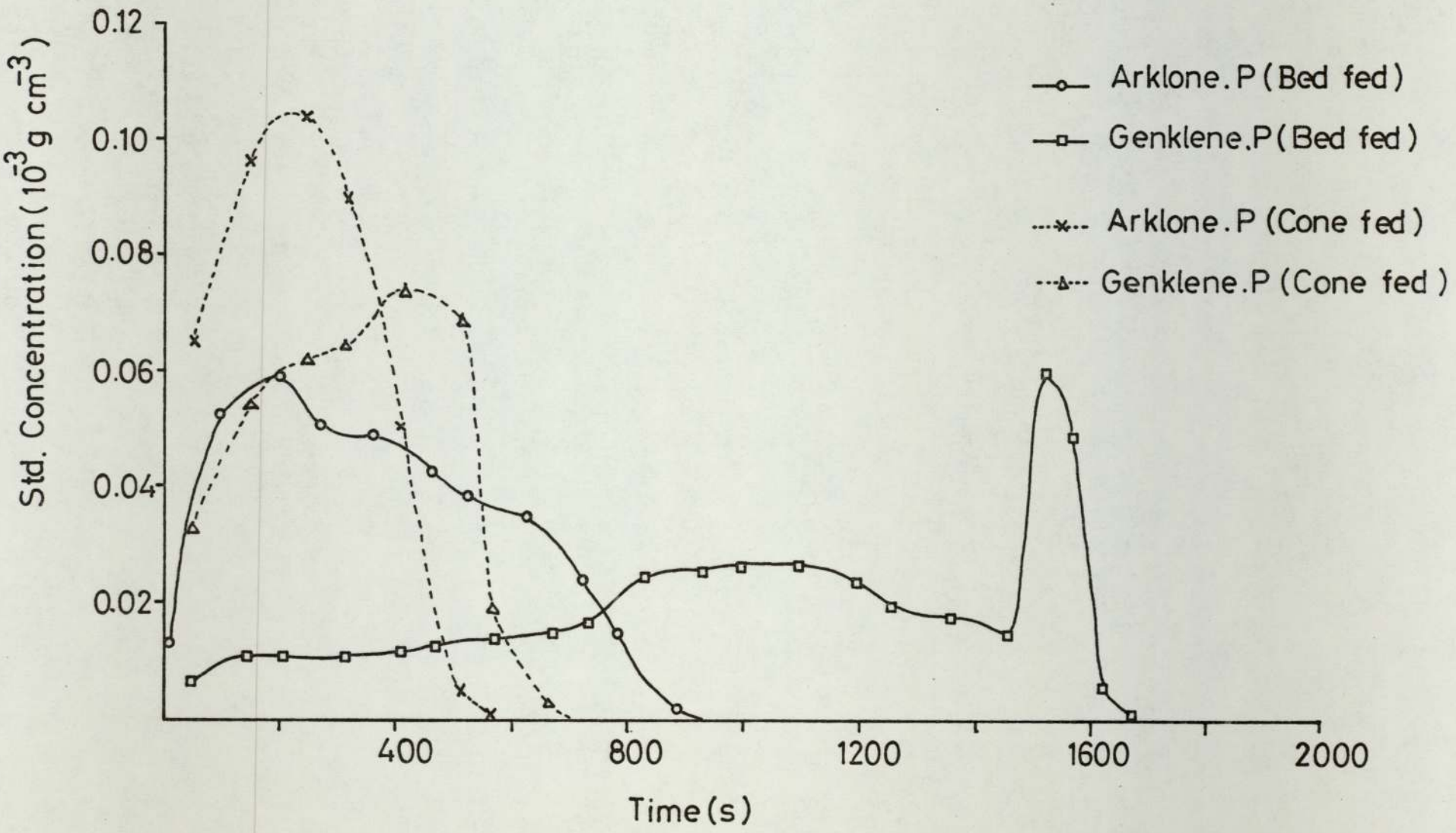

7.4 The Purging Process

At liquid feed rates of 1000 $cm^3.hr^{-1}$ and above, the complete purging of the 'Genklene'.P. bottom product had proved very difficult. In the time available for purging, i.e. one switching interval, only 80-90% of the product was being removed. After the chromatograph had sequenced the remaining 10-20% of the bottom product was exiting from the top product outlet with the 'Arklone'.P., thereby causing severe contamination of that product.

7.4.1 Double Purging

To overcome the contamination problem, a system of 'double-purging' was introduced. This method of operation had successfully been operated by other workers (47,185) using a similar sequential chromatographic unit of twelve 2.5 cm diameter steel columns.

Double-purging involves two columns being purged simultaneously by separate gas supplies. Each column is thereby given a total purging time twice the sequencing interval. One disadvantage inherent in this mode of operation is that it reduces the effective separating section of the chromatograph from eleven to ten columns.

The implementation of a double-purging system to the SCCR1 did not have the desired results. Contamination of the top product still occurred indicating that the purging process was still incomplete.

A closer study of the temperature profile in the unit for a feed rate of only 600 $cm^3.hr^{-1}$, Section 6.5.4, revealed that the temperature in the purge bed could fall to below $-20^{o}K$. At higher feed rates this temperature may be lower still. The effects of this fall in temperature have a very significant effect upon the partition

coefficients of the two solutes in that both thermodynamic theory (180), and experimental results (50), give log K^{∞} as an inverse function of the absolute temperature. At temperatures of $-20^{\circ}K$ more than twice the expected purge gas rate is required. Hence even with a double purge system, complete removal of the bottom product from the isolated columns is not possible.

7.4.2 Heating the Purge Gas

Preventing the fall in temperature within the purging column by some method of heating was a further alternative. Short of a complete redesign of the chromatographic columns the only practical way to achieve this was by fitting a heat exchanger into the inlet purge gas line. The concentric tube type heat exchanger was constructed from a finned copper tube of 1.9 cm i.d. and a 5.1 cm, 'Q.V.F.' glass tube of length 71 cm. The purge gas flowed in the annulus whilst heat was provided by inserting a 'Q.V.F.' 1 KW. 'Red Rod' immersion heater into the copper tube. Control of the air outlet temperature was achieved by connecting the 1 KW heater to a rheostat.

The heat exchanger was operated on a trial and error principle, with the purge gas being heated just enough to ensure complete removal of the product within one sequencing interval. Overheating of the gas could result in the premature purging of the column, and excessive heating of the column packing, whilst underheating would not achieve the desired result of removing all the 'Genklene'.P bottom product.

The results shown in Table 7.2 were taken from a typical separation run for a 50:50 mixture of 'Arklone'.P and 'Genklene'.P. at a feed rate of 600 $cm^3 hr^{-1}$.

The arbitary reference values of 'percentage removal of product', namely 82.5; 95.5, and 99; were obtained by integration of the concentration profile recorded by the Katharometer.

If the average time to remove 99% of the product is considered, it can be seen that some fourteen seconds are saved by heating the purge gas. This small improvement in purging time may seem insignificant when compared with a switching time of 262 seconds, but it must be emphasised that the heating element was only being operated at a little over half its maximum capacity.

Table 7.2

Efficiency of Heat Exchanger

Column N°	Time to Purge 82.5% Product (s)		Time to Purge 95.5% Product (s)		Time to Purge 99% Product (s)	
	Without Heating	With Heating	Without Heating	With Heating	Without Heating	With Heating
1	120	108	155	147	183	167
2	140	130	180	166	213	197
3	139	126	175	172	210	201
4	148	133	192	175	224	205
5	140	130	178	165	206	192
6	154	147	198	188	233	220
7	137	128	172	161	200	188
8	142	138	190	181	228	211
9	135	131	181	168	217	200
10	147	135	192	180	224	209
11	122	115	158	152	189	180
12	131	130	170	170	205	200
Average	138	126	178	169	211	197

Run Conditions:

Sequencing Interval	262 s
Solute Feedrate	600 $cm^3 hr^{-1}$
$G_{m.c}/L'$	260
Carrier Gas Flowrate	1100 $cm^3 s^{-1}$
Purge Gas Flowrate	1700 $cm^3 s^{-1}$
Ambient Temperature	22.0 °C
Purge Gas Temperature	45.0 °C
Power Input to Heater	0.58 $J s^{-1}$

CHAPTER 8

FURTHER STUDIES WITH THE SCCRl IN THE SEPARATING MODE

8.0 Further Studies with the SCCR1 in the Separating Mode

8.1 The Modified Temperature Profile

8.1.1 Results

Moving the feed entry ports to the column end cones has allowed for better vaporisation of the solutes (Section 7.3.1). The vaporisation having been made easier by virtue of the spray nozzle distributor, and the improved heat transfer medium in the end cones.

The ultimate aim of the studies into the temperature profile is to try to define the perturbations in terms of physical parameters so that an accurate profile may be introduced into the mathematical model of the process. The type of temperature profile obtained when feeding was to the column centre, (Figure 6.27), is extremely difficult to simulate accurately. In any form of modelling whilst account can be taken of the sorption processes, it is desirable that the assumption of instantaneous vaporisation of the solute feed be made, with any heat effects resulting from this instantaneous vaporisation being assumed to be negligible. The validity or not of these stipulations needs to be determined experimentally. Section 7.3.2 dealt with the faster rates of evaporation obtained in the column end cones, and to investigate any temperature fluctuations, a shortened version of the experimental programme given in Section 6.5 was undertaken.

Using the same system operating under identical flow conditions as given in Section 6.5.4.1, the temperature profiles were obtained for a feedrate of 600 $cm^3.hr^{-1}$. These profiles are illustrated in Figures 8.2 to 8.6, with the detailed experimental data presented in Table 8.2 and Appendix A.7.2 to A.7.6.

The following test was also carried out to determine the degree of heat conduction through the packing and also to determine the true temperatures within the columns.

Three thermocouples were positioned 23 cm down column 1 at distances of 1.3, 2.5 and 3.8 cm from the column wall. Shortly before the maximum temperature was reached at the various measuring points, the carrier gas was cut off by energising the transfer solenoid valve at the column inlet. Movement of solute molecules continued for a short distance until the pressure in the column had been equalised. After the solute molecules have effectively come to a halt, no further temperature changes occur which can be attributed to sorption effects. The cooling down of the packing material which then occurred was due solely to heat conduction through the packing material and the thermocouples towards the column wall. The cooling per unit of time, $\Delta T/\Delta z$, (where ΔT = temperature difference, Δz = time increment in appropriate units) at the individual measuring points was determined, and the value so obtained related to the mean temperature difference, θ, between the measuring point and the column wall. These results with the corresponding cooling curves are given in Table 8.1 and Figure 8.1, with the full experimental details given in Appendix A.7.1.

8.1.2 Discussion

From the results shown in Table 8.1 it can be seen that cooling rates are essentially independent of position in the packed column and that therefore better thermal conductivity conditions do not exist in the peripheral zones. This finding is in contrast to the results of Hupe (72), who found that for a 10 cm diameter column

packed with silica gel (0.2-0.3 mm) cooling occurred much faster near to the column wall. An explanation of the disagreement of the results can be found when consideration is taken of the different methods of column packing. Hupe (72) used a method of packing proposed by Guillemin (88), in which the packing is fluidised and then allowed to settle. This method produces a very low uneven packed density in columns over 6 cm diameter (72), which may well explain the higher cooling rates in the peripheral regions. The method of packing used for the 7.6 cm diameter columns in the SCCR1 inherently involves increasing the packed density in the regions near to the column wall and therefore it is not surprising that the cooling rates in these areas are in contrast to results published by Hupe (72).

On the basis of the results shown in Table 8.1 it is possible to estimate the influence of the cooling rates upon the temperature changes in the column. Taking the results for Run 600-265-262-E6, Appendix A.7.4, a temperature rise of $5.8^{\circ}C$ above ambient is registered in a time of 100 seconds for the region around the feed point. For these figures $\Delta T/\Delta z$. $\theta = 0.15^{\circ}K.min^{-1}$. The cooling due to thermal conductivity during that time is thus, 2.7 x 1.66 x 0.15 i.e. $0.67^{\circ}C$. Similarly in the purge section a drop of $6.2^{\circ}C$ was recorded in a time of 50 seconds, from which it can be calculated that a cooling of $0.38^{\circ}C$ occurs through thermal conductivity. The examples quoted above show that the operation of the SCCR1 is far from adiabatic. If a true adiabatic system could be constructed we would observe a time/temperature relationship (for the feed region) which would rise to a maximum positive temperature and then fall off to the base line at ambient but not below it. This would be so, as the heat of adsorption is equivalent to the heat of desorption. However as shown, the system

is far from adiabatic and a considerable amount of heat is lost not only during the temperature rise of 100 seconds but also whilst the temperature remains at this elevated value. The heat lost at this stage will later be observed as a depression below the base line.

Alternatively in a true isothermal system a sample of solute would be absorped onto a section of column packing to raise it to a certain maximum temperature above ambient. If this section could then be cooled to ambient without any vaporisation of sample a negative peak exactly equal in size to the positive peak would be observed upon vaporisation of the sample. This situation could never occur because the sample cannot be prevented from vaporising, and in practice the system is between the two extremes of adiabatic and isothermal operation. The method of continuously feeding to a column for a time equivalent to one sequencing interval will tend to approach an isothermal system, but the size of the column and poor heat conduction will more than cancel out the effect from the broad feed band. The reduction in size of the temperature fluctuations, resulting from the repositioning of feed distributors are shown in Figures 8.2 to 8.6. Virtually the whole of the separating section of the SCCR1 now operates between $\pm 6^{\circ}C$ about ambient. The absence of internal/external column heating still leaves a sharp drop of $-10^{\circ}C$ in the isolated column, although this may be partly offset by preheating the purge gas stream.

Relating the experimental temperature profile to heats of absorption and desorption still remains difficult especially in the feed zone region. The discontinuous nature of operation in which the feed point advances a whole column length at the end of every sequencing interval will lead to a partial cancelling out of the sorption effects,

in that the heats of absorption from the vaporised feed solutes will in part be reduced by the desorption of the solutes already present in the liquid phase in the column. A depression in temperature recorded by the thermocouple nearest to the feed point indicates that the initial vaporisation of the solute is still to a small extent affecting the performance of the columns. Although the rates of vaporisation and heat transfer are greatly enhanced by spraying liquid feed into the column end cones, it will only be by supplying the solutes direct to the column in the vapour state that all deleterious vaporisation effects will be removed.

The isothermal diagram Figure 8.7 was produced from the results shown in Figures 8.2 to 8.6 and provides a simple means of describing the temperature distribution. It must be emphasised that the isothermal diagrams whilst proving valuable for comparative purposes with Figure 6.27, cannot be taken as being exact as the isotherms were produced by interpolation between the temperature measurements shown in Figures 8.2 to 8.6.

TABLE 8.1
Cooling Rates at 3 Positions within the Column

	3.8cm from Column Wall			2.6cm from Column Wall			1.3cm from Column Wall		
Time	ΔT	Mean Temp	$\frac{\Delta T}{\Delta Z.\theta}$	ΔT	Mean Temp	$\frac{\Delta T}{\Delta Z.\theta}$	ΔT	Mean Temp	$\frac{\Delta T}{\Delta Z.\theta}$
min	°C	°C	°C min^{-1}	°C	°C	°C min^{-1}	°C	°C	°C min^{-1}
0-1	3.3	-11.15	0.3	1.6	-8.4	0.19	1.1	-6 55	0.17
1-2	1.8	-8.6	0.21	1.2	-7.0	0.17	0.85	-5.6	0.15
2-3	1.2	-7.1	0.17	1.0	-5.9	0.17	0.75	-4.8	0.16
3-4	1.1	-5.95	0.18	0.8	-5.0	0.16	0.6	-4.1	0.15
4-5	0.8	-5.0	0.16	0.7	-4.3	0.16	0.5	-3.55	0.14
5-6	0.6	-4.3	0.14	0.55	-3.75	0.15	0.45	-3.1	0.15
6-7	0.5	-3.75	0.13	0.5	-3.25	0.15	0.45	-2.7	0.16
7-8	0.4	-3.3	0.12	0.4	-2.8	0.14	0.40	-2.2	0.18
8-9	0.4	-2.9	0.14	0.35	-2.4	0.15	0.3	-1.85	0.16
9-10	0.35	-2.5	0.14	0.3	-2.0	0.15	0.3	-1.55	0.19
10-11	0.3	-2.2	0.14	0.3	-1.7	0.18	0.25	-1.2	0.21

All Temperatures Referenced to Ambient

TABLE 8.2 Summary of Results for the Temperature Profile at a Feedrate of 600 $cm^3 hr^{-1}$

Run Title	Solute Feed Rate	I_s	$\frac{G_{m.c}}{L'}$	T_{amb}	Inlet Gas Temp	Position of Thermocouples															
						TC1		TC2		TC3		TC4		TC5		TC6		TC7		TC8	
						A	R	A	R	A	R	A	R	A	R	A	R	A	R	A	R
	$cm^3 hr^{-1}$	s		°C	°C	cm	cm	cm	cm	cm	cm	cm	cm	cm	cm	cm	cm	cm	cm	cm	cm
600-265-262-E1	591	261	255	21.2	21.2	\	\	7.6	3.8	22.9	3.8	38.1	3.8	45.7	3.8	53.3	3.8	Carrier Inlet		Ambient	
600-265-262-E4	591	261	255	21.0	21.1	\	\	7.6	2.5	22.9	2.5	38.1	2.5	45.7	2.5	53.3	2.5	"		"	
600-265-262-E6	591	261	255	21.0	21.0	\	\	7.6	1.3	22.9	1.3	38.1	1.3	45.7	1.3	53.3	1.3	"		"	
600-265-262-F1	621	261	258	21.0	22.0	\	\	7.6	0.0	22.9	0.0	38.1	0.0	45.7	0.0	53.3	0.0	"		"	
600-265-262-F3	621	261	258	21.0	22.0	\	\	15.2	1.3	15.2	2.5	15.2	3.8	30.5	3.8	\	\	"		"	

TC1, TC2 ... = Thermocouple N° 1,2 ... etc

A = Axial Distance from Top of Column

R = Radial Distance from Column Wall

Figure 8.1 Cooling Rates within the Columns

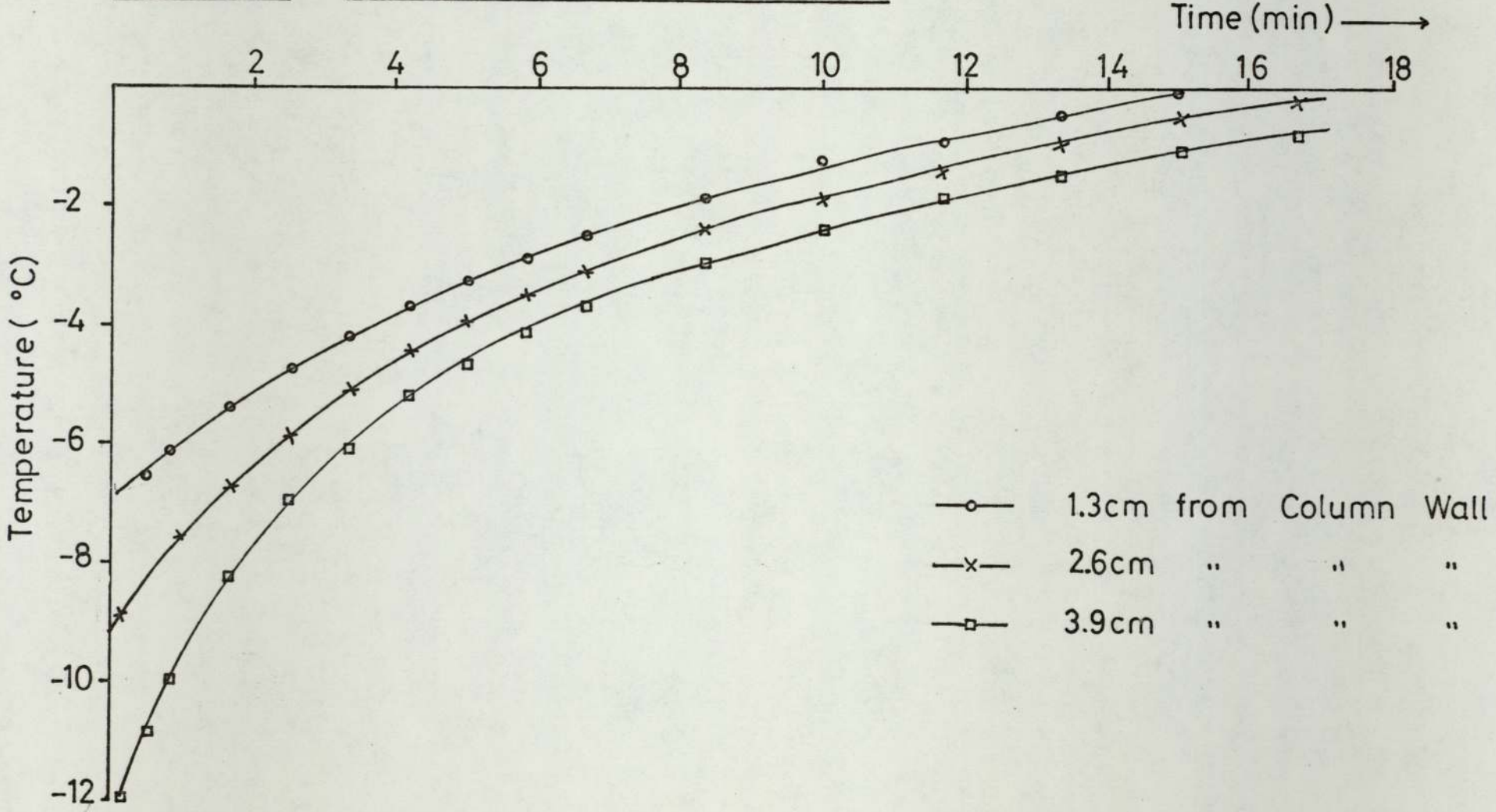

Figure 8.2 Temperature Profile for a Feedrate of 600cm^{3}hr^{-1} (TC's 3.8cm into Column)

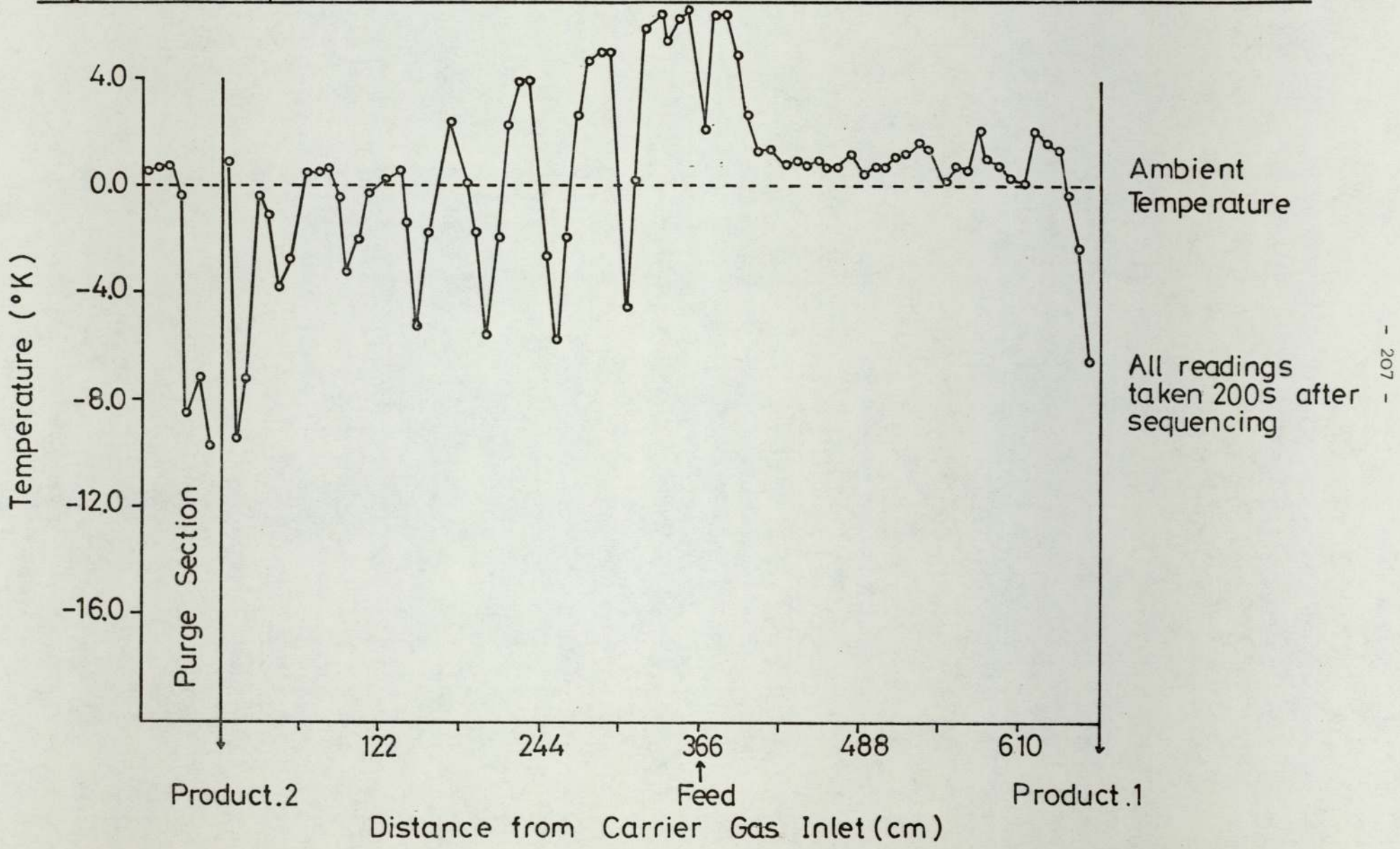

Figure 8.3 Temperature Profile for a Feedrate of 600cm^{3}hr^{-1} (TC's 2.5cm into Column)

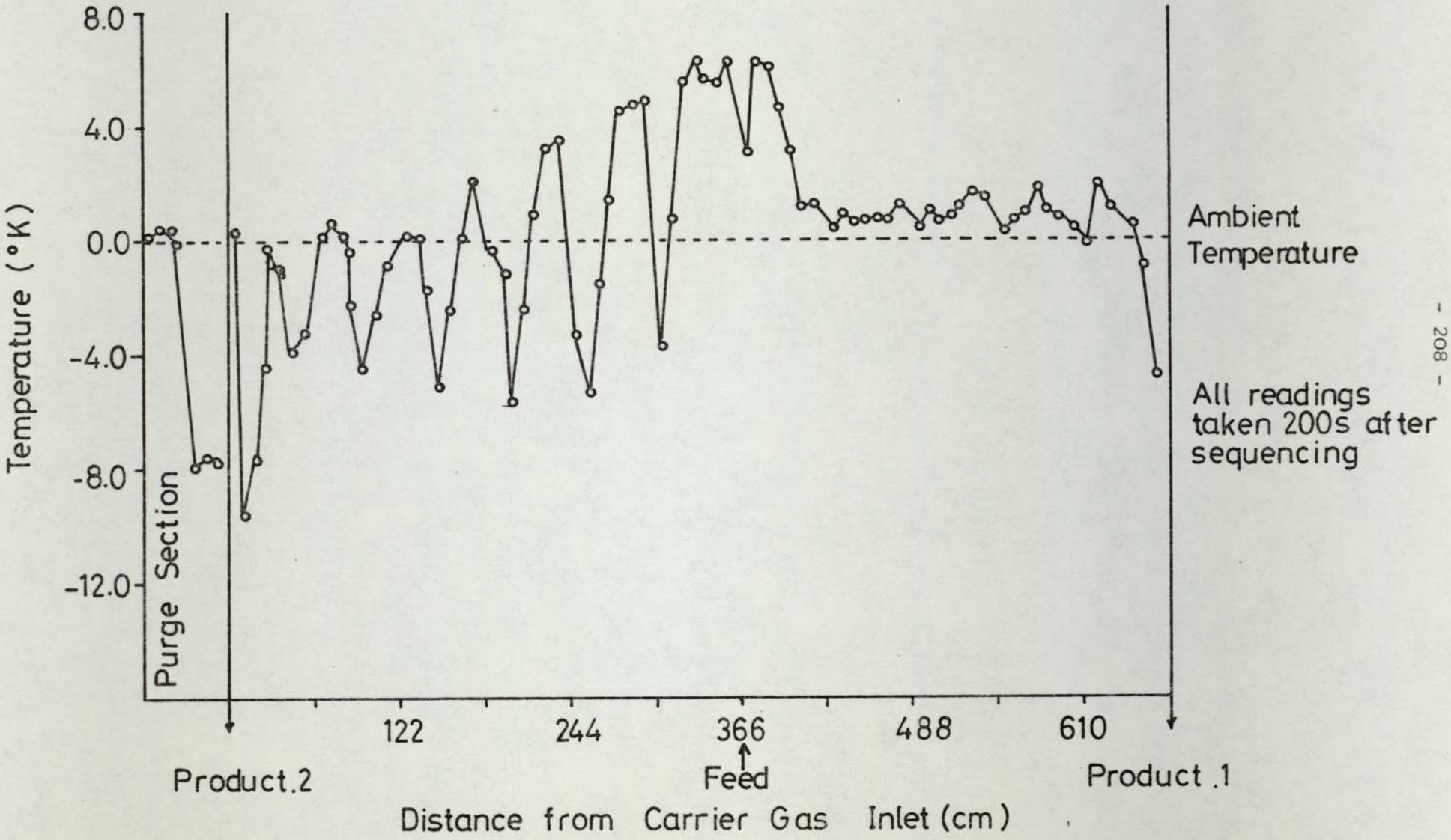

Figure 8.4 Temperature Profile for a Feedrate of 600 $cm^3 hr^{-1}$ (TC's 1.3cm into Column)

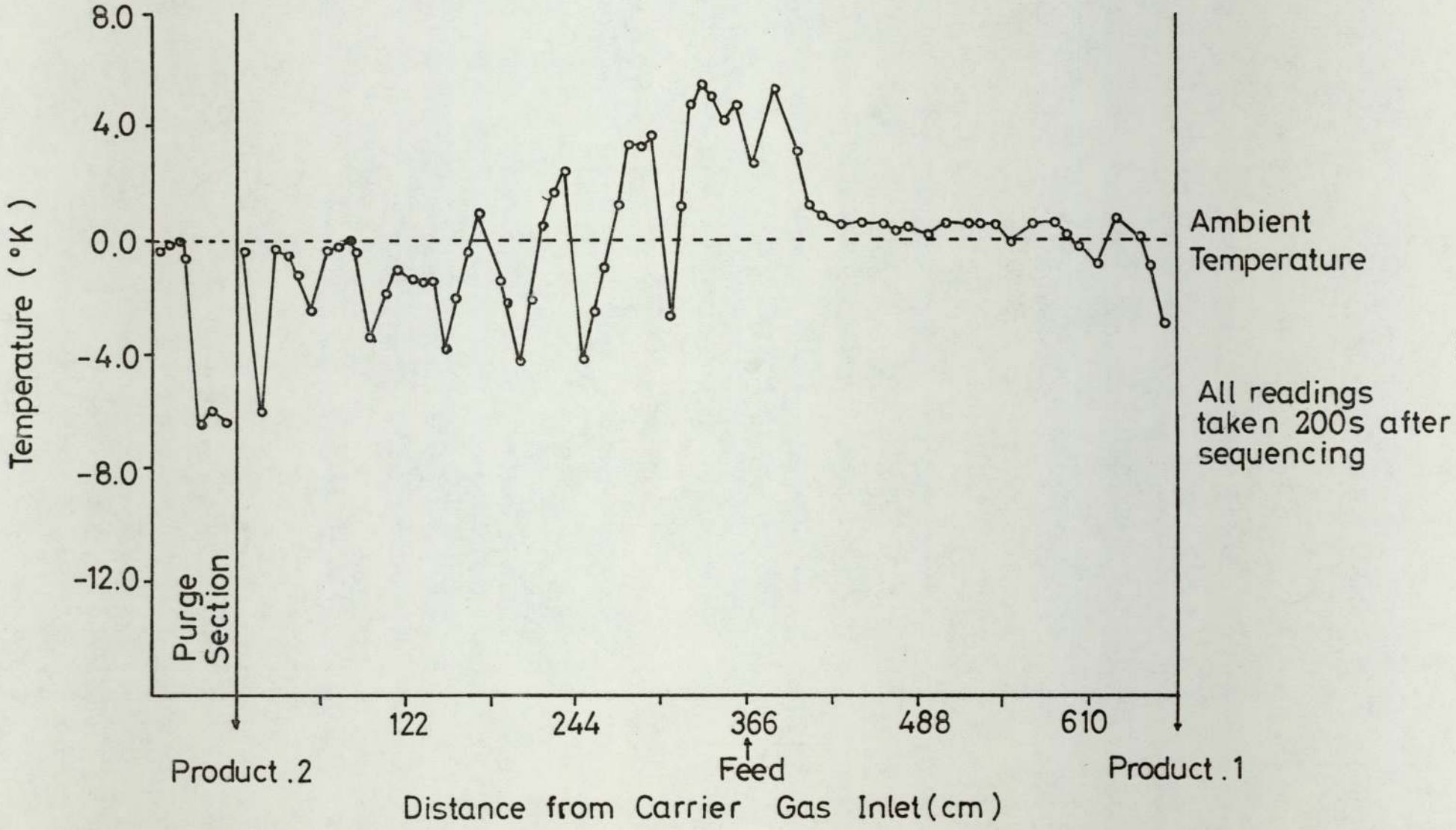

Figure 8.5 Temperature Profile for a Feedrate of 600cm^3 hr^{-1} (TC's at Column Wall)

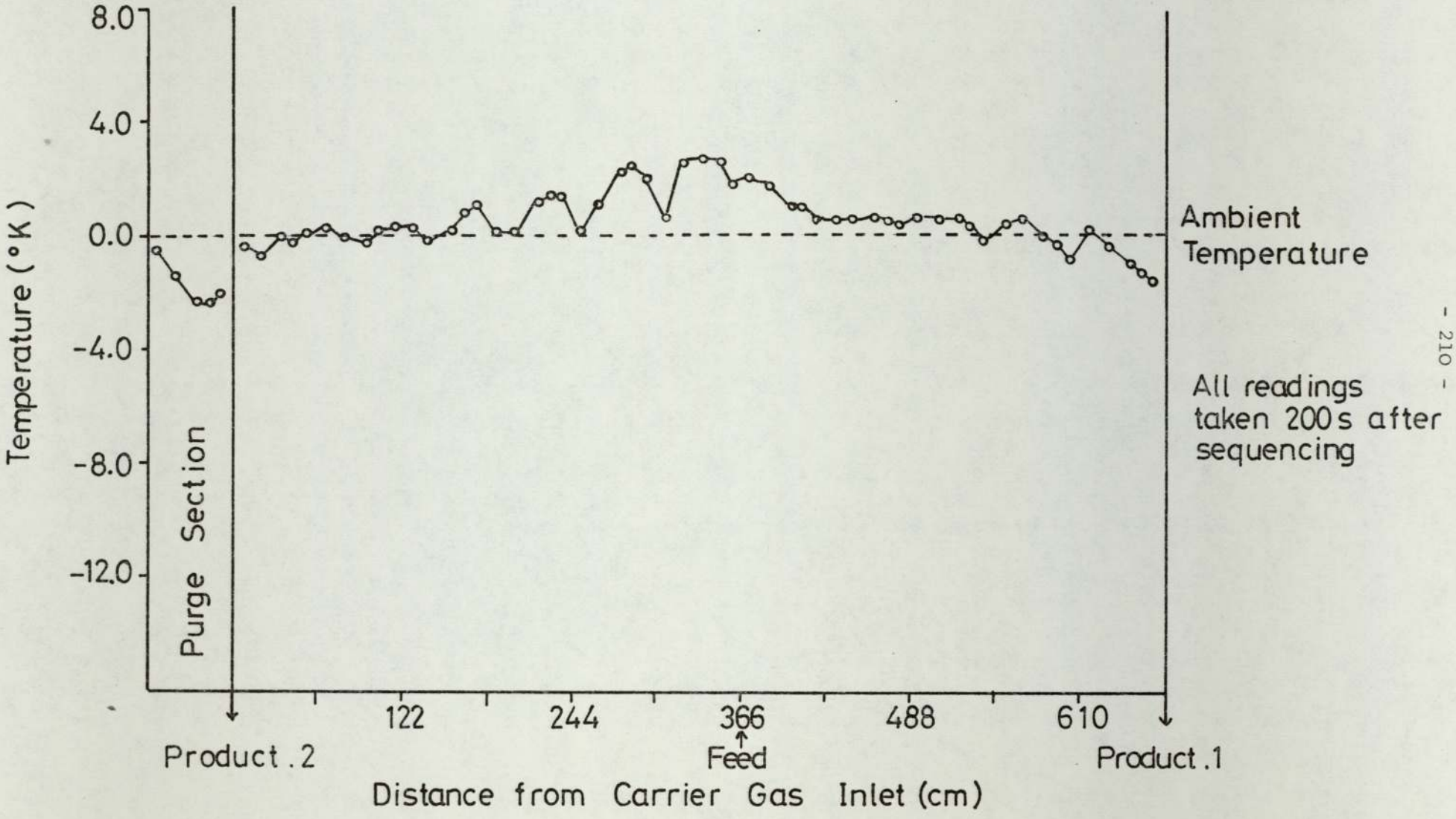

Figure 8.6 Temperature Profile for a Feedrate of 600 $cm^3 hr^{-1}$ (TC's 3.8cm into Column)

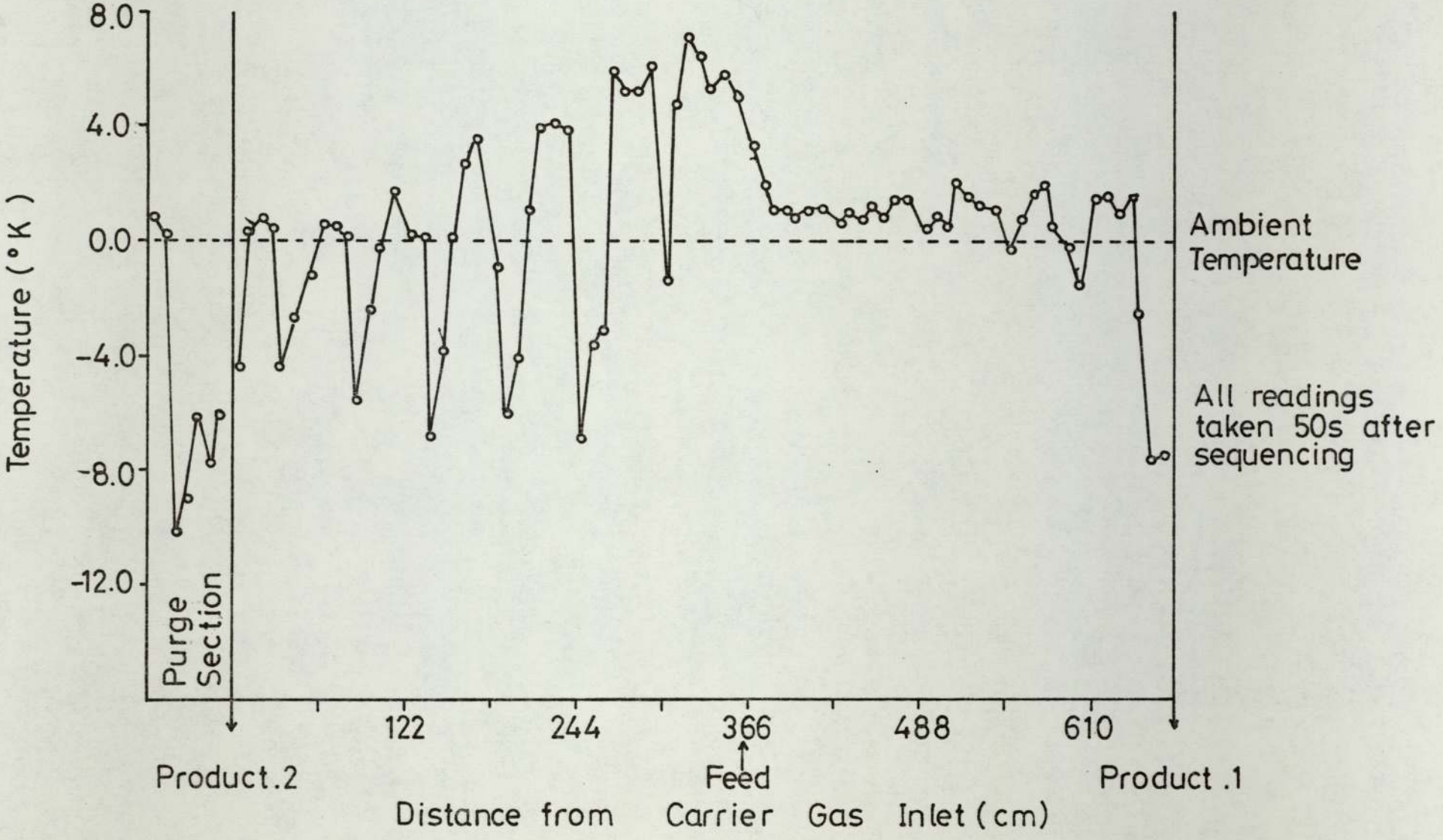

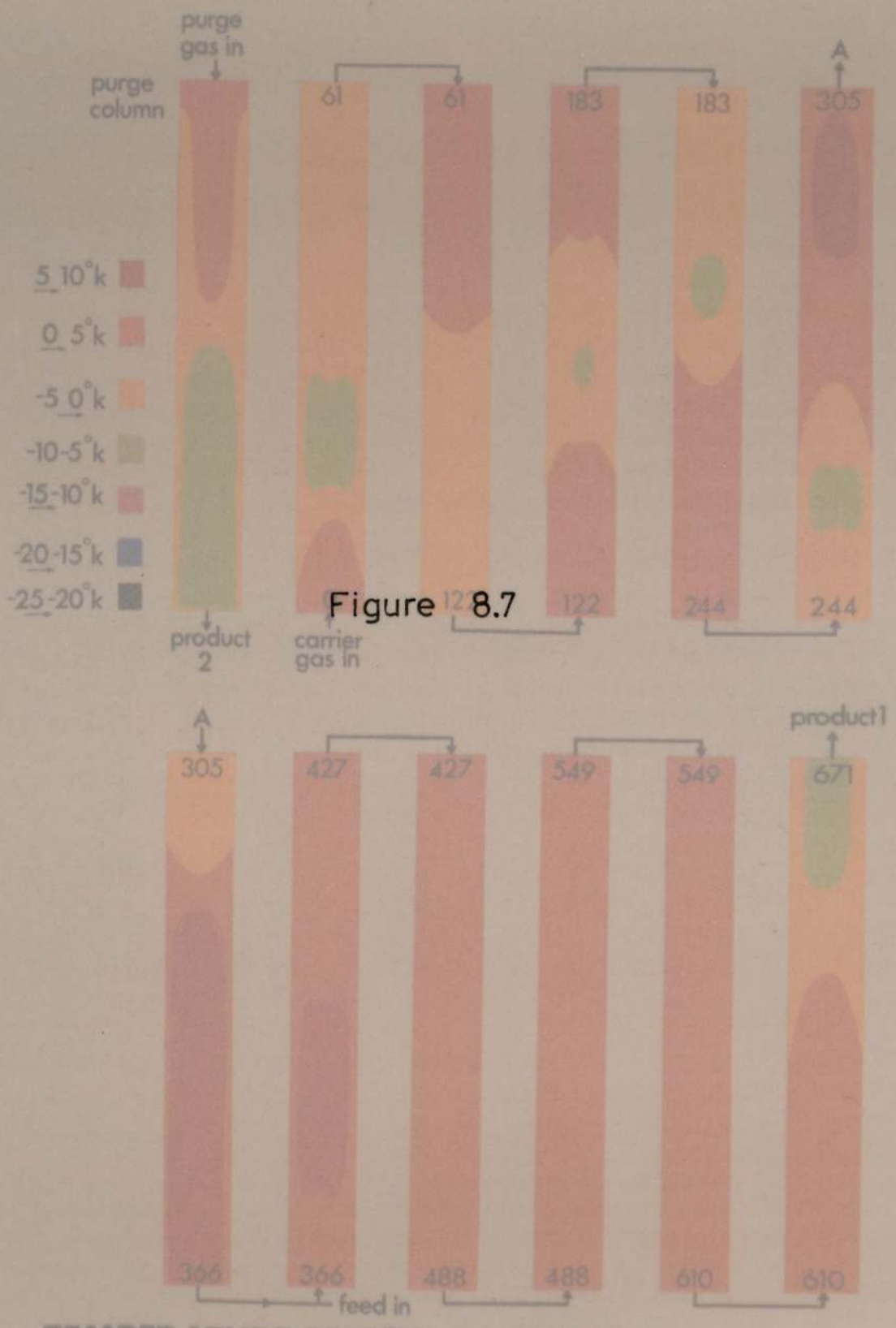

Figure 8.7

TEMPERATURE EFFECTS IN SEQUENTIAL CHROMATOGRAPHIC UNIT WITH FEED INTO END CONE

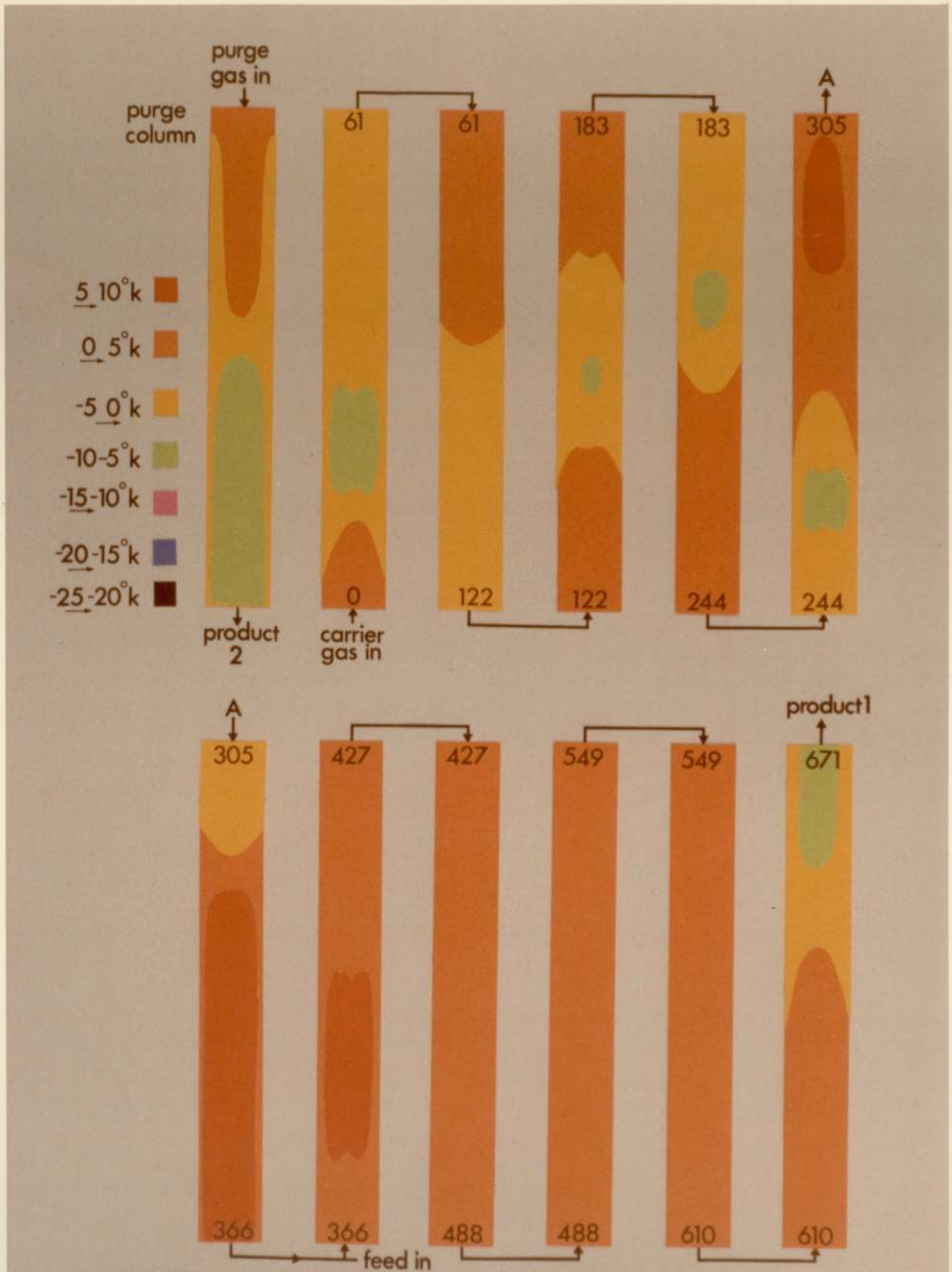

TEMPERATURE EFFECTS IN SEQUENTIAL CHROMATOGRAPHIC UNIT WITH FEED INTO END CONE

8.2 Maximising Solute Feedrate for the System Arklone.P./Genklene.P.

8.2.1 Results

A similar experimental programme was conducted as that illustrated in Section 6.4.

Using a 50:50 by volume mixture of Arklone.P. and Genklene.P., the feedrate was increased from 400 cm^3hr^{-1} up to 1200 cm^3hr^{-1} in intervals of 200 cm^3hr^{-1}. After a successful separation was obtained at 1200 cm^3hr^{-1}, the feedrate was increased by 100 cm^3hr^{-1} intervals until severe contamination of the products occurred. A successful separation may be defined as one having reproducible solute concentration profiles with product purities at all times greater than 99.5%. It must be emphasised that the product purities quoted in Table 8.4 were at their worst possible value during the sequencing interval, and had they been recorded at an optimum time during the interval all purities barring those for Run 1500-265-262-A would have been in excess of 99.9%.

The ratio of $G_{m.c}$ to L' was again specified at 265, although accurate determinations of $G_{m.c}/L'$ later showed these values to be slightly lower than anticipated. In earlier runs (Section 6.4), it had been possible to increase the purge gase flowrate up to 2850 $cm^3.s^{-1}$, however during these later studies the maximum purge flowrate obtainable was 2300 $cm^3.s^{-1}$. This loss of efficiency was attributed entirely to decreasing mechanical efficiency in the SCCR1, caused by continual operation over a period of 4 years. Although regular maintenance was carried out, it is recommended that should further studies be conducted with the unit a complete overhaul be carried out with replacement of all the air distribution networks and associated filtration system.

A summary of experimental and computed results is given in Tables 8.3, 8.4, with the concentration profiles being illustrated in

Figures 8.8 to 8.15. Full details of the runs appear in Appendices A.7.7 to A.7.14.

8.2.2 Discussion

Consideration of Figures 8.8 to 8.15, shows a marked improvement in the separating capabilities of the SCCR1. The mechanical design changes discussed in Chapter 7 have allowed the maximum feed throughput to be increased to 1400 $cm^3.hr^{-1}$. Without a major redesign of the unit, incorporating internal column heating, and recoating of the packing it would appear that the limits of feed throughput from both a mechanical and a chromatographic sense have been reached.

Comparison of the individual solute profiles is again valuable in giving an insight into the mechanisms of separation. With respect to Arklone.P., the mean level of gas phase concentration rises proportionately with increasing feedrate. Up to a feedrate of 1000 $cm^3.hr^{-1}$ the trailing edge of the profile has not extended more than three column lengths behind the feed point. Beyond 1000 $cm^3.hr^{-1}$ the profile gradually extends towards the isolated section until for Run 1500-265-262-A contamination of the Genklene.P., Product 2 occurs. The gradual decrease in Arklone.P. concentration between the feedpoint and the isolated column indicates that the whole of this section, i.e. 6 columns is being utilised for separation purposes. Prior to repositioning the feed valves no more than 3 columns in this section could be utilized for separation because of the presence of unvaporised feed. [See for example Figure 6.15, Section 6.4.2, where the Arklone.P. profile has extended more than two column lengths behind the feed point before separation commences and the Arklone.P. concentration level starts to fall].

Saturation point in the gas phase has not been reached with Arklone.P. The highest recorded on-column concentration was 1.18 x 10^{-3} $g.cm^{-3}$ for Run 1500-265-262 A. The partial pressure exerted by the Arklone.P. was calculated to be 16.7 $kN.m^{-2}$, whereas the saturated vapour pressure at 22°C was found to be 38.0 $kN.m^{-2}$.

N.B. The S.V.P. for Arklone.P. was calculated at 22°C as this was the ambient temperature for Run 1500-265-262.A. It is well appreciated that temperature fluctuations are present giving rise to variations in S.V.P's. However the maximum on-column Arklone.P. concentration was measured in front of the feed point where it is very unlikely that the temperature of the gas phase is below ambient. Hence the value of 38.0 $kN.m^{-2}$ will be a conservative estimate of the saturated vapour pressure at the position of maximum concentration.

The behaviour of the Genklene.P. profile during the study was in marked contrast to the results shown in Chapter 6. The profile was very much 'flatter', in that for the seven columns where Genklene.P. was present, six of columns exhibited concentrations of the same order of magnitude. The leading edge of the profile was again very sharp and even at feed rates of 1400 $cm^3 hr^{-1}$ Genklene.P. had not advanced more than 1 column in front of the feedpoint. The mean level of gas phase concentration increased with increasing feedrate up to Run 1200-265-262-A, at which point the standardised concentration was approximately 0.11 x 10^{-3} $g.cm^{-3}$. Above a feedrate of 1200 cm^3 hr^{-1} the mean level of Genklene.P. gas phase concentration did not appear to increase beyond 0.11 x 10^{-3} $g.cm^{-3}$.

The situation where the concentration reaches a maximum level and does not exceed this value even though the feedrate continues to increase, was experienced in previous separation studies in Section 6.4.2.

The maximum level for these previous results was approximately 0.05 $g.cm^{-3}$. Saturation of the gas phase with Genklene.P. vapour was put forward to explain the experimental results, and again this would seem to be occurring for the later experimental runs above a feedrate of 1200 $cm^3 hr^{-1}$.

Although repositioning the feed values has reduced cooling effects through vaporisation, cooling of the gas phase still occurs at points between the feedpoint and the isolated section. It is probable that at these positions the partial pressure of Genklene.P. reaches saturation point and condensation from the gas phase may even occur. Verification of this hypothesis may be obtained from a consideration of the vapour pressures of Genklene.P. within the unit.

From a standardised concentration of 0.11×10^{-3} $g.cm^{-3}$ the maximum on-column concentration will be approximately 0.44×10^{-3} cm^{-3}, at which value the partial pressure of Genklene.P. is 9.1 $kN.m^{-2}$. At $20^{\circ}C$, $P^{\circ}_{G.P}$ is 12.1 $kN.m^{-2}$, and it only requires the temperature to fall to $13^{\circ}C$ before the gas phase becomes saturated with Genklene.P. vapour. A temperature of $13^{\circ}C$ is very possible within the SCCRl especially at the feedrates above 1000 $cm^3.hr^{-1}$.

Table 8.3
The Study of Feedrate for the System Arklone.P / Genklene.P

Experimental Settings

Run Title	Solute Feed Rate	I_s	L'	P_a	T_a	Separating Section				Purge Section			
						G_a	P_{in}	P_{out}	G_{mc}/L'	S_a	P_{in}	P_{out}	S_{mc}/L'
	$cm^3 hr^{-1}$	s	$cm^3 s^{-1}$	$kN m^{-2}$	°C	$cm^3 s^{-1}$	$kN m^{-2}$	$kN m^{-2}$		$cm^3 s^{-1}$	$kN m^{-2}$	$kN m^{-2}$	
400-265-262-E	390	264	1.476	101	21.0	1150	396	197	256	1766	273	214	488
600-265-262-D	604	262	1.487	100	22.0	1150	395	188	254	2180	272	215	596
800-265-262-F	823	262	1.487	99	20.0	1150	394	187	252	2180	271	202	604
1000-265-262-B	1040	261	1.493	101	21.5	1150	396	197	253	2300	273	211	639
1200-265-262-A	1216	261	1.493	101	23.0	1150	396	197	253	2300	273	214	636
1300-265-262-A	1316	261	1.493	102	22.5	1150	397	189	258	2300	274	200	660
1400-265-262-A	1385	263	1.482	101	22.0	1150	400	194	254	2300	273	194	667
1500-265-262-A	1504	261	1.493	101	23.0	1150	396	194	254	2300	273	211	639

Table 8.4
The Study of Feedrate for the System Arklone.P / Genklene.P

Computed Results

Run Title	K^{∞}_{+} K_{max}		Sepn' Sect'		Purge Sect'		% Product Purity		Conc' Analysis Results in Appendix	Conc' Profile in Figure
	A.P	G.P	G_{min} L'	G_{max} L'	S_{min} L'	S_{max} L'	A.P	G.P		
400-265-262-E	137	411	198	400	442	564	>99.8	>99.8	A.7.7	8.8
600-265-262-D	133	396	196	411	539	681	>99.7	>99.5	A.7.8	8.9
800-265-262-F	144	429	194	409	535	718	>99.8	>99.6	A.7.9	8.10
1000-265-262-B	136	406	196	395	570	737	>99.8	>99.7	A.7.10	8.11
1200-265-262-A	129	384	196	395	570	727	>99.8	>99.2	A.7.11	8.12
1300-265-262-A	126	391	198	416	573	786	>99.8	>99.7	A.7.12	8.13
1400-265-262-A	124	369	196	404	574	808	>99.7	>99.6	A.7.13	8.14
1500-265-262-A	130	382	196	401	570	737	84	93	A.7.14	8.15

Figure 8.8 Standardised Concentration Profile for Run 400-265-262-E

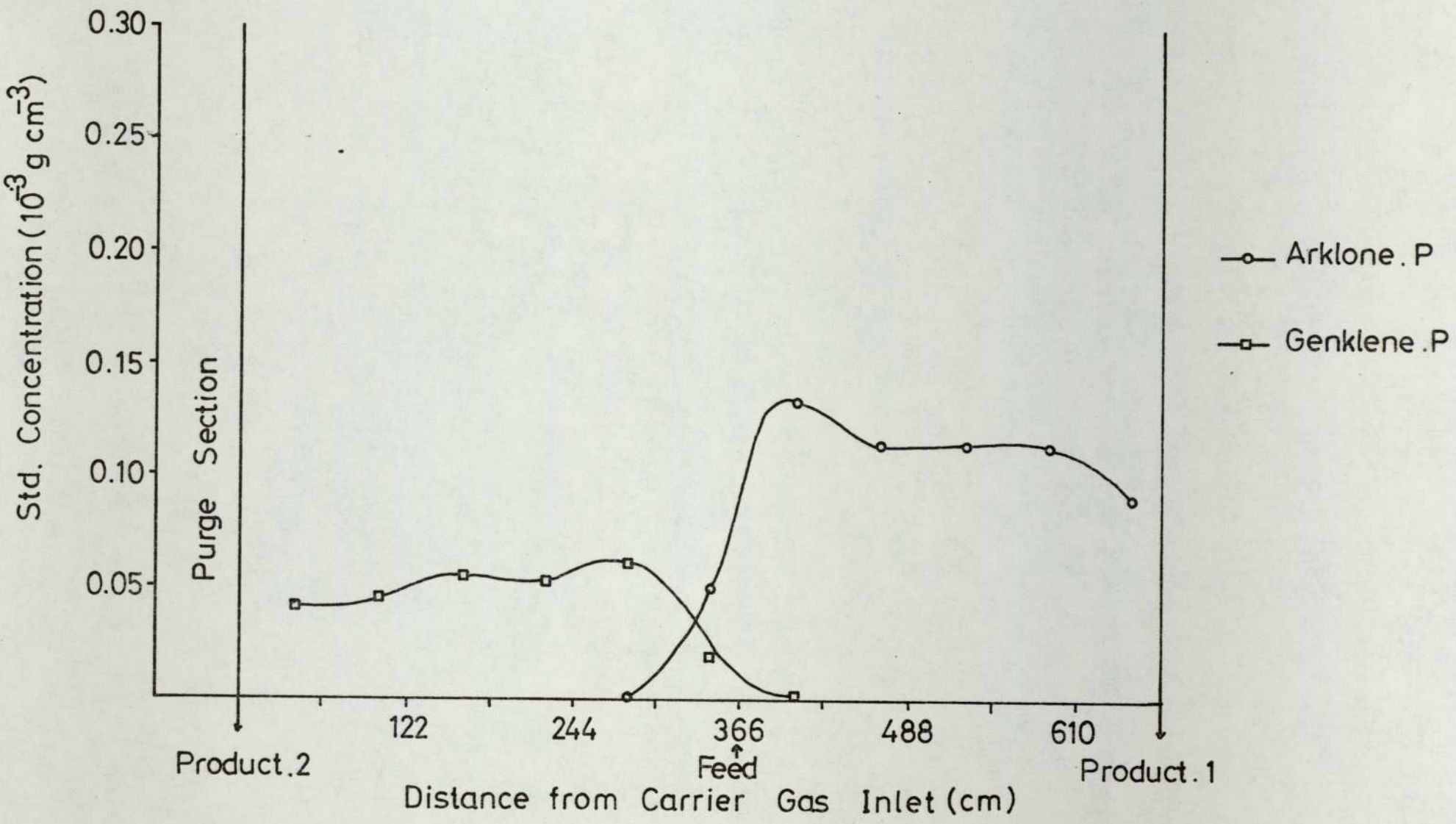

Figure 8.9 Standardised Concentration Profile for Run 600-265-262-D

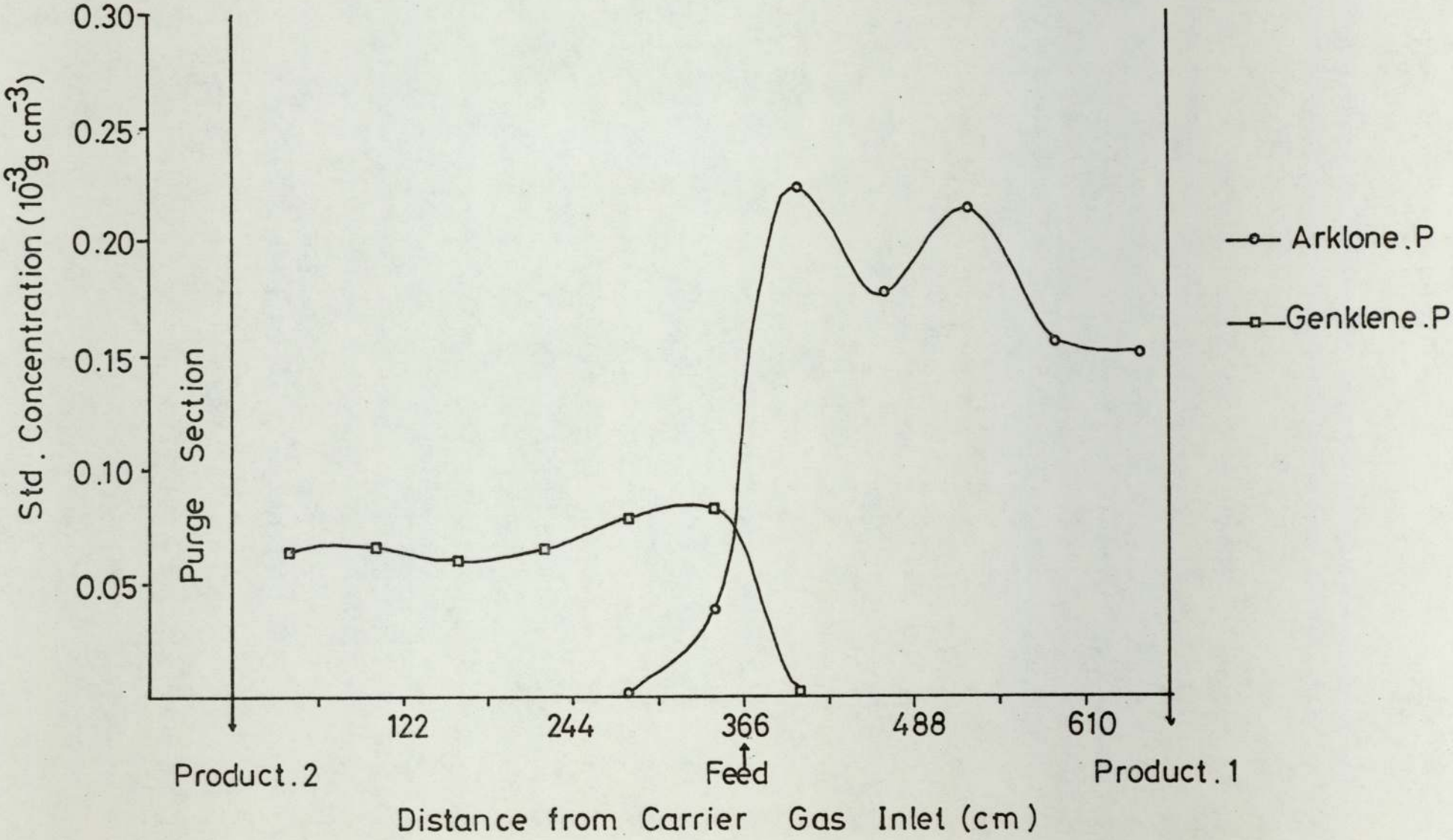

Figure 8.10 Standardised Concentration Profile for Run 800-265-262-F

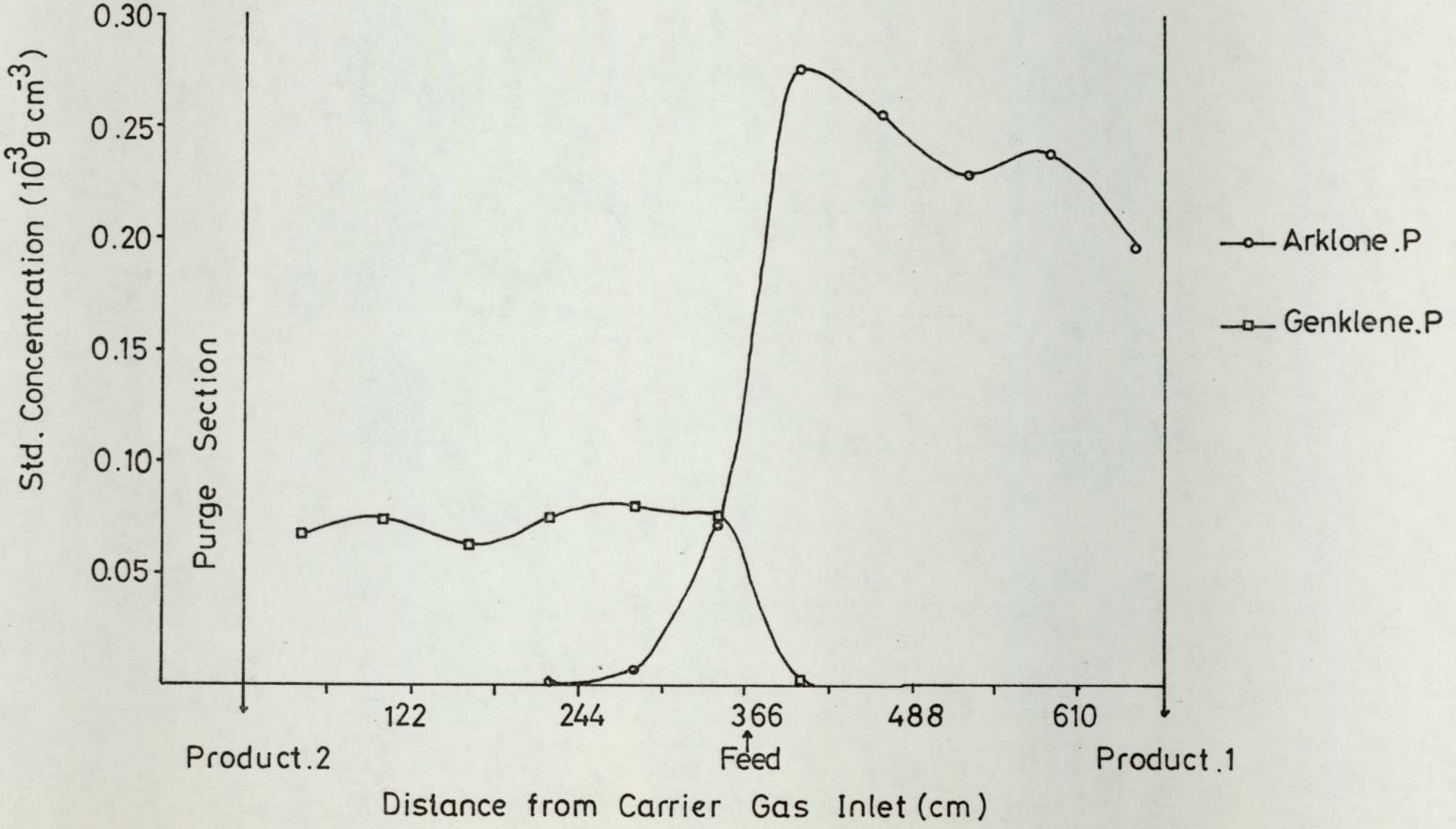

Figure 8.11 Standardised Concentration Profile for Run 1000-265-262-B

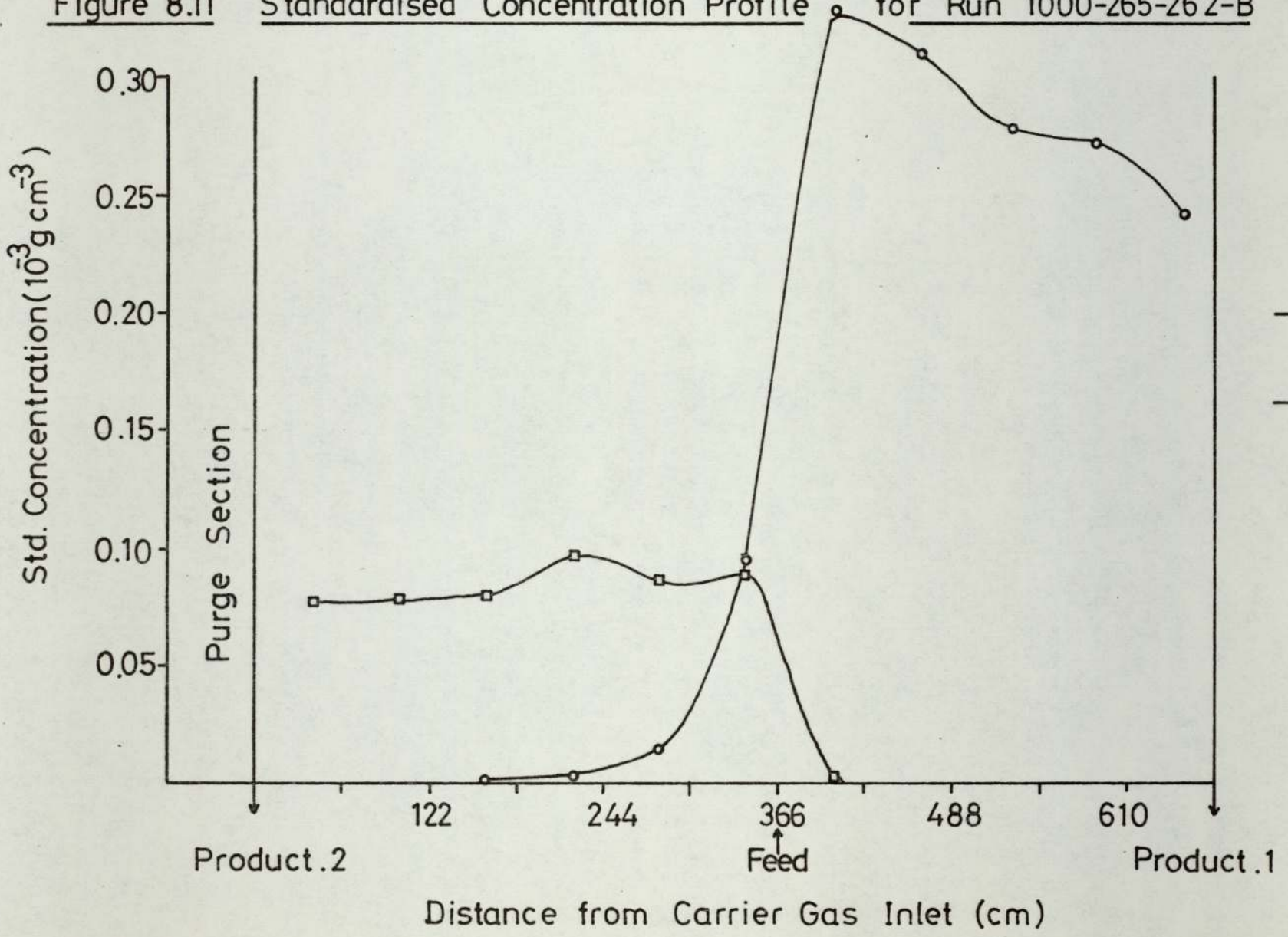

Figure 8.12 Standardised Concentration Profile for Run 1200-265-262-A

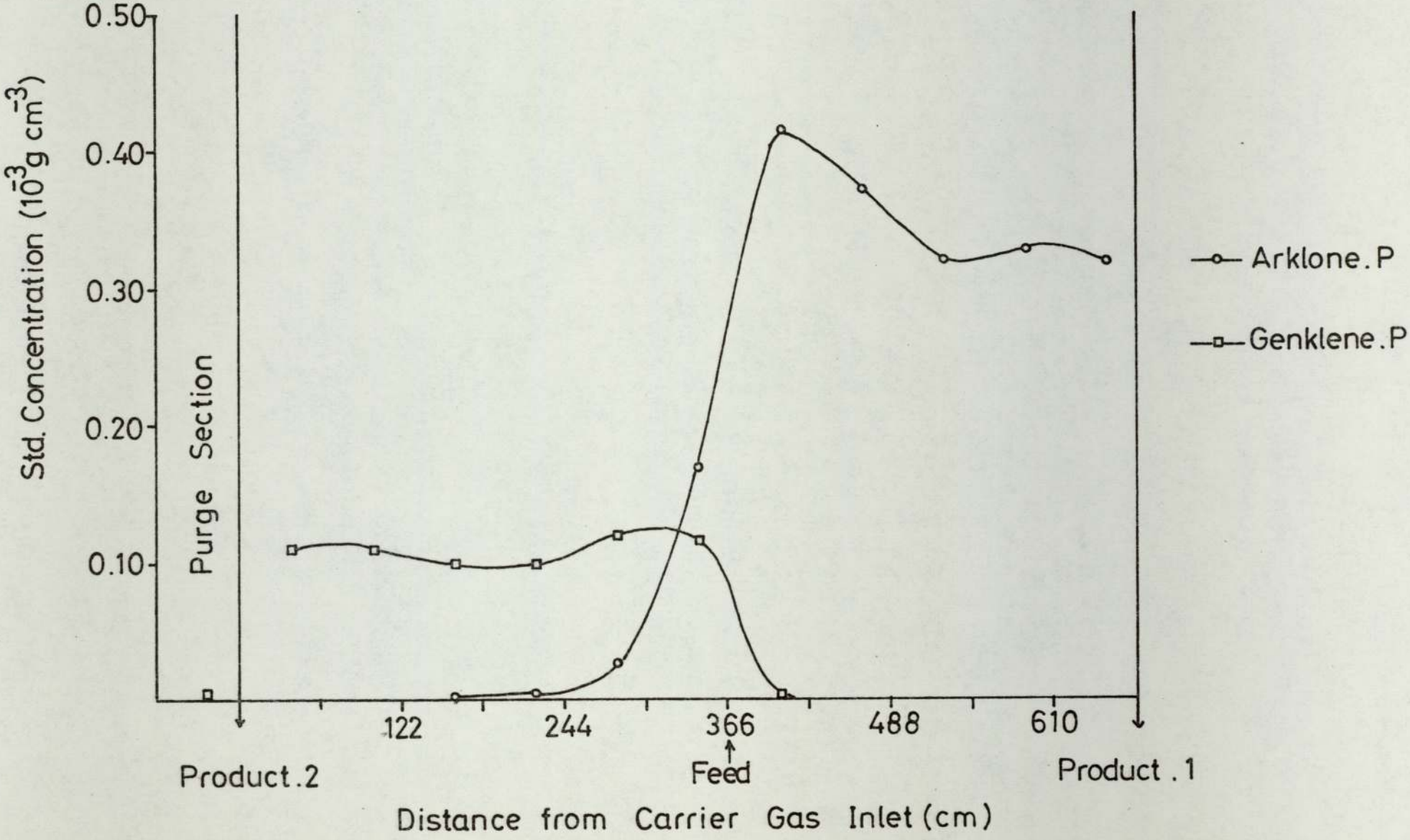

Figure 8.13 Standardised Concentration Profile for Run 1300-265-262-A

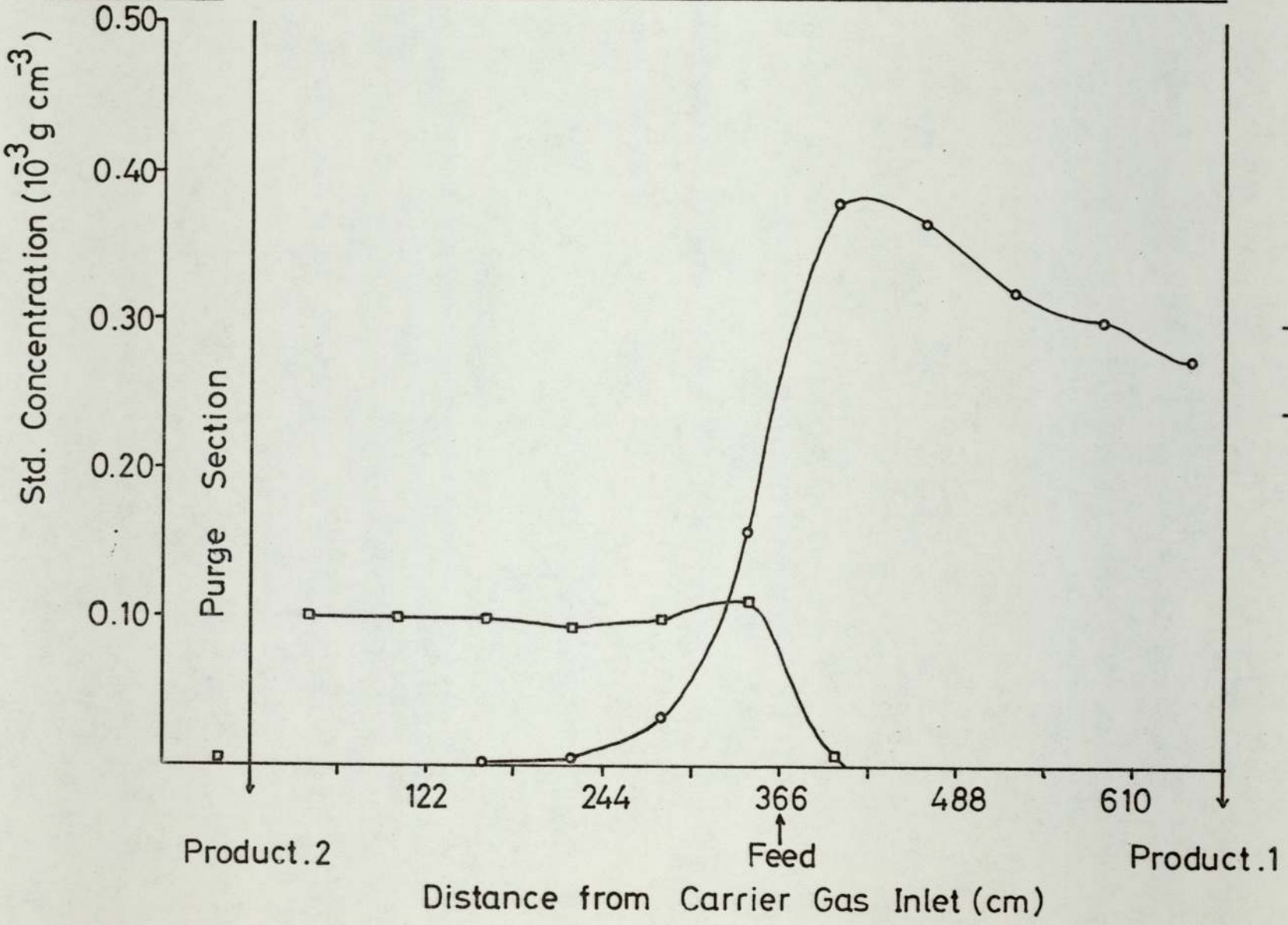

Figure 8.14 Standardised Concentration Profile for Run 1400-265-262-A

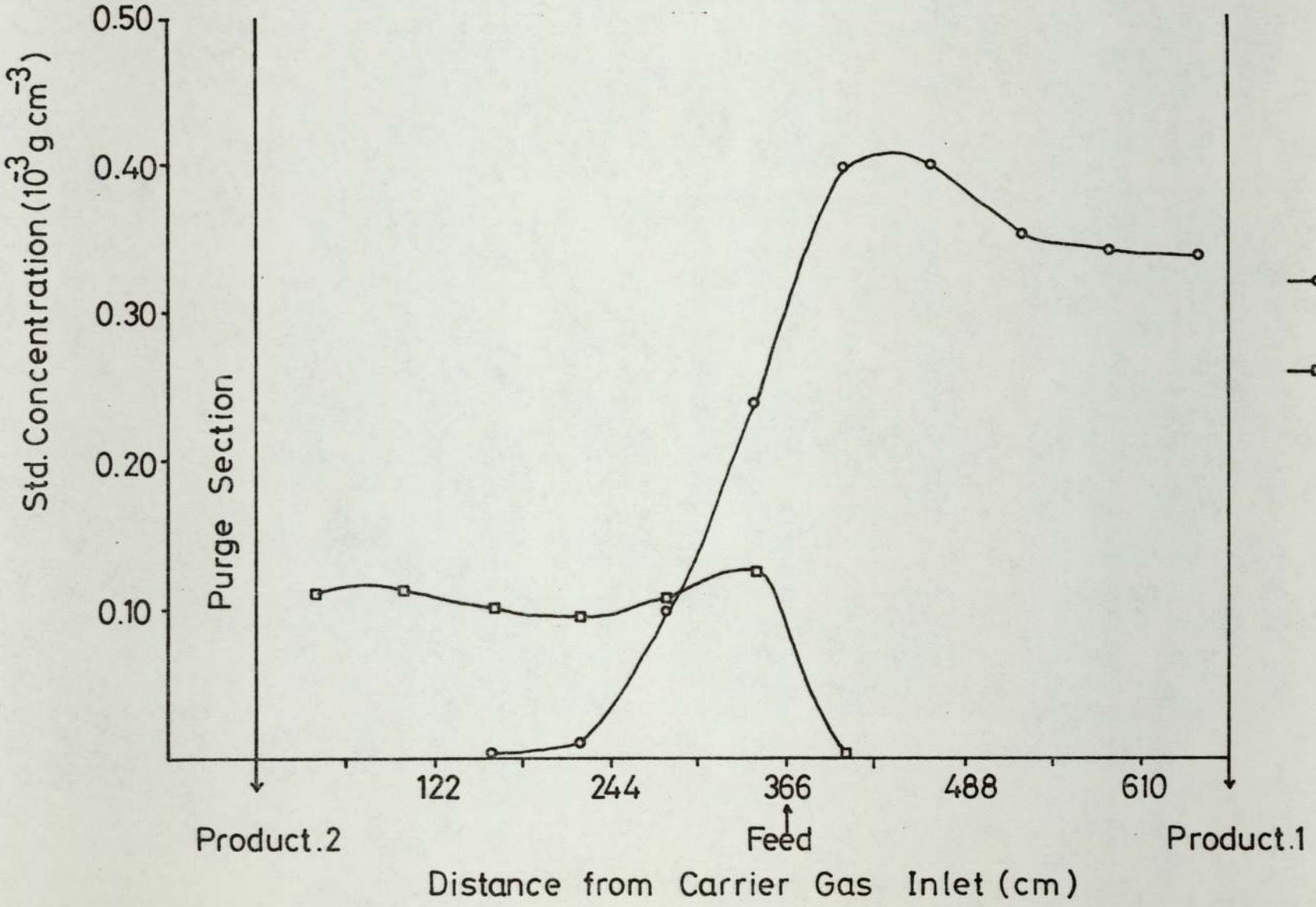

Figure 8.15 Standardised Concentration Profile for Run 1500-265-262-A

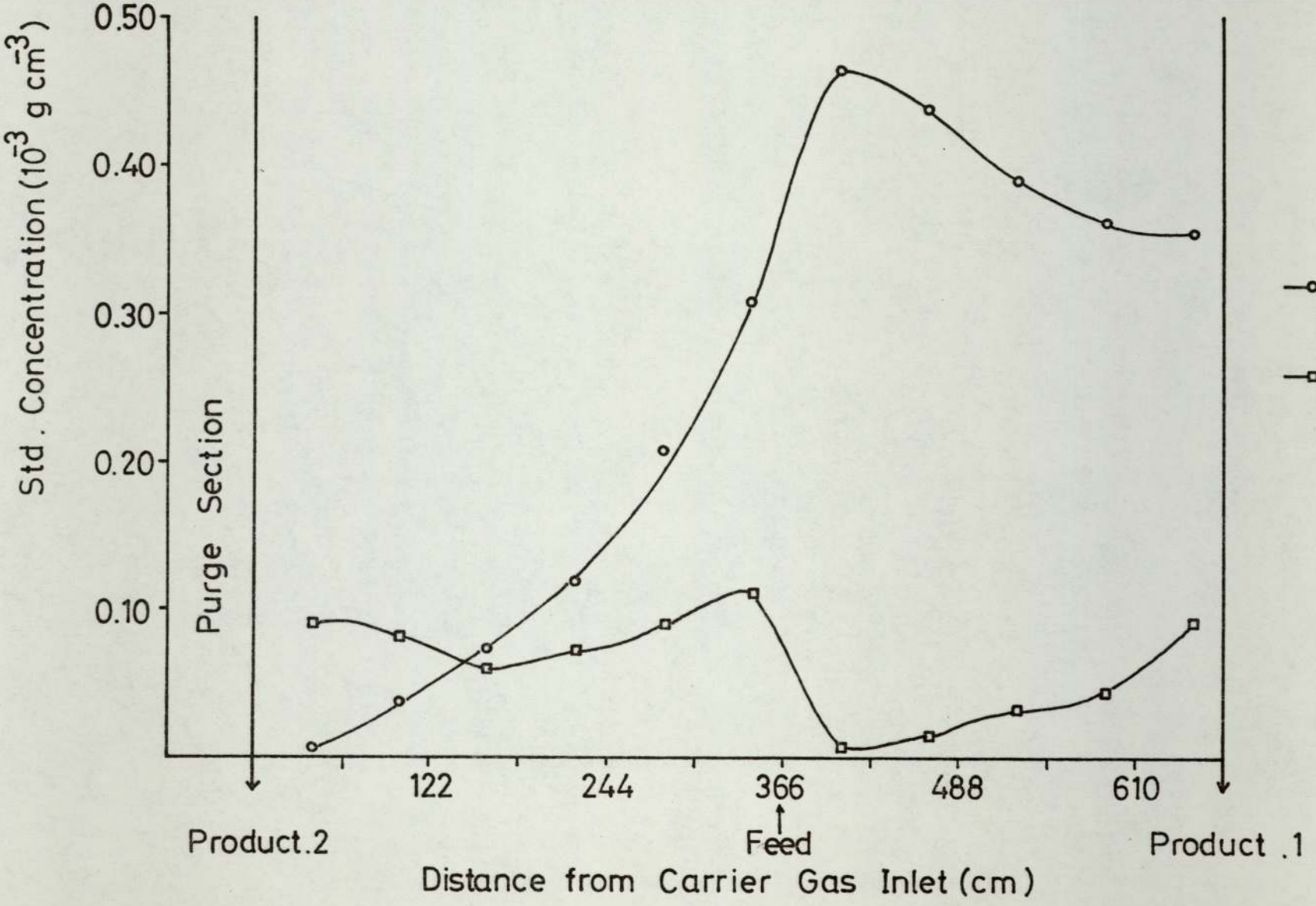

8.3 Investigations with the System Arklone.P./Dichloromethane

8.3.1 Introduction

The results presented so far in Chapters 6, 7 and 8, have followed a chronological pattern with the initial studies being followed by the design changes and then the later investigations with Arklone.P./Genklene.P. The studies with the system Arklone.P./Dichloromethane were not as extensive as for Arklone.P./Genklene.P. and therefore for clarity all results both before and after the redesign of the unit have been grouped together under one heading.

The restrictions governing the choice of a second system for study have been outlined in Section 4.1, and consequently dichloromethane (d.c.m) along with Arklone.P. was the only possible combination of solutes giving a separation factor of less than two. At 20^{o}C the partition coefficients at infinite dilution for Arklone.P. and d.c.m., indicated a separation factor of 1.17 for the pair, and even ignoring any temperature and concentration effects upon the partition coefficients, a successful separation of the system into two pure streams would be highly unlikely solely from the fact that the value of G/L' will roughly double between the carrier gas inlet and outlet.

8.3.2 Results Prior to Mechanical Design changes in the SCCR1

Inherent with any system of low separation factor is the fact that throughputs will be comparatively small and therefore it was proposed to operate the unit at the lowest possible feedrate that the feed pump could accurately deliver, this feedrate having a value of approximately 100 $cm^3.hr^{-1}$, for a 50:50 mixture of Arklone.P./dichloromethane.

In selecting a value for $G_{m.c}/L'$ a similar procedure was adopted as for the system Arklone.P./Genklene.P., in that $G_{m.c}/L'$ was set midway between the partition coefficients for Arklone.P. and dichloromethane, measured at infinite dilution and 20°C. These values were 141 and 120 respectively, giving $G_{m.c}/L'$ as 130.5, for which an arbitary sequencing interval of 150 seconds was programmed into the automatic sequencing/timer unit.

Operating the SCCR1 unit with the above conditions produced no separation whatsoever, with both solutes being carried in the direction of mobile phase flow and exiting from the Product 1 port. A trial and error procedure followed to determine the range of $G_{m.c}/L'$ over which a measure of separation could be achieved. Results presented in Table 8.5 were obtained for $G_{m.c}/L'$ values of 120, 115 and 110, with the relevant concentration profiles given in Figures 8.16 to 8.19. Further details for the runs are given in Appendix A.7.15 to A.7.18.

8.3.3 Discussion

Dichloromethane possessing a lower partition coefficient than Arklone.P. is preferentially carried with the mobile phase, whilst the Arklone.P. travels in the direction of packing to exit in the purge column as Product 2. (c.f. system Arklone.P./Genklene.P., where the Arklone.P. travelled in the direction of carrier gas flow and exited as Product 1.).

At the low solute feedrate used, i.e. 100 $cm^3.hr^{-1}$, it is unlikely that any feed is remaining in the liquid state within the columns, and therefore the poor separations obtained cannot be attributed

to this cause. The saturated vapour pressure for dichloromethane is considerably higher than that of Genklene.P. at the same temperature, and hence it is to be expected that a system of Arklone.P./d.c.m. will prove easier to vaporise than the system Arklone.P./Genklene.P.

A mechanical defect which may well be producing inefficiencies concerned the feed distribution network. This network was not designed for low feed throughputs, and to achieve a mean feedrate of 100 $cm^3.hr^{-1}$ the reciprocating feed pump had to be fitted with 5:1 reduction gear. This immediately has the effect of producing 'slugs' of solute rather than a continuous input. More importantly perhaps is the fact that the discontinuous nature of operation at the end of a sequencing interval involves a pressure change of approximately 20 kN m^{-2}, as the feed port is switched to an adjacent column. Accurate monitoring of feedrate requires that the pressure in the central feed distributor be equalised with the pressure in the columns to which the solutes are to enter. The sudden change in column pressure of 20 $kN.m^{-2}$ will produce a surge of feed from the distributor into the column and whilst at the most this will be only 1-2 cm^3 it does mean that possibly 25% of the feed due to enter the column during a sequencing interval is entering in one surge. Obviously at higher feedrates the effects of this surge will be greatly reduced.

The results shown in Figures 8.16 to 8.19 show the sensitivity of the system to changes in $G_{m.c}/L'$. For Run 100-120-150-A the Product 2 purity is considerably higher than Product 1 and yet changing the $G_{m.c}/L'$ value by only 10, i.e. Run 100-110-150-A, has the effect of retarding the movement of solute in the direction of carrier flow and reversing the relative product purities. Reproducibility of the

profiles and purities as such proved impossible. Run 100-120-150-B was performed to try to duplicate the profile for Run 100-120-150-A but as comparison of the respective profiles shows little success was obtained. Not only was reproducibility between successive runs unobtainable, but the concentration profile between successive cycles of operation also changed appreciably and an equilibrium situation was never attained. The separation of Arklone.P./dichloromethane into even one pure product stream was thus thought to be beyond the separating capabilities of the SCCR1.

8.3.4 Results Taken after the Design Changes

For the system Arklone.P./dichloromethane a further modification to the unit was adopted, in that the reciprocating feed pump was fitted with a smaller delivery head thereby allowing the removal of the reduction gear. Greater accuracy in the monitoring of solute feed throughputs resulted.

Three runs, were performed in which the ratio of $G_{m.c}/L'$ varied between 135 and 115. Further tests were then carried out to observe the ability of the unit to reproduce the profiles. All runs were at a constant feedrate of 100 $cm^3.hr^{-1}$, and a sequencing interval of 150 seconds. The results are given in Tables 8.6, 8.7, Figures 8.20 to 8.24, and Appendix A.7.19 to A.7.25.

8.3.5 Discussion

The definition of a successful separation for Arklone.P./Genklene.P. has been given as one having product purities in excess of 99.5% and reproducible solute concentration profiles. The same

stringent limits cannot be applied to a system possessing a separation factor of 1.17, however an arbitary definition gives a successful separation as one in which the concentration profile can be easily reproduced and one product is at a purity of greater than 99%.

Comparing the results for the experimental runs conducted at constant solute feedrate of 100 $cm^3.hr^{-1}$, re-emphasises the importance of the $G_{m.c.}/L'$ ratio to the successful separation of this chemical system. The shape of the solute concentration profiles given in Figures 8.20 to 8.24, are as expected for a system having similar partition coefficients, with the maximum concentrations for both solutes centreing around the feed point. The profiles then fall away gently to their respective product streams. Sharp leading and trailing edges to the profiles, common to the system Arklone.P. and Genklene.P. were understandably not present for the above system. Run 100-135-150-A produced a Product.2 purity of 99.2% but with very poor Product 1. purity (59%). Decreasing the value of $G_{m.c}/L'$ leads to the two components exhibiting a greater preference to move in the direction of the packing, and as Run 100-125-150-A demonstrates, the expected increase in Product 1 purity occurs without any loss of Product 2 purity. Further reduction of $G_{m.c}/L'$ retards the progress of the concentration profile to the point where the Arklone.P no longer extends over the whole of the separating section, and a very high value for Product 1. is recorded for Run 100-115-150-A4. The retardation of the profiles has however lead to contamination of the bottom Product,2, where purity has now fallen to approximately 81%. Continued investigations at a $G_{m.c}/L'$ value of 115 demonstrated the stability of the separation and several profiles have been plotted to show the reproducibility of the separation, Figures 8.22 to 8.24. A profile recorded eleven cycles after

equilibrium had been reached, possessed the same levels of concentration and purities as those recorded at 4, 5 and 6 cycles after equilibrium. These results were also able to be repeated in separate runs, i.e. Run 100-115-150-B4 a fact which fulfills perhaps the most important criteria for separation and in complete contrast to earlier separation studies with the system Arklone.P./dichloromethane.

The results discussed above demonstrate the capabilities of the SCCR1 in dealing with a system having a low separation factor. The conditions of operation may be far from being the optimum values and in any further investigations a study into the optimum sequencing interval is essential. With the SCCR1 having a finite column length, it would seem very unlikely that the situation will be reached where two pure product streams can be obtained. However, in an industrial situation a majority of separations would be concerned in the upgrading of the purity of a chemical substance, or the removal of a specific compound from a mixture, both of which require only one pure stream. The ability of the SCCR1 to produce either a pure top or bottom product has already been shown, although studies into the recycling of the impure product are still required.

In concluding the studies into the system Arklone.P./ dichloromethane it is anticipated that were the design changes recommended in Chapter 10 to be adopted a substantial increase in throughput may be effected and separations of systems having lower separation factors than 1.17 should be possible provided the purity of only one product is specified.

Table 8.5

System Arklone.P/Dichloromethane, Study of $G_{m.c}/L$ ratio

Experimental Settings

Run Title	Solute Feed Rate	I_s	L'	P_a	T_a	Separating Section				Purge Section			
						G_a	P_{in}	P_{out}	$G_{m.c}/L$	S_a	P_{in}	P_{out}	$S_{m.c}/L$
	$cm^3 hr^{-1}$	s	$cm^3 s^{-1}$	$kN m^{-2}$	°C	$cm^3 s^{-1}$	$kN m^{-2}$	$kN m^{-2}$		$cm^3 s^{-1}$	$kN m^{-2}$	$kN m^{-2}$	
100-120-150-A	112.5	148	2.866	101	21.0	941	376	166	117	1730	235	197	282
100-115-150-A	112.5	148	2.866	101	22.0	917	376	173	113	1730	235	197	288
100-110-150-A	111.6	148	2.866	100	21.0	883	376	173	108	1770	234	196	287
100-120-150-B	110.0	148	2.866	101	21.0	941	376	170	116.5	1770	235	197	288

Computed Results

Run Title	$K^{\infty}+K_{max}$		Sepn' Sect'		Purge Sect'		% Product Purity		Conc' Analysis Results in Appendix	Conc' Profile in Figure
	A.P	d.c.m	G_{min}/L'	G_{max}/L'	S_{min}/L'	S_{max}/L'	A.P	d.c.m		
100-120-150-A	138	126	88	200	259	309	>84	>68	A.7.15	8.16
100-115-150-A	131	122	86	187	265	317	>63	>85	A.7.16	8.17
100-110-150-A	139	127	82	178	264	316	>63	>83	A.7.17	8.18
100-120-150-B	138	125	88	193	265	317	>87.5	>73	A.7.18	8.19

Table 8.6 Separation Studies for the System Arklone.P/Dichloromethane

Experimental Settings

Run Title	Solute Feed Rate	I_s	L'	P_a	T_a	Separating Section				Purge Section			
						G_a	P_{in}	P_{out}	G_{mc}/L'	S_a	P_{in}	P_{out}	S_{mc}/L'
	$cm^3 hr^{-1}$	s	$cm^3 s^{-1}$	$kN m^{-2}$	°C	$cm^3 s^{-1}$	$kN m^{-2}$	$kN m^{-2}$		$cm^3 s^{-1}$	$kN m^{-2}$	$kN m^{-2}$	
100-135-150-A	113	148	2.633	100	21.5	1000	375	158	135	1690	236	188	302
100-125-150-A	113	148	2.633	100	21.5	941	375	165	126	1690	236	188	302
100-115-150-A4	130	148	2.633	100	22.5	875	375	176	116	1650	236	188	294
100-115-150-A5	130	148	2.633	100	22.5	875	375	176	116	1650	236	188	294
100-115-150-A6	130	148	2.633	100	22.5	875	375	176	116	1650	236	188	294
100-115-150-A11	130	148	2.633	100	22.5	875	375	176	116	1650	236	188	294
100-115-150-B	130	148	2.633	100	22.5	875	375	176	116	1650	236	188	294

Table 8.7 Separation Studies for the System Arklone.P/Dichloromethane

Computed Results

Run Title	K_{max}		Sepn' Sect'		Purge Sect'		% Product Purity		Conc' Analysis Results in Appendix	Conc' Profile in Figure
	A.P	D.C.M	G_{min} / L'	G_{max} / L'	S_{min} / L'	S_{max} / L'	A.P	D.C.M		
100-135-150-A	136	122	101	240	272	341	> 99.2	> 59	A.7.19	8.20
100-125-150-A	136	123	95	217	272	341	> 99.5	> 72	A.7.20	8.21
100-115-150-A4	131	119	89	189	266	333	> 92	>99.5	A.7.21	8.22
100-115-150-A5	131	119	89	189	266	333	> 80	>99.5	A.7.22	8.23
100-115-150-A6	131	119	89	189	266	333	> 81	>99.5	A.7.23	8.23
100-115-150-A11	131	119	89	189	266	333	> 81	>99.5	A.7.24	8.24
100-115-150-B	131	119	89	189	266	333	> 81	>99.5	A.7.25	8.25

Figure 8.16 Standardised Concentration Profile for Run 100-120-150-A

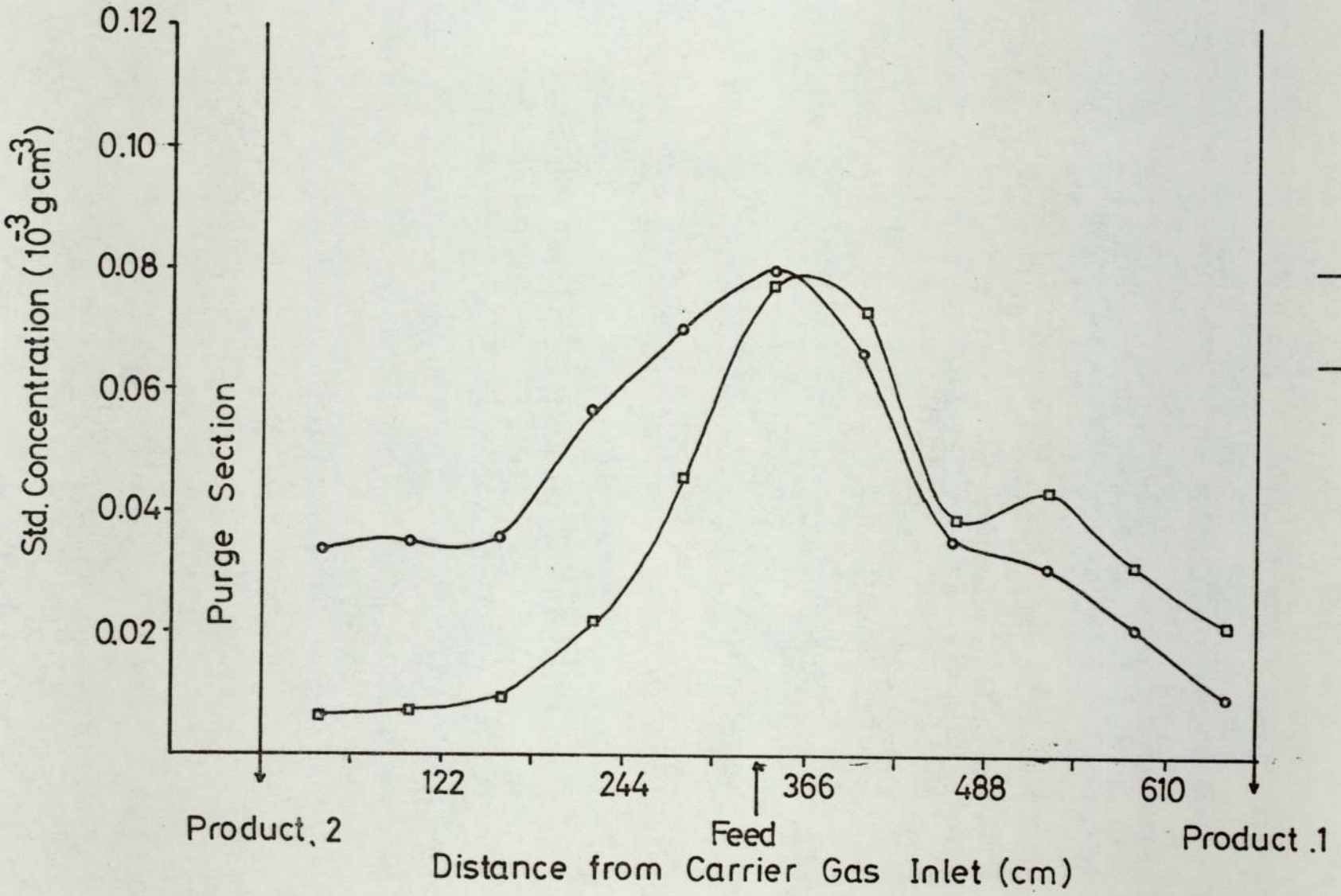

Figure 8.17 Standardised Concentration Profile for Run 100-115-150-A

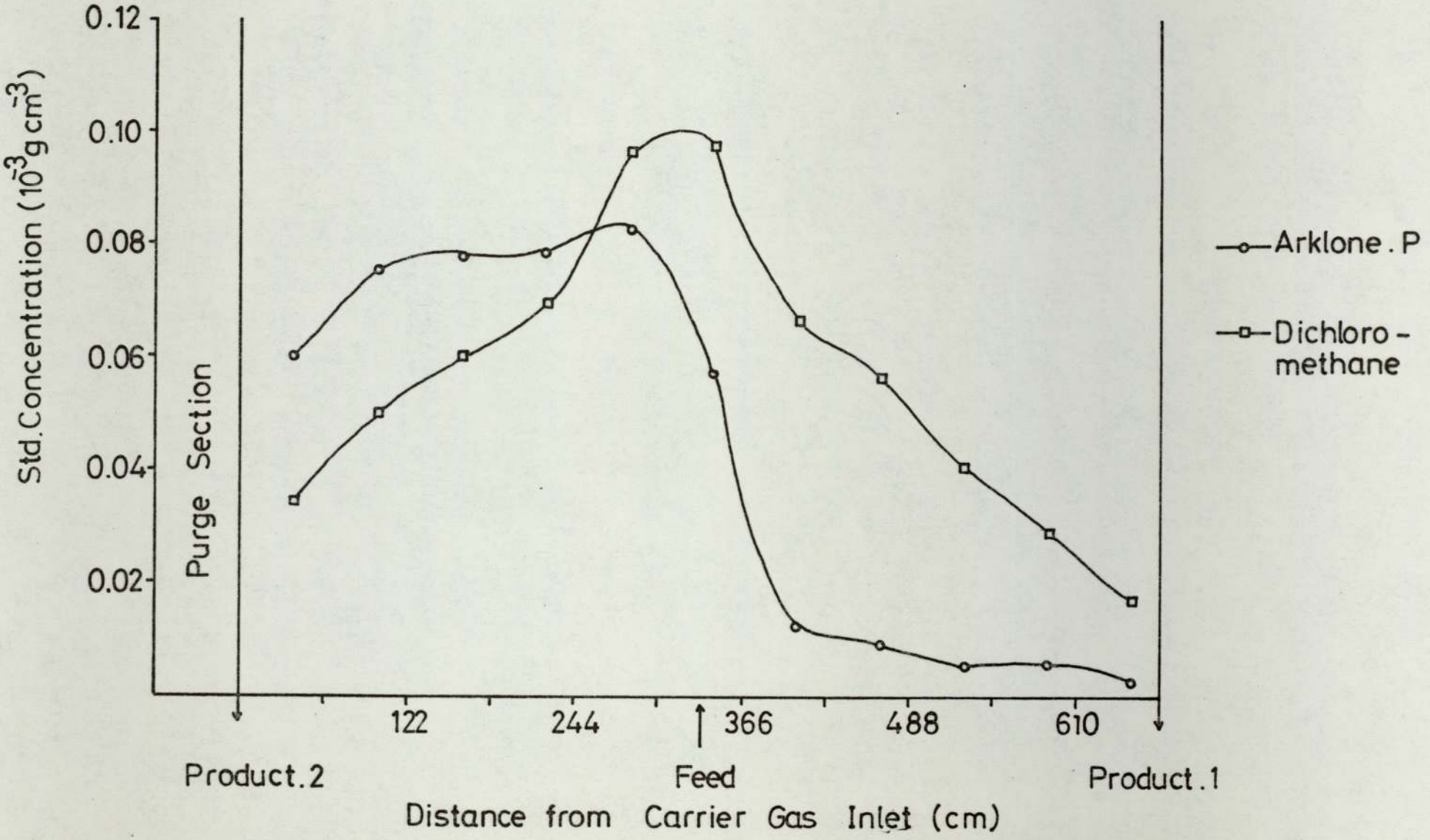

Figure 8.18 Standardised Concentration Profile for Run 100-110-150-A

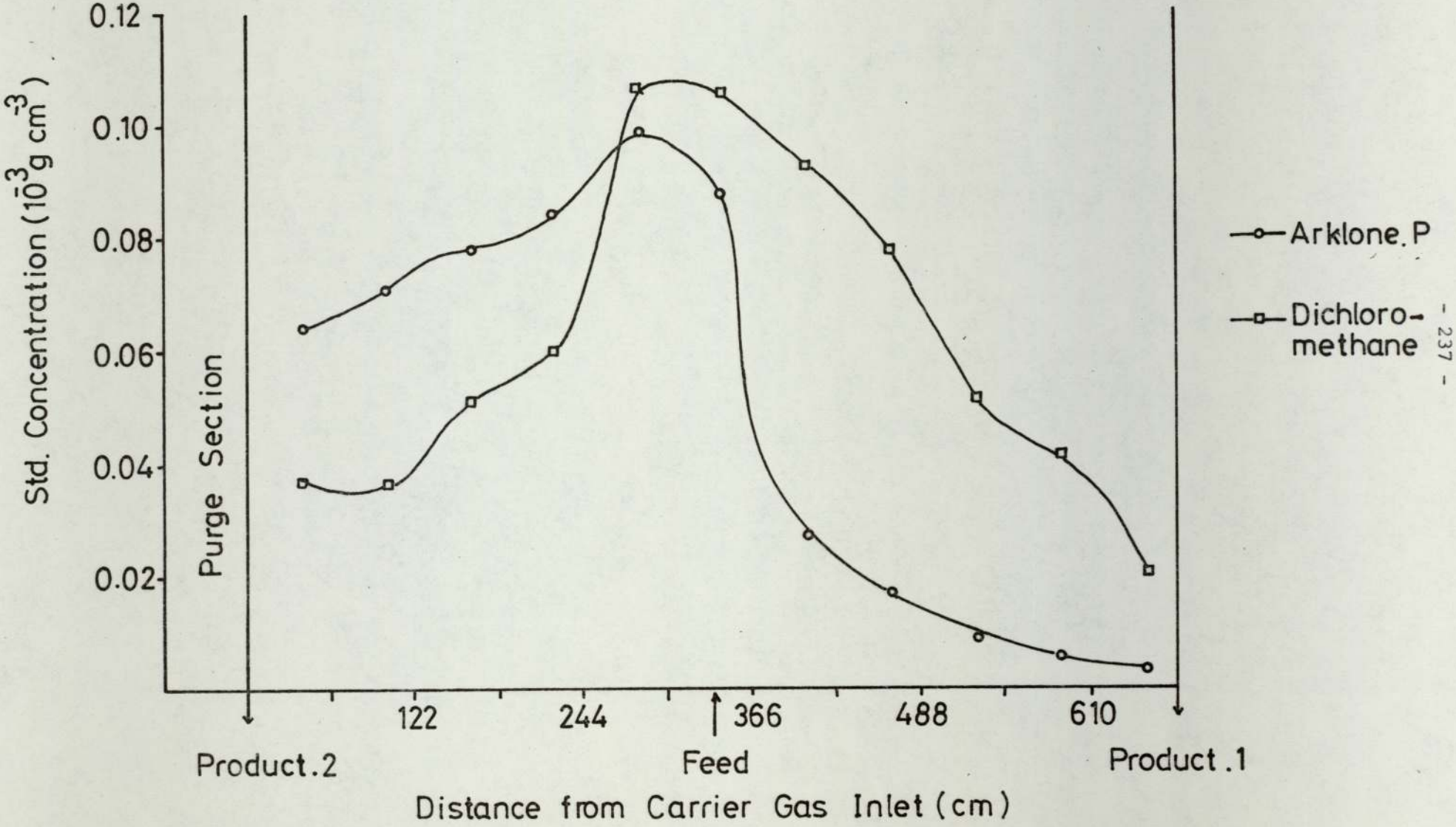

Figure 8.19 Standardised Concentration Profile for Run 100-120-150-B

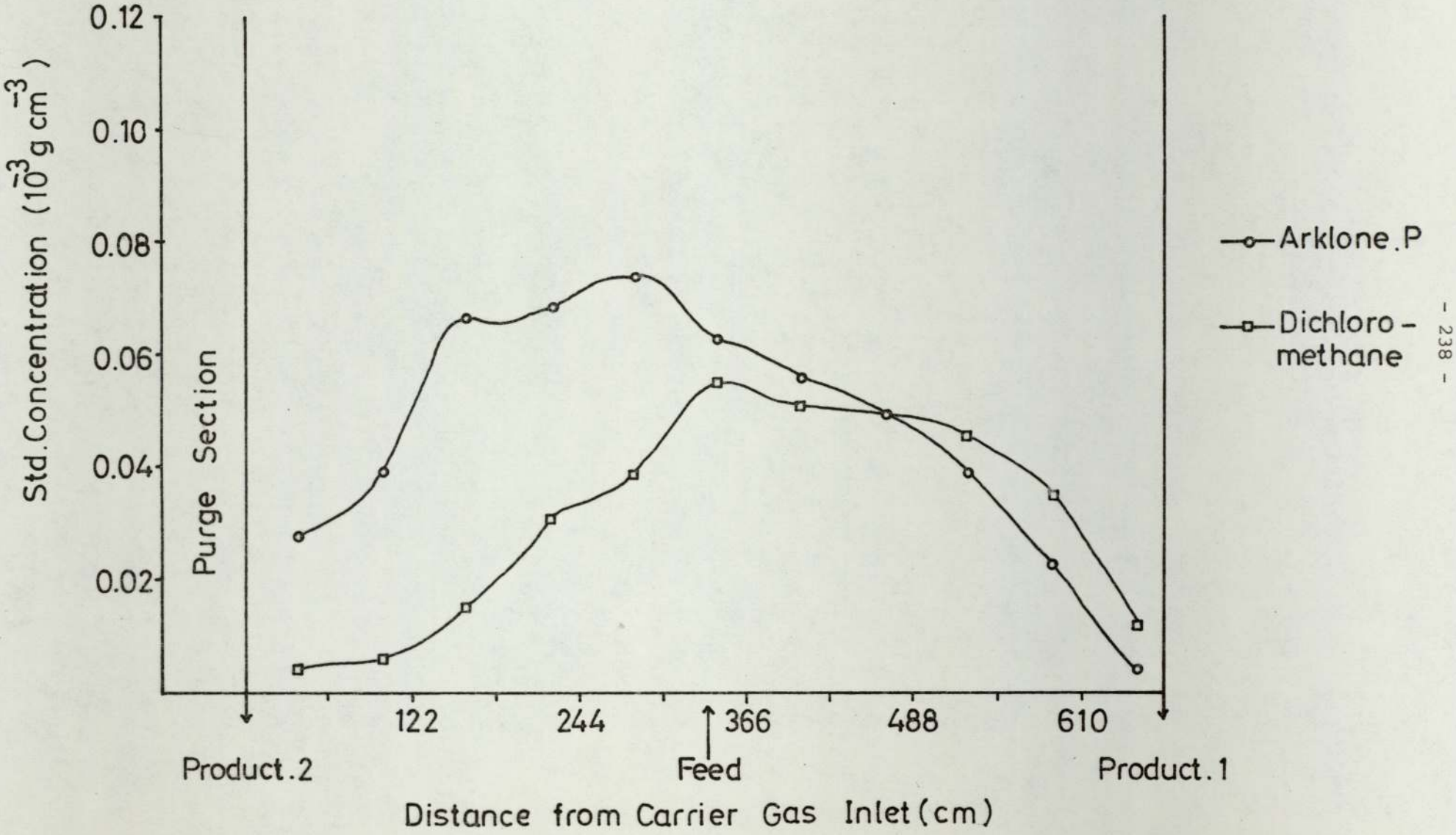

Figure 8.20 Standardised Concentration Profile for Run 100-135-150-A

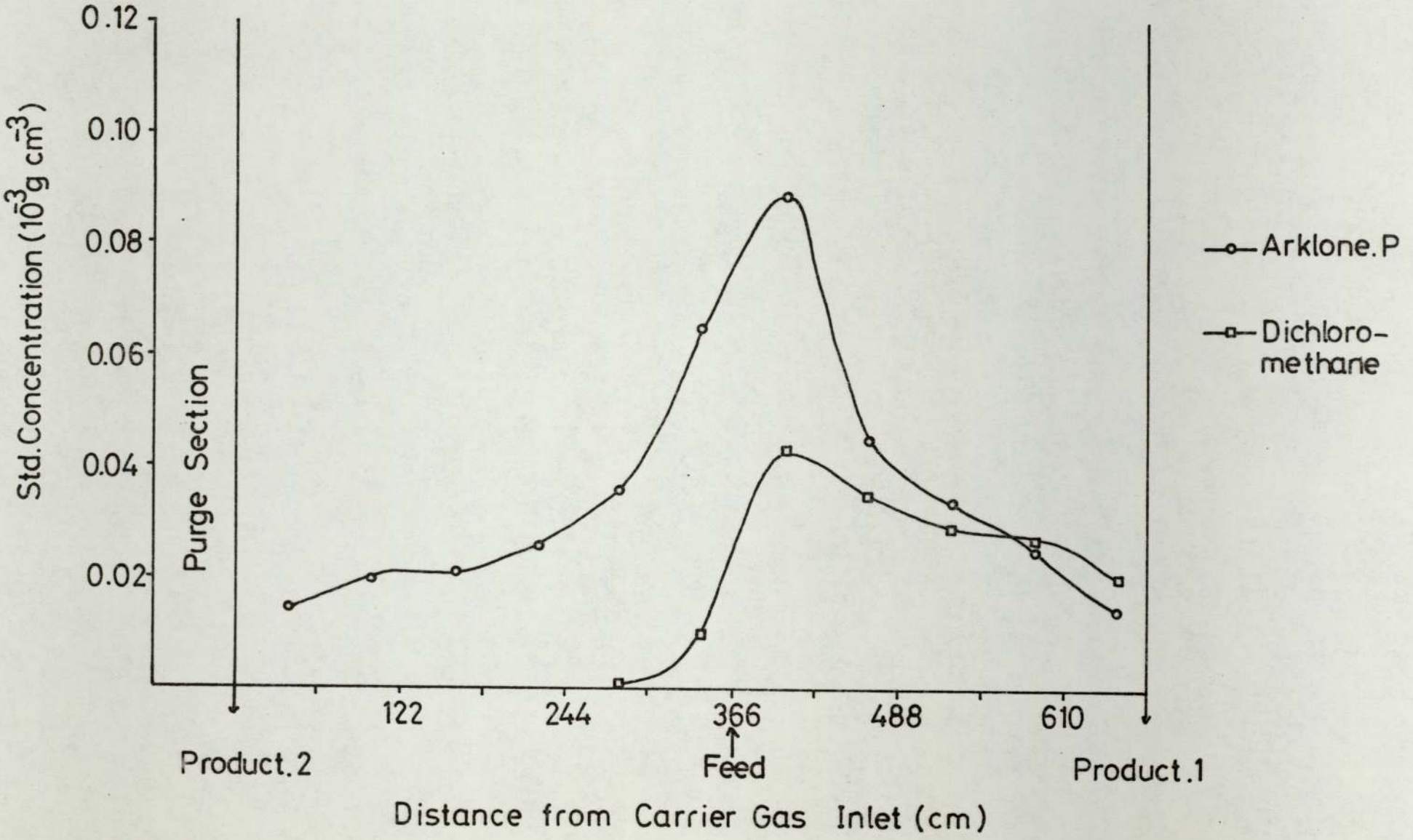

Figure 8.21 Standardised Concentration Profile for Run 100-125-150-A

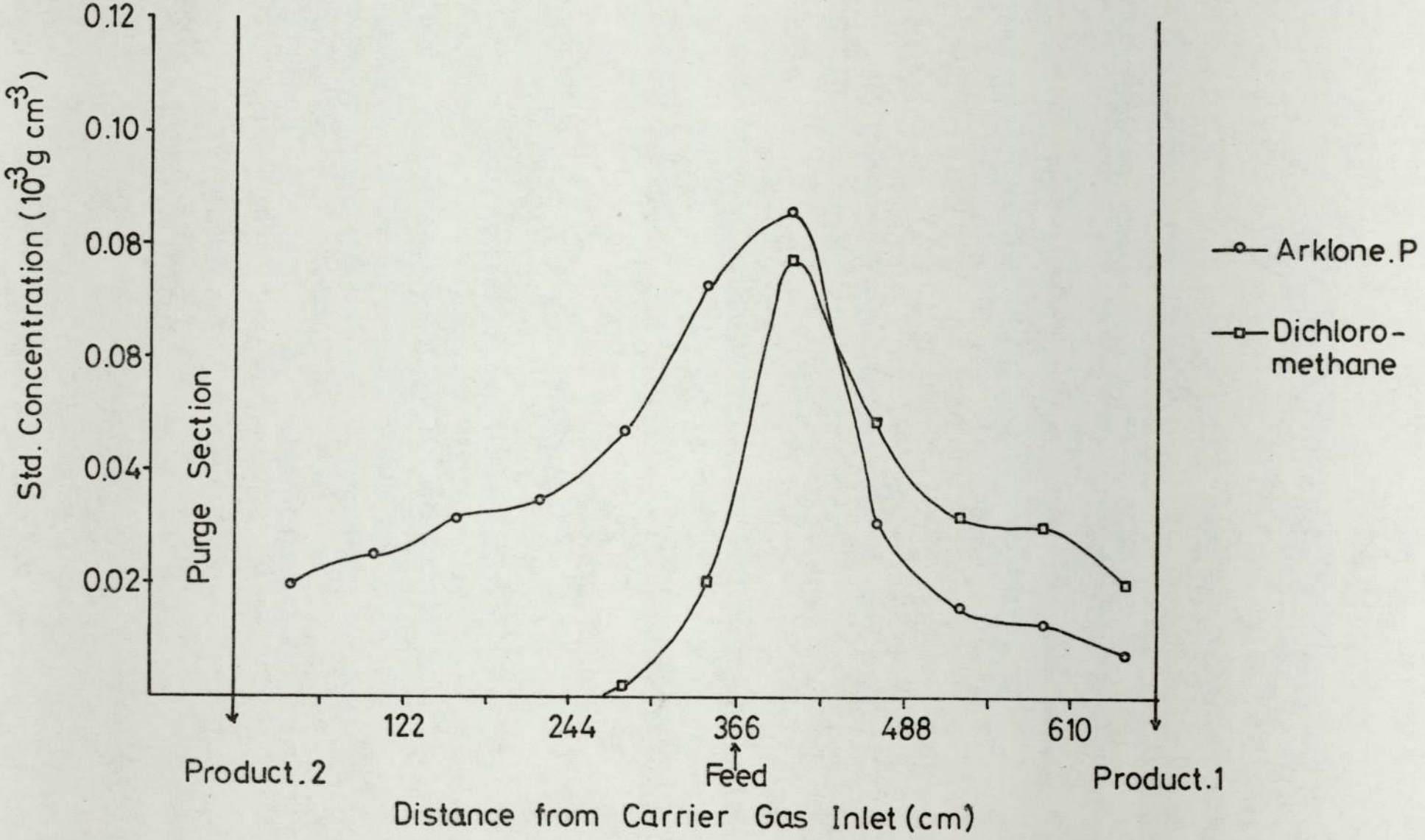

Figure 8.22 Standardised Concentration Profile for Run 100-115-150-A4

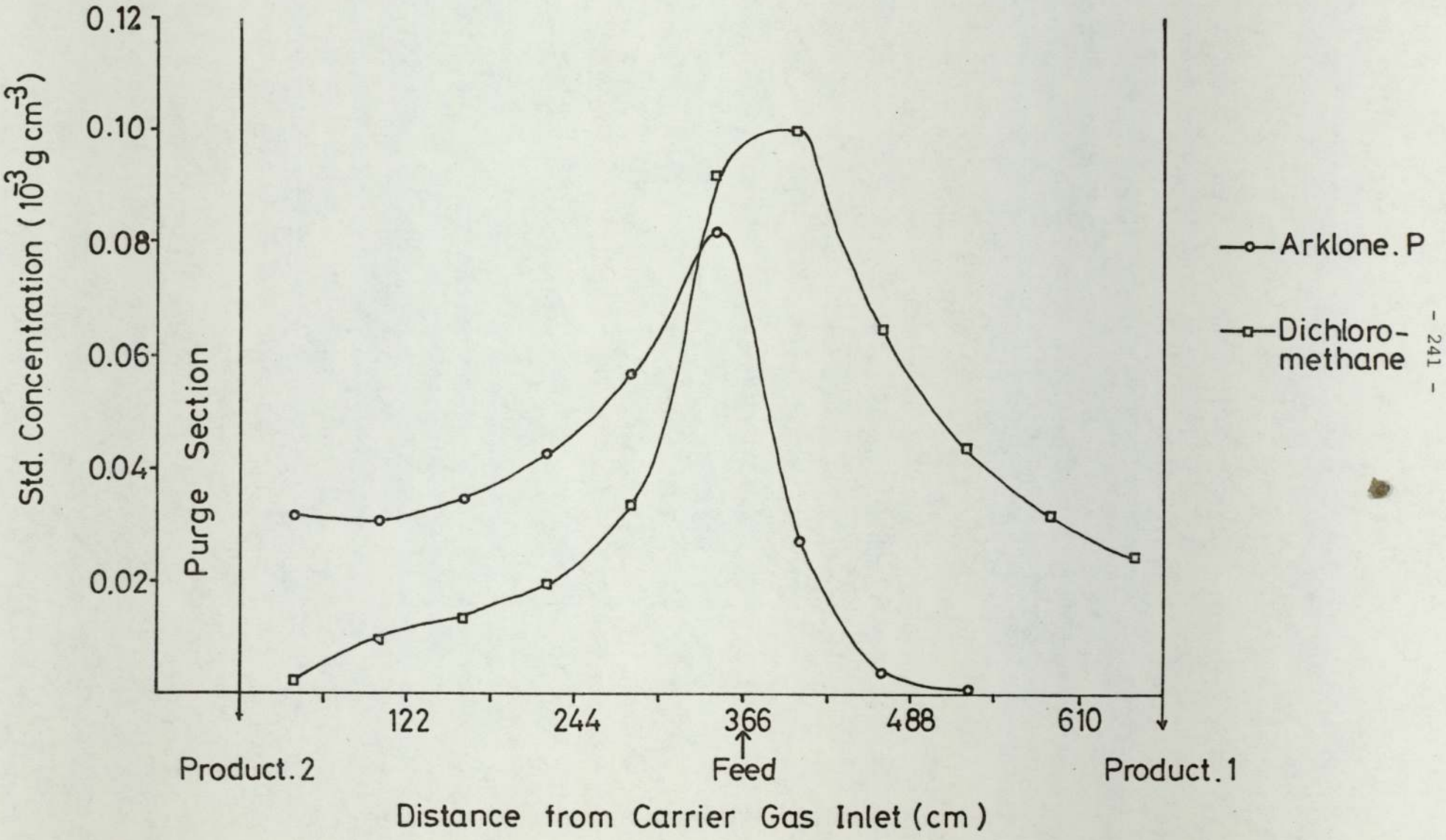

Figure 8.23 Standardised Concentration Profile for Runs 100-115-150-A5 & 100-115-150-A6

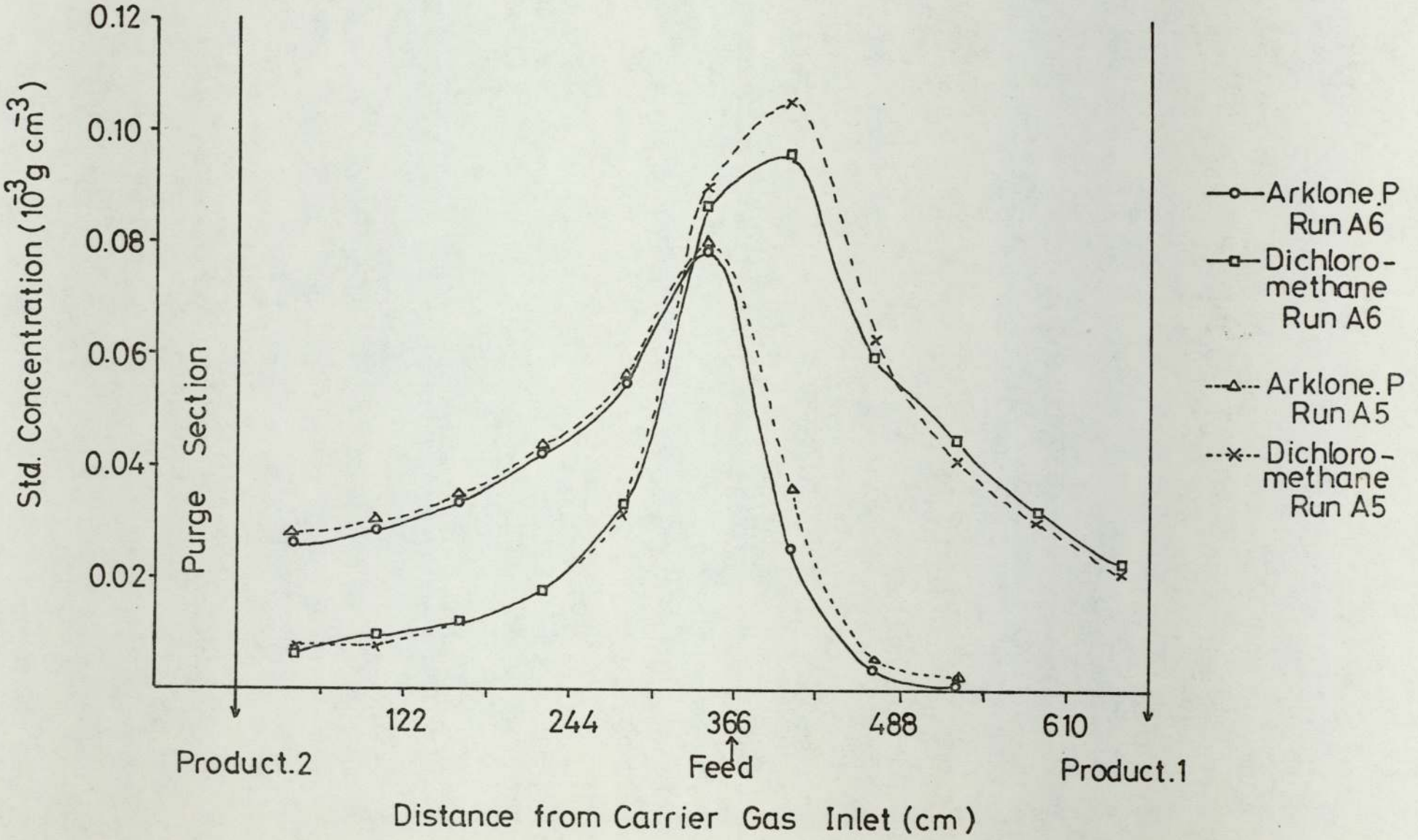

Figure 8.24 Standardised Concentration Profile for Runs 100-115-150-A11 & 100-115-150-B4

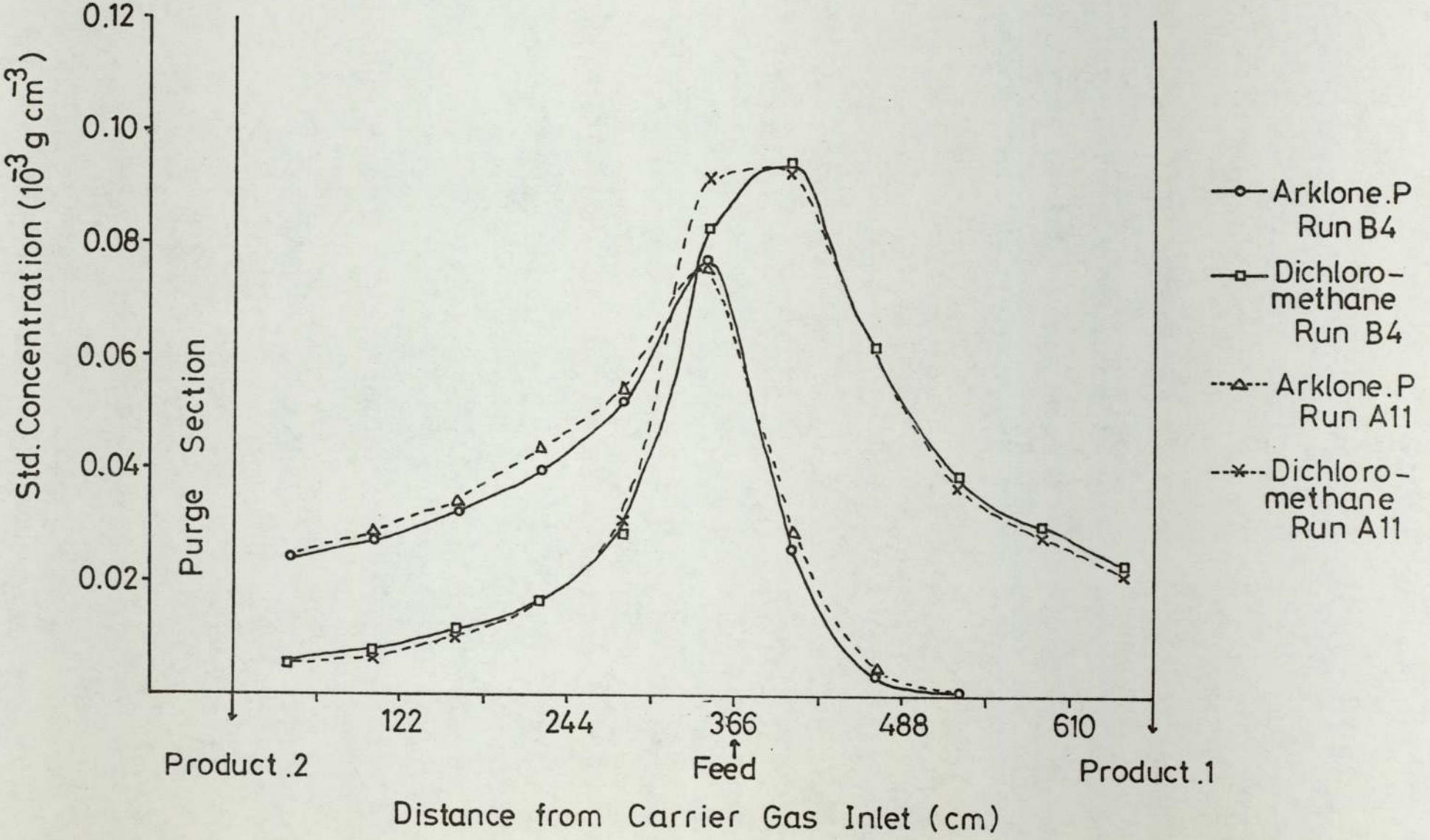

CHAPTER 9

MATHEMATICAL MODELLING OF THE CONTINUOUS COUNTER-CURRENT CHROMATOGRAPHIC PROCESS

9.1 Introduction

A statistically based model for the moving-bed form of continuous chromatography has been developed by Sciance and Crosser (190), relating the operating flowrates, feed-point location, degree of separation and the required column length for a binary feed mixture. For components A and B introduced into the mid-point of the column they obtained:

$$\ell n\ (u_z)_i = \frac{\ell . k''_i}{2.u.} \quad (K_i^{\infty} - \psi) \tag{9.1}$$

$$\ell n\ [1-(u_z)_{ii}] = \frac{-\ell k''_{ii}}{2.u.} \quad (K_{ii}^{\infty} - \psi) \tag{9.2}$$

$(u_z)_i$ = Bottoms/feed mass flowrate ratio of component A

$(u_z)_{ii}$ = Tops/feed mass flowrate ratio of component B

k'' = rate constant of desorption

u = average mobile phase velocity

ψ = operating mobile phase/stationary phase velocity ratio

ℓ = required column length

Although experimentally determined values of k''_i, k''_{ii} have to be used as published values are scarce, Equations 9.1 and 9.2 do yield the inequality:

$$K_i^{\infty} < \psi < K_{ii}^{\infty} \tag{9.3}$$

The fundamental criteria for continuous operation.

Applying the random walk approach (Section 2.2.3.2), Al-Madfai (38) obtained the expression to describe zone broadening in continuous counter-current g.l.c.:

$$H = d_p + \frac{2D_m}{u} + \frac{2r'.r''}{u.r''-u_L r'} \left(\frac{u + u_L}{r' + r''}\right)^2 \qquad (9.4)$$

r' = rate of transfer of molecules from gas to liquid

r" = rate of transfer of molecules from liquid to gas

u_L = stationary phase velocity

Equation 9.4 is of a similar form to a static column expression for HETP, which does not include a zone broadening term to account for movement of the stationary phase:

$$H = d_p + \frac{2D_m}{u} + \frac{2.r'.u}{(r'+r'')^2} \qquad (9.5)$$

The theoretical plate height determined from a continuous counter-current model is not equivalent to the co-current plate height usually associated with elution chromatography. Al-Madfai (38) using the work of Gluekauf (53) as a basis, related the two plate height definitions through the equation:

$$\frac{N_{cc}}{N} = 3(\alpha''-1) \qquad (9.6)$$

N_{cc} = number of counter-current theoretical plates or stages

N = number of co-current theoretical plates (elution chromatography)

α'' = separation factor = K_2/K_1

The first inference from the above equation is that for separation factors below 1.33, less theoretical plates would be required for the continuous case than for a static column. As α approaches unity, N_{cc}/N tends towards zero indicating that continuous counter-current operation may be especially viable for difficult separations. Rony (191-193) developed the relationship between the number of stages in a counter-current multistage system (operated at total reflux), N_{cc}, that are required to obtain a separation identical to that achieved in a co-current chromatographic system with N theoretical plates:

$$\frac{N_{cc}}{N} = \frac{(1+K_i)^2}{\sqrt{2\pi}\ (u_m.t/\sigma)} \qquad (9.7)$$

K_i = partition coefficient of component i

u_m = molar velocity of mobile phase

t = time

σ = peak standard deviation (units of length)

Following the work of Fitch et al (135), Barker and Huntington (33,37,41) adapted the theory of stagewise liquid/liquid extraction given by Alders (194), for the separation, to an equal degree of purity, of a two component equimolar feed mixture. For a solute mixture feed point at the centre of the separating section:

$$\log \frac{(G/L)_R}{(G/L)_S} = \log\ (K_{ii}/K_i) + \frac{2}{N_{cc}} \left[\log\left(1 - \frac{(E_i)}{f_i}\right) 1 + \log \frac{(E_{ii})}{f_{ii}}\ 1\right] \qquad (9.8)$$

where $(G/L)_R, (G/L)_S$ = ratio of gas to liquid phase flowrates in the rectifying and stripping sections respectively

$(E_i)_1$, $(E_{ii})_1$ = mass production rates of component i and ii at the top of the column

f_i, f_{ii} = mass feedrates of components i and ii to the column.

One major disadvantage of Equations 9.7 and 9.8 is the inherent assumption of a constant partition coefficient, i.e. the infinite dilution value. Introduction of a non-linear absorption isotherm into a stage-to-stage calculation for a vertical moving-bed column was accomplished by Tiley (195), who studied the effect of stage number, flow conditions and temperature on the column concentration profiles. Two significant conclusions were drawn in that a limiting feed throughput was found for a given solvent rate, product purity and number of stages which is dependent on the phase equilibrium characteristics, and secondly Tiley found an optimum operating temperature just below the main boiling points of the feed mixture. In a later paper Pritchard et al (136) compared the results of a multi-stage computational procedure with experimental results and provided an HETP of 13-18 mm was assumed, very approximate agreement was obtained between experiment and theory. Pritchard et al (136) also argue that a theoretical analysis of the process in terms of the height of a transfer unit (H.T.U.) is the more logical concept for the packed columns in their work, although plate to plate models are more amenable to computation in non-equilibrium systems. From theoretical considerations Arkenbout and Smit (196) conclude that it is incorrect to assume that the H.T.U. analysis will always be more satisfactory than a theoretical-plate analysis. Holland et al (197) have attempted a synthesis of the two concepts by introducing the idea of a 'mass

transfer section' enabling the computational procedure for a packed column to be similar to that for a stagewise process. Rony (193) has suggested the use of the concept of 'extent of separation' to enable valid comparisons to be made between various types of separation processes.

Methods employing the H.T.U. concept for treatment of the counter-current gas/liquid chromatographic process have been developed by Barker and Lloyd (30,41), who derived the following equations:

$$(N_{OG})_R = \frac{1}{Q_G/(KQ_L-1)} \quad \ell n\left[\frac{M_A/KQ_L-y_1}{M_A/KQ_L-y_2} \frac{(Q_G/KQ_L-1)}{(Q_G/KQ_L-1)} \right] \tag{9.9}$$

$$(N_{OG})_S = \frac{1}{(1-Q_G/KQ_L)} \quad \ell n\left[\frac{M_B/KQ_L-y_1}{M_B/KQ_L-y_2} \frac{(1-Q_G/KQ_L)}{(1-Q_G/KQ_L)} \right] \tag{9.10}$$

Q_G = gas volumetric flowrate

Q_L = liquid volumetric flowrate

M_A, M_B = mass flowrate of solute leaving the column in the product A and Product B streams respectively

$(N_{OG})_R$ $(N_{OG})_S$ = number of overall gas phase transfer units in the 'rectifying' and 'stripping' sections respectively.

y_1, y_2 = gas phase solute concentrations at points 1 and 2 in the column.

Barker and Lloyd applied this technique to the vertical moving-bed column shown in Figure 2.7, and found a first order relationship between the logarithm of H_{OG} and the solvent phase flowrate, with H_{OG} values of the order of 10 cm for the systems and conditions studied (29,30,41).

Sunal (50) developed a computer model of the continuous chromatographic process based on the 'two film theory' of mass transfer. Comparing the experimental results of Huntington (33) with predicted values he concluded that the effect of axial mixing on separation efficiency was negligible.

The theoretical treatments of the counter-current chromatographic process discussed above are all based upon a true steady state process and as such should only be applied to the moving bed or moving stationary phase systems, discussed in Sections 2.4.2 and 2.4.3. For the sequential units, the operating principle is similar to the frontal elution technique with an imposed column sequencing action necessitating the introduction of time as an additional variable. Sunal (50) has developed a computer model based on a plate to plate operation to describe the operation of the compact circular counter-current chromatograph discussed in Section 2.4.3.2.1, and a similar approach was adopted by Deeble (45) for the simulation of the functioning of the SCCR1. In this latter model, inherently requiring many experimentally determined parameters, Deeble (45) investigated the effects of number of theoretical plates per column, feedrate, and column temperature, and one of the most significant conclusions drawn was that the inclusion of a temperature profile would greatly enhance the accuracy of the simulation.

Sakodynskii et al. (198,199) have developed a plate model of a chromatographic column to include the effects of a non-linear isotherm and interaction between feed components. In a recent publication (200) they have developed a model for calculating the distribution of concentrations at the column outlet based on a semicontinuous chromatographic column model and using as their initial equation a material balance of the form derived by Deeble (45).

In the present work the concept of the plate to plate model used by Deeble has been retained with theoretically determined temperature, pressure and concentration profiles being introduced. The H.E.T.P. has also been determined from a purely theoretical background in an attempt to exclude all experimental results from the model.

9.2 The Computer Model

9.2.1 Estimation of the Theoretical Plate Height

Chapter 2 presented several theories expressing the behaviour of a chromatographic column in terms of the H.E.T.P. Giddings (11) developed the non-equilibrium theory in which the mass transfer or non-equilibrium terms were expressed as functions of diffusivity, particle diameter, stationary phase dimensions, etc., and obtained a definition of the theoretical plate height as Equation 2.19;

$$H = \frac{2\,\gamma' D_m}{u} + q'R(1-R)\,\frac{d_f^2.u}{D_s} + \left[\frac{1}{2\lambda d_p} + \frac{D_m}{w.d_p^2.u}\right]^{-1} \qquad (2.19)$$

In developing the above equation to apply to the SCCR1 unit the evaluations of many physical parameters are required, many of which are specific to individual solute components, e.g. molar volumes, collision diameters. To attempt to evaluate certain parameters inherent in Equation 2.19 in terms of individual solutes is too complex a problem and therefore the simplifying assumption has been made that in the cases where parameters vary for the individual solutes (i.e. Arklone.P/ Genklene.P), the mean value is taken.

Individual terms from Equation 2.19 will be discussed below with an estimation of their physical value.

a) Labyrinth Factor γ'

The structural parameter γ' is found to be a function of the independent terms for tortuosity and constriction and has been evaluated at $\gamma' = 0.46$ for crushed firebrick (186).

b) Configuration factor q'

The above factor is to allow for the shape of the stationary phase layer, and Giddings (11) has given a typical value of 0.25.

c) Retention Ratio R

The fraction of solute in the mobile phase (R) is given by

$$R = \frac{V_m}{V_m + \sum_i K.V_s} \qquad (9.11)$$

which for the solutes Arklone.P, Genklene.P. evaluates at 0.0096.

d) Stationary Phase Film Thickness d_f

Giddings (11) has related the film thickness to the particle diameter via $\frac{d_f}{d_p} \leq 0.03$, for the solid support in question we find that $d_f \leq 12 \times 10^{-4}$ cm = 12 μ.

e) Particle Diameter d_p

The size range of Chromosorb P, used as packing in the SCCR1 was between 500 and 355 micron, giving a mean particle diameter of 4.28×10^{-4} m.

f) Flow Velocity u

The mean flow velocity will obviously change as the carrier gas expands during its passage through the SCCR1. The variation in HETP with mobile phase velocity has been illustrated in Section 2.2.3.1 and therefore it is necessary to define a mean column velocity, u_{mc}, for use in Equation 2.19. A typical value for u_{mc} is 0.09 $m.s^{-1}$.

g) Mobile and Stationary Phase Molecular Diffusion Coefficient D_m, D_s

The mobile phase diffusion coefficient may be calculated from the Hirschfelder-Bird-Spotz equation (187).

$$D_m = \frac{0.00186\ T^{\frac{1}{2}} \left(\frac{1}{M_1} + \frac{1}{M_2}\right)^{\frac{1}{2}}}{p.\sigma_{12}^2 \cdot r_{12}} \qquad (9.12)$$

where M_1 = molecular weight of solvent (carrier gas)

M_2 = molecular weight of solute

p = absolute pressure in atmospheres

r_{12} = mean collision diameter

$$= \frac{(r_o)_1 + (r_o)_2}{2} \qquad (9.13)$$

$(r_o)_1 (r_o)_2$ = individual solvent, solute, collision diameters

σ_{12} = collision integral for diffusion

The collision diameters may be calculated directly from viscosity measurements, or from the empirical equation below (181)

$$r_o = 1.18\ V_b^{1/3} \qquad (9.14)$$

where V_b is the molar volume of the fluid at the normal boiling point determined by the method of addition. For air, V_b was found to be 20.1 cm^3, and for a 50:50 mixture of Arklone.P/Genklene.P, V_b was evaluated as 122.1.

The collision integral, σ_{12}, is a function of $K_b.T/\varepsilon_{12}$ where K_b is Boltzmann's constant and ε_{12} is the energy of molecular interaction. Values of, σ_{12}, are tabulated in reference (181).

Substitution into Equation 9.12 yields a value for D_m at 20°C of 0.059 $cm^2.s^{-1}$. It must be emphasised that this value is an average value for the two solutes. Arklone.P/Genklene.P. evaluated at a mean column pressure of 2.46 atmospheres.

A recommended relation (181) for estimation of diffusivities of non-electrolytes in liquids at low concentration of the diffusing component is the Wilke and Chang equation (188).

$$\frac{D_s.\mu}{T} = 7.4 \times 10^{-8} \frac{(X.M_L)^{\frac{1}{2}}}{V_b^{0.6}} \qquad (9.15)$$

where μ = viscosity of liquid phase

X = association parameter (1.0 for non-associated liquids)

M_L = molecular weight of liquid phase

The above equation shows that D_s depends strongly on the solvent mainly through reciprocal viscosity, $^1/\mu$, but this effect is tempered somewhat by the fact that D_s increases with the square root of solvent molecular weight. It can be seriously questioned whether the inverse viscosity relationship holds for the long snake-like molecules used as solvents in gas chromatography (189) and therefore it is perhaps fortunate that the plate height terms containing D_s terms contribute very little to the overall plate height. The absolute value for the viscosity of the silicone oil solvent has not been tabulated and neither is it possible to calculate it. An estimation of this value based on similar solvent phases can be given as 2000 cp, resulting in stationary phase molecular diffusion coefficient in the order of 1×10^{-6} $cm^2.s^{-1}$. Whilst this value can be no more than an estimation it does hold with the opinion of Giddings (11) that for gas chromatography the ratio of diffusion coefficients, liquid to gas, is about 10^{-5}.

h) Eddy Diffusion Factor λ

The above factor, present in the coupled part of Equation 2.19, may be defined as

$$\lambda_i = w_\beta^2 . w_\lambda / 2 \qquad (9.16)$$

where $w_\beta^2 . w_\lambda$ is evaluated for each of 5 categories of velocity inequality highlighted in Section 2.2.3.2. Giddings (11) has estimated the individual contributions to λ_i as approximately,

$$\lambda_1 = 0.5;\ \lambda_2 = 10^4;\ \lambda_3 = 0.5;\ \lambda_4 = 0.1;\ \lambda_5 = 0.02\ (\frac{d_c}{d_p})^2$$

giving λ_i as 1.1×10^4.

This value for λ can only be a very approximate value, however, as the term for eddy diffusion, $(\frac{1}{2.\lambda.d_p})$, in the coupled expression (Equation 2.19), is not the dominant term, contributing less than 1% for SCCR1 conditions, then further accuracy in the estimation of λ is not thought necessary,

i) Diffusional Flow Parameter w

In a similar manner to evaluating λ, the parameter w may be defined as

$$w_i = w_\alpha^2 . w_\beta^2 / 2 \qquad (9.17)$$

evaluated again for the five types of velocity inequality occuring within the packed columns. The non-equilibrium approach to evaluating w requires specific information regarding the velocity profile, which for the SCCR1 is not available. However Giddings (11) has also

evaluated w for use in the 'random-walk'method of determining, H, and has reported that the numerical results so obtained were not inferior to those developed from the non-equilibrium theory. The approximate magnitude of the velocity inequalities are as follows:

Transchannel, $w_1 = 0.01$

Transparticle, $w_2 = 0.10$

Short-range interchannel, $w_3 = 0.5$

Long-range interchannel, $w_4 = 2.0$

Transcolumn, $w_5 = 0.001 \left(\frac{d_c}{d_p}\right)^2$

It is the final velocity inequality for the transcolumn effects that is of particular importance to large diameter columns and from the above definition it becomes apparent that the plate height becomes a function of the column diameter squared for a constant particle diameter. Contrary to this definition, Pretorius and de Clerk (76) indicate that plate height increases with d_c at constant $\frac{d_p}{d_c}$ and reaches a maximum at $\frac{d_p}{d_c} = 0.05$ and then decreases with increasing d_c. Support for this theory is given by Spencer and Kucharski (77) and Knox (78). Taking the value to give a maximum plate height contribution, w_5 is calculated at 0.4. The overall summed value for w_i then becomes 3.01.

Having defined and estimated all the parameter in Equation 2.19 the theoretical plate height is given by:

$$H = \frac{2 \times 0.46 \times 0.059}{9.0} + \frac{0.25 \times 0.0096(1-0.0096)(12\times10^{-4})^2 9.0}{1.0\times10^{-6}}$$

$$+ \left[\frac{1}{2 \times 1.1\times10^{4} \times 0.0428} + \frac{0.059}{3.01\times(0.0428)^2 \times 9.0} \right]^{-1}$$

$= 0.876$ cm

In Section 2.3.1.1 further mechanisms leading to zone broadening were discussed. Of particular importance to the SCCRl were two additional plate height contributions resulting from cross-column temperature fluctuations, H_t, and the unevenness of the flow velocity, H_c. The contribution from these terms must be evaluated and added to the overall plate height.

H_t, has previously been defined (11) in Section 2.3.1.2 and is given by

$$H_t = \alpha_t . (\Delta T)^2 \quad \frac{r_c^2 . u}{900 . D_m} \qquad (2.26)$$

ΔT in the above equation is the temperature difference between the column axis and wall, which will have a specific value for each axial point within the SCCRl. As the HETP defined by Equation 2.19 is not a point value but an average value for conditions within the SCCRl, the average temperature difference between the axis and wall for the eleven separating columns is required. For a typical separation run this average temperature difference was found by integration of the axial temperature profile to be approximately $3.0^{o}C$, giving a contribution from H_t of 0.09 cm.

Many approaches have been made for theoretically formulating the term H_c, (68,19,75,76). Hupe (19) using a statistical treatment generated an expression of

$$H_c = \frac{2.83 . r_c^{0.58}}{u^{1.886}} \qquad (9.18)$$

and whilst the cross-sectional velocity profile corresponding to this relationship was an unusual shape, the fit to a variety of experimental results on columns between 1.3 and 10 cm diameter was very good.

For SCCR1 conditions the contribution H_c makes to the overall plate height is 0.096 cm.

The final height equivalent to a theoretical plate expression becomes

$$H = \frac{2\gamma' D_m}{u} + q'R(1-R)\frac{d_f^2 u}{D_s} + \left[\frac{1}{2.\lambda.d_p} + \frac{D_m}{w.d_p^2.u}\right]^{-1} + H_c + H_t \qquad (9.19)$$

$$= \underline{1.062 \text{ cm}}$$

It is the opinion of the author that the above equation may be rewritten to include the term H_c as a coupled parameter. H_c is included in the van Deemter equation to allow for cross column velocity fluctuations and will therefore inherently contain the transcolumn velocity inequality defined by Giddings as w_5. The addition of separate contributions to plate height is only valid if those contributions are independent from one another [c.f. addition of variances in the random-walk theory]. Therefore if the term H_c includes a contribution for the transcolumn velocity inequality it will not be independent from the other velocity correction terms (w_1-w_4) and may be included in the coupled part of Equation 9.19 to give

$$H = \frac{2\gamma' D_m}{u} + q'R(1-R)\frac{d_f^2.u}{D_s} + \left[\frac{1}{2.\lambda.d_p} + \frac{D_m}{w'd_p^2.u} + \frac{1}{H_c}\right]^{-1} + H_t \qquad (9.20)$$

where w' does not include a contribution from w_5, the transcolumn effect.

9.2.2 Development of a Concentration Profile

9.2.2.1 Mass Balance over a Theoretical Plate

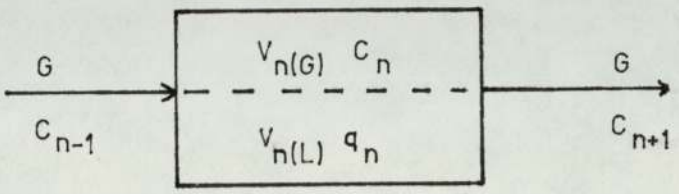

The chromatographic column is considered to consist of a series of idealized mixing stages or theoretical plates. $V_{n(G)}$ and $V_{n(L)}$ are the gas and liquid phase volumes respectively with c_n and q_n being the average gas and liquid phase concentrations of a single solute occurring in plate n over a small time increment $t \rightarrow t+\Delta t$. G represents the gas phase volumetric flowrate and is assumed to be constant over plate n.

A mass balance over plate n for the time increment $t \rightarrow t+\Delta t$ gives:

$$G.c_{n-1} = G\,c_n + V_{n(G)} \frac{dc_n}{dt} + V_{n(L)} \frac{dq_n}{dt} \qquad (9.21)$$

Substituting $K = q_n/c_n$:

$$G.c_{n-1} = G.c_n + (V_{n(G)} + K\,V_{n(L)}) \frac{dC_n}{dt} \qquad (9.22)$$

If the time increment, Δt, over which Equation 9.22 is integrated, is sufficiently small so that C_{n-1} may be considered constant, then integration of Equation 9.22 gives:

$$C_n = C_{n-1}\left(1-e^{-\frac{G.\Delta t}{V_n}}\right) + C_n(O)\,e^{-\frac{G.\Delta t}{V_n}} \qquad (9.23)$$

where V_n is known as the effective plate volume, equalling $(V_{n(G)}+K.V_{n(L)})$, reference (8).

The first term on the right hand side of Equation 9.23 represents the contribution to c_n on plate n, from the preceding plate, (n-1). For the plate which is receiving solute feed, this term will include a factor c_f, to give the total input gas phase concentration to that plate. The second term in Equation 9.23 represents the contribution from material present on the n^{th} plate at the start of the time increment, and is equivalent to the average gas phase concentration in plate n in the preceding time interval.

Starting from time zero, a plate to plate calculation for a single solute may be performed by substitution of successive values of c_{n-1} into Equation 9.23, $c_{n(O)}$ being zero for the first time increment. The resultant concentration profile is then updated by repeating the calculations for successive time increments, c_n in the first time increment becoming $c_{n(o)}$ in the second and so on. The sequencing action occurring in the SCCR1 unit is superimposed on the plate to plate calculations by stepping the concentration profile backwards, by one column, at the end of a sequencing interval. Mathematically this technique is identical with the port advancement found in the practical operation but provides a more compact method for digital programming.

9.2.2.2 Solute Concentration Effects

With the solute partition coefficients not being constant, a factor must be introduced into the model to allow for the relationship between the partition coefficient and the gas phase concentration. The non linear relationship is best represented by a polynomial of the form

$$K_i = (a_o)_i + (a_1.c_n)_i + (a_2.c_n^2)_i + (a_3.c_n^3)_i \qquad (9.24)$$

however it was found (Section 5.2.1.2 and Appendix 3), that for the gas phase concentrations present in the SCCR1, the above relationship could be approximated to a straight line without any significant loss of accuracy. Above gas phase concentrations of 0.5×10^{-3} g.cm^{-3}, a full polynomial expansion for the dependence of K upon concentration should be used.

A further correction resulting from the presence of solute molecules in the gas phase needs to be made to the value of the gas flowrate, G.

$$G' = G\left[1 + M_v \left(\frac{c_{n(i)}}{M_i} + \frac{c_{n(ii)}}{M_{ii}}\right)\right] \qquad (9.25)$$

where G = volumetric flowrate of solute free carrier gas

M_v = molar volume at column operating temperature

M_i, M_{ii} = respective molecular weights

For solute feedrates below 600 cm^3.hr^{-1} the contribution from the solutes may be assumed negligible, but at higher throughputs a correction is required with a contribution of approximately 8% to the

total gas flowrate at the maximum feedrates.

9.2.3 The Introduction of a Pressure Gradient

For flexibility in the computer model a relationship between pressure drop and gas flowrate that was applicable to all types of flow was introduced (201):

$$\frac{\Delta P}{\ell} \cdot g_c = 150 \frac{(1-\varepsilon)^2}{\varepsilon^3} \frac{\mu . u_m}{D'^2_p} + 1.75 \frac{(1-\varepsilon)}{\varepsilon^3} \cdot \frac{G_E u_m}{D'_p} \qquad (9.26)$$

where u_m = superficial velocity measured at mean column pressure

G_E = mass flow rate of gas

ℓ = length of column

ε = voidage

D'_p = effective particle diameter as defined by:

$$D'_p = \frac{6\ (1-\varepsilon)}{\phi'\ S_s} \qquad (9.27)$$

where ϕ' = shape factor for non-spherical particles = 0.65, ref.(181)

S_s = specific surface of particle per unit volume of bed = $1.9\ m^2.cm^{-3}$, reference (45).

In practice the type of flow found in the SCCR1 was laminar, with Reynolds numbers based on the above definition for effective particle diameter, being well below 1.0. Equation 9.26 for these conditions approximates to the Kozeny equation (202) in that the second term on the right hand side of Equation 9.26, to account for kinetic energy losses becomes negligible. Inclusion of this second term will allow the model to simulate the chromatographic process at pressures and

flowrates far in excess of those available in practice, under which conditions it is believed that improved separations will result. Considering the possible inaccuracy in determining ϕ' and S_s, the predicted values for pressure drop were in close agreement with those found in practice. The overall pressure drop for a typical experimental separation run has been recorded as 199 kN m^{-2}, whereas under identical flow conditions the model will predict a pressure drop of 204 $kN.m^{-2}$.

9.2.4 Development of a Temperature Profile

9.2.4.1 Heat Balance over a Theoretical Plate

Scott (83) has derived an expression relating the excess temperature of a plate to the volume of gas flowing through the plate (expressed in plate volumes) during a specific time interval. The final expression is a standard differential equation of the form:

$$\frac{d\Theta}{dV} + \beta_c \Theta = \alpha_c \frac{dX_{gn}}{dV} \qquad (9.28)$$

α_c, β_c = constants (functions of plate heat capacity and heat losses)

Θ = excess temperature of plate above its surroundings

V = volume of gas passed through a plate in terms of "plate volumes"

X_{gn} = concentration of solute in the gas phase in plate n.

Solution of Equation 9.28 is a complex procedure and requires the use of statistical tables, making the derivation unsuitable for inclusion in the digital computer simulation. For use in the SCCR1 model, Equation 9.28 may be greatly simplified as the term $\frac{dX_{gn}}{dV}$, i.e. the change in gas phase concentration during the passage of a

certain volume of gas, is not an unknown factor but is inherently calculated by the program for each time increment.

The following postulates will be made; a) The gas flowrate through the plate is constant. b) The temperature of the surroundings of the plate is constant. c) The heat capacity of the gas in the plate is insignificant compared with the heat capacities of the liquid phase and support. d) Linear absorption isotherms are assumed.

Considering a heat balance over the plate, then;
(Heat capacity of plate) X (rise in temperature) = (heat evolved in plate) - -(heat conducted radially from plate).

Considering the number of plates in a column the temperature of adjacent plates may be assumed to be the same, so that axial heat conduction is negligible compared with heat conducted radially from the column, hence,

$$(V_2\rho_L.S_L + V_1.\rho_p.S_p)\Theta = [h_i.K_i \frac{d\ c_n}{dt}] - Ap.z.\ dt.\Theta \qquad (9.29)$$

V_1, V_2 = volumes of liquid phase and solid support

S_L, S_p = specific heats of liquid phase and solid support

ρ_L, ρ_p = densities of liquid phase and solid support

h_i = heat of solution of component i in the liquid phase

A_p = surface area of theoretical plate

z = composite thermal conductivity of packed bed

The term $[h_i.k_i \frac{d\ c_n}{dt}]$ in Equation 9.29, has to be evaluated for each of the components Arklone.P., Genklene.P. Values for h_i were obtained from Sunal (52), whilst the composite thermal conductivity, Z, was evaluated from the expression given by Perry (181).

Knowing the change in gas phase concentration over the time increment dt, Equation 9.29 may be solved to yield the change in temperature of the plate during the same dt.

9.2.4.2 Limiting Saturated Vapour Pressures

Experimentally it has been shown that the under certain conditions the gas phase concentration may reach saturation point and condensation may even occur (Chapter 8). To attempt to program for condensation and the inherent effects such as multiple feed points, rate of condensation and rate of re-evaporation, is beyond the scope of the present work, and may well be unneccessary as condensation is not a fault of the mathematical simulation but of the experimental equipment and can be prevented by a redesign of the unit. However, for the present model the maximum permissible gas phase solute concentrations must be specified for each plate to prevent the on-column concentrations rising above saturation point. The saturated vapour pressures are therefore calculated for each plate, at the temperature of the plate, and if the on-column concentration reaches this level it is assumed that the condensate has no further effect on the simulation and is simply removed from the unit in the purge column.

9.2.5 The Program

Figure 9.1 gives a detailed flow chart of the computation, with the listing of the program written in Fortran IV presented in Appendix 2. A listing of the variable names is also given in Appendix 2. The program is compatible for running on 'International Computers Limited' machines, and was computed on a series CDC 7600 machine at the University of Manchester Regional Computer Centre.

Figure 9.1

Flowchart for the Computer Simulation of the SCCR1

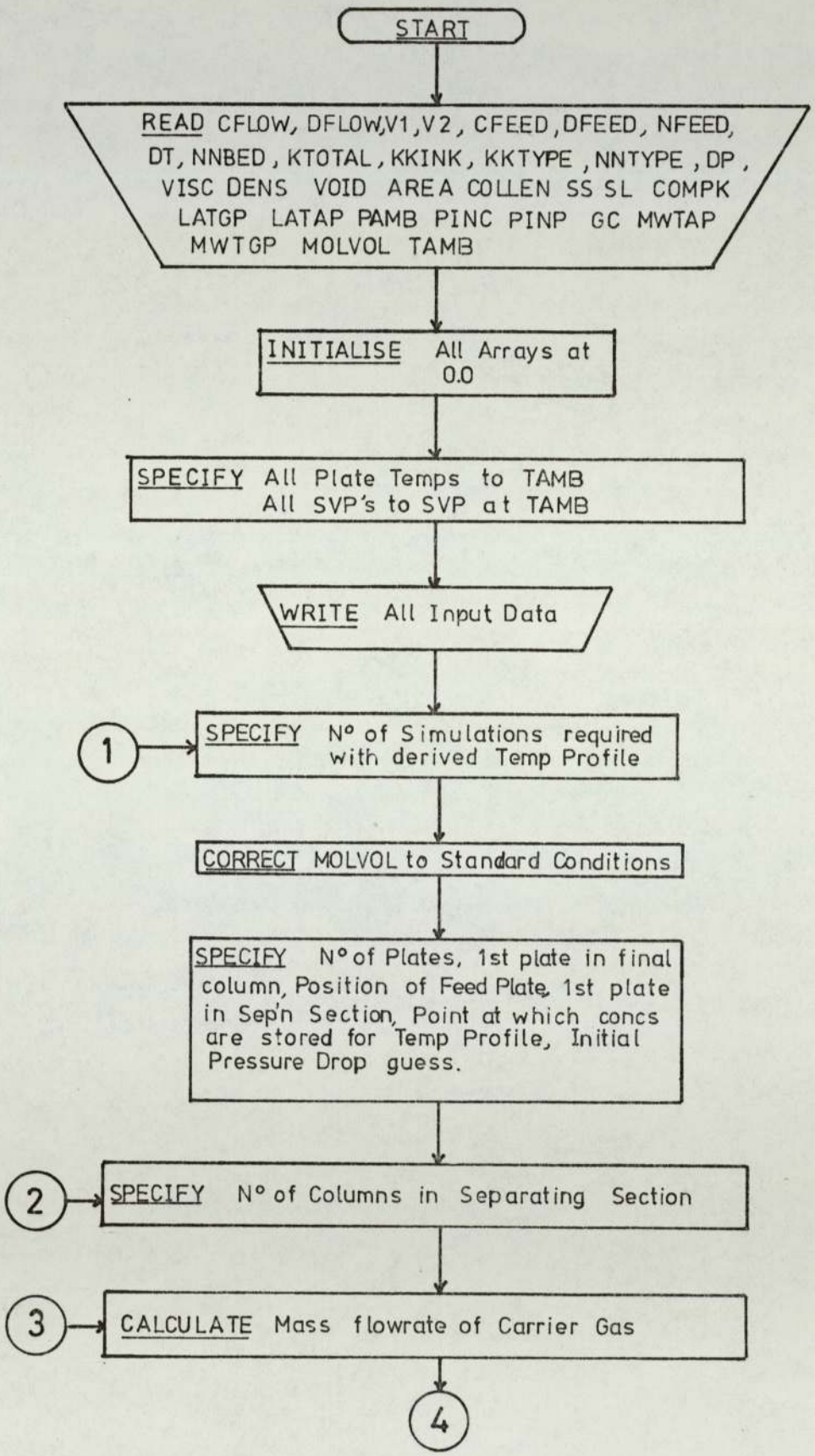

Figure 9.1 (cont'd)

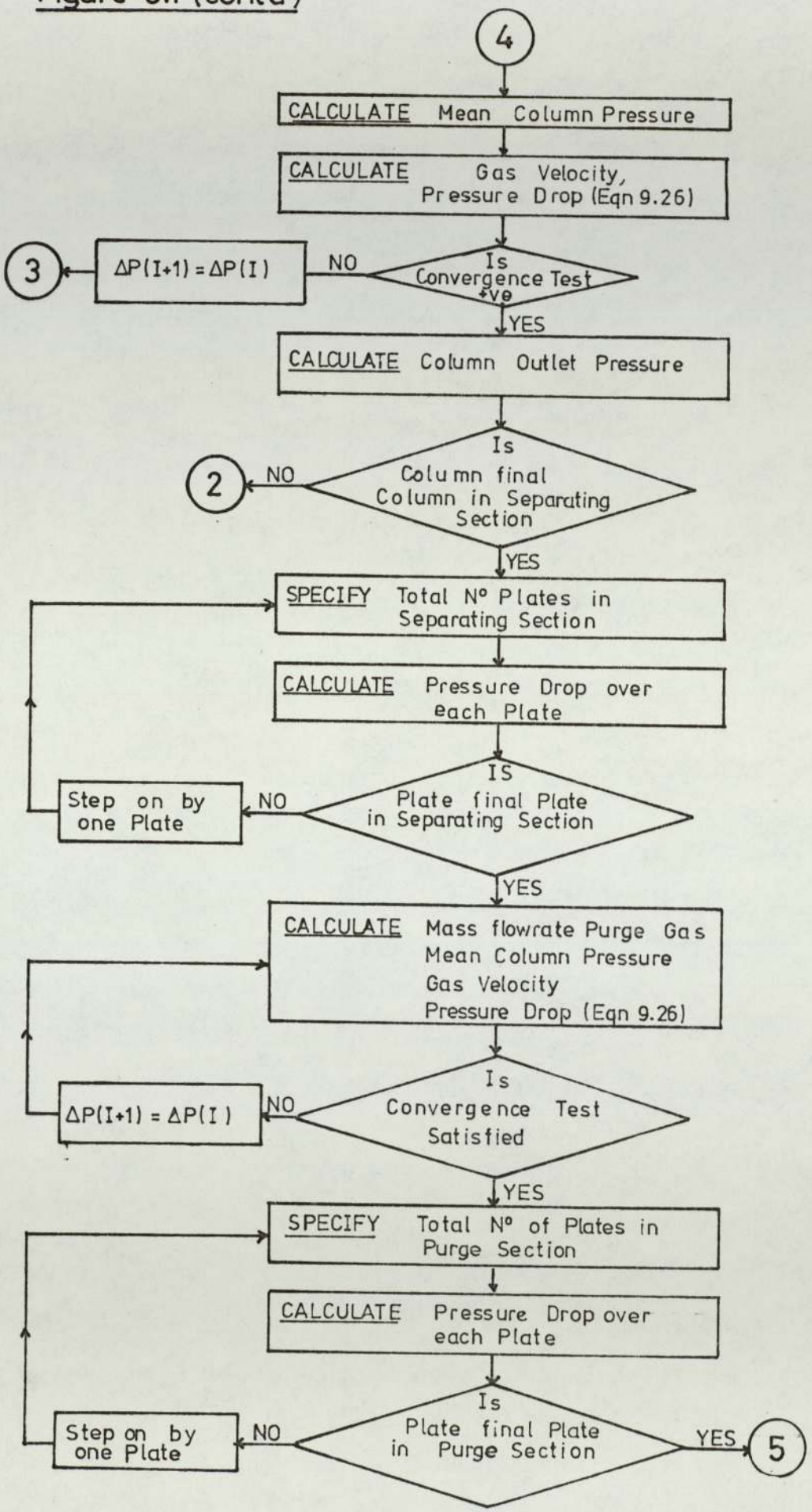

Figure 9.1 (contd)

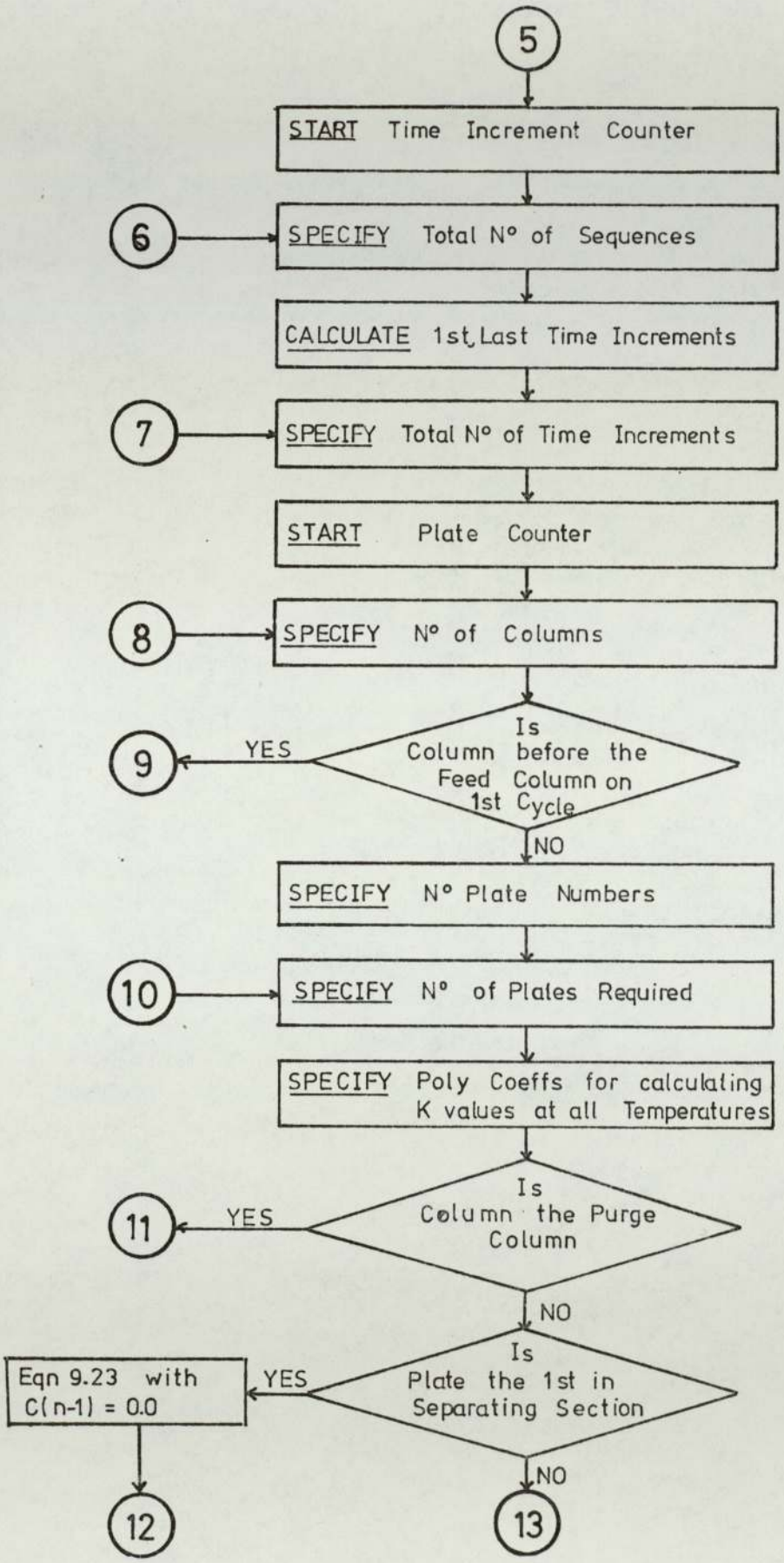

Figure 9.1(cont'd)

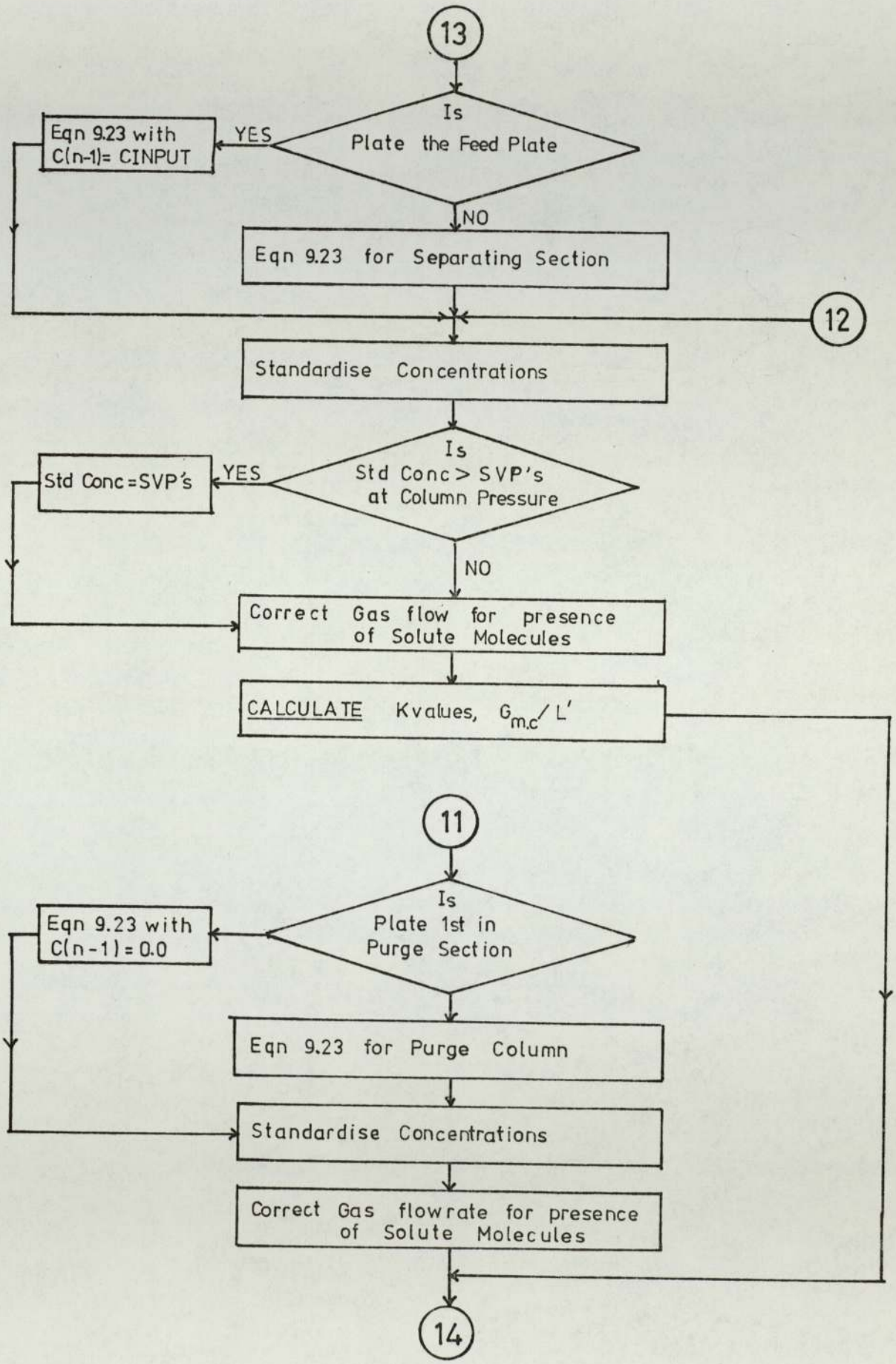

Figure 9.1(cont'd)

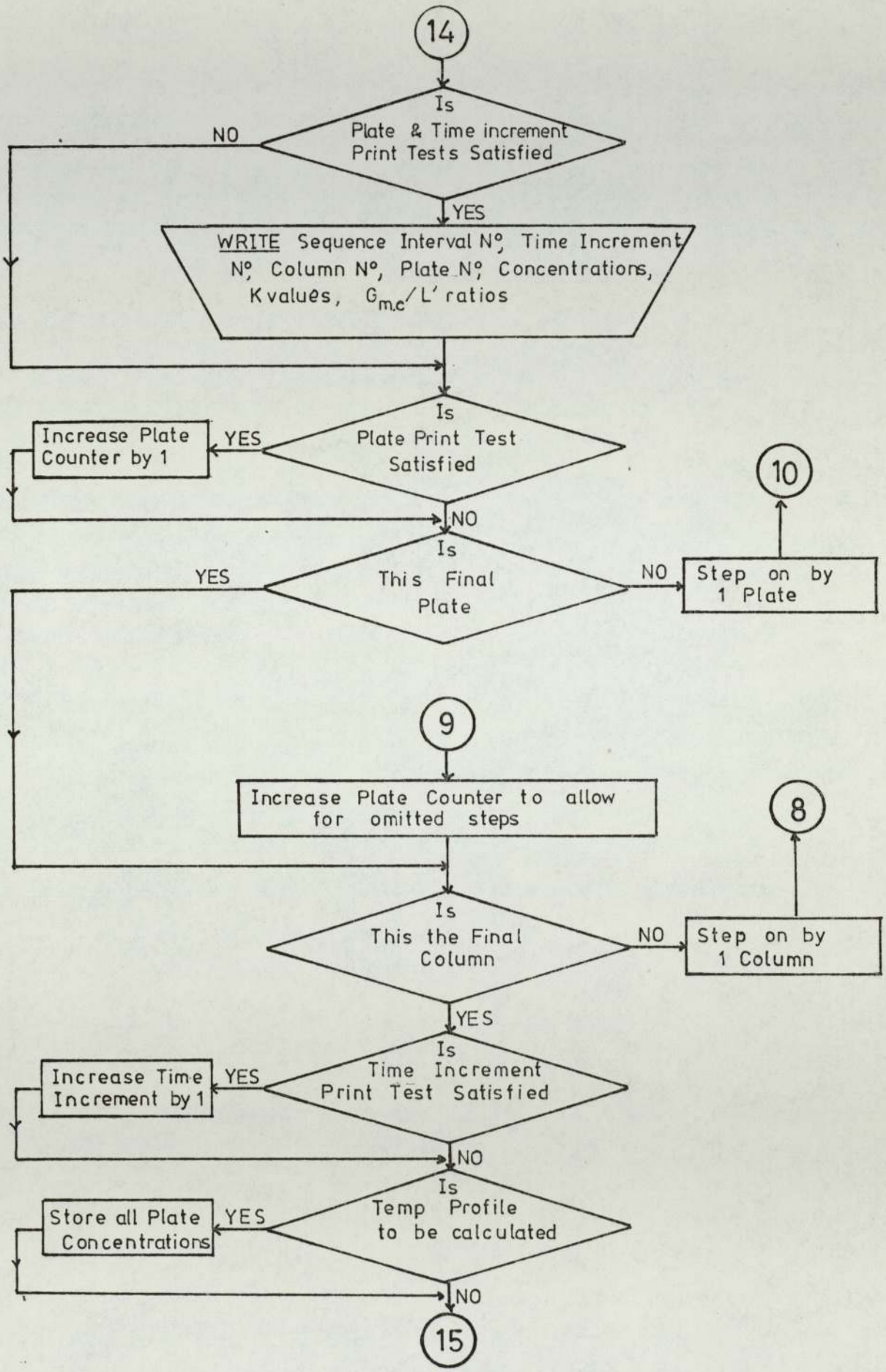

Figure 9.1 (cont'd)

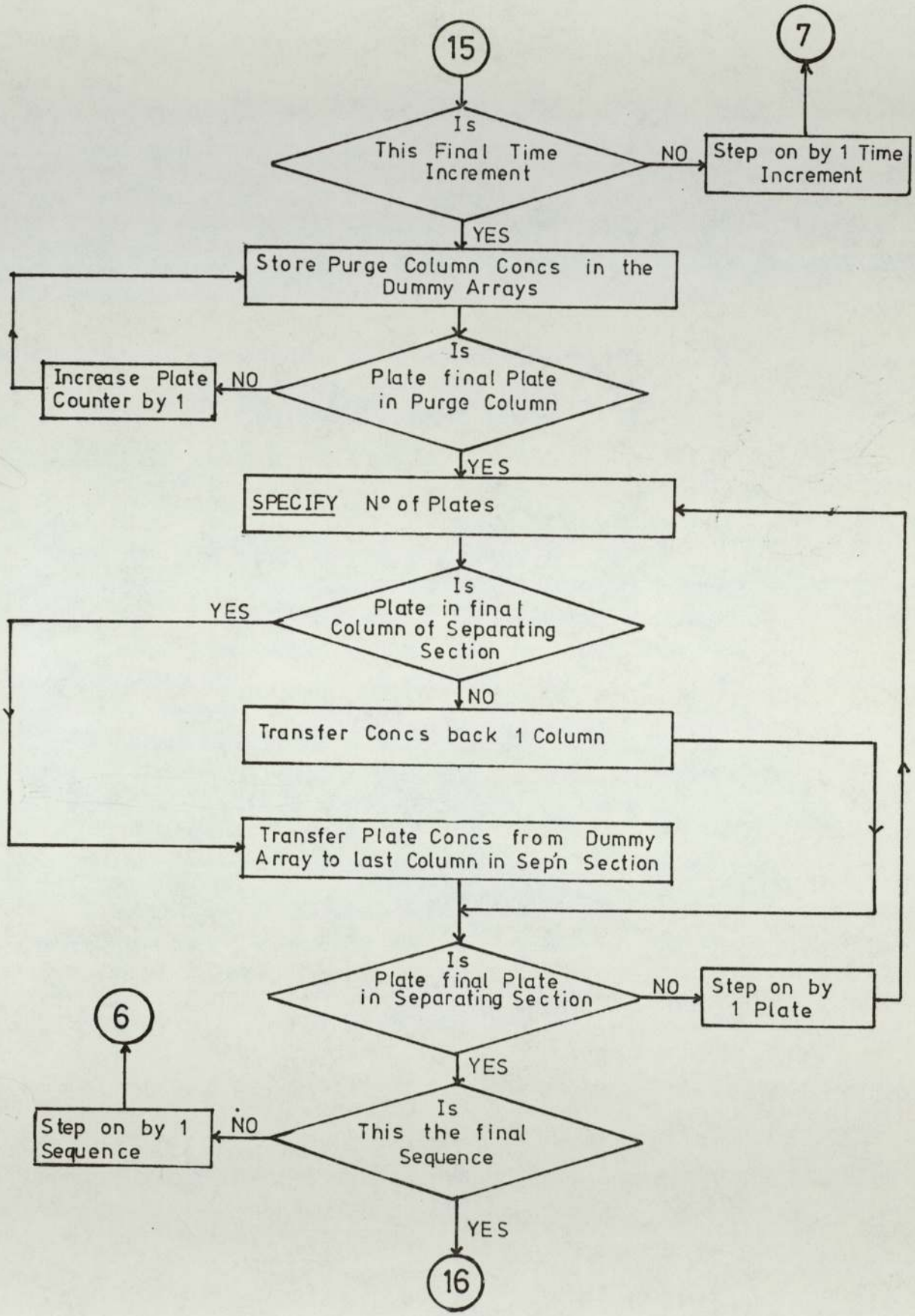

Figure 9.1(cont'd)

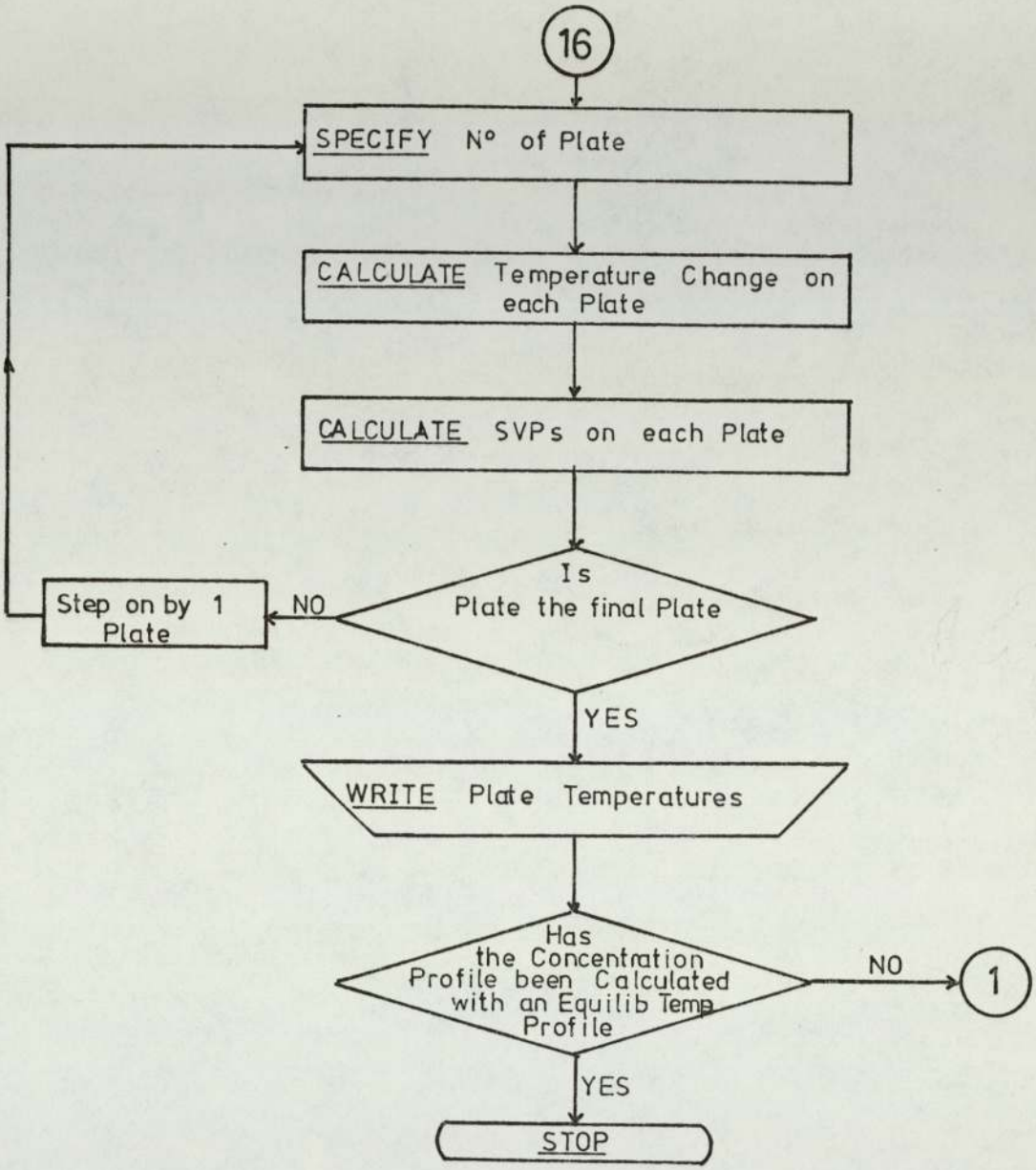

9.3 Results

Five computer runs are given for a range of solute feedrates. For all runs, the sequencing rate, number of plates per column,time increment, ambient temperature, and column packing characteristics are held constant. In developing the model to its present state several parameters have had to be optimised with a view to curtailing the execution time of the program.

The time increment (Δt) over which the column concentrations are assumed to be constant has been determined as 1 second. Using a Δt greater than 1s was found to invalidate the constant concentration assumption and resulted in the program not reaching an equilibrium value. For values of Δt below 1s the change in level or form of the respective concentration profiles was minimal and did not warrant the increase in computational time.

In Section 9.2.1 the theoretical plate height was estimated as 1.062 cm, yielding 57 plates/column. It has been shown (45) that for the system Arklone.P./Genklene.P. with a separation factor of approximately 2.7, that the number of plates/column is not a major factor in determining a successful separation until either the number of plates/column is reduced to below 20, or the difficulty of separation is increased. As the program execution time is in direct proportion to the number of theoretical plates in the model, then as a compromise between accuracy and time, the number of plates per column was specified as 40. It must be emphasised however that the above findings recorded by Deeble (45) and further substantiated with unrecorded runs of the present model, apply only to a system of high separation factor and that for a system such as dichloromethane/Arklone.P. with a low separation factor, the number of plates is expected to be a

major influence in the type of separation obtained. Conder (121,122), working with large scale batch units has also arrived at similar conclusions.

The concentration profiles for solute feedrates of 600,800, 1000,1200, and 1400 $cm^3.hr^{-1}$ are given in Figures 9.2 to 9.6 with the input data required by the model having the same values as that set experimentally.

9.4 Discussion

The major criticism of the model is the execution time of the simulation. The plate to plate calculation method requires that more than 10^8 calculations be performed and hence the necessity for optimising the time increment and the number of plates per column. It has been suggested (204) that considerable time will be saved if the basic mass balance differential equation (9.22) is solved by a method of numerical integration incorporating the Runge-Kutta-Merson technique (205). Without a basic mathematical restructuring of the model, further refinements will be limited by the processing time and therefore cost of running the model.

9.4.1 Accuracy of the Simulation

The five runs presented in Figures 9.2 to 9.6 may be compared with the experimental profiles shown in Chapter 8. In so doing it will be noticed that the shape of both solute profiles are of a similar form to that found experimentally although the Arklone.P. profile from the model does possess a more pronounced 'plateau region'. The levels of concentration predicted for Arklone.P., are in close agreement with experimental values up to a feedrate of 1200 $cm^3.hr^{-1}$., after which predicted levels tend to exceed the measured values. Regarding the Genklene.P. profile, the predicted values whilst accurately modelling the profile shape, consistently give values in excess of those found experimentally. The explanation for this is probably because the model is not capable of dealing completely with situations where solute condensation from the gas phase may occur. In practice any condensed Genklene.P. will revaporise and cool the localised region of the packed bed. Although the model is programmed so that the s.v.p's of Genklene.P. may not be exceeded, it cannot allow for the heating/cooling

effect of any condensing/revaporising of the solute, and it is this anomaly which it is believed is resulting in the predicted values for Genklene.P. being higher than those measured experimentally. As previously mentioned (9.2.4.2) preventing condensation of solutes is a relatively simple matter and if this were to be implemented then it is believed that the experimentally determined concentrations would increase, and match more closely those predicted by the model.

Although it is not possible to present it graphically, the rate of build up of concentrations is of importance. At the start of each simulation the rate of build up in gas phase concentration of the component with least affinity for the stationary phase (Arklone.P.), is faster than for the Genklene.P. gas phase concentration. The reason for this is that the Genklene.P. has a larger liquid volume accessible to it in the column, and consequently its concentration in the mobile phase is reduced to a greater degree than for the Arklone.P. The time taken for the profiles to reach pseudo-equilibrium was therefore not only dependent upon the input concentrations but also upon the component K values. For the simulation of Run 1200-265-262, Arklone.P. had reached equilibrium after only 9 sequences whilst the Genklene.P. required more than 15 sequences. In practice observations from the Katharometer product traces showed that Arklone.P. required 12 sequences with the Genklene.P. reaching pseudo-equilibrium after approximately 19 sequences, which perhaps demonstrates the idealistic nature of the simulation.

Using numerical integration techniques to solve the mass balance equation is one approach that will improve the efficiency of the model. The accuracy of simulation may also be improved, and possible ways of achieving this are listed below.

9.4.2 Methods for Improving the Accuracy of Simulation

(i) Temperature Profile:- At present the temperature profile is calculated under equilibrium concentration conditions, and the concentration profile is then recalculated with the equilibrium temperature profile present. Ideally, as temperature is a function of the rate of change of concentration within the columns, a non-equilibrium temperature profile should be developed concurrently with the concentration profile. The importance of including a temperature profile can be seen from Figure 9.6, where the concentration profiles are portrayed for operation of the model under both isothermal and non-isothermal conditions. The change in levels of concentration for both modes of operation can be seen to be greater than 10% and hence it is desirable to model a temperature profile as accurately as possible, however small the fluctuations may be. The heat balance over a theoretical plate is at present calculated based on the concentration change over the plate during one sequencing interval. Again accuracy may be improved if this calculation were to be accomplished based on the concentration change over the plate during one time increment. Programming-wise this may be accomplished basically by placing the temperature difference equations inside the inner loop of the mathematical simulation. The reason this has not been performed is the execution time limit, as the time required in the production of the temperature profile then becomes comparable to that required by the concentration profile, and the program again becomes too lengthy.

(ii) H.E.T.P.;- The value for H.E.T.P. defined in Section 9.2.1 can be considered as the mean column value and is used as an input parameter by the model. Throughout the simulation this value for

H.E.T.P. is regarded as a constant, independent from concentration, temperature, and more importantly mobile phase velocity. Equation 9.20 shows H to be a complex function of the velocity, u, which may be simplified to yield,

$$H = A + B/u + C_s u + C_m u \qquad (2.16)$$

The fact that the mobile phase velocity may change by more than 100% within the separating section of the SCCRl emphasises the importance of defining H.E.T.P's at different positions within the unit. In the above expression it has been found that it is the mobile phase resistance to mass transfer term ($c_m u$) which predominates, and that therefore H can be considered to increase in the direction of mobile phase flow. In practice the solutes are fed to the unit at approximately the mid-point of the separating section. In terms of number of theoretical plates available for separation the feed location may be well away from the mid-point of the separating section.

Whilst the assumption of a constant H.E.T.P. may remain valid for an easy separation it is anticipated that for more difficult systems H will be evaluated in conjunction with the pressure drop calculations so that each column then has a unique number of plates dependent upon the flow conditions.

(iii) Physical Data:- The absorption isotherms for Arklone.P. and Genklene.P. have been considered as linear in the simulation, a valid assumption up to gas phase concentrations of 0.5×10^{-3} $g.cm^{-3}$. At solute feedrates of greater than 1200 $cm^3.hr^{-1}$ these concentrations are

being predicted, and therefore the absorption isotherms should then be described by a more accurate non-linear polynomial.

A further source of error may occur through the assumption that the two solute profiles are independent from each other. Sunal (50) has experimentally measured and correlated activity coefficients for the solutes Arklone.P., Genklene.P, on the silicone fluid phase, in the presence of each other. Improvement may be gained by using this data for the prediction of partition coefficients within the unit, although Sunal (50) reported that the accuracy of the interaction correlation data was less than for the pure solute case.

9.4.3 The Role of the Model

In conclusion several possible uses for the model will be given. Perhaps the major practical limitation in continuous gas-liquid chromatography is the compressible carrier gas giving rise to large changes in G_{mc}/L' within the units. A possible way to minimise this effect is to have the carrier gas entering at a very much higher pressure. Practically this cannot be achieved as the present unit is not designed to operate at pressures greater than 500 $kN.m^{-2}$, and therefore the model should be able to provide answers to the question of high pressure operation.

A further practical application concerns the optimum sequencing interval. Experimental results presented in Section 6.3 indicated that the separating efficiency increased as the sequencing interval was reduced. Mechanical limitations prevented any definite conclusions to be drawn from the study, and hence the model could be used to further investigate this area of study.

Work is presently being conducted in the Chemical Engineering Department of Aston University into continuous g.l.c. separations of industrial importance. The sequential unit used for these studies has been reported briefly elsewhere in this thesis and the above mathematical model may be readily converted to simulate these type of separations provided the necessary physical data ia available. Ellison (49), has used a precursor of the model to simulate gel-permeation chromatographic separations in a 5.2 cm diameter sequential unit with encouraging results.

Figure 9.2 Computer Simulation for Run 600-265-262

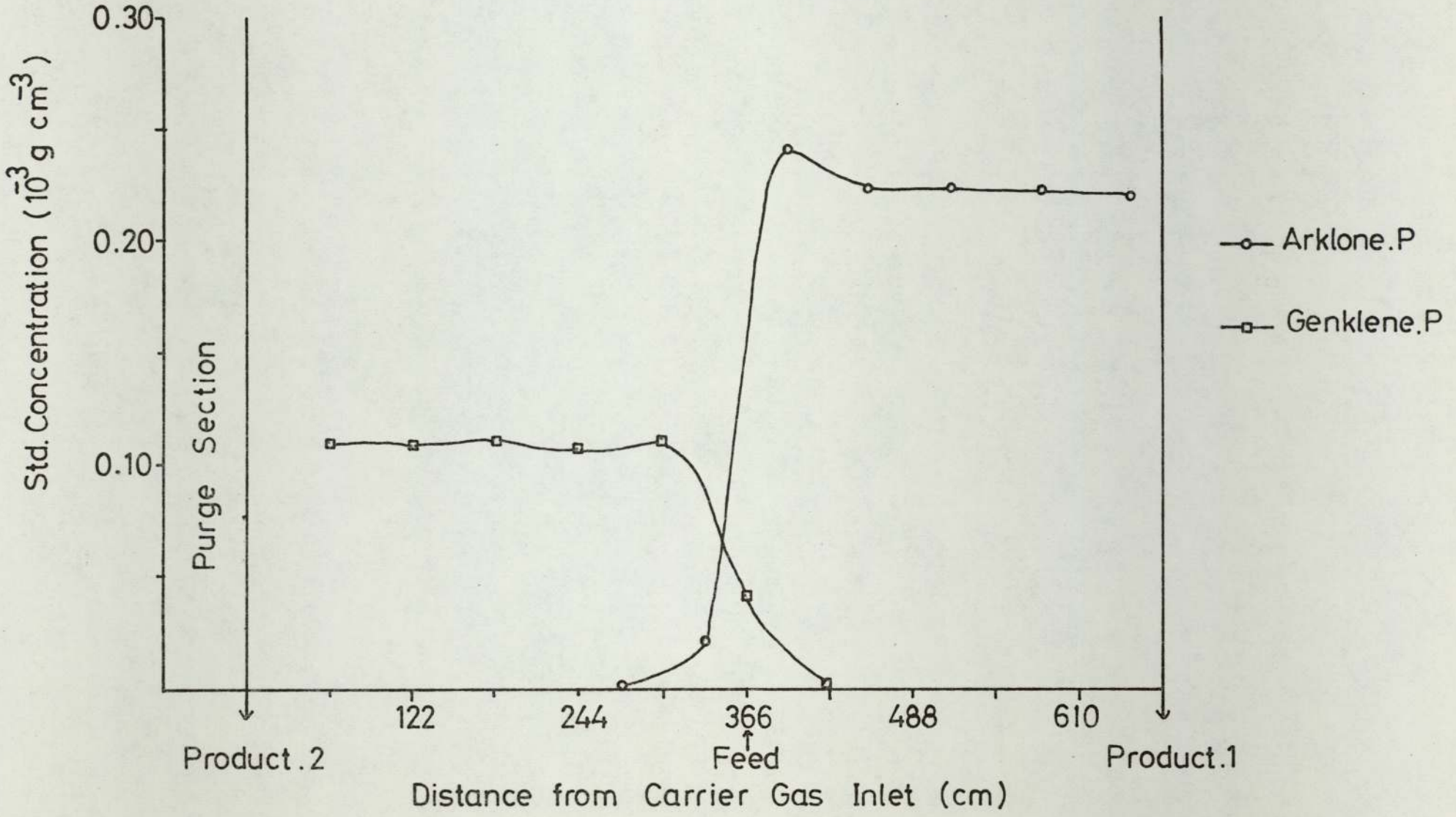

Figure 9.3 Computer Simulation for Run 800-265-262

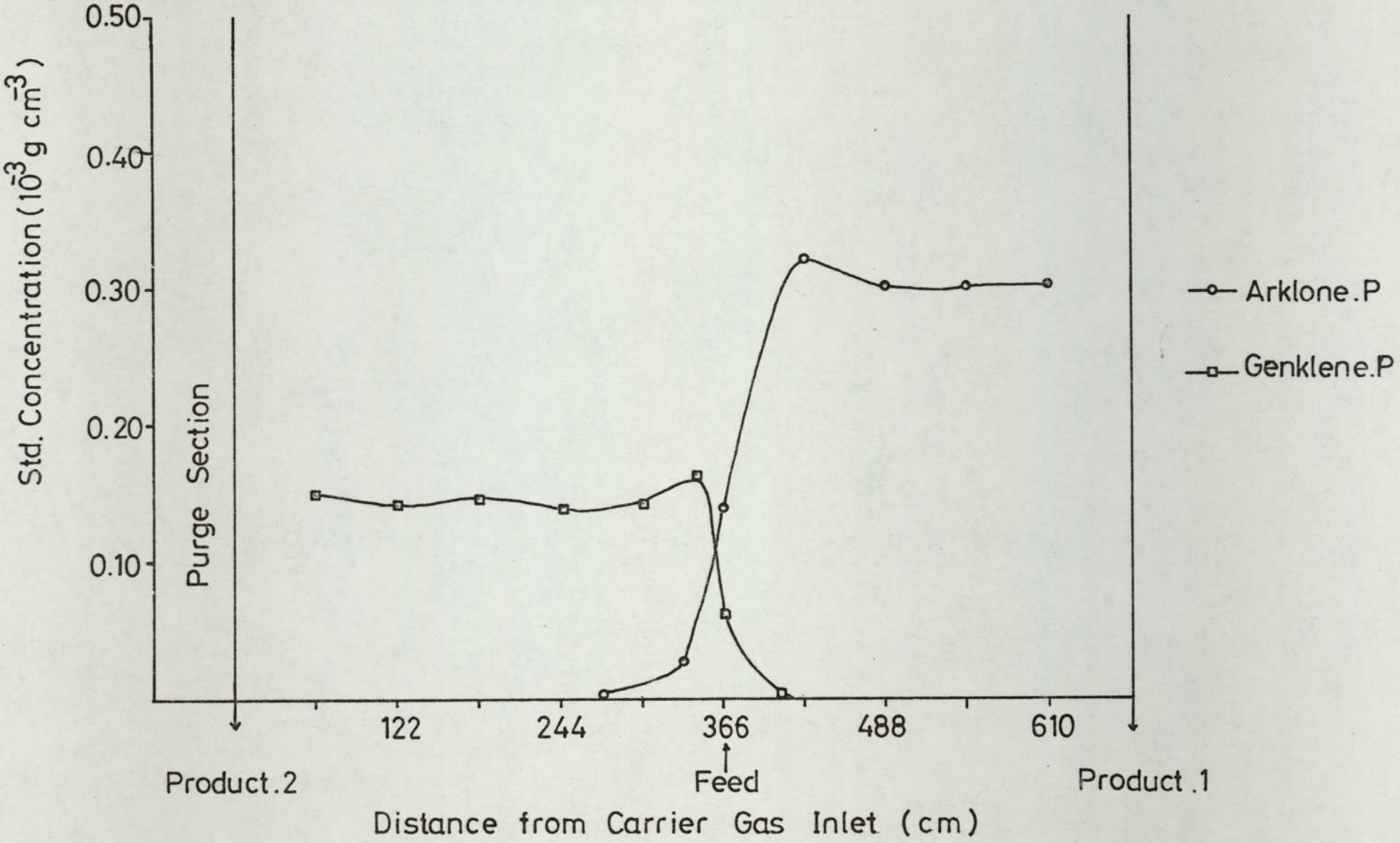

Figure 9.4 Computer Simulation for Run 1000-265-262

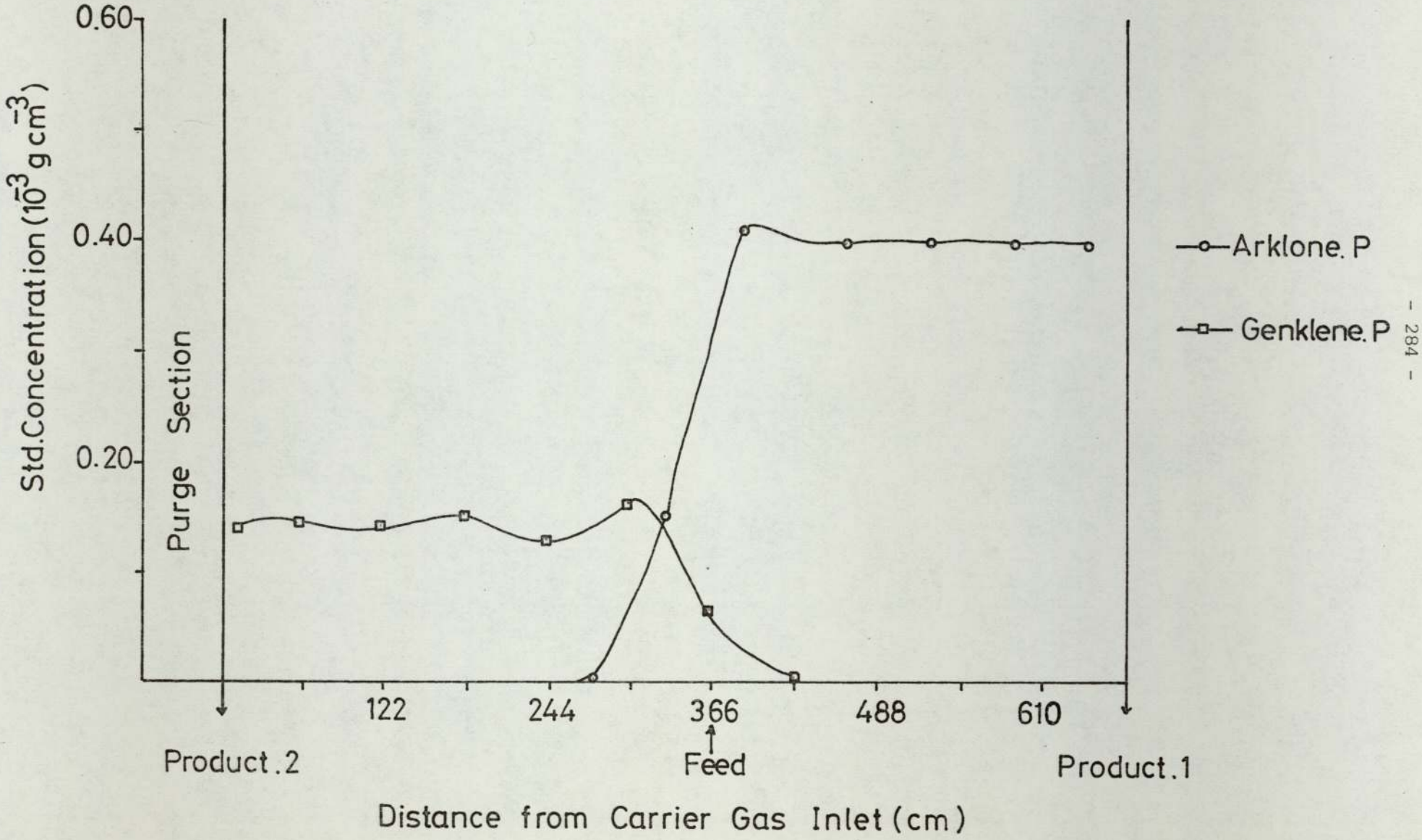

Figure 9.5 Computer Simulation for Run 1200-265-262

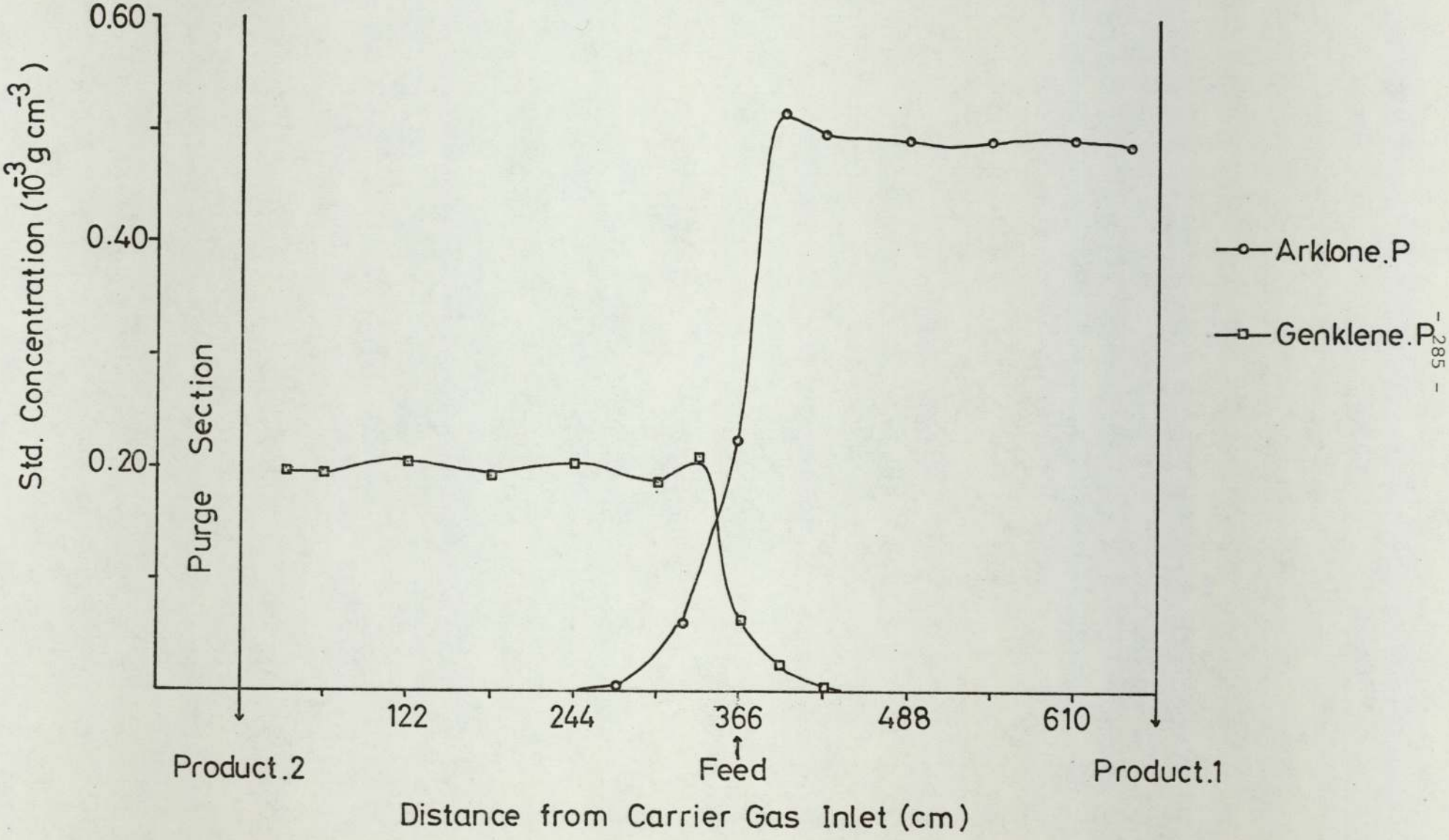

Figure 9.6 Computer Simulation for Run 1400-265-262

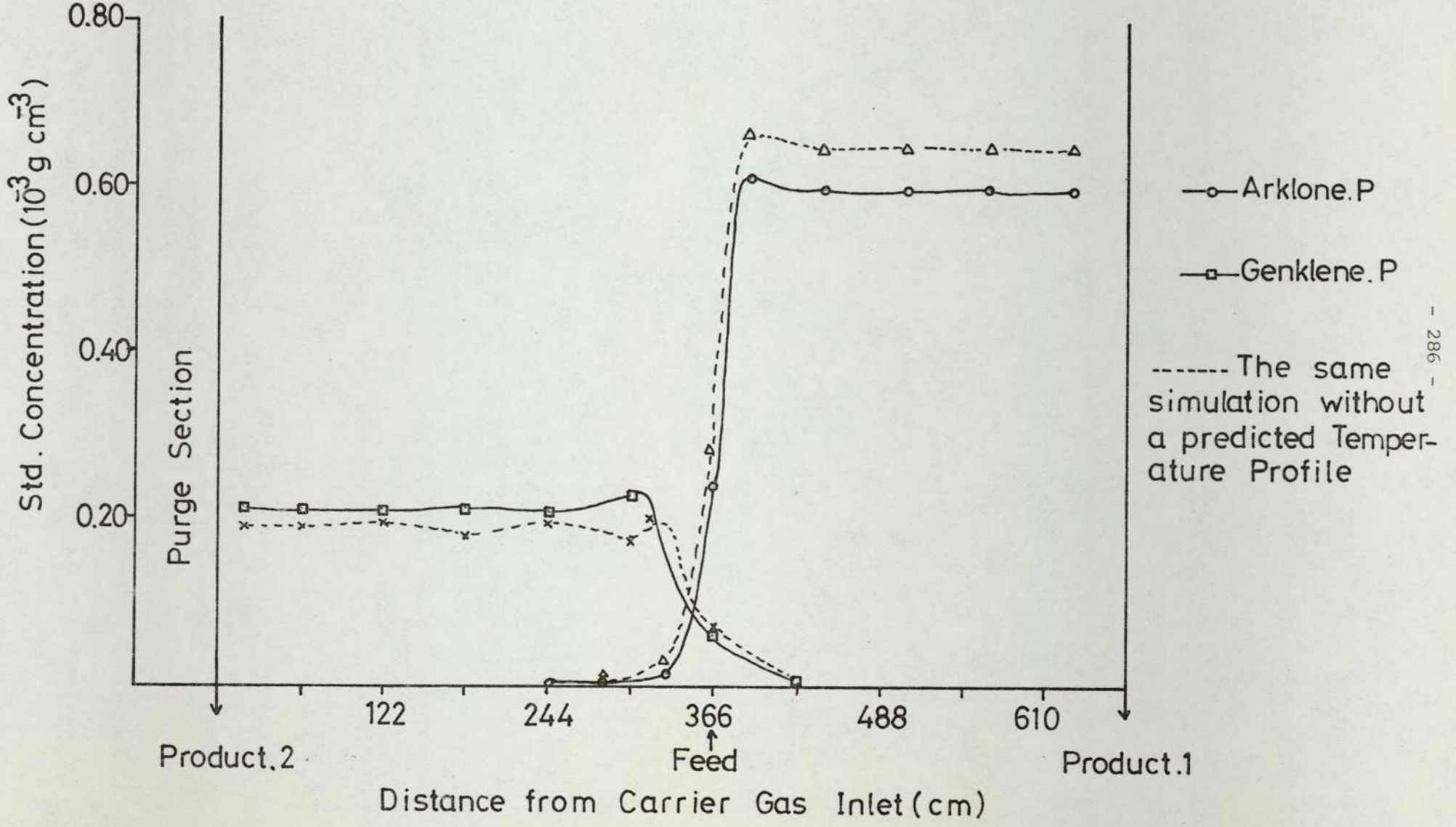

CHAPTER 10

CONCLUSIONS AND RECOMMENDATIONS FOR FUTURE WORK

The ability of a sequential continuous chromatographic unit to fractionate the system Arklone.P./Genklene.P. at high purity, on the phase silicone fluid DC 200/50 at equivolume feedrates up to 1400 $cm^3.hr^{-1}$ has been demonstrated. Above this throughput it is believed that a significant proportion of the higher boiling point solute (Genklene.P) is reaching saturation point in the gas phase and condensing out. For future investigations it is recommended that the ambient temperature of the unit be raised by enclosement in a thermostatically controlled environment. Literature suggests (133) the optimum temperature of operation near to the solute boiling points although consideration must be given to product degradation and the maximum allowable temperature of the solvent phase.

It has been shown that temperature has a significant effect upon the solute distribution coefficients, and that a reduction of temperature perturbations within the sequential unit leads to higher separating efficiencies. The deleterious results from feeding the solutes in the liquid state emphasises the need for their introduction in the gaseous phase. The low, uneven, thermal conductivity possessed by the packed columns has led to very poor heat redistribution. To overcome this, internal fins may be placed in the columns prior to packing. As well as increasing radial heat transfer, it has been suggested (113) that the creation of smaller partially enclosed cross-sections should aid in reducing column profiles. A final recommendation to reduce the temperature fluctuations is to provide heating/cooling facilities for individual columns. Through monitoring changes in column concentration via a katharometer, a suitable control network may be constructed to provide a positive or negative external heat

flow to each column and so cancel the internal heat changes.

The ability of the SCCR1 to separate a more difficult chemical system of Arklone.P./dichloromethane, (separation factor 1.17) has been investigated. Results have shown that the present unit is incapable of producing two pure product streams, although either product may be produced above 99.5% purity provided the second stream is not required at greater than 80%. Because of the closeness of the solute partition coefficients it is essential to have an accurate knowledge of the stationary phase liquid loading. Over the period of operation of the SCCR1, it has been shown that a considerable redistribution of liquid phase has occurred and also that the original 25% wt/wt loading has been reduced to below 23%. It is strongly recommended therefore that prior to any further investigations the stationary phase is recoated and that regular checks be carried out to determine the on-column liquid phase loading. 'Purging off' of expensive liquid phase has been one of the major reasons why the large diameter columns at Abcor Inc.(20-22) have proved uneconomic.

Using a compressible gas as a carrier fluid produces a wide variation in the $G_{m.c}/L'$ ratio throughout the columns. Minimising the change in $G_{m.c}/L'$ is particularly important when difficult separations are being attempted, and operation of the unit at higher pressures would have this desired effect. The type of solenoid valves in operation on the SCCR1 make this recommendation impractical, however, it may be possible to investigate this proposal with the pneumatically operated SCCR2.

To summarize, the practical recommendations may be defined in two categories.

For production purposes, throughputs and efficiencies should be increased in one or more of the following ways:

(i) Operation at a temperature closer to the solute boiling points.

(ii) Temperature programming of individual columns

(iii) Redesign of columns to incorporate internal fins

(iv) Packing the inlet/outlet cones with inert glass or metallic spheres.

(v) Increasing the diameter of the columns

(vi) Re-coating of the stationary phase.

Future areas of investigation, which have been indicated by the present research, are:

(i) Investigation of the effect of inlet pressure upon separating capabilities.

(ii) Determination of the optimum sequencing rate. Results have indicated the use of faster sequencing rates in conjunction with increased carrier gas flowrates. The resultant increase in pressure gradient may be reduced by using a larger particle size solid support.

(iii) Investigation of the effect of changing the feed input position within the separating section of the SCCR1 unit to enable a more efficient use of the available separating length.

(iv) Investigation into the length or number of columns required to meet given product specifications.

(v) Investigation into the carrier gas velocity profile and solute zone velocity profile. The literature has reported (68-80) the differences of opinion that exist as to the shape and effect of velocity profiles in large diameter columns, and these differences have given rise to a number of conflicting expressions to account for zone broadening in large diameter columns.

From a theoretical standpoint a digital computer model has been developed to simulate the operation of the SCCR1, the model is also readily convertable to simulate other SCCR machines. Based on the development of concentration, temperature, and pressure profiles, continuously over a series of theoretical plates, the predicted results have been compared with experimental values. Agreement of the two sets of results becomes less accurate at high feedrates although methods by which the accuracy of the simulation may be improved have been reported, with the most important recommendation being the inclusion of a variable H.E.T.P. parameter. Under dilute conditions the accuracy is such that useful predictive information may be produced with possible avenues of research being:

(i) Investigation of high pressure operation

(ii) Determination of optimum operating conditions

(iii) Determination of the minimum number of theoretical plates for a given separation.

(iv) Investigating in isolation, the individual factors affecting the performance of the sequential unit, defined by Equation 5.18.

Two final theoretical considerations concern the degree of non-equilibrium and the significance of the zone spreading cross-column velocity inequalities. The effect of the finite time required by the mass transfer process may be investigated by redefining the basic mass balance equation so that the gas phase solute concentration on plate n is not in equilibrium with the liquid phase solute concentration on that plate but with the concentration on plate (n-1) or (n-2),(n-3) etc.

An attempt has been made to include the largely empirical term H_c, as a coupled parameter in the plate height equation 9.20. The relationship between this term and the velocity inequality terms defined by Giddings (11) as w_1-w_5 may prove useful.

Appendix .1

Figure A.1.1 Rotameter Calibration

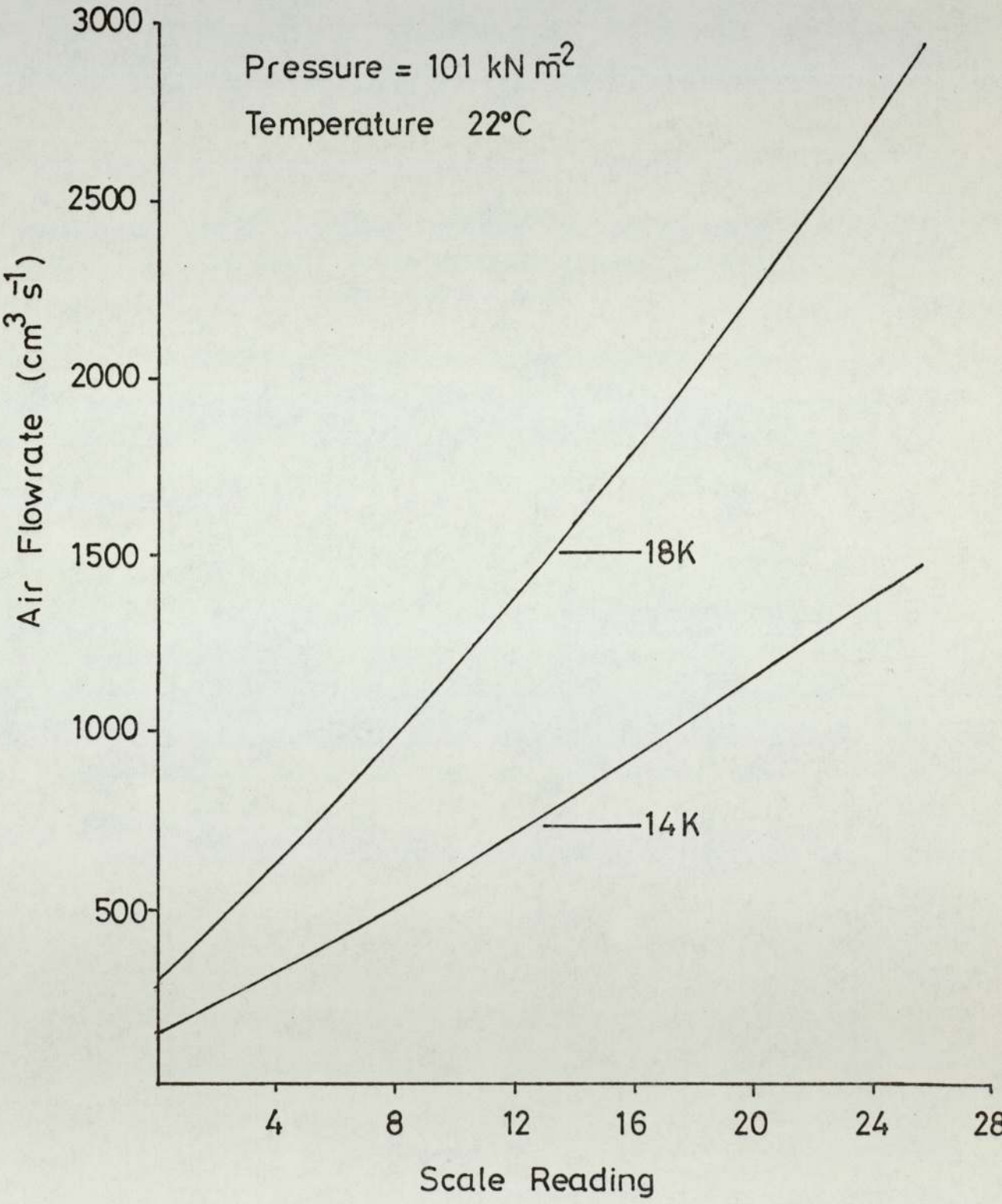

Figure A.1.2 $G_{m.c}$ versus Rotameter Scale for various Column Inlet Pressures

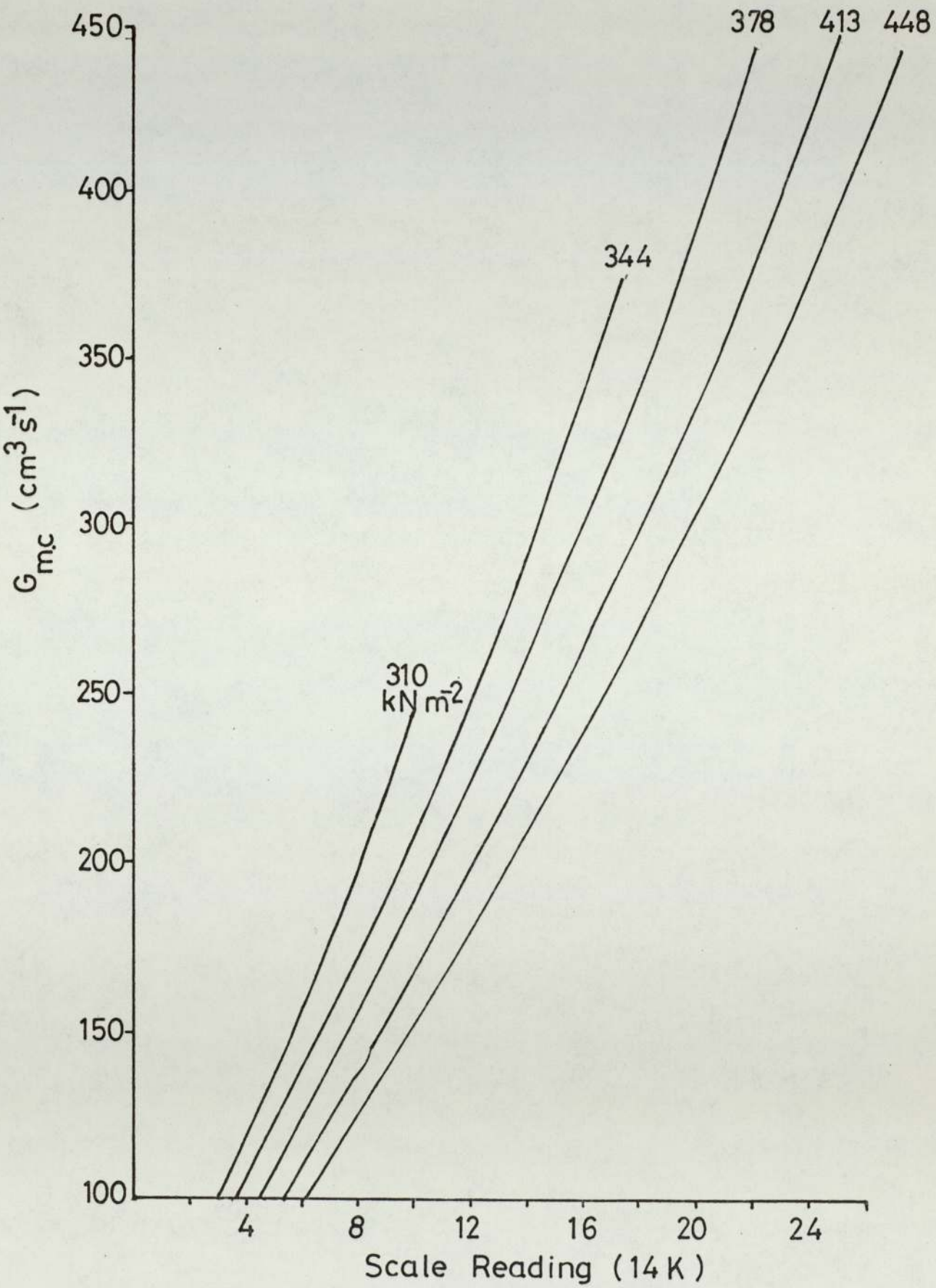

Figure A.1.3 $S_{m.c}$ versus Rotameter Scale for various Column Inlet Pressures

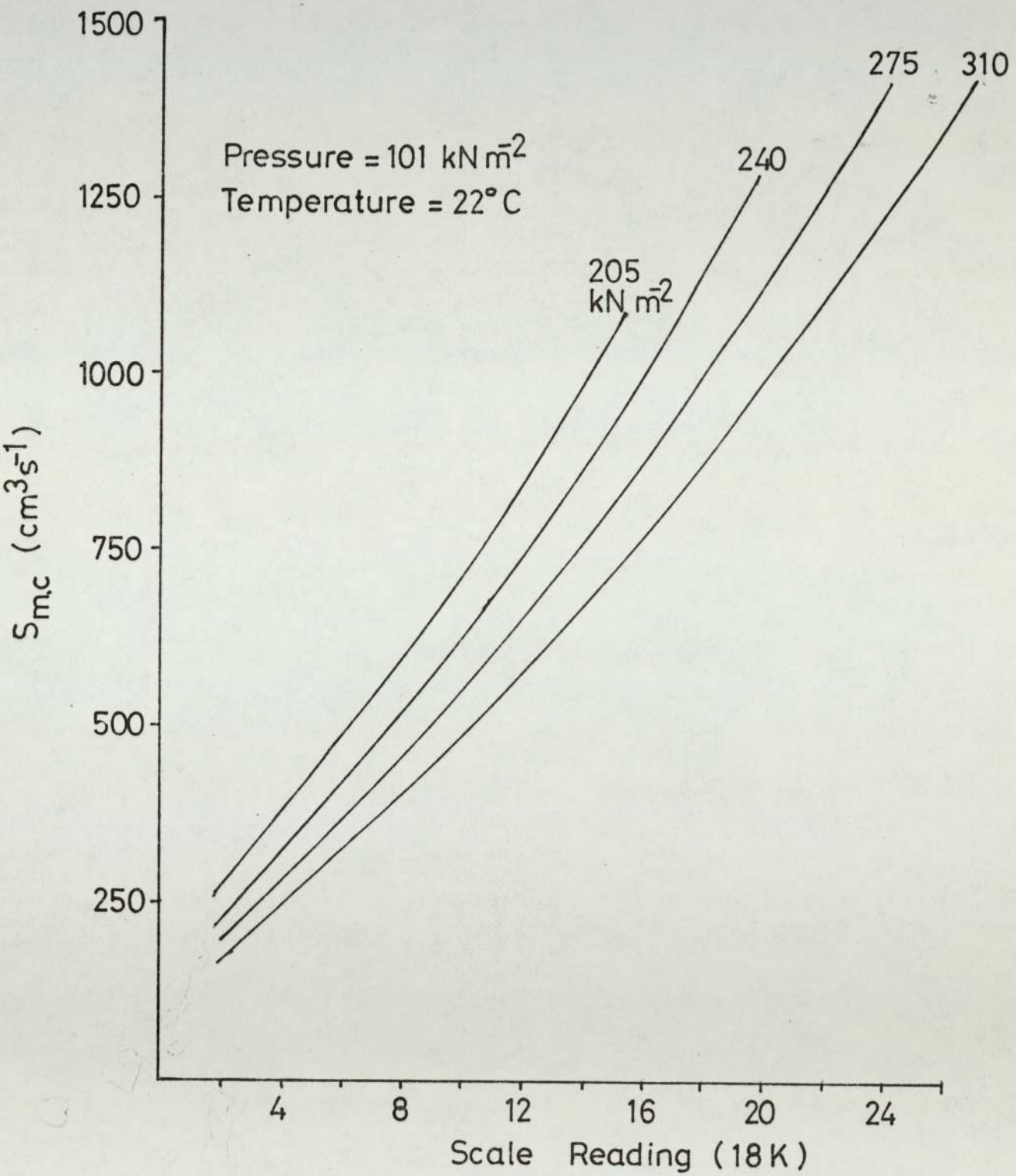

Figure A.1.4 Feed Pump Calibration

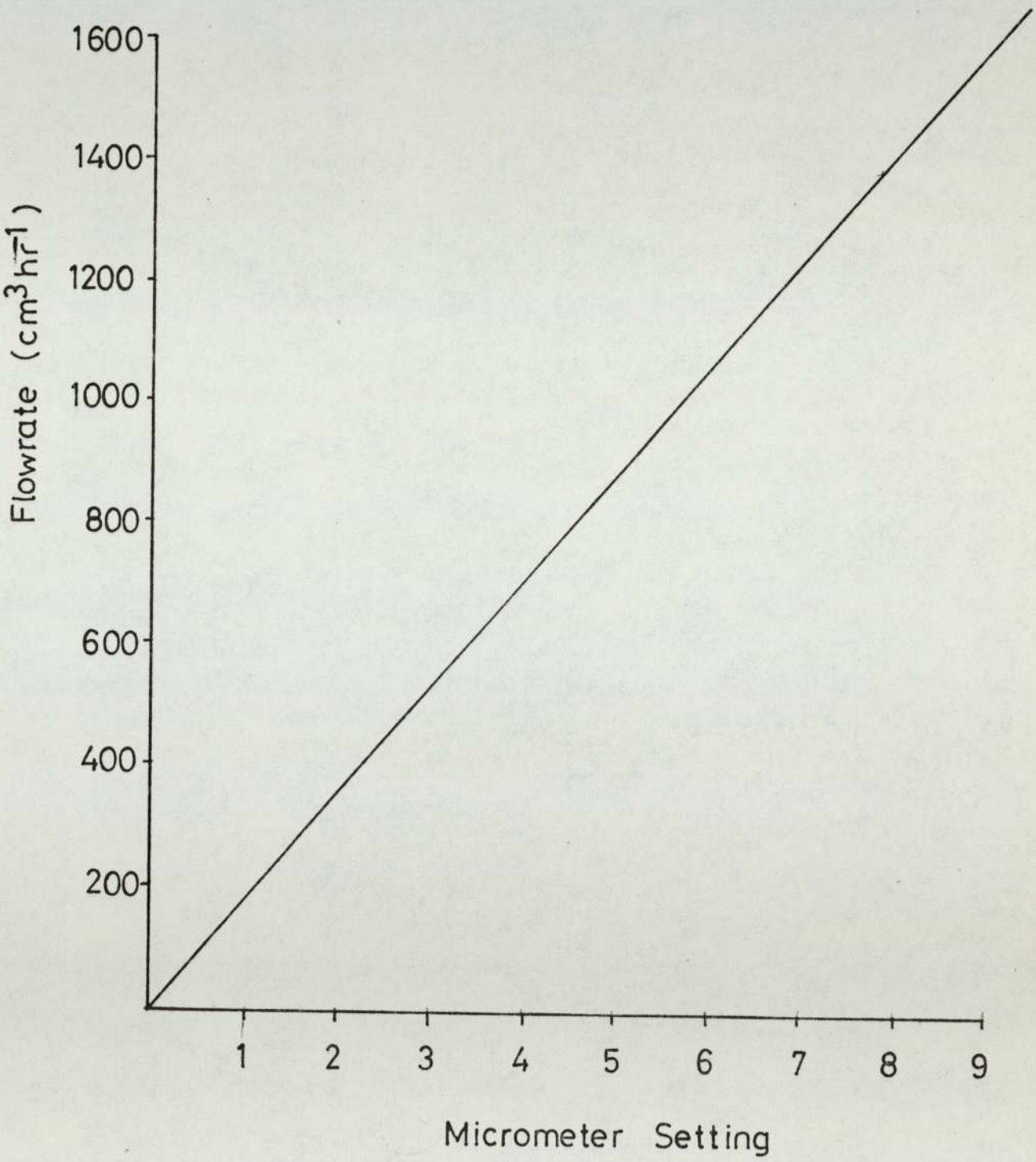

Figure A.1.5 Calibration of Automatic Timed Sequencing Unit

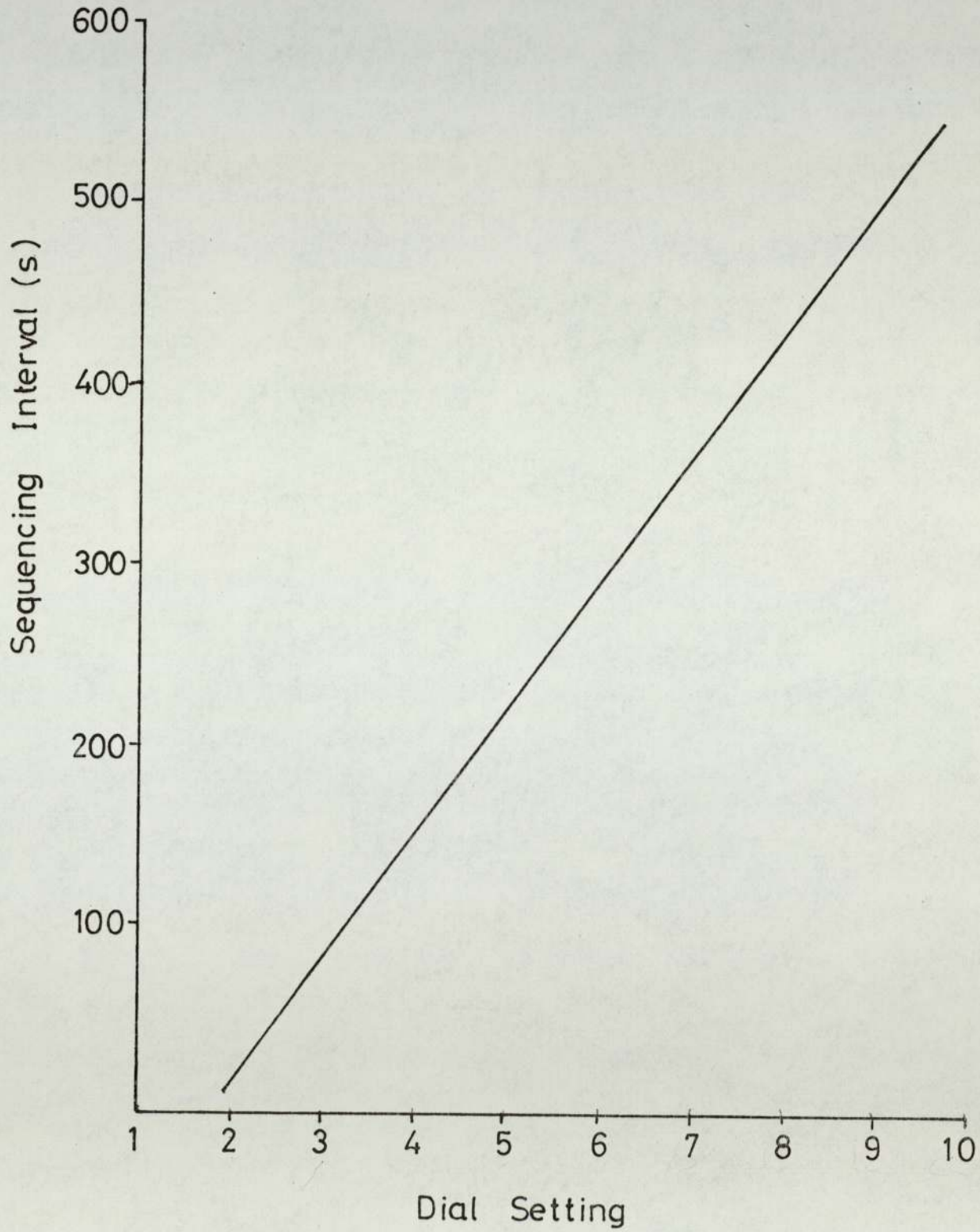

Figure A.1.6 Calibration of Thermocouples 1→8

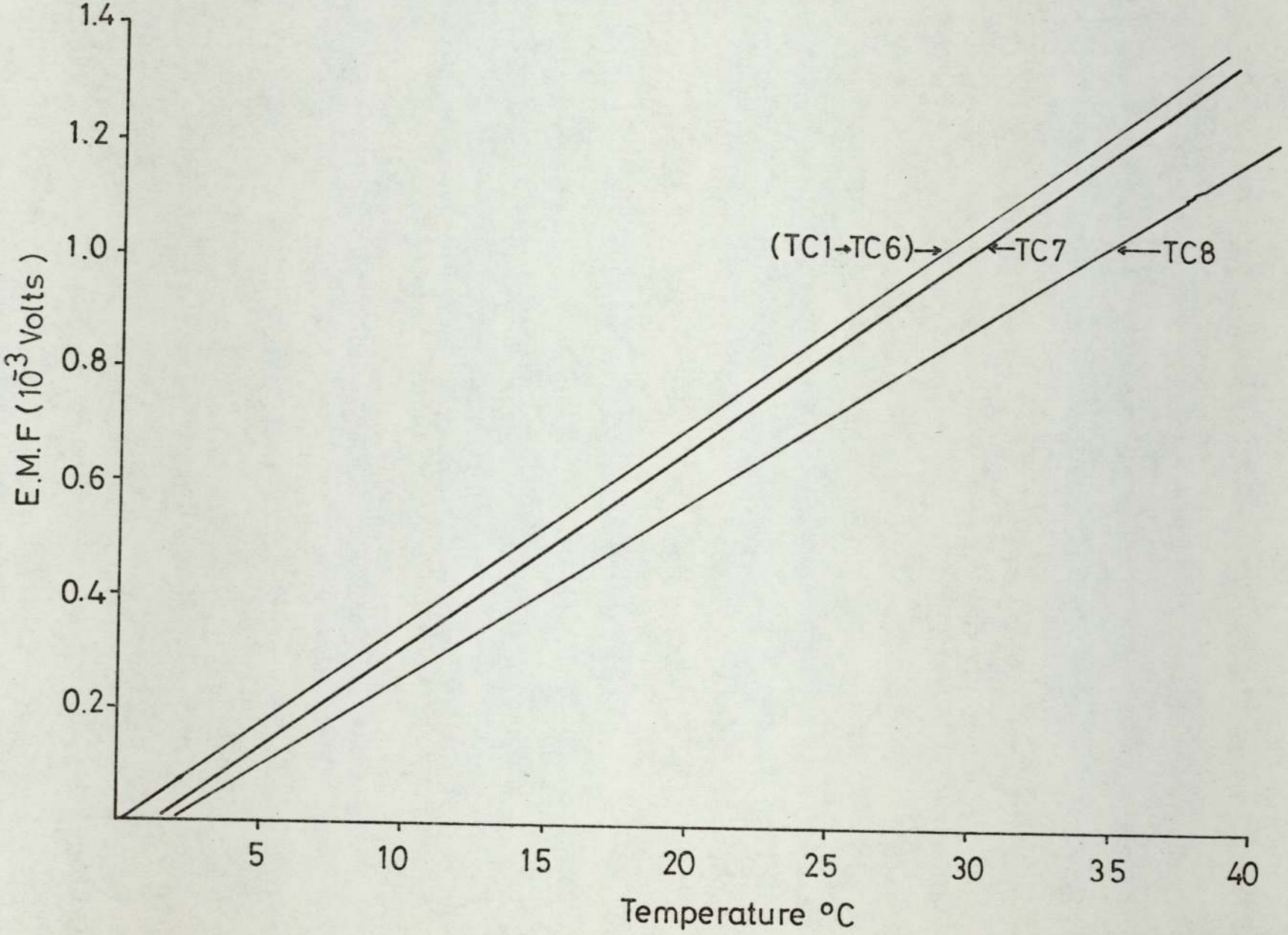

Appendix . 2

Figure A.2.1 Listing of Program to Calculate K value Polynomials

```
      DIMENSION XI(100),XL(100),GAMMA(100),RK(100),CONC(100)
      DIMENSION X(100),Y(100),P(400),FC(20),FRMS(20),R(100),W(100)
      DIMENSION S(100),T(100),U(100)
      TI=0.008101
      SI=0.9547
      TEMP=270.2
      FML=7100.0
      FDCM=84.93
      RHOL=0.97
      RG=8.3144E07
      A=7575.57
      B=8.1833
      NC=4
      NP=40
   20 VAP =EXP((B-((0.2185*A)/TEMP))*2.3026)
      VAPP=VAP*1.3594
      WRITE(2,400)
      WRITE(2,200) TEMP,VAPP
      WRITE(2,300)
      DO 30 K=1,40
      XI(K)=0.02*K
      XL(K)=1.0-XI(K)
      S(K)=TI/((TI*XI(K))+XL(K))
      T(K)=XL(K)*(1.0-TI)/((TI*XI(K))+XL(K))
      U(K)=((XL(K)/((TI*XI(K))+XL(K)))**2)*SI
      GAMMA(K)=S(K)*EXP(T(K)+U(K))
      RK(K)=RG*TEMP*RHOL/((GAMMA(K)*VAPP*FML*XL(K))*980.665)
      CONC(K)=XI(K)*RHOL*FDCM/(RK(K)*XL(K)*FML)
   30 CONTINUE
      WRITE(2,800)S(1),T(1),U(1),GAMMA(1),RK(1),CONC(1)
      NMAX=NC+1
      MM=5*NMAX+2*NP+3
      P(1)=-1
      P(3)=1
      P(4)=1
      P(5)=0
      DO 25 L=1,NC
      CALL F4CFORPL(NP,NMAX,MM,CONC,RK,R,W,FC,P)
   25 FRMS(L)=P(2)
      DO 301 M=1,NC
  301 WRITE(2,600) FC(M),FRMS(M)
      WRITE(2,300)
      WRITE(2,300)
      DO 302 J=1,NP
      WRITE(2,500)X(J),Y(J),R(J),XI(J),XL(J),GAMMA(J),RK(J),CONC(J)
  302 CONTINUE
      TEMP=TEMP+0.5
      IF(TEMP.EQ.303.2) GO TO 40
      GO TO 20
   40 CONTINUE
  100 FORMAT(20X,F10.5,10X,F10.5)
  200 FORMAT(20X,'TEMPERATURE=',2X,F10.5,10X,'VAPOUR PRESSURE=',2X,
     1 F10.5)
  300 FORMAT(1H0)
  400 FORMAT(1H1)
  500 FORMAT(5X,F10.7,5X,F10.7,5X,F10.7,5X,F10.7,5X,F10.7,5X,F10.7,
     1  5X,F10.4,5X,F10.7)
  600 FORMAT(2E15.8)
  700 FORMAT(10X,E15.8,5X,E15.8,5X,E15.8)
  800 FORMAT(10X, F10.6,5X,F10.6,5X,F10.6,5X,F10.6,5X,F15.6,5X,F15.1
      STOP
      END
```

Figure A.2.2 Listing of Program for the Calculation and Plotting of the Standardised Concentration Profile

```
      MASTER SQUIRREL
      DIMENSION A(50),B(50),C(50),D(50),E(50),F(50),G(50),H(50),WW(50
      DIMENSION YY(200),M(50),V(50),W(50),X(50),Y(50),Z(50)
      DIMENSION AA(200),XX(200),ZZ(200)
      DO 131 J=1,6
      READ(1,10) LSRATE,LFRATE,LRUNNO,LDATE,LFTIME,LSTIME
   10 FORMAT(I4,I4,I4,I6,I4,I4)
      READ(1,20) TAMB,AVPPIN,AVPPOU,AVCAIN,AVCAOU,PURROT,CARROT
   20 FORMAT(7F10.5)
   30 FORMAT(12I2)
   40 FORMAT(12F5.2)
      READ(1,30)(M(I),I=1,12)
      READ(1,40)(A(I),I=1,12)
      READ(1,40)(AA(I),I=1,12)
      READ(1,50)(B(I),I=1,12)
      READ(1,50)(C(I),I=1,12)
      READ(1,50)(D(I),I=1,12)
      READ(1,50)(E(I),I=1,12)
   50 FORMAT(10F8.1)
      VOL=0.1
      N=12
      SENS=200.0
      GA=20.0/340000.0
      GG=20.0/455000.0
      NN=128
      WRITE(2,80)
      WRITE(2,86)
   86 FORMAT(40X,'**********************************')
      WRITE(2,201) LRUNNO,LDATE
      WRITE(2,86)
  201 FORMAT(40X,'RUN NUMBER',I4,5X,'DATE',2X,I6)
      WRITE(2,70)
      WRITE(2,202) LSRATE,LFRATE,TAMB
  202 FORMAT(40X,'SWITCHING RATE',2X,I4,'FEED RATE',I4,'AMBIENT TEMP',
     12X,F4.1)
      WRITE(2,70)
      WRITE(2,203) AVPPIN
  203 FORMAT(40X,'AVERAGE PURGE PRESSURE IN',F5.2)
      WRITE(2,204) AVPPOU
  204 FORMAT(40X,'AVERAGE PURGE PRESSURE OUT',F5.2)
      WRITE(2,205) AVCAIN
  205 FORMAT(40X,'AVERAGE CARRIER PRESSURE IN',F5.2)
      WRITE(2,206) AVCAOU
  206 FORMAT(40X,'AVERAGE CARRIER PRESSURE OUT',F5.2)
      WRITE(2,207) PURROT
  207 FORMAT(40X,'PURGE ROTAMETER READING',F5.2)
      WRITE(2,208) CARROT
  208 FORMAT(40X,'CARRIER ROTAMETER READING',F5.2)
      WRITE(2,70)
      WRITE(2,70)
      WRITE(2,70)
      WRITE(2,70)
      WRITE(2,70)
      DO 100 I=1,12
      F(I)=((A(I)+14.7)/14.7)*VOL
      G(I)=((AA(I)+14.7)/14.7)*VOL
  100 CONTINUE
```

Figure A.2.2 cont'd

```
      DO 200 I=1,12
      W(I)=(B(I)*GA)/F(I)
      X(I)=(C(I)*GG)/F(I)
      Y(I)=(D(I)*GA)/G(I)
      Z(I)=(E(I)*GG)/G(I)
  200 CONTINUE
      WRITE(2,110)
      WRITE(2,111)
      DO 300 I=1,12
      WRITE(2,60) M(I),A(I),F(I),B(I),W(I),C(I),X(I)
  300 CONTINUE
      WRITE(2,80)
      WRITE(2,110)
      WRITE(2,111)
      DO 400 I=1,12
      WRITE(2,60) M(I),AA(I),G(I),D(I),Y(I),E(I),Z(I)
  400 CONTINUE
   60 FORMAT(10X,I2,5X,F5.2,5X,F6.4,5X,F8.1,5X,F6.2,5X,F8.1,5X,F6.2)
      WRITE(2,80)
   70 FORMAT(1H0)
   80 FORMAT(1H1)
      DO 500 I=1,200
      WW(I)=0.0
      XX(I)=0.0
      YY(I)=0.0
      ZZ(I)=0.0
  500 CONTINUE
      DO 600 I=1,12
      WW(I*10)=W(I)
      XX(I*10)=X(I)
      YY(I*10)=Y(I)
      ZZ(I*10)=Z(I)
  600 CONTINUE
      WRITE(2,122)
      WRITE(2,121)
      WRITE(2,122)
      CALL GRAPH3(WW,XX,XX,NN)
      CONTINUE
      WRITE(2,80)
      WRITE(2,122)
      WRITE(2,125)
      WRITE(2,122)
  110 FORMAT(11X,'BED',4X,'PRESSURE',3X,'VOLUME',6X,'ARKLONE',5X,'CO
     1',8X,'GENKLENE',6X,'CONC')
  111 FORMAT((5X,'ISOLATED',5X,'DSI',8X,'MLS',6X,'PEAK AREA',4X,'*E-
     1',6X,'PEAK AREA',4X,'*E-08'))
  122 FORMAT(40X,'**********************************************************
  121 FORMAT(40X,'CONCENTRATION PROFILE FOR ARKLONE/GENKLENE AT 100
     1')
  125 FORMAT(40X,'CONCENTRATION PROFILE FOR ARKLONE/GENKLENE AT 250
     1')
      CALL GRAPH3(YY,ZZ,ZZ,NN)
  131 CONTINUE
      CONTINUE
      STOP
      END
```

Figure A.2.3 Listing of Program for the Simulation of the SCCR1

```
      PRØGRAM PLATES2(INPUT,ØUTPUT,TAPE1=INPUT,TAPE2=ØUTPUT)
C     FØRTRAN PLATE TØ PLATE CALCULATIØN
      DIMENSIØN C(720),D(720),X(60),Y(60)
      DIMENSIØN DELT(720),TEMP(720),T(720),P(720),SVP(720)
      DIMENSIØN DDF(720),DDL(720),CCF(720),CCL(720),DELD(720),DELC(72
      DIMENSIØN PINCAR(20)
      REAL M1AP,M2AP,M3AP,M4AP,M1GP,M2GP,M3GP,M4GP,MWTAP,MWTGP,MØLVØL
      REAL ML,MS,LATGP,LATAP,LRATE,MASSF
C     READ INPUT DATA
      READ(1,3) CFLØW,SFLØW,V1,V2,CFEED,DFEED,DT
      READ(1,4) NFEED,NNBED,KTØTAL,KKINK,KKTYPE,NNTYPE
      READ(1,715) DP,VISC,DENS,VØID,AREA,CØLLEN
      READ(1,794)SS,SL,CØMPK,LATGP,LATAP
      READ(1,5)PAMB,PINC,PINP,GC
      READ(1,14)MWTAP,MWTGP,MØLVØL,TAMB
C     SET DUMMY ARRAYS EQUAL TØ ZERØ
      DØ 1 NN=1,720
      T(NN)=TAMB
      SVP(NN)=0.69E-03
    1 CØNTINUE
C     ØUTPUT DATA
      WRITE(2,22)
      WRITE(2,23)
      WRITE(2,24)
      WRITE(2,25)
      WRITE(2,25)
      WRITE(2,26)
      WRITE(2,25)
      WRITE(2,27)
      WRITE(2,25)
      WRITE(2,28)
      WRITE(2,25)
      WRITE(2,29)
      WRITE(2,25)
      WRITE(2,31)
      WRITE(2,25)
      WRITE(2,7)CFLØW,SFLØW,V1,V2
      WRITE(2,25)
      WRITE(2,8)CFEED,DFEED,DT
      WRITE(2,25)
      WRITE(2,9)NFEED,NNBED,KTØTAL,KKINK,KKTYPE,NNTYPE
      WRITE(2,25)
      WRITE(2,10)PAMB,PINC,PINP
      WRITE(2,25)
      WRITE(2,720) DP,VISC,DENS,VØID,AREA,CØLLEN
      WRITE(2,25)
      WRITE(2,19)MWTAP,MWTGP,MØLVØL,TAMB
      WRITE(2,25)
      WRITE(2,1095) SS,SL,CØMPK,LATGP,LATGP
      WRITE(2,25)
      WRITE(2,22)
C     DEFINE PRØGRAM PARAMETERS
      XX=1.0
      GØ TØ 466
  467 XX=XX+1.0
  466 CØNTINUE
      DØ 937 NN=1,720
```

Figure A.2.3 cont'd

```
      C(NN)=0.0
      D(NN)=0.0
      P(NN)=0.0
  937 CONTINUE
      DO 2 NN=1,60
      X(NN)=0.0
      Y(NN)=0.0
    2 CONTINUE
      M1AP=0.0
      M2AP=0.0
      M1GP=0.0
      M2GP=0.0
      MOLVOL=MOLVOL*(TAMB/273.2)*(101./PAMB)
      NNTOT=NNBED*12
      NNELEV=NNBED*11+1
      NNFEED=NFEED*NNBED+1
      NNBED1=NNBED+1
      KKKK=(KTOTAL*KKINK)-(KKINK-1)
      KKK=KTOTAL*KKINK-1
      PINCAR(1)=PINC
C     START PRESSURE DROP CALCULATIONS
      DELP1=20.0
      DO 712 I=1,11
      MASSF=DENS*CFLOW
  711 PMEAN=PINCAR(I)-(DELP1/2.0)
      VEL=(CFLOW*PAMB)/(AREA*PMEAN)
      A1=150.0*((1-VOID)**2)*VISC*VEL/((VOID**3)*(DP**2))
      A2=1.75*(1-VOID)*MASSF*VEL/((VOID**3)*DP)
      DELP=(A1+A2)*COLLEN/(GC*10000.0)
      IF(ABS(DELP1-DELP).LE.0.1)GO TO 710
      DELP1=DELP
      GO TO 711
  710 CONTINUE
      PINCAR(I+1)=PINCAR(I)-DELP
  712 CONTINUE
      PINPUR=PINP
      DELP1=20.0
      MASSF=DENS*CFLOW
  714 PMEAN=PINPUR-DELP1/2.0
      VEL=(SFLOW*PAMB)/(AREA*PMEAN)
      A1=150.0*((1-VOID)**2)*VISC*VEL/((VOID**3)*(DP**2))
      A2=1.75*(1-VOID)*MASSF*VEL/((VOID**3)*DP)
      DELP=(A1+A2)*COLLEN/(GC*10000.0)
      IF(ABS(DELP1-DELP).LE.0.5) GO TO 716
      DELP1=DELP
      GO TO 714
  716 CONTINUE
      POPUR=PINPUR-DELP
      NNBED2=NNBED*2+1
      NNBED3=NNBED*3+1
      NNBED4=NNBED*4+1
      NNBED5=NNBED*5+1
      NNBED6=NNBED*6+1
      NNBED7=NNBED*7+1
      NNBED8=NNBED*8+1
      NNBED9=NNBED*9+1
      NNBTEN=NNBED*10+1
```

Figure A.2.3 cont'd

```
      NDUM1=NNBED*2
      NDUM2=NNBED*3
      NDUM3=NNBED*4
      NDUM4=NNBED*5
      NDUM5=NNBED*6
      NDUM6=NNBED*7
      NDUM7=NNBED*8
      NDUM8=NNBED*9
      NDUM9=NNBED*10
      NDUM10=NNBED*11
      NDUM11=NNBED*12
      DØ 210 NN=NNBED1,NDUM1
      P(NN)=(PINCAR(1)-(((PINCAR(1)-PINCAR(2))/(NNBED))*(NN-NNBED)))
     1/PAMB
  210 CØNTINUE
      DØ 220 NN=NNBED2,NDUM2
      P(NN)=(PINCAR(2)-(((PINCAR(2)-PINCAR(3))/(NNBED))*(NN-NDUM1)))
     1/PAMB
  220 CØNTINUE
      DØ 230 NN=NNBED3,NDUM3
      P(NN)=(PINCAR(3)-(((PINCAR(3)-PINCAR(4))/(NNBED))*(NN-NDUM2)))
     1/PAMB
  230 CØNTINUE
      DØ 240 NN=NNBED4,NDUM4
      P(NN)=(PINCAR(4)-(((PINCAR(4)-PINCAR(5))/(NNBED))*(NN-NDUM3)))
     1/PAMB
  240 CØNTINUE
      DØ 250 NN=NNDED5,NDUM5
      P(NN)=(PINCAR(5)-(((PINCAR(5)-PINCAR(6))/(NNBED))*(NN-NDUM4)))
     1/PAMB
  250 CØNTINUE
      DØ 260 NN=NNBED6,NDUM6
      P(NN)=(PINCAR(6)-(((PINCAR(6)-PINCAR(7))/(NNBED))*(NN-NDUM5)))
     1/PAMB
  260 CØNTINUE
      DØ 270 NN=NNBED7,NDUM7
      P(NN)=(PINCAR(7)-(((PINCAR(7)-PINCAR(8))/(NNBED))*(NN-NDUM6)))
     1/PAMB
  270 CØNTINUE
      DØ 280 NN=NNBED8,NDUM8
      P(NN)=(PINCAR(8)-(((PINCAR(8)-PINCAR(9))/(NNBED))*(NN-NDUM7)))
     1/PAMB
  280 CØNTINUE
      DØ 290 NN=NNBED9,NDUM9
      P(NN)=(PINCAR(9)-(((PINCAR(9)-PINCAR(10))/(NNBED))*(NN-NDUM8)))
     1/PAMB
  290 CØNTINUE
      DØ 310 NN=NNBTEN,NDUM10
      P(NN)=(PINCAR(10)-(((PINCAR(10)-PINCAR(11))/(NNBED))*(NN-NDUM9)))
     1/PAMB
  310 CØNTINUE
      DØ 320 NN=NNELEV,NDUM11
      P(NN)=(PINCAR(11)-(((PINCAR(11)-PINCAR(12))/(NNBED))*(NN-NDUM10)))
     1/PAMB
  320 CØNTINUE
      DØ 330 NN=1,NNBED
      P(NN)=(PINPUR-(((PINPUR-PØPUR)/(NNBED))*(NN)))/PAMB
```

Figure A.2.3 cont'd

```
  330 CØNTINUE
      WRITE(2,12)
      KKSUM=1
C     START SCCR1 SIMULATIØN
C     SWITCHING LØØP
      DØ 100 K=1,KTØTAL
      ISTKK=KKINK*(K-1)+1
      LSTKK=KKINK*K
C     DT LØØP,DT SET AT 1 SECØND,CØNCS ASSUMED CØNSTANT ØVER DT
      DØ 200 KK=ISTKK,LSTKK
      NNSUM=1
C     N LØØP, FØR TØTAL NUMBER ØF CØLUMNS USED
      DØ 300 N=1,12
      IF(N.LE.(NFEED-K)) GØ TØ 500
      NNFST=NNBED*(N-1)+1
      NNLST=NNBED*N
C     NN LØØP FØR TØTAL NUMBER ØF PLATES IN UNIT
      DØ 400 NN=NNFST,NNLST
      IF((T(NN).LE.300.0).AND.(T(NN).GE.294.0))GØ TØ 461
      IF((T(NN).LE.294.0).AND.(T(NN).GE.292.0))GØ TØ 462
      IF((T(NN).LE.292.0).AND.(T(NN).GE.290.0))GØ TØ 463
      IF(T(NN).LE.290.0)GØ TØ 464
  461 M3AP=0.3385E05
      M4AP=0.1305E03
      M3GP=0.3089E06
      M4GP=0.3874E03
      GØ TØ 465
  462 M3AP=0.4192E05
      M4AP=0.1405E03
      M3GP=0.3633E06
      M4GP=0.4200E03
      GØ TØ 465
  463 M3AP=0.4890E05
      M4AP=0.1517E03
      M3GP=0.4281E06
      M4GP=0.4560E03
      GØ TØ 465
  464 M3AP=0.5716E05
      M4AP=0.1640E03
      M3GP=0.5058E06
      M4GP=0.4956E03
  465 CØNTINUE
      IF(N.EQ.1)GØ TØ 80
      IF((N.EQ.2).AND.(NN.EQ.NNFST)) GØ TØ 40
      IF(NN.EQ.NNFEED)GØ TØ 50
      CCØN=C(NN-1)
      DCØN=D(NN-1)
      CINPUT=0.0
      DINPUT=0.0
      GØ TØ 60
   40 C(NN-1)=0.0
      D(NN-1)=0.0
      CCØN=C(NN)
      DCØN=D(NN)
      GØ TØ 70
   50 CINPUT=CFEED
      DINPUT=DFEED
```

Figure A.2.3 cont'd

```
      CC0N=CINPUT+C(NN-1)
      DC0N=DINPUT+D(NN-1)
   60 IF(C(NN-1).LT.0.1E-10)C(NN-1)=0.0
      IF(D(NN-1).LT.0.1E-10)D(NN-1)=0.0
   70 CC0L=CC0N*P(NN)
      DC0L=DC0N*P(NN)
      IF(DC0L.GE.SVP(NN))DC0L=SVP(NN)
      CFL0WC=CFL0W*(1.+M0LV0L*(CC0N/MWTAP+DC0N/MWTGP))
      A=CFL0WC*DT/P(NN)
      LRATE=4676.0/(12.0*KKINK)
      ZZ=A/LRATE
      AA=EXP(-A/(V1+V2*(((M1AP*CC0L+M2AP)*CC0L+M3AP)*CC0L+M4AP)))
      GG=EXP(-A/(V1+V2*(((M1GP*DC0L+M2GP)*DC0L+M3GP)*DC0L+M4GP)))
      WW=(((M1AP*CC0L+M2AP)*CC0L+M3AP)*CC0L+M4AP)
      RR=(((M1GP*DC0L+M2GP)*DC0L+M3GP)*DC0L+M4GP)
      C(NN)=(1.-AA)*(C(NN-1)+CINPUT)+AA*C(NN)
      D(NN)=(1.-GG)*(D(NN-1)+DINPUT)+GG*D(NN)
      GO TO 150
   80 IF(NN.EQ.NNFST)GO TO 90
      IF(C(NN-1).LT.0.1E-10)C(NN-1)=0.0
      IF(D(NN-1).LT.0.1E-10)D(NN-1)=0.0
      CC0N=C(NN-1)
      DC0N=D(NN-1)
      GO TO 95
   90 C(NN-1)=0.0
      D(NN-1)=0.0
      CC0N=C(NN)
      DC0N=D(NN)
   95 CC0L=CC0N*P(NN)
      DC0L=DC0N*P(NN)
      IF(DC0L.GE.SVP(NN))DC0L=SVP(NN)
      SFL0WC=SFL0W*(1.+M0LV0L*(CC0N/MWTAP+DC0N/MWTGP))
      A=SFL0WC*DT/P(NN)
      LRATE=4676.0/(12.0*KKINK)
      ZZ=A/LRATE
      AA=EXP(-A/(V1+V2*(((M1AP*CC0L+M2AP)*CC0L+M3AP)*CC0L+M4AP)))
      GG=EXP(-A/(V1+V2*(((M1GP*DC0L+M2GP)*DC0L+M3GP)*DC0L+M4GP)))
      WW=(((M1AP*CC0L+M2AP)*CC0L+M3AP)*CC0L+M4AP)
      RR=(((M1GP*DC0L+M2GP)*DC0L+M3GP)*DC0L+M4GP)
      C(NN)=(1.-AA)*C(NN-1)+AA*C(NN)
      D(NN)=(1.-GG)*D(NN-1)+GG*D(NN)
  150 IF((NN.EQ.(NNTYPE*NNSUM)).AND.(KK.EQ.(KKTYPE*KKSUM)))GO TO 160
      GO TO 170
  160 WRITE(2,161)K,KK,N,NN,C(NN),D(NN),WW,RR,ZZ
  170 IF(NN.EQ.(NNTYPE*NNSUM))NNSUM=NNSUM+1
  400 CONTINUE
      GO TO 300
  500 NNSUM=NNSUM+NNBED/NNTYPE
  300 CONTINUE
      IF(KK.EQ.(KKTYPE*KKSUM)) GO TO 180
      GO TO 212
  180 KKSUM=KKSUM+1
      WRITE(2,185)
      GO TO 200
  212 CONTINUE
      IF(KK.NE.KKKK) GO TO 778
      DO 779 I=1,NNTOT
```

Figure A.2.3 cont'd

```
      CCF(I)=C(I)
      DDF(I)=D(I)
  779 CØNTINUE
  778 CØNTINUE
      IF(KK.NE.KKK) GØ TØ 200
      DØ 781 I=1,NNTØT
      CCL(I)=C(I)
      DDL(I)=D(I)
  781 CØNTINUE
  200 CØNTINUE
      WRITE(2,190)
      WRITE(2,195)
C     SIMULATIØN ØF SØLENØID SWITCHING SEQUENCE
      DØ 1500 NN=1,NNBED
      X(NN)=C(NN)
      Y(NN)=D(NN)
 1500 CØNTINUE
      DØ 2000 NN=1,NNTØT
      IF(NN.GE.NNELEV)GØ TØ 2010
      NNADJ=NN+NNBED
      C(NN)=C(NNADJ)
      D(NN)=D(NNADJ)
      GØ TØ 2000
 2010 NNADJ=NN+1-NNELEV
      C(NN)=X(NNADJ)
      D(NN)=Y(NNADJ)
 2000 CØNTINUE
  100 CØNTINUE
      WRITE(2,25)
      WRITE(2,25)
C     TEMPERATURE CALCULATIØN
      DØ 803 I=1,NNTØT
      DELC(I)=CCL(I)-CCF(I)
      DELD(I)=DDL(I)-DDF(I)
  803 CØNTINUE
      WRITE(2,25)
      WRITE(2,804)(DELC(I),I=1,NNTØT)
      WRITE(2,25)
      WRITE(2,804)(DELD(I),I=1,NNTØT)
      ML=4535.4/(NNBED*12)
      MS=14805.0/(NNBED*12)
      SURAR=1456.6/NNBED
      HTCP=(MS*SS)+(ML*SL)
      XXXX=KKINK
      HTLØSS=CØMPK*SURAR*XXXX
      DØ 901 I=1,NNTØT
      DELT(I)=((LATAP*125.6*V2*DELC(I))+(LATGP*372.0*DELD(I)*V2))/(HTC
     1+HTLØSS)
      T(I)=TAMB+DELT(I)
      IF(T(I).GE.294.0)SVP(I)=0.75E-03
      IF((T(I).LE.294.0).AND.(T(I).GE.292.0))SVP(I)=0.69E-03
      IF((T(I).LE.292.0).AND.(T(I).GE.290.0))SVP(I)=0.64E-03
      IF(T(I).LE.290.0)SVP(I)=0.586E-03
  901 CØNTINUE
      WRITE(2,902)(T(I),I=1,NNTØT)
  902 FØRMAT (10X,F10.5,10X,F10.5,10X,F10.5,10X,F10.5)
      IF(XX.EQ.2.0)GØ TØ 468
```

Figure A.2.3 cont'd

```
      GØ TØ 467
  468 CØNTINUE
    3 FØRMAT(7F10.0)
    4 FØRMAT(6I4)
    5 FØRMAT(4F10.0)
    6 FØRMAT(4E13.5)
    7 FØRMAT(1H ,7HCFLØW= ,F8.3,4X,7HSFLØW= ,F8.3,4X,4HV1= ,F10.5,
     14X,4HV2= ,F10.5)
    8 FØRMAT(1H ,7HCFEED= ,E13.6,4X,7HDFEED= ,E13.6,4X,4HDT= ,F10.5)
    9 FØRMAT(1H ,7HNFEED= ,I2,1X,7HNNBED= ,I3,1X,8HKTØTAL= ,I3,
     11X,7HKKINK= ,I4,1X,8HKKTYPE= ,I3,1X,8HNNTYPE= ,I3)
   10 FØRMAT(1H ,6HPAMB= ,F6.1,1X,6HPINC= ,F6.1,1X,6HPINP= ,F6.1)
   11 FØRMAT(1H ,6HM1AP= ,E13.6,10X,6HM1GP= ,E13.6)
   12 FØRMAT(1H ,2H K,5X,5H  KK ,5X,3H N ,5X,5H  NN ,5X,
     114H     C(NN)    ,5X,14H     D(NN)    )
   14 FØRMAT(4F10.0)
   15 FØRMAT(4E13.6)
   16 FØRMAT(1H ,6HM2AP= ,E13.6,10X,6HM2GP= ,E13.6)
   17 FØRMAT(1H ,6HM3AP= ,E13.6,10X,6HM3GP= ,E13.6)
   18 FØRMAT(1H ,6HM4AP= ,E13.6,10X,6HM4GP= ,E13.6)
   19 FØRMAT(1H ,7HMWTAP= ,F6.2,2X,8HMWTGP=  ,F6.2,2X,8HMØLVØL= ,
     1 F6.0,2X,6HTAMB= ,F5.1)
   21 FØRMAT(20X,E13.6,10X,E13.6,10X,E13.6,10X,E13.6)
   22 FØRMAT(1H1)
   23 FØRMAT(10X,' SCCR1 CØMPUTER SIMULATIØN ')
   24 FØRMAT(10X,' ************************** ')
   25 FØRMAT(1HO)
   26 FØRMAT(10X,'RUN NUMBER15A,PRØDUCED ØN 16/4/77,NEW CØNDITIØNS FØR
     1AP/GP AT APPRØX G/L=260  AMB TEMP SET AT 20.0 DEG C')
   27 FØRMAT(10X,'SYSTEM ARKLØNE P /GENKLENE P')
   28 FØRMAT(10X,'FEED RATE=1000MLS/HR')
C     FURTHER INFØRMATIØN REGARDING THIS MØDEL MAY BE ØBTAINED FRØM TH
C     AUTHØR AT 1 THE HEADLANDS DARLINGTØN C0.DURHAM
   29 FØRMAT(10X,'CARRIER GAS =20.7CM AT 45.0PSI')
   31 FØRMAT(1X,'INPUT DATA ')
  161 FØRMAT(1H ,I2,5X,I5,5X,I3,5X,I5,5X,E14.6,5X,E14.6,
     15X,F10.4,5X,F10.4,5X,F10.4)
  185 FØRMAT(1H ,32HNEXT TIME INTERVAL FØR PRINT ØUT)
  190 FØRMAT(1H ,23HNEXT SWITCHING INTERVAL)
  195 FØRMAT(1H ,2H K,5X,5H  KK ,5X,3H N ,5X,5H  NN ,5X,
     114H     C(NN)    ,5X,14H     D(NN)    )
  715 FØRMAT(6F10.0)
  794 FØRMAT(5F10.0)
  720 FØRMAT(1H ,4HDP= ,E11.4,3X,6HVISC= ,E11.4,3X,6HDENS= ,E11.4,
     13X,6HVØID= ,E11.4,3X,6HAREA= ,F10.4,3X,8HC0LLEN= ,F8.4)
  777 FØRMAT(10X,E15.6,10X,E15.6)
  804 FØRMAT(10X,E15.6,10X,E15.6,10X,E15.6,10X,E15.6)
 1095 FØRMAT(1H ,4HSS= ,F10.4,4HSL= ,F10.4,7HC0MPK= ,F10.6,7HLATAP= ,
     1F10.4,7HLATGP= ,F10.4)
      END
```

Figure A.2.4 Example of SCCR1 Simulation Output

NEXT TIME INTERVAL FØR PRINT ØUT
NEXT SWITCHING INTERVAL

K	KK	N	NN	C(NN)	D(NN)	k(AP)	k(GP)
22	5568	1	20	0.	.778082E-06	151.7000	456.4066
22	5568	1	40	0.	.288990E-04	140.5000	556.2007
22	5568	2	60	0.	.174507E-03	140.5000	670.6770
22	5568	2	80	0.	.171454E-03	140.5000	665.9752
22	5568	3	100	0.	.174326E-03	140.5000	665.6060
22	5568	3	120	0.	.177642E-03	140.5000	663.4183
22	5568	4	140	0.	.171849E-03	140.5000	649.4272
22	5568	4	160	0.	.167710E-03	140.5000	641.3609
22	5568	5	180	0.	.177245E-03	140.5000	649.5503
22	5568	5	200	0.	.186241E-03	140.5000	651.9211
22	5568	6	220	0.	.175542E-03	140.5000	627.4082
22	5568	6	240	0.	.142624E-03	130.5000	536.9513
22	5568	7	260	.448468E-04	.154036E-03	145.0356	605.6735
22	5568	7	280	.179349E-03	.181922E-04	163.5621	444.9857
22	5568	8	300	.423194E-03	.293714E-06	194.5153	420.6416
22	5568	8	320	.401773E-03	0.	189.4809	420.0000
22	5568	9	340	.396830E-03	0.	187.3264	420.0000
22	5568	9	360	.398854E-03	0.	185.9087	420.0000
22	5568	10	380	.398244E-03	0.	184.0271	420.0000
22	5568	10	400	.398478E-03	0.	182.2569	420.0000
22	5568	11	420	.398328E-03	0.	180.2674	420.0000
22	5568	11	440	.398451E-03	0.	178.3079	420.0000
22	5568	12	460	.395787E-03	0.	159.1307	387.4000
22	5568	12	480	.187127E-03	.900340E-13	144.2513	387.4000
NEXT TIME INTERVAL FØR PRINT ØUT							
22	5655	1	20	0.	0.	151.7000	456.0000
22	5655	1	40	0.	.866347E-06	140.5000	423.2940
22	5655	2	60	0.	.173041E-03	140.5000	670.6770
22	5655	2	80	0.	.172455E-03	140.5000	667.8637
22	5655	3	100	0.	.176141E-03	140.5000	667.5408
22	5655	3	120	0.	.174916E-03	140.5000	659.1788

Figure A.2.5 Variable Parameters in SCCR1 Model

LØCAL VARIABLES IN PRØGRAM PLATES2

NAME	TYPE	CURRENT VALUE	
C	REAL	ARRAY (720)	STANDARDISED CONC
D	REAL	ARRAY (720)	" "
X	REAL	ARRAY (60)	DUMMY VARIABLE
Y	REAL	ARRAY (60)	" "
DELT	REAL	ARRAY (720)	ΔT OVER PLATE
T	REAL	ARRAY (720)	ABSOLUTE ~~TEMP~~
P	REAL	ARRAY (720)	ABSOLUTE PRESSURE
SVP	REAL	ARRAY (720)	SAT' VAP' "
DDF	REAL	ARRAY (720)	STD' CONC
DDL	REAL	ARRAY (720)	" "
CCF	REAL	ARRAY (720)	" "
CCL	REAL	ARRAY (720)	" "
DELD	REAL	ARRAY (720)	" "
DELC	REAL	ARRAY (720)	" "
PINCAR	REAL	ARRAY (20)	CARRIER INLET PRESSU
M1AP	REAL	0.	K VALUE COEFFICIENTS
M2AP	REAL	0.	" "
M3AP	REAL	41920.0000000	" "
M4AP	REAL	140.500000000	" "
M1GP	REAL	0.	" "
M2GP	REAL	0.	" "
M3GP	REAL	363300.000000	" "
M4GP	REAL	420.000000000	" "
MWTAP	REAL	187.400000000	MOLECULAR WEIGHT
MWTGP	REAL	133.400000000	" "
MØLVØL	REAL	25647.9448865	" VOLUME
ML	REAL	9.44875000000	WT LIQUID PHASE
MS	REAL	30.8437500000	WT PACKING
LATGP	REAL	56.8000000000	LATENT HEAT
LATAP	REAL	38.0200000000	" "
LRATE	REAL	1.49297573436	L'
CFLØW	REAL	1150.00000000	CARRIER GAS FLOWRATE
SFLØW	REAL	2300.00000000	PURGE " "
V1	REAL	47.9000000000	PLATE VOLUME
V2	REAL	9.90400000000	" "
CFEED	REAL	.206760000000E-03	FEED CONCENTRATION
DFEED	REAL	.175340000000E-03	" "
DT	REAL	1.00000000000	TIME INCREMENT
NFEED	INTEGER	7	FEED BED
NNBED	INTEGER	40	N° PLATES/BED
KTØTAL	INTEGER	24	TOTAL N° SEQUENCES
KKINK	INTEGER	261	SEQUENCING INTERVAL
KKTYPE	INTEGER	87	PRINTING INTERVAL
NNTYPE	INTEGER	20	PLATE PRINT "
DP	REAL	.149000000000E-03	PARTICLE DIAM
VISC	REAL	.182000000000E-03	GAS VISCOSITY
DENS	REAL	.122500000000E-02	" DENSITY
VØID	REAL	.693000000000	VOIDAGE
AREA	REAL	45.6100000000	PLATE AREA
CØLLEN	REAL	61.0000000000	COLUMN LENGTH
SS	REAL	.200000000000	SPECIFIC HEAT
SL	REAL	.200000000000	" "

Figure A.2.5 cont'd

CØMPK	REAL	.370000000000E-03	THERMAL CONDUCTIVITY
PAMB	REAL	101.330000000	AMBIENT PRESSURE
PINC	REAL	410.000000000	CARRIER "
PINP	REAL	273.700000000	PURGE "
GC	REAL	981.000000000	GAS CONSTANT
TAMB	REAL	293.200000000	AMBIENT TEMPERATURE
NN	INTEGER	327	COUNTER
XX	REAL	2.00000000000	CONSTANT
NNTØT	INTEGER	480	TOTAL N° PLATES
NNELEV	INTEGER	441	LAST BED, 1ST PLATE
NNFEED	INTEGER	281	FEED PLATE
NNBED1	INTEGER	41	SEP' SECT' " "
KKKK	INTEGER	6004	COUNTER
KKK	INTEGER	6263	"
DELP1	REAL	45.2607773085	ΔP IN PURGE BED
I	INTEGER	12	COUNTER
MASSF	INTEGER	1	MASS FLOWRATE
PMEAN	REAL	251.069611346	MEAN PRESSURE
VEL	REAL	20.3522137943	GAS VELOCITY
A1	REAL	7087267.31233	DUMMY
A2	REAL	220496.707078	"
DELP	REAL	45.4407344734	CØRRECTED ΔP
PINPUR	REAL	273.700000000	PURGE PRESSURE IN
PØPUR	REAL	228.259265527	" " ØUT
NNBED2	INTEGER	81	1ST PLATE IN BED
NNBED3	INTEGER	121	" " "
NNBED4	INTEGER	161	" " "
NNBED5	INTEGER	201	" " "
NNBED6	INTEGER	241	" " "
NNBED7	INTEGER	281	" " "
NNBED8	INTEGER	321	" " "
NNBED9	INTEGER	361	" " "
NNBTEN	INTEGER	401	" " "
NDUM1	INTEGER	80	LAST " "
NDUM2	INTEGER	120	" " "
NDUM3	INTEGER	160	" " "
NDUM4	INTEGER	200	" " "
NDUM5	INTEGER	240	" " "
NDUM6	INTEGER	280	" " "
NDUM7	INTEGER	320	" " "
NDUM8	INTEGER	360	" " "
NDUM9	INTEGER	400	" " "
NDUM10	INTEGER	440	" " "
NDUM11	INTEGER	480	" " "
KKSUM	INTEGER	62	COUNTER
K	INTEGER	21	"
ISTKK	INTEGER	5221	"
LSTKK	INTEGER	5481	"
KK	INTEGER	5370	"
NNSUM	INTEGER	17	"
N	INTEGER	9	"
NNFST	INTEGER	321	"
NNLST	INTEGER	360	"
CCØN	REAL	.546837573887E-03	PLATE CONC'
DCØN	REAL	.528313701808E-04	
CINPUT	REAL	0.	PLATE N FEED CONC'
DINPUT	REAL	0.	" " "

Figure A.2.5 cont'd

CCØL	REAL	.158431337665E-02	ON-COLUMN CONC'.
DCØL	REAL	.153064548746E-03	" " "
CFLØWC	REAL	1247.74867009	CORRECTED FLOWRATE
A	REAL	430.669756140	DUMMY
ZZ	REAL	288.464002616	$G_{m.c}$ /L'
AA	REAL	.814708136245	DUMMY
GG	REAL	.913733571539	"
WW	REAL	207.026772654	K ARKLONE.P
RR	REAL	476.408813225	K GENKLENE.P
SFLØWC	REAL	2317.25651480	PURGE FLOWRATE
NNADJ	INTEGER	40	DUMMY
SURAR	REAL	36.4150000000	SURFACE AREA
HTCP	REAL	8.05850000000	HEAT CAPACITY
HTLØSS	REAL	3.41210000000	" LOSS

TRACE BACK TRAIL ENDS IN PRØGRAM PLATES2

Appendix .3

Figure A.3.1 K Value Coefficients for Arklone.P

$K = A + B(\text{concentration})^2$

Temperature	Vapour Pressure	A	B
°C	millibar		
283.2	236.5	208.7	92578.5
284.2	247.2	200.4	85303.1
285.2	258.4	192.4	78646.5
286.2	269.9	184.8	72552.3
287.2	281.9	177.6	66969.6
288.2	294.4	170.6	61852.3
289.2	307.3	164.0	57158.8
290.2	320.7	157.7	52851.5
291.2	334.6	151.7	48896.2
292.2	348.9	146.0	45262.0
293.2	363.8	140.5	41921.1
294.2	379.2	135.5	36508.8
295.2	395.2	130.5	33850.6
296.2	411.7	125.6	31402.7
297.2	428.7	121.1	29147.2
298.2	446.4	116.7	27067.8
299.2	464.6	112.4	25149.7
300.2	483.5	108.4	23379.6
301.2	503.1	104.6	21745.1
302.2	523.3	100.9	20234.9

Figure A.3.2 K Value Coefficients for Genklene.P

$K = A + B(conc)^2$

Temperature	Vapour Pressure	A	B
°C	millibar		
283.2	87.5	641.1	846344
284.2	91.8	613.7	775537
285.2	96.2	587.7	711107
286.2	100.7	562.9	652441
287.2	105.5	539.4	598990
288.2	110.5	516.9	550250
289.2	115.6	495.6	505795
290.2	121.0	475.3	465210
291.2	126.6	456.0	428135
292.2	132.3	437.6	394250
293.2	138.4	420.0	363258
294.2	144.6	403.3	334897
295.2	151.1	387.4	308928
296.2	157.7	372.1	285134
297.2	164.7	357.6	263321
298.2	171.9	343.8	243312
299.2	179.4	330.4	224947
300.2	187.2	317.9	208082
301.2	195.2	305.8	192585
302.2	203.5	294.3	178337

Figure A.3.3 K Value Coefficients for Dichloromethane

$K = A + B(conc)^2$

Temperature	Vapour Pressure	A	B
°C	millibar		
283.2	296.4	194.7	117383
284.2	310.7	186.4	107532
285.2	325.7	178.4	98569.9
286.2	341.2	170.9	90412.1
287.2	357.5	163.7	82981.3
288.2	374.3	156.9	76208.4
289.2	391.8	150.4	70031.2
290.2	410.0	144.2	64393.7
291.2	428.9	138.3	59245.7
292.2	448.6	132.7	54541.5
293.2	469.0	127.4	50240.4
294.2	490.1	122.3	46305.4
295.2	512.1	117.5	42703.2
296.2	535.0	112.8	39403.6
297.2	558.7	108.4	36379.4
298.2	583.2	104.2	33606.2
299.2	608.6	100.2	31061.5
300.2	635.0	96.3	28725.2
301.2	662.4	92.7	26579.0
302.2	690.7	89.2	24606.4

Appendix . 4

Figure A.4.1 Calculation of G_{mc}/L (Run 300-275-400-A

$$j = \frac{3}{2}\frac{(P_{io})^2 - 1}{(P_{io})^3 - 1} = \frac{3}{2}\frac{(\frac{378}{186})^2 - 1}{(\frac{378}{186})^3 - 1} = 0.635$$

$$G_{mc} = G_a \times j \times \frac{P_a}{P_o} = 875 \times 0.635 \times \frac{101}{186} = 301.7 \text{ cm}^3 \text{ s}^{-1}$$

$$L' = \frac{\text{Total volume of solvent in columns}}{\text{Time for 1 cycle}}$$

$$= \frac{5090}{12 \times I_s}$$

I_s = Sequencing interval

$$L' = \frac{5090}{12 \times 399} \quad 1.063 \text{ cm}^3 \text{ s}^{-1}$$

$$\frac{G_{mc}}{L'} = \frac{301.7}{1.063} = 284$$

Figure A.4.2 Calculation of Partial Pressure of Genklene.P

As an example, use results from run 800-265-262-A

For an ideal gas $P_i = P_{col} \times y_i$

and substituting for y_i from equation 5.17,

$$P_i = \frac{P_{col} \times C_{i(std)} \times R_g \times T}{M_i \times P_{std}}$$

From run 800-265-262-A the maximum value of $C_{G.P.(std)} = 0.097 g\, cm^{-3}$ (Appendix 5), at a pressure of 379 kN m^{-2}, and minimum temperature of 8°C

Hence $$P_i = \frac{379 \times 0.097 \times 10^{-3} \times 0.896 \times 10^{4} \times 281.2}{133.4 \times 101.1}$$

$$= 6.868 \text{ kN } m^{-2}$$

The saturated vapour pressure of Genklene.P at 8°C = 7.14 kN. m^{-2} (reference 190), and therefore the gas phase was very close to being saturated with Genklene.P

Figure A.4.3 Calculation of Liquid Phase Loading

Weight of packing in analytical column = 9.828 g

Column temperature = 60.5 °C

Ambient temperature = 22.5 °C

Column inlet pressure = 180.1 $kN.m^{-2}$

Column outlet pressure (ambient) = 101.1 $kN\ m^{-2}$

Flowrate (F) of carrier gas = 116.5 $cm^3\ min^{-1}$

Retention time for methane (unretained) = 11.5 s

Retention time for Arklone.P = 72.0 s

$K^{\infty}_{A.P}$ at 60.5 °C = 40.79

j = 0.700

$$V_l = F \times \frac{T_c}{T_a} \times \frac{P_o}{P_a} \times j \times (t_r - t_m) / K$$

$$= 116.5 \times \frac{333.7}{295.7} \times 1.0 \times 0.7 \times \left(\frac{72.0 - 11.5}{60}\right) \times \frac{1}{40.79}$$

$$= 2.275\ cm^3$$

$\therefore$ Weight of liquid phase $= V_l \times \rho = 2.207$ g

and % liquid loading $= \frac{2.207}{9.828} \quad \underline{22.45}$

Appendix . 5

Figure A.5.1 Concentration Profile Results Run 300-265-400-

Distance from Carrier Gas Inlet	Time after Sequenc	Sample Point Pressure	Peak Area		Column Concentration		Standardised Concentration	
			A.P	G.P	A.P	G.P	A.P	G.P
cm	s	$kN\,m^{-2}$			10^{-3} g cm^{-3}		10^{-3} g cm^{-3}	
717	100	207	2243	38080	0.002	0.014	0.001	0.007
717	300	204	1022	1471	0	0	0	0
656	100	193	145700	715	0.082	0	0.043	0
656	300	197	222300	1233	0.128	0	0.066	0
595	100	211	225200	1579	0.127	0	0.061	0
595	300	211	315000	1323	0.179	0	0.086	0
534	100	232	265000	2302	0.151	0	0.066	0
534	300	239	261200	1350	0.153	0	0.065	0
473	100	245	287300	2603	0.162	0	0.067	0
473	300	259	286700	224	0.164	0	0.064	0
412	100	266	288600	828	0.163	0	0.062	0
412	300	273	273000	1133	0.156	0	0.058	0
351	100	290	297300	18360	0.166	0.006	0.058	0.002
351	300	290	258300	144100	0.143	0.048	0.050	0.017
290	100	304	195800	334000	0.111	0.114	0.037	0.038
290	300	307	8780	365100	0.006	0.127	0.002	0.042
229	100	321	3130	480100	0.003	0.165	0.001	0.052
229	300	321	1403	351400	0.001	0.120	0	0.038
168	100	338	2729	567400	0.002	0.197	0	0.059
168	300	338	1121	592500	0.001	0.207	0	0.062
107	100	359	371	520000	0	0.181	0	0.051
107	300	359	714	514600	0	0.182	0	0.051
46	100	376	1400	311900	0	0.107	0	0.029
46	300	376	7100	439500	0.004	0.152	0.001	0.041

Figure A.5.2 Concentration Profile Results for Run 300-265-300-A

Distance from Carrier Gas Inlet	Time after Sequence	Sample Point Pressure	Peak Area		Column Concentration		Standardised Concentration	
			A.P	G.P	A.P	G.P	A.P	G.P
cm	s	$kN\,m^{-2}$			10^{-3} g cm^{-3}		10 g cm^{-3}	
717	100	233	< 100	5824	0	0.032	0	0.014
717	250	233	< 100	769	0	0.004	0	0.002
656	100	190	15150	987	0.139	0.004	0.074	0.002
656	250	197	17880	171	0.163	0	0.084	0
595	100	214	19140	< 100	0.175	0	0.083	0
595	250	214	21430	< 100	0.197	0	0.093	0
534	100	238	23160	< 100	0.212	0	0.090	0
534	250	238	24750	< 100	0.226	0	0.096	0
473	100	262	23090	< 100	0.212	0	0.082	0
473	250	262	21890	< 100	0.199	0	0.077	0
412	100	287	24680	< 100	0.227	0	0.080	0
412	250	287	32910	< 100	0.304	0	0.107	0
351	100	307	29130	177	0.267	0	0.088	0
351	250	307	20990	1005	0.191	0.006	0.063	0.002
290	100	324	5608	4231	0.051	0.022	0.016	0.007
290	250	328	1192	14140	0.010	0.074	0.003	0.023
229	100	341	992	13600	0.010	0.070	0.003	0.021
229	250	341	164	28560	0	0.155	0	0.046
168	100	362	< 100	32860	0	0.175	0	0.049
168	250	362	< 100	31810	0	0.172	0	0.048
107	100	383	< 100	22520	0	0.121	0	0.032
107	250	383	< 100	20740	0	0.113	0	0.030
46	100	396	< 100	32020	0	0.172	0	0.044
46	250	403	< 100	30510	0	0.163	0	0.041

Figure A.5.3 Concentration Profile Results Run 300-265-250-A

Distance from Carrier Gas Inlet	Time after Sequence	Sample Point Pressure	Peak Area		Column Concentration		Standardised Concentration	
			A.P	G.P	A.P	G.P	A.P	G.P
cm	s	kNm^{-2}			10^{-3} g cm^{-3}		10^{-3} g cm^{-3}	
717	50	225	<100	16700	0	0.089	0	0.040
717	200	225	<100	<100	0	0	0	0
656	50	156	9612	<100	0.090	0	0.058	0
656	200	156	10480	<100	0.097	0	0.063	0
595	50	190	12650	<100	0.116	0	0.062	0
595	200	190	14120	<100	0.131	0	0.070	0
534	50	218	16050	<100	0.148	0	0.069	0
534	200	218	17750	<100	0.164	0	0.076	0
473	50	242	19370	<100	0.179	0	0.075	0
473	200	242	21820	<100	0.203	0	0.085	0
412	50	266	24130	<100	0.223	0	0.085	0
412	200	269	25150	<100	0.234	0	0.088	0
351	50	293	23920	<100	0.223	0	0.077	0
351	200	293	16320	4667	0.150	0.026	0.052	0.009
290	50	314	7635	14160	0.070	0.077	0.023	0.025
290	200	314	223	27850	0	0.149	0	0.048
229	50	335	<100	28340	0	0.152	0	0.046
229	200	335	<100	29450	0	0.159	0	0.048
168	50	362	<100	31990	0	0.172	0	0.048
168	200	362	<100	32420	0	0.175	0	0.049
107	50	379	<100	33820	0	0.183	0	0.049
107	200	379	<100	32500	0	0.176	0	0.047
46	50	396	<100	32360	0	0.176	0	0.045
46	200	396	<100	30980	0	0.168	0	0.043

Figure A.5.4 Concentration Profile Results Run 400-265-262-

Samples 200s after sequence

Distance from Carrier Gas Inlet	Sample Point Pressure	Peak Area		Column Concentration		Standardised Concentration	
		A.P	G.P	A.P	G.P	A.P	G.P
cm	kNm^{-2}			10^{-3} g cm^{-3}		10^{-3} g cm^{-3}	
717	221	<100	<100	0	0	0	0
656	163	17250	<100	0.160	0	0.099	0
595	190	19350	<100	0.179	0	0.095	0
534	221	24270	<100	0.225	0	0.103	0
473	249	30950	<100	0.288	0	0.117	0
412	273	35750	<100	0.332	0	0.123	0
351	300	32350	11680	0.300	0.062	0.101	0.021
290	321	4727	28330	0.044	0.156	0.014	0.049
229	342	164	40880	0	0.223	0	0.066
168	362	131	30980	0	0.168	0	0.047
107	383	129	32550	0	0.178	0	0.047
46	400	<100	35400	0	0.190	0	0.049

Figure A.5.5 Concentration Profile Results Run 500-265-262-A

Samples 200s after sequence

Distance from Carrier Gas Inlet	Sample Point Pressure	Peak Area		Column Concentration		Standardised Concentration	
		A.P	G.P	A.P	G.P	A.P	G.P
cm	$kN\,m^{-2}$			10^{-3} g cm^{-3}		10^{-3} g cm^{-3}	
717	225	<100	1143	0	0.006	0	0.002
656	159	18780	< 100	0.173	0	0.110	0
595	194	24550	< 100	0.229	0	0.119	0
534	218	29300	< 100	0.272	0	0.126	0
473	245	35940	< 100	0.332	0	0.137	0
412	273	44040	< 100	0.408	0	0.151	0
351	293	46980	12080	0.435	0.064	0.150	0.022
290	321	24170	16890	0.222	0.092	0.070	0.029
229	338	1225	31450	0.010	0.170	0.003	0.051
168	362	< 100	33390	0	0.183	0	0.051
107	383	<100	32500	0	0.174	0	0.046
46	400	< 100	38330	0	0.210	0	0.053

Figure A.5.6 Concentration Profile Results Run 600-265-262-A

Samples 200s after sequence

Distance from Carrier Gas Inlet	Sample Point Pressure	Peak Area		Column Concentration		Standardised Concentration	
		A.P	G.P	A.P	G.P	A.P	G.P
cm	kNm^{-2}			10^{-3} g cm^{-3}		10^{-3} g cm^{-3}	
717	238	<100	<100	0	0	0	0
656	149	22720	<100	0.211	0	0.143	0
595	183	29250	<100	0.272	0	0.150	0
534	214	32520	<100	0.301	0	0.142	0
473	238	37860	<100	0.316	0	0.149	0
412	266	51690	<100	0.479	0	0.182	0
351	293	54170	13260	0.502	0.072	0.173	0.025
290	311	40660	13620	0.378	0.073	0.123	0.024
229	335	657	48900	0.006	0.268	0.002	0.081
168	355	159	57500	0	0.319	0	0.091
107	376	191	55800	0	0.304	0	0.082
46	393	<100	46470	0	0.252	0	0.065

Figure A.5.7 Concentration Profile Results Run 700-265-262-A

Samples 200s after sequencing

Distance from Carrier Gas Inlet	Sample Point Pressure	Peak Area		Column Concentration		Standardised Concentration	
		A.P	G.P	A.P	G.P	A.P	G.P
cm	kNm^{-2}			10^{-3} g cm^{-3}		10^{-3} g cm^{-3}	
717	225	<100	1097	0	0.006	0	0.003
656	153	19840	285	0.185	0	0.122	0
595	187	33420	<100	0.311	0	0.168	0
534	214	38140	<100	0.354	0	0.167	0
473	238	52770	<100	0.490	0	0.208	0
412	266	53930	<100	0.500	0	0.190	0
351	293	54030	12840	0.502	0.070	0.173	0.024
290	317	52430	20820	0.493	0.116	0.157	0.037
229	338	15420	25800	0.144	0.141	0.043	0.042
168	362	1053	56150	0.011	0.304	0.003	0.085
107	379	<100	64700	0	0.352	0	0.094
46	400	<100	43920	0	0.242	0	0.061

Figure A.5.8 Concentration Profile Results Run 800-265-262-A

Samples 200s after sequence

Distance from Carrier Gas Inlet	Sample Point Pressure	Peak Area		Column Concentration		Standardised Concentration	
		A.P	G.P	A.P	G.P	A.P	G.P
cm	kNm^{-2}			10^{-3} g cm^{-3}		10^{-3} g cm^{-3}	
717	214	<100	<100	0	0	0	0
656	156	31570	<100	0.293	0	0.190	0
595	187	39200	<100	0.364	0	0.197	0
534	221	50660	<100	0.468	0	0.214	0
473	245	54570	<100	0.499	0	0.206	0
412	273	59980	<100	0.556	0	0.206	0
351	297	54800	10030	0.508	0.052	0.173	0.018
290	321	54960	25430	0.508	0.139	0.160	0.044
229	338	19460	39650	0.180	0.217	0.054	0.065
168	359	213	52310	0.001	0.284	0	0.080
107	379	< 100	66830	0	0.363	0	0.097
46	400	<100	49760	0	0.269	0	0.068

Figure A.5.9 Concentration Profile Results Run 1000-265-262-A

Samples 200s after sequence

Distance from Carrier Gas Inlet	Sample Point Pressure	Peak Area		Column Concentration		Standardised Concentration	
		A. P	G. P	A.P	G. P	A.P	G.P
cm	$kN\,m^{-2}$			10^{-3} g cm^{-3}		10^{-3} g cm^{-3}	
717	214	100	248	0	0	0	0
656	156	37120	100	0.344	0	0.223	0
595	190	52400	100	0.485	0	0.258	0
534	218	52020	100	0.483	0	0.224	0
473	245	63470	100	0.579	0	0.239	0
412	276	64410	100	0.598	0	0. 219	0
351	297	67290	19960	0.626	0.108	0.213	0.037
290	314	66380	26640	0.615	0.146	0.198	0.047
229	338	66540	31410	0.619	0.170	0.185	0.051
168	362	62060	41800	0.577	0.161	0.229	0.064
107	379	26110	48700	0.243	0.065	0.262	0.070
46	403	290	73430	0.001	0.267	0	0.067

Figure A.5.10 Temperature Profile Results Run 400-265-262-B1

Bed Isolated	TC1		TC4		TC5		TC6	
	EMF mV	Temp °C	EMF mV	Temp °C	EMF mV	Temp °C	EMF mV	Temp °C
9	855	0.4	507	-9.8	789	-1.7	658	-5.5
10	854	0.1	893	1.2	801	-1.4	703	-4.2
11	841	-0.3	918	2.0	814	-1.0	860	-0.3
12	787	-1.8	849	0.0	810	-1.1	834	-0.5
1	731	-3.4	557	-8.4	737	-3.2	646	-5.8
2	778	-2.1	677	-4.7	733	-0.5	679	-4.9
3	797	-1.5	816	-1.0	756	-2.7	774	-2.2
4	804	-1.3	848	-0.1	777	-2.1	801	-1.4
5	807	-1.2	822	-0.8	788	-1.8	803	-1.3
6	813	-1.1	830	-0.6	797	-1.5	810	-1.1
7	824	-0.7	765	-2.4	807	-1.2	862	0.3
8	812	-1.1	336	-13.9	784	-1.9	638	-6.1

Figure A.5.11 Run 400-265-262-C1

Bed Isolated	TC1		TC2		TC3		TC4		TC5		TC6	
	emf mV	Temp °C	emf mV	Temp °C	emf mV	Temp °C	emf mV	Temp °C	emf mV	Temp °C	emf mV	Temp °C
3	842	2.1	814	1.3	772	0.1	805	1.0	702	-1.9	779	0.3
4	807	1.1	811	1.2	782	0.3	826	1.6	818	1.4	818	1.4
5	816	1.3	807	1.1	789	0.5	808	1.1	823	1.5	821	1.5
6	822	1.5	814	1.3	793	0.6	816	1.3	819	1.4	816	1.4
7	851	2.3	133	-18.2	800	0.9	740	-0.9	920	4.3	916	4.2
8	814	1.3	174	-17.0	784	0.4	304	-13.3	544	-6.5	474	-8.5
9	876	3.0	856	2.5	797	0.8	460	-8.9	506	-7.5	470	-8.6
10	893	3.5	880	3.1	814	1.3	837	1.9	511	-7.4	476	-8.4
11	830	1.7	862	2.6	813	1.2	876	3.0	869	2.8	822	1.5
12	756	-0.4	797	0.8	796	0.7	833	1.8	873	2.9	873	2.9
1	576	-8.4	442	-9.4	698	-2.1	530	-6.9	570	-5.7	567	-5.8
2	811	1.2	767	-0.1	734	-1.0	701	-2.0	544	-6.5	516	-7.3

Figure A.5.12 Temperature Profile Results Run 400-265-262-C3

Bed Isolated	TC1		TC2		TC3		TC4		TC5		TC6	
	emf	Temp	emf	Temp	emf	Temp	emf	Temp	emf	Temp	emf	Temp
	mV	°C	mV	°C	mV	°C	mV	°C	mV	°C	mV	°C
9	867	2.8	868	2.8	859	2.5	862	2.6	770	0.0	710	-1.0
10	839	2.0	883	3.2	878	3.1	885	3.3	796	0.7	829	1.7
11	809	1.1	833	1.8	883	3.5	876	3.0	809	1.1	838	2.0
12	671	-2.8	750	-0.6	810	1.1	801	0.9	797	0.8	804	1.0
1	773	-0.1	623	-4.2	484	-8.2	442	-9.4	704	-1.9	627	-4.1
2	796	0.7	801	0.9	736	-1.0	773	0.1	718	-1.5	726	-1.3
3	789	0.5	819	1.4	799	0.8	806	1.0	746	-0.7	763	-0.2
4	793	0.7	788	0.5	810	1.1	804	1.0	763	-0.2	779	0.3
5	801	0.9	799	0.8	797	0.8	801	0.9	774	0.1	782	0.3
6	804	1.0	806	1.0	807	1.1	809	1.1	780	0.3	788	0.5
7	823	1.5	831	1.7	536	-6.7	116	-18.7	782	0.3	734	-1.0
8	788	0.5	794	0.7	610	-4.6	259	-14.6	753	-0.5	590	-5.1

Figure A.5.13 Run 400-265-262-D1

Bed Isolated	TC1		TC2		TC3		TC4		TC5		TC6	
	emf	Temp	emf	Temp	emf	Temp	emf	Temp	emf	Temp	emf	Temp
	mV	°C	mV	°C	mV	°C	mV	°C	mV	°C	mV	°C
3	847	0.9	837	0.6	839	0.7	855	1.1	858	1.2	900	2.4
4	855	1.1	840	0.7	843	0.8	854	1.1	854	1.1	848	0.9
5	862	1.3	845	0.9	848	0.9	866	1.5	864	1.4	861	1.3
6	884	2.0	851	1.0	854	1.1	871	1.6	869	1.5	869	1.5
7	860	1.3	856	1.2	863	1.4	906	2.6	902	2.5	904	2.5
8	901	2.5	856	1.2	859	1.3	864	1.4	862	1.3	872	1.6
9	863	1.4	861	1.3	875	1.7	957	4.1	951	3.9	940	3.6
10	834	0.5	850	1.0	865	1.4	890	2.1	897	2.4	949	3.8
11	796	-0.5	833	0.5	848	0.9	830	0.4	840	0.7	867	1.5
12	838	0.7	800	-0.4	789	-0.7	563	-7.2	622	-5.5	752	-1.8
1	847	09	812	-0.1	801	-0·4	852	1.1	838	0.7	624	-5.5
2	834	0.5	823	0.2	822	0.2	882	1.9	871	1.6	869	1.5

Figure A.5.14 Temperature Profile Results Run 400-265-262-D3

Bed Isolated	TC1		TC2		TC3		TC4		TC5		TC6	
	emf mV	Temp °C	emf mV	Temp °C	emf mV	Temp °C	emf mV	Temp °C	emf mV	Temp °C	emf mV	Temp °C
3	847	0.9	837	0.6	839	0.7	855	1.1	852	1.2	900	2.4
4	848	0.9	838	0.6	851	1.0	843	0.8	842	0.8	833	0.5
5	856	1.2	846	0.9	862	1.3	854	1.1	852	1.1	839	0.7
6	881	1.9	848	1.5	871	1.6	862	1.3	860	1.3	838	0.7
7	850	1.0	842	0.8	871	1.6	860	1.3	859	1.3	850	1.0
8	899	2.4	892	2.2	895	2.3	889	2.1	883	1.9	857	1.2
9	848	1.0	844	0.8	904	2.5	896	2.3	896	2.3	876	1.7
10	819	0.1	818	0.1	857	1.2	846	0.9	862	1.3	871	1.6
11	792	-0.7	784	-0.9	792	-0.7	790	-0.7	818	0.1	852	1.1
12	860	1.3	838	0.7	511	-8.7	518	-8.5	602	-6.1	796	-0.5
1	867	1.5	851	1.0	864	1.4	849	1.0	833	0.5	786	-0.8
2	848	0.9	838	0.6	851	1.0	843	0.8	842	0.8	833	0.5

Figure A.5.15 Run 600-265-262-B1

Bed Isolated	TC1		TC2		TC3		TC4		TC5		TC6	
	emf mV	Temp °C	emf mV	Temp °C	emf mV	Temp °C	emf mV	Temp °C	emf mV	Temp °C	emf mV	Temp °C
12	836	0.3	816	-0.2	272	-15.8	352	-13.5	490	-9.5	784	-1.1
1	858	1.0	847	0.7	844	0.6	837	0.4	816	-0.2	752	-2.1
2	792	-0.9	797	-0.8	909	2.4	896	2.1	861	1.1	796	-0.8
3	811	-0.4	807	-0.5	808	-0.5	812	-0.3	821	-0.1	811	-0.4
4	828	0.1	823	0.0	829	0.1	821	-0.1	821	-0.1	813	-0.3
5	837	0.4	833	0.3	842	0.5	841	0.5	839	0.4	821	-0.1
6	873	1.4	870	1.3	863	1.1	862	1.1	857	0.9	829	0.1
7	840	0.5	836	0.3	863	1.1	870	1.3	863	1.1	848	0.7
8	813	-0.3	810	-0.4	799	-0.7	797	-0.8	809	-0.4	826	0.1
9	831	0.2	843	0.5	891	1.9	893	2.0	887	1.8	834	0.3
10	791	-0.9	797	-0.8	841	0.5	856	0.9	862	1.1	849	0.7
11	771	-1.5	774	-1.4	799	-0.7	813	-0.3	830	0.2	841	0.5

Figure A.5.16 Temperature Profile Results Run 600-265-262-B3

BED Isolated	TC1		TC2		TC3		TC4		TC5		TC6	
	emf mV	Temp °C	emf mV	Temp °C	emf mV	Temp °C	emf mV	Temp °C	emf mV	Temp °C	emf mV	Temp °C
4	816	-0.2	810	-0.4	811	-0.4	823	0.0	823	0.0	817	-0.2
5	828	0.1	818	-0.2	819	-0.1	842	0.5	840	0.5	836	0.3
6	861	1.1	829	0.1	829	0.1	854	0.9	852	0.8	851	0.8
7	832	0.2	836	0.3	843	0.5	904	2.3	902	2.2	902	2.2
8	812	-0.3	824	0.0	822	-0.1	792	-0.9	791	-0.9	830	0.2
9	849	0.7	832	0.2	836	0.3	878	1.5	876	1.4	836	0.3
10	810	-0.4	826	0.1	840	0.5	920	2.8	917	2.6	922	2.8
11	792	-0.9	814	-0.3	827	0.1	857	0.9	854	0.9	903	2.3
12	786	-1.1	761	-1.8	736	-2.5	620	-5.8	614	-6.0	809	-0.4
1	813	-0.3	778	-1.3	760	-1.8	821	-0.1	821	-0.1	615	-6.0
2	791	-0.9	792	-0.9	797	-0.8	873	1.4	872	1.4	854	0.9
3	793	-0.9	793	-0.9	799	-0.7	820	-0.1	819	-0.2	876	1.5

Figure A.5.17 Run 600-265-262-B5

Bed Isolated	TC1		TC2		TC3		TC4		TC5		TC6	
	emf mV	Temp °C	emf mV	Temp °C	emf mV	Temp °C	emf mV	Temp °C	emf mV	Temp °C	emf mV	Temp °C
12	684	-3.9	817	-0.1	889	1.9	880	1.7	856	1.0	852	0.9
1	788	-0.9	549	-7.8	400	-12.0	360	-13.2	602	-6.2	624	-5.6
2	837	0.5	851	0.9	779	-1.2	799	-0.6	747	-2.1	747	-2.1
3	816	-0.1	874	1.5	849	0.8	850	0.8	794	-0.8	789	-0.9
4	814	-0.2	810	-0.3	848	0.8	839	+0.5	818	-0.1	813	-0.2
5	827	0.2	829	0.2	826	0.1	828	0.2	814	-0.2	812	-0.3
6	833	0.3	841	0.6	841	0.6	842	0.6	826	0.1	823	0.1
7	875	1.5	894	2.1	364	-13.1	351	-13.5	792	-0.8	788	-0.9
8	791	-0.9	823	0.1	620	-5.8	159	-18.9	588	-6.7	610	-6.0
9	859	1.1	826	0.1	829	0.3	820	0.0	576	-7.0	594	-6.5
10	888	1.9	912	2.6	882	1.8	887	1.9	766	-1.6	774	-1.3
11	846	0.7	894	2.1	914	2.7	913	2.6	856	1.0	850	0.8

Figure A.5.18 Temperature Profile Results Run 600-265-262-C1

Bed Isolated	TC1		TC2		TC3		TC4		TC5		TC6	
	emf mV	Temp °C	emf mV	Temp °C	emf mV	Temp °C	emf mV	Temp °C	emf mV	Temp °C	emf mV	Temp °C
11	807	1.5	796	1.2	761	0.2	578	-5.0	481	-7.7	459	-8.4
12	744	-0.3	781	0.7	760	0.2	830	2.2	499	-7.3	492	-7.5
1	516	-6.8	422	-9.5	629	-3.6	468	-8.1	538	-6.1	542	-6.0
2	752	0.0	722	-0.9	686	-1.9	626	-3.6	444	-8.8	407	-9.9
3	774	0.6	751	-0.1	720	-1.0	764	0.3	727	-0.7	731	-0.6
4	746	-0.2	744	-0.3	731	-0.6	793	1.1	778	0.7	790	1.1
5	753	0.0	741	-0.3	733	-0.6	756	0.1	774	0.6	781	0.8
6	766	0.4	753	0.0	742	-0.3	773	0.6	770	0.5	773	0.6
7	802	1.4	506	-7.1	751	0.1	719	-1.0	901	4.2	904	4.3
8	764	0.3	713	-1.1	735	-0.5	306	-12.8	578	-5.0	524	-6.5
9	722	-0.9	710	-1.2	713	-1.1	226	-15.1	261	-14.1	197	-15.9
10	790	1.1	766	0.4	731	-0.6	386	-10.5	436	-9.1	398	-10.1

Figure A.5.19 Run 600-265-262-C3

Bed Isolated	TC1		TC4		TC5		TC6	
	emf mV	Temp °C	emf mV	Temp °C	emf mV	Temp °C	emf mV	Temp °C
4	763	-1.1	829	0.8	736	-1.9	768	-1.0
5	778	-0.7	791	-0.3	758	-1.3	776	-0.7
6	789	-0.4	811	0.3	774	-0.8	791	-0.3
7	811	0.4	783	-0.5	791	-0.3	864	1.8
8	802	0.0	347	-13.0	782	-0.6	666	-3.9
9	780	-0.6	235	-16.2	724	-2.3	520	-8.1
10	801	0.0	386	-11.9	724	-2.2	573	-6.5
11	816	0.4	769	-0.9	752	-1.4	634	-4.8
12	798	-0.1	880	2.2	773	-0.8	783	-0.5
1	693	-3.1	546	-7.3	697	-3.0	604	-5.7
2	761	-1.2	620	-5.2	702	-2.9	626	-5.0
3	787	-0.4	821	0.6	736	-1.9	764	-1.1

Figure A.5.20 Temperature Profile Results Run 800-265-262-B1

Bed Isolated	TC1		TC2		TC3		TC4		TC5		TC6	
	emf mV	Temp °C	emf mV	Temp °C	emf mV	Temp °C	emf mV	Temp °C	emf mV	Temp °C	emf mV	Temp °C
5	830	-0.2	832	-0.2	830	-0.2	836	-0.1	819	-0.5	809	-0.8
6	882	1.3	883	1.3	872	1.0	870	0.9	852	0.4	818	-0.6
7	859	0.6	859	0.6	894	1.6	893	1.6	869	0.9	836	-0.1
8	852	0.4	851	0.4	857	0.5	853	0.4	843	0.1	844	0.2
9	791	-1.3	793	-1.3	808	-0.9	808	-0.9	811	-0.8	823	-0.4
10	774	-1.8	782	-1.6	776	-1.8	773	-1.8	793	-1.3	796	-1.2
11	774	-1.8	790	-1.4	834	-0.1	837	0.0	836	-0.1	806	-0.9
12	810	-0.8	780	-1.7	310	-15.1	340	-14.2	470	-10.5	770	-1.9
1	836	-0.1	830	-0.2	823	-0.4	820	-0.5	787	-1.5	722	-3.5
2	773	-1.9	786	-1.5	900	1.7	891	+1.3	839	0.0	772	-1.9
3	780	-1.7	783	-1.6	783	-1.6	782	-1.6	791	-1.3	787	-1.5
4	804	-1.0	804	-1.0	806	-0.9	806	-0.9	806	-0.9	790	-1.4

Figure A.5.21 Run 800-265-262-C1

Bed Isolated	TC1		TC2		TC3		TC4		TC5		TC6	
	emf mV	Temp °C	emf mV	Temp °C	emf mV	Temp °C	emf mV	Temp °C	emf mV	Temp °C	emf mV	Temp °C
6	756	0.8	730	-0.3	727	-0.4	760	0.6	753	0.4	759	0.5
7	759	0.6	742	0.1	750	0.3	824	2.4	817	2.2	820	2.3
8	776	1.1	753	0.4	762	0.6	814	2.1	809	2.0	842	2.9
9	758	0.5	752	0.3	763	0.7	804	1.8	798	1.7	810	2.0
10	722	-0.5	742	0.1	752	0.3	760	0.6	759	0.8	780	1.1
11	677	-1.8	713	-0.8	722	-0.5	673	-1.9	678	-1.8	698	-1.2
12	690	-1.4	670	-2.0	650	-2.6	540	-5.7	570	-4.9	630	-3.1
1	730	-0.3	690	-1.4	672	-2.0	750	0.3	730	-0.3	530	-6.0
2	707	-0.9	711	-0.8	712	-0.8	809	2.0	792	1.5	791	1.5
3	700	-1.1	707	-0.9	712	-0.8	725	-0.4	729	-0.3	816	2.2
4	720	-0.6	713	-0.8	718	-0.6	717	-0.7	717	-0.7	708	-0.9
5	736	-0.1	724	-0.5	730	-0.3	746	0.2	744	0.1	740	0.0

Figure A.5.22 Temperature Profile Results Run 800-265-262-D1

Bed Isolated	TC1		TC2		TC3		TC4		TC5		TC6	
	emf mV	Temp °C	emf mV	Temp °C	emf mV	Temp °C	emf mV	Temp °C	emf mV	Temp °C	emf mV	Temp °C
9	804	0.1	827	0.8	862	1.8	856	1.6	734	-1.9	330	-13.4
10	761	-1.1	773	-0.8	804	0.1	793	-0.2	720	-2.3	270	-15.1
11	710	-2.6	698	-2.9	738	-1.8	729	-2.0	703	-2.8	248	-15.8
12	650	-4.2	714	-2.5	731	-2.0	726	-2.1	696	-3.0	376	-12.1
1	691	-3.1	318	-13.8	430	-10.6	388	-11.8	603	-5.6	440	-10.3
2	753	-1.3	783	-0.5	672	-3.4	714	-2.5	636	-4.7	616	-5.3
3	746	-1.5	802	0.1	782	-0.5	782	-0.5	687	-3.2	753	-1.3
4	738	-1.8	737	-1.8	790	-0.3	778	-0.6	714	-2.5	782	-0.5
5	754	-1.3	754	-1.3	757	-1.2	756	-1.3	728	-2.1	754	-1.3
6	768	-0.9	777	-0.7	779	-0.6	779	-0.6	741	-1.7	769	-0.9
7	821	0.6	846	+1.3	467	-9.5	387	-11.8	752	-1.4	690	-3.1
8	816	0.5	862	1.8	643	-4.5	272	-15.1	736	-1.8	364	-12.5

Figure A.5.23 Run 800-265-262-E1

Bed Isolated	TC1		TC2		TC3		TC4		TC5		TC6	
	emf mV	Temp °C	emf mV	Temp °C	emf mV	Temp °C	emf mV	Temp °C	emf mV	Temp °C	emf mV	Temp °C
11	810	-1.1	803	-1.3	772	-2.2	446	-11.5	440	-11.7	420	-12.2
12	811	-1.1	826	-0.7	791	-1.7	573	-7.9	527	-9.2	490	-10.3
1	707	-4.1	454	-11.3	656	-5.5	461	-11.1	-71	-26.1	495	-10.1
2	810	-1.1	784	-1.9	733	-3.3	762	-2.5	594	-7.3	498	-10.1
3	830	-0.6	809	-1.2	766	-2.4	821	-0.8	800	-1.4	803	-1.3
4	788	-1.8	800	-1.4	777	-2.1	845	0.1	836	-0.4	848	-0.1
5	806	-1.2	804	-1.3	791	-1.7	816	-1.0	840	-0.3	859	0.3
6	824	-0.7	823	-0.7	804	-1.3	830	-0.6	840	-0.3	849	0.0
7	870	0.9	599	-7.2	817	-0.9	771	-2.3	987	3.9	983	3.8
8	874	0.7	833	-0.5	816	-1.0	472	-10.8	656	-5.5	710	-4.0
9	826	-0.7	840	-0.3	808	-1.2	390	-13.1	507	-9.8	529	-9.2
10	784	-2.2	790	-1.7	783	-1.9	326	-15.0	355	-14.1	377	-13.5

Figure A.5.24 Temperature Profile Results Run 800-265-262-E2

Bed Isolated	TC1		TC4		TC5		TC6	
	emf mV	Temp °C	emf mV	Temp °C	emf mV	Temp °C	emf mV	Temp °C
11	806	-1.3	333	-14.8	738	-3.2	552	-8.5
12	800	-1.4	743	-3.1	760	-2.6	640	-6.0
1	720	-3.7	516	-9.5	682	-4.8	579	-7.7
2	787	-1.8	757	-2.7	704	-4.2	658	-5.5
3	814	-1.0	859	0.2	747	-2.9	794	-1.9
4	812	-1.1	898	-1.4	779	-2.0	831	0.5
5	819	-0.9	849	0.0	800	-1.4	837	-0.4
6	827	-0.7	860	0.3	813	-1.1	842	-0.2
7	866	0.5	840	-0.3	840	-0.3	949	2.8
8	860	0.3	508	-9.8	834	-0.5	796	-1.5
9	837	-0.4	386	-13.3	799	-1.5	661	-5.4
10	801	-1.4	285	-16.1	753	-2.8	548	-8.6

Figure A.6.1 Feed Distributor Analysis (A.P/G.P 400cm^3 hr

Feed Bed

Arklone.P			Genklene.P		
Time	Peak Area	Std' Conc'	Time	Peak Area	Std' Conc'
s		10^{-3}g cm^{-3}	s		10^{-3}g cm^{-3}
10	1162	0.003	50	1347	0.002
100	8762	0.020	150	4164	0.006
200	12690	0.028	312	5801	0.008
262	13770	0.028	474	6371	0,008
362	12960	0.027	674	12130	0.015
462	9079	0.019	836	10900	0.013
524	5955	0.012	998	7585	0.009
624	1197	0.002	1198	1134	0.001

Feed Cone

50	17470	0.038	50	17820	0.026
150	22770	0.053	150	24740	0.035
250	23330	0.056	250	23670	0.034
312	21140	0.044	312	29010	0.038
362	504	0.001	362	12010	0.016
462	206	0	462	1413	0.002
524	< 100	0	524	314	0

Figure A.6.2 Feed Distributor Analysis (A.P/G.P 600$cm^3 hr^{-1}$)

Feed Bed

Arklone. P			Genklene, P		
Time	Peak Area	Std' Conc'	Time	Peak Area	Std' Conc'
s		10^{-3}g cm^{-3}	s		10^{-3}g cm^{-3}
10	3329	0.007	50	2940	0.004
100	15730	0.035	212	6535	0.009
200	18650	0.041	474	8651	0.011
362	20000	0.040	736	18000	0.021
462	17200	0.035	998	17830	0.020
624	9123	0.018	1198	12970	0.014
724	2503	0.004	1460	4688	0.005
786	222	0	1622	3780	0.006

Feed Cone

50	20380	0.045	50	18470	0.026
150	25650	0.066	150	30020	0.043
250	26630	0.071	250	32150	0.046
312	24620	0.057	312	36120	0.048
412	3074	0.008	412	36350	0.048
512	340	0	512	5822	0.008
574	<100	0	574	855	0.001

Figure A.6.3 Feed Distributor Analysis (A.P/G.P 800cm^{3}hr^{-1})

Feed Bed

Arklone.P			Genklene.P		
Time	Peak Area	Std' Conc'	Time	Peak Area	Std' Conc'
s		10^{-3}g cm^{-3}	s		10^{-3}g cm^{-3}
10	5897	0.013	50	3290	0.005
100	19560	0.044	212	6822	0.009
200	22300	0.053	412	9426	0.013
262	23470	0.052	574	10720	0.013
362	22740	0.050	836	19190	0.022
462	20620	0.042	1098	22380	0.025
524	19670	0.035	1360	16520	0.018
624	17800	0.034	1460	1654	0.002
724	13290	0.026	1522	37130	0.063
786	7803	0.014	1572	29650	0.050
886	1834	0.003	1672	6437	0.011

Feed Cone

50	23260	0.055	50	21140	0.030
150	28330	0.081	150	35030	0.050
250	29500	0.089	250	38440	0.055
312	27910	0.072	312	40310	0.057
412	8784	0.052	412	43880	0.068
512	379	0.001	512	11610	0.015
574	100	0	574	1767	0.002
674	0	0	674	385	0

Figure A.6.4 Feed Distributor Analysis (A.P/G.P 1000 $cm^3 hr^{-1}$)

Feed Bed

Arklone.P			Genklene.P		
Time	Peak Area	Std' Conc'	Time	Peak Area	Std' Conc'
s		10^{-3} g cm^{-3}	s		10^{-3} g cm^{-3}
10	5696	0.013	50	5015	0.007
100	22440	0.053	150	7755	0.011
200	23950	0.059	312	8649	0.011
262	23260	0.051	574	11540	0.014
362	22500	0.049	936	22140	0.026
462	20770	0.043	1198	21530	0.024
624	18340	0.035	1360	16590	0.018
724	12650	0.024	1460	13880	0.015
786	7822	0.015	1522	35120	0.060
886	1250	0.002	1622	3322	0.006
986	258	0	1672	448	0.001

Feed Cone

50	25390	0.065	50	23220	0.033
150	30540	0.096	150	36940	0.053
250	31550	0.104	250	41460	0.062
312	30490	0.090	312	42760	0.064
412	21880	0.047	412	45860	0.074
512	2754	0.005	512	44190	0.069
564	370	0.001	564	15120	0.019
664	283	0	664	2413	0.003

Appendix .7

Figure A.7.1 Cooling Rates Within the Columns

Time	Temperature 3.8cm from Column Wall		Temperature 1.3cm from Column Wall		Temperature 2.6cm from Column Wall	
s	mV	°C	mV	°C	mV	°C
0	300	-12.8	500	-7.1	414	-9.3
10	328	-12.1	507	-6.9	429	-8.9
50	368	-10.9	537	-6.1	468	-7.8
100	462	-8.2	561	-5.4	508	-6.7
150	504	-7.0	581	-4.8	537	-5.9
200	538	-6.1	602	-4.2	566	-5.1
250	568	-5.2	621	-3.7	587	-4.5
300	584	-4.7	633	-3.3	605	-4.0
350	603	-4.2	648	-2.9	620	-3.6
400	619	-3.7	661	-2.5	634	-3.2
500	646	-3.0	685	-1.9	663	-2.4
600	666	-2.4	703	-1.3	681	-1.9
700	684	-1.9	720	-0.9	696	-1.5
800	698	-1.5	732	-0.5	712	-0.9
900	712	-1.1	745	-0.1	732	-0.5
1000	722	-0.8	753	-0.1	739	-0.3

Figure A.7.2 Temperature Profile Results Run 600-265-262-E1

Bed Isolated	TC1		TC2		TC3		TC4		TC5		TC6	
	emf mV	Temp °C	emf mV	Temp °C	emf mV	Temp °C	emf mV	Temp °C	emf mV	Temp °C	emf mV	Temp °C
11	768	0.5	770	0.6	776	0.7	629	-3.5	690	-2.0	745	-0.1
12	768	0.5	784	1.0	500	-7.1	715	-1.0	622	-3.7	658	-2.6
1	768	0.5	767	0.5	783	0.9	452	-8.5	500	-7.1	410	-9.7
2	763	0.4	747	-0.1	808	1.7	743	-0.2	674	-2.2	526	-6.4
3	760	0.3	761	0.3	774	0.7	790	1.1	781	0.9	763	0.4
4	767	0.5	771	0.6	781	0.9	800	1.4	808	1.7	802	1.5
5	770	0.6	784	1.0	783	0.9	781	0.9	783	0.9	796	1.3
6	740	-0.3	830	2.3	972	6.3	845	2.7	797	1.5	801	1.5
7	720	-0.9	596	-4.4	961	6.0	943	5.5	973	6.4	982	6.6
8	730	-0.6	663	-2.5	684	-1.9	921	4.9	928	5.1	930	5.1
9	753	0.1	747	-0.1	549	-5.7	829	2.3	890	4.0	890	4.0
10	758	0.2	759	0.3	704	-1.3	690	-1.7	774	0.7	837	2.5

Figure A.7.3 Run 600-265-262-E4

Bed Isolated	TC1		TC2		TC3		TC4		TC5		TC6	
	emf mV	Temp °C	emf mV	Temp °C	emf mV	Temp °C	emf mV	Temp °C	emf mV	Temp °C	emf mV	Temp °C
1	749	0.3	755	0.4	760	0.6	462	-7.9	472	-7.7	468	-7.8
2	747	0.2	741	0.0	793	1.2	760	0.6	712	-0.8	576	-4.7
3	751	0.3	750	0.3	780	1.4	781	1.2	767	0.8	747	0.2
4	760	0.6	757	0.5	767	0.8	781	1.2	798	1.7	794	1.5
5	763	0.7	762	0.6	766	0.7	762	0.6	766	0.7	784	1.3
6	730	-0.3	847	3.1	953	6.1	856	3.3	787	1.3	787	1.3
7	696	1.3	646	2.5	966	6.5	940	5.7	936	5.6	956	6.2
8	727	-0.4	628	-3.2	690	-1.4	900	4.6	910	4.9	916	5.0
9	740	0.0	731	-0.3	555	-5.3	774	1.0	854	3.3	870	3.7
10	746	0.2	751	0.3	685	-1.6	660	-2.3	742	0.1	816	2.2
11	743	0.1	743	0.1	747	+0.2	587	-4.4	653	-2.5	711	-0.8
12	744	0.1	752	0.4	470	-7.7	710	-0.9	606	-3.8	630	-3.1

Figure A.7.4 Temperature Profile Results Run 600-265-262-E6

Bed Isolated	TC1		TC2		TC3		TC4		TC5		TC6	
	emf mV	Temp °C	emf mV	Temp °C	emf mV	Temp °C	emf mV	Temp °C	emf mV	Temp °C	emf mV	Temp °C
3	748	0.2	741	0.0	763	0.7	765	0.7	743	0.1	740	0.0
4	758	0.5	751	0.3	758	0.5	762	0.6	763	0.7	764	0.7
5	763	0.7	764	0.7	764	0.7	762	0.6	760	0.6	764	0.7
6	728	-0.3	836	2.7	930	5.4	852	3.2	786	1.3	775	1.0
7	696	-1.3	648	-2.6	907	4.8	917	5.1	890	4.3	913	4.9
8	722	-0.6	596	-4.1	709	-0.9	860	3.4	859	3.4	878	3.9
9	740	0.0	690	-1.4	594	-4.2	760	0.6	801	1.7	829	2.5
10	746	0.2	690	-1.4	691	-1.4	671	-2.0	728	0.4	776	1.0
11	744	0.2	731	-0.3	740	0.0	626	-3.3	678	-1.9	705	-1.0
12	746	0.2	732	-0.2	529	-6.0	721	-0.5	701	-1.1	656	-2.4
1	746	0.2	738	-0.1	741	0.0	519	-6.3	529	-6.0	521	-6.3
2	742	0.1	716	-0.7	771	0.9	742	0.1	707	-0.9	640	-2.9

Figure A.7.5 Run 600-265-262-F1

Bed Isolated	TC1		TC2		TC3		TC4		TC5		TC6	
	emf mV	Temp °C	emf mV	Temp °C	emf mV	Temp °C	emf mV	Temp °C	emf mV	Temp °C	emf mV	Temp °C
3	776	1.1	761	0.6	759	0.5	748	0.2	738	-0.1	723	-0.5
4	782	1.3	764	0.7	764	0.7	761	0.6	756	0.5	745	0.1
5	783	1.3	769	0.8	767	0.8	765	0.7	763	0.7	760	0.6
6	705	-1.0	812	2.1	806	1.9	780	1.1	780	1.1	768	0.8
7	701	1.1	763	0.7	833	2.7	842	2.9	834	2.7	810	2.0
8	758	0.5	738	-0.1	783	1.2	824	2.4	830	2.6	812	2.1
9	770	0.8	742	0.1	746	0.2	786	1.3	796	1.6	793	1.5
10	773	0.9	752	0.4	740	0.0	751	0.3	771	0.9	780	1.1
11	761	0.6	754	0.4	745	0.1	738	-0.1	741	0.3	754	0.4
12	774	1.0	728	-0.3	722	-0.6	742	0.1	743	0.1	746	0.2
1	764	0.7	733	-0.2	688	-1.5	660	-2.2	664	-2.2	681	-1.7
2	759	0.5	751	0.3	742	0.1	718	-0.6	707	-0.9	693	-1.3

Figure A.7.6 Temperature Profile Results Run 600-265-262-F3

Bed Isolated	TC2		TC3		TC4		TC5	
	emf	Temp	emf	Temp	emf	Temp	emf	Temp
	mV	°C	mV	°C	mV	°C	mV	°C
12	520	-6.3	409	-9.5	411	-9.4	728	-0.3
1	734	-0.2	762	0.6	765	0.7	734	-0.2
2	770	0.9	812	2.1	816	2.2	801	1.7
3	758	0.5	773	0.9	776	1.0	828	2.5
4	763	0.7	779	1.1	781	1.2	788	1.4
5	767	0.8	783	1.2	788	1.4	785	1.3
6	687	1.5	891	4.3	963	6.3	914	5.0
7	682	1.7	810	2.0	770	0.9	753	0.4
8	654	2.5	553	5.3	542	5.7	833	2.7
9	696	-1.3	704	-1.0	713	-0.8	677	-1.8
10	730	-0.3	753	0.4	757	0.5	558	-5.2
11	743	0.1	764	0.7	767	0.8	725	-0.4

Figure A.7.7 Concentration Profile Results Run 400-265-262-E

Samples at 200s

Distance from Carrier Gas Inlet	Sample Point Pressure	Peak Area		Standardised Concentration	
		A.P	G.P	A.P	G.P
cm	kNm^{-2}			10^{-3} g cm^{-3}	
717	242	<100	375	0	0.003
656	197	6360	<100	0.091	0
595	224	8951	<100	0.113	0
534	249	10040	<100	0.114	0
473	273	11013	<100	0.114	0
412	290	13770	<100	0.134	0
351	307	2238	7760	0.021	0.050
290	324	218	10100	0.002	0.062
229	341	<100	9037	0	0.053
168	359	<100	10150	0	0.056
107	379	<100	8641	0	0.045
46	396	<100	8360	0	0.042

Figure A.7.8 Concentration Profile Results Run 600-265-262-D

Samples at 200s

Distance from Carrier Gas Inlet	Sample Point Pressure	Peak Area		Standardised Concentration	
		A.P	G.P	A.P	G.P
cm	kNm^{-2}			10^{3} g.cm^{-3}	
717	225	<100	<100	0	0
656	190	7195	<100	0.151	0
595	214	11800	<100	0.156	0
534	238	18420	<100	0.218	0
473	262	16160	<100	0.174	0
412	287	23000	<100	0.227	0
351	304	4181	12740	0.039	0.083
290	324	330	12940	0.003	0.079
229	341	<100	11320	0	0.066
168	359	<100	10890	0	0.060
107	379	<100	12510	0	0.066
46	396	<100	12690	0	0.064

Figure A.7.9 Concentration Profile Results Run 800-265-262-F

Samples at 200s

Distance from Carrier Gas Inlet	Sample Point Pressure	Peak Area		Standardised Concentration	
		A.P	G.P	A.P	G.P
cm	kNm^{-2}			10^{-3} g cm^{-3}	
717	211	<100	<100	0	0
656	190	13060	<100	0.195	0
595	225	18870	<100	0.238	0
534	252	20430	<100	0.229	0
473	273	24690	<100	0.256	0
412	293	28800	100	0.278	0
351	307	7960	11640	0.073	0.075
290	324	852	13260	0.007	0.081
229	341	<100	13080	0	0.076
168	359	<100	11400	0	0.063
107	376	<100	14020	0	0.074
46	396	<100	13640	0	0.068

Figure A.7.10 Concentration Profile Results Run 1000-265-262-B

Samples at 200s

Distance from Carrier Gas Inlet	Sample Point Pressure	Peak Area		Standardised Concentration	
		A.P	G.P	A.P	G.P
cm	kNm^{-2}			10^{-3} g cm^{-3}	
717	211	<100	<100	0	0
656	190	17460	<100	0.242	0
595	221	21990	<100	0.273	0
534	256	26160	<100	0.289	0
473	280	30120	<100	0.316	0
412	297	33660	<100	0.338	0
351	310	11810	14360	0.096	0.090
290	324	2066	14680	0.015	0.087
229	345	502	17390	0.004	0.098
168	362	642	15000	0.004	0.081
107	376	277	15080	0.002	0.078
46	396	<100	16270	0	0.080

Figure A.7.11 Concentration Profile Results Run 1200-265-262-A

Samples at 200s

Distance from Carrier Gas Inlet	Sample Point Pressure	Peak Area		Standardised Concentration	
		A.P	G.P	A.P	G.P
cm	kNm^{-2}			10^{-3} g cm^{-3}	
717	214	<100	228	0	0002
656	200	23140	<100	0.319	0
595	232	26680	<100	0.328	0
534	249	27710	<100	0.321	0
473	276	33960	<100	0.372	0
412	293	38770	<100	0.416	0
351	310	19900	18430	0.171	0.116
290	328	3565	20070	0.027	0.119
229	345	961	17560	0.007	0.099
168	362	707	18500	0.005	0.099
107	383	398	21210	0.003	0.108
46	396	146	22200	0001	0109

Figure A.7.12 Concentration Profile Results Run 1300-265-262-A

Samples at 200 s

Distance from Carrier Gas Inlet	Sample Point Pressure	Peak Area		Standardised Concentration	
		A.P	G.P	A.P	G.P
cm	kNm^{-2}			10^{-3} g cm^{-3}	
717	197	<100	<100	0	0
656	201	20440	<100	0.274	0
595	225	23220	<100	0.302	0
534	245	27480	<100	0.321	0
473	272	33320	<100	0.367	0
412	290	35960	1321	0.382	0.009
351	307	18620	17680	0.161	0.112
290	324	4531	16630	0.034	0.100
229	348	826	16800	0.006	0.094
168	362	668	18700	0.005	0.101
107	383	379	19780	0.003	0.101
46	396	<100	20830	0	0.102

Figure A.7.13 Concentration Profile Results Run 1400-265-262-A

Samples at 200s

Distance from Carrier Gas Inlet	Sample Point Pressure	Peak Area		Standardised Concentration	
		A.P	G.P	A.P	G.P
cm	kNm^{-2}			10^{-3} g cm^{-3}	
717	211	<100	1150	0	0.011
656	204	24600	< 100	0.338	0
595	235	27980	< 100	0.343	0
534	259	31030	< 100	0.355	0
473	276	36060	< 100	0.403	0
412	297	38220	474	0.401	0.003
351	317	26760	20710	0.240	0.127
290	331	13190	18200	0.102	0.107
229	348	1893	17220	0.013	0.096
168	365	1024	19240	0.007	0.103
107	383	766	22360	0.005	0.114
46	400	<100	23100	0	0.113

Figure A.7.14 Concentration Profile Results Run 1500-265-262-A

Samples at 200s

Distance from Carrier Gas Inlet	Sample Point Pressure	Peak Area		Standardised Concentration	
		A.P	G.P	A.P	G.P
cm	kNm^{-2}			10^{-3} g cm^{-3}	
717	211	<100	3128	0	0.029
656	201	25510	7432	0.357	0.072
595	228	28710	5242	0.364	0.045
534	256	33330	4110	0.392	0.031
473	276	38600	2274	0.440	0.016
412	293	42210	1389	0.466	0.009
351	310	32080	18070	0.309	0.113
290	324	24590	15380	0.210	0.092
229	345	15930	13210	0.121	0.075
168	362	11040	11490	0.076	0.062
107	379	6253	16030	0.041	0.082
46	396	1536	18700	0.009	0.092

Figure A.7.15 Concentration Profile Results Run 100-120-150-A

Samples at 75s

Distance from Carrier Gas Inlet	Sample Point Pressure	Peak Area		Standardised Concentration	
		A.P	D.C.M	A.P	D.C.M
cm	kNm^{-2}			10^{-3} g cm^{-3}	
290	309	31000	20940	0.070	0.045
229	329	26540	11220	0.057	0.023
168	350	17740	5001	0.036	0.009
107	361	18610	4136	0.036	0.007
46	378	18620	3972	0.034	0.007
717	214	2670	390	0.009	0.001
656	177	2521	5497	0.010	0.021
595	200	6046	9597	0.022	0.032
534	221	9900	14330	0.032	0.044
473	246	12330	14150	0.036	0.039
412	267	25190	28800	0.067	0.073
351	290	33830	33770	0.083	0.079

Figure A.7.16 Run 100-115-150-A

717	214	9112	3409	0.030	0.011
656	177	829	4832	0.003	0.017
595	200	1608	8720	0.006	0.029
534	221	1690	13810	0.005	0.040
473	246	3067	20790	0.009	0.057
412	267	4736	26600	0.013	0.067
351	290	23410	42160	0.058	0.098
290	309	36620	45070	0.083	0.096
229	329	36850	34640	0.079	0.070
168	350	39220	27580	0.075	0.050
107	361	38540	31550	0.078	0.060
46	378	32010	19640	0.061	0.035

Figure A.7.17 Concentration Profile Results Run 100-110-150-A

Samples at 75s

Distance from Carrier Gas Inlet	Sample Point Pressure	Peak Area		Standardised Concentration	
		A.P	D.C.M	A.P	D.C.M
cm	$kN\,m^{-2}$			$10^{-3}\ g\,cm^{-3}$	
717	216	1529	366	0.005	0.002
656	179	1189	5764	0.004	0.002
595	201	1905	13020	0.007	0.042
534	221	2933	17570	0.009	0.051
473	244	6167	29220	0.018	0.078
412	265	10670	36710	0.028	0.093
351	288	36100	42910	0.088	0.107
290	306	43030	45180	0.099	0.106
229	325	31030	29290	0.085	0.060
168	348	38360	26970	0.078	0.052
107	361	36860	20150	0.072	0.037
46	378	34930	21320	0.065	0.037

Figure A.7.18 `Run 100-120-150-B

717	214	3361	414	0.011	0.002
656	168	910	326	0.004	0.001
595	200	6632	10330	0.023	0.035
534	222	12590	15420	0.039	0.045
473	244	17320	18270	0.050	0.050
412	266	20840	20160	0.056	0.051
351	287	25760	23630	0.063	0.055
290	305	32400	18280	0.074	0.039
229	327	31650	15230	0.069	0.031
168	349	32900	7842	0.067	0.015
107	363	19900	3286	0.039	0.006
46	378	15000	2520	0.028	0.004

Figure A.7.19 Concentration Profile Results Run 100-135-150-A

Samples at 100s

Distance from Carrier Gas Inlet	Sample Point Pressure	Peak Area		Standardised Concentration	
		A.P	D.C.M	A.P	D.C.M
cm	$kN\,m^{-2}$			10^{-3}	$g\,cm^{-3}$
717	204	< 100	< 100	0	0
656	164	1844	2740	0.014	0.020
595	197	3788	4183	0.025	0.027
534	220	5894	5085	0.034	0.029
473	242	8660	6939	0.045	0.035
412	264	18750	10830	0.089	0.043
351	286	14770	2312	0.065	0.010
290	304	8795	< 100	0.036	0
229	327	6654	< 100	0026	0
168	348	5721	< 100	0.021	0
107	365	5809	< 100	0.020	0
46	378	4569	< 100	0.015	0

Figure A.7.20 Run 100-125-150-A

717	204	< 100	< 100	0	0
656	168	1134	2882	0.008	0.020
595	197	1983	4898	0.013	0.030
534	222	2822	5890	0.016	0.032
473	244	5987	9814	0.031	0.049
412	266	18000	16815	0086	0.077
351	286	16550	4751	0.073	0020
290	305	11550	405	0.047	0.002
229	327	9052	< 100	0.035	0
168	348	8711	< 100	0.032	0
107	365	7172	< 100	0.025	0
46	378	5900	< 100	0.020	0

Figure A.7.21 Concentration Profile Results Run 100-115-150-A4

Distance from Carrier Gas Inlet	Sample Point Pressure	Peak Area		Standardised Concentration	
		A.P	D.C.M	A.P	D.C.M
cm	kNm^{-2}			10^{-3} g cm^{-3}	
717	204	<100	<100	0	0
656	179	<100	3644	0	0.025
595	204	<100	5399	0	0.032
534	222	256	8497	0.001	0.044
473	244	861	13820	0.004	0.065
412	265	6167	22650	0.028	0.100
351	288	18570	21820	0.082	0.093
290	306	13870	8486	0.057	0.034
229	325	11410	5271	0.043	0.020
168	348	9683	3923	0.035	0.014
107	361	8886	3036	0.031	0.010
46	378	9400	1086	0.032	0.003

Figure A.7.22 Run 100-115-150-A5

717	204	<100	<100	0	0
656	179	<100	3246	0	0.022
595	204	<100	4949	0	0.030
534	222	217	7998	0.002	0.041
473	244	825	13360	0.004	0.063
412	265	7787	23920	0.036	0.106
351	288	18060	21050	0.080	0.090
290	306	13710	8216	0.056	0.033
229	325	11240	4870	0.044	0.018
168	348	9447	3563	0.035	0.013
107	361	8762	2909	0.031	0.010
46	378	8420	2219	0.028	0.007

Figure A.7.23 Concentration Profile Results Run 100-115-150-A6

Distance from Carrier Gas Inlet	Sample Point Pressure	Peak Area		Standardised Concentration	
		A.P	D.C.M	A.P	D.C.M
cm	$kN\,m^{-2}$			$10^{-3}\ g\ cm^{-3}$	
717	204	<100	<100	0	0
656	179	<100	3387	0	0.023
595	204	<100	5336	0	0.032
534	222	263	8821	0.001	0.045
473	244	800	12770	0.004	0.060
412	265	5594	21600	0.026	0.096
351	288	17950	20500	0.079	0.087
290	306	13410	8142	0.055	0.032
229	325	11010	4700	0.043	0.018
168	348	9344	3423	0.034	0.012
107	361	8331	2439	0.029	0.008
46	378	7941	2311	0.027	0.007

Figure A.7.24 Run 100-115-150-A11

717	204	<100	<100	0	0
656	179	<100	3111	0	0.022
595	204	<100	4788	0	0.029
534	222	270	7450	0.001	0.038
473	244	1047	13060	0.005	0.062
412	265	6303	20920	0.029	0.093
351	288	19120	21610	0.084	0.092
290	306	13360	7841	0.055	0.031
229	325	11310	4508	0.044	0.017
168	348	9318	3034	0.034	0.011
107	361	8285	2295	0.029	0.008
46	378	7485	1718	0.025	0.006

Figure A.7.25 Concentration Profile Results Run 100-115-150-B4

Distance from Carrier Gas Inlet	Sample Point Pressure	Peak Area		Standardised Concentration	
		A.P	D.C.M	A.P	D.C.M
cm	$kN\,m^2$			$10^{-3}\ g\ cm^{-3}$	
717	201	<100	<100	0	0
656	173	<100	3400	0	0.023
595	201	<100	4950	0	0.030
534	224	205	7574	0.001	0.039
473	246	871	13160	0.004	0.062
412	266	5687	21100	0.026	0.094
351	285	17590	19420	0.077	0.083
290	305	12650	7321	0.052	0.029
229	327	10430	4487	0.040	0.017
168	349	8932	3255	0.033	0.012
107	363	7975	2445	0.028	0.008
46	378	7524	1864	0.025	0.006

Nomenclature

A	term accounting for eddy diffusion in chromagraphic theoretical plate height equation
A'	constant in the theoretical costing equation
A"	molar heat of vaporisation
A_p	cylindrical surface area of a theoretical plate
a	factor in the costing equation defined by $a = 2\left(\frac{\alpha-1}{\alpha+1}\right)\left(\frac{K}{1+K}\right)$
B	term accounting for longitudinal diffusion in chromatographic theoretical plate height equation
B'	constant in theoretical costing equation
C'	constant in theoretical costing equation
C_m	term accounting for mobile phase resistance to mass transfer in chromatographic theoretical plate height equation
C_s	term accounting for stationary phase resistance to mass transfer in chromatographic theoretical plate height equation
c	solute concentration in mobile phase
D_m	mobile phase molecular diffusivity
D'_p	effective diameter of particles, as defined by Equation 9.27.
D_r	radial diffusion coefficient
D_s	stationary phase molecular diffusivity
d_c	internal column diameter
d_f	thickness of stationary phase liquid film
d_p	mean particle diameter
d_{pc}	ratio of particle to column diameter
E	eddy diffusivity
$(E_i)_1, (E_{ii})_1$	mass production rates of components i and ii at the top of a column.
E_p	production rate of a given component
F	carrier gas volumetric flowrate measured at ambient conditions

Nomenclature continued...

F_m fractional volume of mobile phase in a chromatographic column

F_s fractional volume of stationary phase in a chromatographic column

f feedrate of component to a column

f' factor to allow for the effect on column length of increasing the mole fraction of solute in the liquid phase

G gas phase volumetric flowrate in the main separating section of the sequential unit, solute free.

G' gas phase volumetric flowrate in the main separating section of the sequential unit including a contribution from solute molecules.

G_E mass flowrate of fluid as defined by Ergun equation

$(G/L)_R, (G/L)_S$ ratio of gas to liquid flowrates in the rectifying and stripping sections of the column

$G_{m.c}$ gas phase volumetric flowrate measured at mean column pressure

$G_{T.c}$ summation of capital and running costs for a production chromatograph

G_2 constant in the plate height equation for large diameter columns

g_c gravitational constant

H height equivalent to a (chromatographic) theoretical plate, H.E.T.P.

H' intrinsic plate height for packing, as measured on an analytical column

H'_c theoretical plate height of a large diameter column without mixing devices.

H_c contribution to H in large diameter columns caused by non-uniformity of the velocity profile

H_{CN} theoretical plate height for a large diameter column with mixing devices.

H_t contribution ot H, caused by thermal fluctuations across the column

H_{tp} contribution to H produced by thermal lag in temperature programmed columns

Nomenclature continued (2)

h_i	heat of solution of component i in the liquid phase
h_o	reference value of H as defined by $h_o \frac{10.h}{u} (\frac{4}{d})^{0.5}$
I'	Aris integral describing the velocity profile gradient in the chromatographic plate height equation for large diameter columns
I_s	the length of a sequencing interval
j	James and Martin gas phase compressibility factor
K	partition coefficient of solute between mobile and stationary phases
K_i	partition coefficient of component i
K^∞	partition coefficient at infinite dilution
ΔK	change in K^∞ with increasing solute concentration
$\Delta K'$	change in K^∞ with change in temperature
k'	mass distribution ratio = $F_m/K.F_s$
k"	rate constant of desorption in probabilistic model (190)
k_b	Boltzmann constant = 1.38×10^{-6} erg/^oK
L	liquid solvent volumetric flowrate
L'	apparent liquid solvent flowrate in the sequential unit
L_m	distance migrated by the centre of a component zone
ℓ	column length
ℓ'	root mean square step length in random walk model
M_A	mass flowrate of solute leaving the column as product A stream, H.T.U. model
M_B	mass flowrate of solute leaving the column in the product B stream, H.T.U. model
M_f	molecular weight of feed component
M_i	molecular weight of solute
M_L	molecular weight of solvent liquid phase
M_V	solute molar volume at column operating temperature

Nomenclature continued (3)

M_1	molecular weight of mobile phase
M_2	molecular weight of solute
m'	factor to allow for shape of velocity profile in chromatographic plate height equation for large diameter columns
m_i	mass of component i in given sample
Δm_i	mass of component i, recycled during fraction cutting
$m_i(L)$	mass of solute in the liquid phase
$m_i(G)$	mass of solute in the gas phase
m_L	mass of solvent per unit volume
N	number of theoretical co-current chromatographic plates, or stages, within a column (N.T.P.)
N_{cc}	number of counter-current theoretical plates
N_f	number of theoretical plates occupied by feed band at column inlet
$(N_{OG})_R$	number of overall gas phase transfer units in the rectifying section of a column, H.T.U. model
$(N_{OG})_S$	number of overall gas phase transfer units in the stripping section of a column, H.T.U. model
n	normalised value of the number of theoretical plates in the column = $N.a^2/36$
n'	number of steps in random walk model
n_f	normalised value of the number of theoretical plates in the column, defined by $n_f = N_f.a/6$.
n_l	number of mixing devices in chromatographic plate height equation
P_a	ambient pressure
P^o_a	vapour pressure of component
P_{IO}	ratio of column inlet to outlet pressure
P_O	column outlet pressure
p	absolute pressure in atmospheres
p_f	partial pressure of feed component in gas stream, immediately before entering column

Nomenclature continued (4)

Q_G	gas volumetric flowrate from H.T.U. model
Q_L	liquid volumetric flowrate from H.T.U. model
q	solute concentration in stationary phase
q'	configuration factor dependent on shape of stationary phase layer
q_r	throughput of a production chromatograph
R	retention ratio = elution volume/total bed volume
R_g	gas constant
R_s	resolution = $t_{R2}-t_{R1}/\frac{1}{2}\ (w_1+w_2)$
r	recovery ratio after fraction cutting
r'	rate of transfer of molecules from gas to liquid phase in random walk model for continuous chromatography.
r"	rate of transfer of molecules from liquid to gas phase in random walk model for continuous chromatography
r_c	column radius
r_o	individual molecular collision diameter
r_{12}	mean molecular collision diameter for components 1 and 2
S	volumetric gas flowrate in the purge section of the sequential unit.
S_L	specific heat of liquid phase
$S_{m.c}$	volumetric gas flowrate measured at mean purge column pressure
S_p	specific heat of packing
S_s	specific surface of particle per unit volume of bed
T	absolute temperature
ΔT	temperature difference between column axis and wall
T_a	ambient temperature
T_c	column temperature
t	time
t_c	cycle time between repetitive injections

Nomenclature continued (5)

t_m	elution or retention time of unretained component
t_r	elution or retention time of retained component
u	average interstitial gas phase velocity
u_L	stationary phase velocity in random walk model for continuous chromatography
$u_{m.c.}$	interstitial gas phase velocity at mean column pressure
u_m	superficial column velocity
$(u_s)_i$	bottoms/feed mass flowrate ratio of component, i, in probabilistic model
$(u_z)_{ii}$	tops/feed mass flowratio of component ii in probabilistic model
V_b	molar volume at boiling point
V_G	volume of gas phase in a column corrected for gas compressibility = $j.V_m$
V_L	volume of liquid phase impregnated on the solid support
V_m	mobile phase volume of column
$V_n(G)$	gas phase volume in plate n of a chromatographic model
$V_n(L)$	liquid phase volume in plate n of a chromatographic model
V_R	elution or retention volume of component
V_R^o	corrected retention volume
V_S	stationary phase volume in column
V_1	volume of packing per theoretical plate
V_2	volume of liquid phase per theoretical plate
v	volumetric gas flowrate expressed in terms of plate volumes
W	characteristic baseline width of a single solute chromatographic peak
W_{to}	chromatographic baseline peak width at column outlet
$w, w_\alpha, w_\beta, w_\lambda$	factors in chromatographic theoretical plate height equation to allow for non-uniformity of the velocity profile.

Nomenclature continued (6)

X	association parameter in Wilke and Chang equation
X_{gn}	concentration of solute in gas phase over the nth plate of theoretical model proposed by Scott
y_i	mole fraction in the gas phase
y_1	gas phase solute concentration at point 1 in the column, H.T.U. model.
y_2	gas phase solute concentration at point 2 in the column, H.T.U. model
z	composite thermal conductivity of packed bed

Greek

α	relative volatility of key solute components
α'	packing geometry factor in chromatographic plate height equation for large diameter columns
α''	chromatographic separation factor = K_2/K_1
α_c	constant in the excess plate temperature equation
α_t	constant of value 0.004 in the theoretical plate height equation for heating rate
β	heating rate
β'	factor in costing equation defined by $= \frac{a.t_R}{6.t_c} \cdot \frac{M_f p_f}{R_g.T} \frac{\pi.\varepsilon.u}{4}$
β_c	constant in excess plate temperature equation
γ'	labyrinth factor
γ_A^{∞}	activity coefficient at infinite dilution
$\gamma_A^{'\infty}$	activity coefficient at infinite dilution including correction for non ideality
$\gamma_i(L)$	activity coefficient for component i in the liquid phase
γ_s	obstructive factor within solid particles
$\delta_i, \delta_i', \delta_i''$	series of factors to correct theoretical operating (G/L) limits of the SCCR1 unit
ε	void fraction of a packed bed

Nomenclature continued (7)

ε_{12}	energy of molecular interaction
Θ	excess temperature of plate above its surroundings
λ	eddy diffusion factor
μ	dynamic viscosity
ν	reduced velocity = $u\, d_p/D_m$
ℓ	density
ℓ_L	density of liquid phase
ℓ_p	density of solid support
σ	standard deviation
σ^2	variance
σ_{to}	standard deviation at column outlet
σ_{12}	collision integral for diffusion
τ_i	fitted experimental constant in Flory-Huggins equation
ϕ'	shape factor
ψ	operating mobile phase/stationary phase velocity ratio in probabilistic model
ψ_i	fitted experimental constant in Flory-Huggins equation

References

1. M.S. Tswett, Proc. Warsaw Soc. Nat. Sci. Biol. Sec., 14, No.6 (1903).

2. M.S. Tswett, Ber. deut. botan. Ges. 24, 316, 384 (1906).

3. A.J.P. Martin and R.L.M. Synge, Biochem. J., 35, 1358 (1941).

4. A.T. James and A.J.P. Martin, Biochem. J., 50, 679 (1952).

5. A.T. James, A.J.P. Martin and G.H. Smith, Biochem. J., 52, 238 (1952).

6. A.T. James, Biochem. J., 52, 242 (1952).

7. A.T. James and A.J.P. Martin, Analyst (London), 77, 915 (1952).

8. J.J. van Deemter, F.J. Zuiderweg and A. Klinkenberg, Chem. Eng. Sci., 5, 271 (1955).

9. J.C. Giddings and H. Eyring, J. Phys. Chem., 59, 416 (1955).

10. J.C. Giddings, J. Chem. Phys., 31, 1462 (1959).

11. J.C. Giddings, "Dynamics of Chromatography", Part 1, Principles and Theory, Marcel Dekker, New York, 1965, pp.323.

12. A.T. James, "Gas Chromatography", H.J. Noebels, N. Brenner and R.F. Wall. Eds. Academic Press, New York, 1961, p.247.

13. D.E.M. Evans and J.C. Tatlow, J. Chem. Soc., London, 1184 (1955).

14. J.J. Kirkland, "Gas Chromatography", H.J. Noebels, V.J. Coates, and I.S. Fagerson, Eds., Academic Press, New York, 1958, p.203.

15. D.W. Carle and T. Johns, Nat. Symp. on Instrumental Methods of Analysis, Instr. Soc. Amer., Houston, Texas, 1958.

16. M.J.E. Golay, "Gas Chromatography", H.J. Noebels, N. Brenner and R.F. Wall, Eds., Academic Press, New York, 1961, p.1.

17. F.H. Huyten, W. van Beersum and G.W.A. Rijnders, "Gas Chromatography", R.P.W. Scott, Ed., Butterworths, London, 1960, p.224.

18. G.J. Friscone, J. Chromatogr., 6, 97 (1961).

19. E. Bayer, K.P. Hupe and H. Mack, Anal. Chem., 35, 492 (1963).

20. U.S. Patent, 3,250,058 (1966); 3,491,512 (1968).

21. J.M. Ryan, R.S. Timmins and J.F. O'Donnell, Chem. Eng. Prog., 64, 53 (1968).

22. R.S. Timmins, L. Mir and J.M. Ryan, Chem. Eng., 76, 170 (1969).

23. J.W. Amy, L. Brand and W. Baitinger, 12th Pittsburg Conference of Analytical Chemistry and Applied Spectroscopy, Pittsburgh, Pennsylvania, 1961.

24. A.B. Carel, R.E. Clement and G. Perkins, "Advances in Chromatography", A. Zlatkis Ed., Preston Tech. Abstracts Co., Evanston, Illanois, 1969, p.113.

25. P. Valentin, G. Hagenbach, B. Roz and G. Guiochon, "Gas Chromatography", S.G. Perry, Ed., Applied Science Publishers, London, 1973, p.157.

26. E. Wolf and T. Vermenlen, Ind. Eng. Chem., Process Des. Dev., 15, 485 (1976).

27. P.E. Barker and D. Critcher., Chem., Eng. Sci., 13, 82 (1960).

28. D. Critcher, Ph.D. Thesis, Univ. of Birmingham, 1963.

29. P.E. Barker and D. Lloyd, Symposium on the less Common Means of Separation, 1963, Inst. Chem. Eng. London, 1964, p.68.

30. D. Lloyd, Ph.D. Thesis, Univ. of Birmingham, 1963.

31. P.E. Barker and D. Lloyd, U.S. Patent, 3,338,031.

32. P.E. Barker and D.H. Huntington, J. Gas Chromatogr., 4, 59 (1966).

33. D.H. Huntington, Ph.D. Thesis, Univ. of Birmingham, 1967.

34. P.E. Barker and D.H. Huntington, "Advances in Gas Chromatography 1965", A. Zlatkis and L.S. Eltre, Eds., 1966, p.162.

35. P.E. Barker and Universal Fisher Engineering Co.Ltd., British Patent Applications 33630/65, 43629/65, 5764/68, 44375/68.

36. P.E. Barker and D.H. Huntington, "Gas Chromatography 1966". A.B. Littlewood, Ed., Inst. of Petroleum, 1967, p.135.

37. P.E. Barker and D.H. Huntington, Dechema Monograph, 62, 153 (1969).

38. S. Al-Madfai, Ph.D. Thesis, Univ. of Birmingham, 1969.

39. P.E. Barker and S. Al-Madfai, J. Chromatog. Sci., 7, 425 (1969).

40. P.E. Barker and S. Al-Madfai, Proc. 5th International Symposium on Advances in Chromatography, Las Vegas, 1969, Preston Technical Abstracts Co., Evanston, Illinois, 1969, p.123.

41. P.E. Barker, "Preparative Gas Chromatography", A. Zlatkis, Ed., Wiley-Interscience, London, 1971, p.135.

42. P.E. Barker and R.E. Deeble, Symposium on Less Common Means of Separation, Inst. of Chem. Eng., London, 1972.

43. P.E. Barker and R.E. Deeble, Anal. Chem., 45, 1121 (1973).

44. P.E. Barker and R.E. Deeble, British Patent, 1,418,503, U.S. Patent 4,001,112.

45. R.E. Deeble, Ph.D. Thesis, Univ. of Aston in Birmingham, 1974.

46. P.E. Barker and R.E. Deeble, Chromatographia, 8 (2), 67 (1975).

47. S. Liodakis, unpublished work, Univ. Aston in Birmingham, 1976.

48. P.E. Barker, J.F. Ellison and B.W. Hatt, "Advances in Chromatographic Fractionation of Macromolecules," Chemical Society, London, 1976.

49. J.F. Ellison, Ph.D. Thesis, Univ. of Aston in Birmingham, 1976.

50. A.B. Sunal, Ph.D. Thesis, Univ. of Aston in Birmingham, 1973.

51. K.P. Hupe and E. Bayer, "Gas Chromatography 1964", A. Goldup, Ed., 1965, p.62.

52. S.W. Mayer and E.R. Tompkins, J. Am. Chem. Soc., 69, 2866 (1947).

53. E. Gluekauf, Trans. Faraday, Soc., 51, 34 (1955).

54. J.C. Giddings, J. Chromatogr., 2, 44 (1959).

55. L. Lapidus and N.R. Amundson, J. Phys. Chem., 56, 984 (1952).

56. J.J. Van Deemter, 2nd Informal Symp., Gas Chromatography Discussion Group, Cambridge, 1957.

57. E. Kucera, J. Chromatogr., 19, 237 (1965).

58. O. Grubner, "Advances in Chromatography Vol. 6", R.A. Keller and J.C. Giddings, Eds., Marcel Dekker Inc., New York, 1968, p.173.

59. E. Grushka, J. Phys. Chem., 76, 2586 (1972).

60. M. Golay, "Gas Chromatography 1958", D.H. Desty, Ed., Butterworths, London, 1958, p.36.

61. J.H. Purnell, "Gas Chromatography", J. Wiley & Sons, London, 1962.

62. J.C. Giddings, J. Chem. Ed., 35, 588 (1958).

63. A. Einstein, Ann. der Physik, 17, 549 (1905).

64. J.M. Harper and E.G. Hammond, Anal. Chem., 37, 486 (1965).

65. K. de Clerk and T.S. Buys, Separation Sci., 7, 653 (1972).

66. R. Aris, Proc. Roy. Soc., Ser. A., 252, 538 (1959).

67. J.C. Giddings, J. Chromatogr., 5, 46 (1961).

68. J.C. Giddings, J. Gas Chromatogr., 1 (1), 12 (1963).

69. J.C. Giddings and G.E. Jensen, J. Gas Chromatogr., 2 (9),290(1964).

70. G.M.C. Higgins and J.F. Smith, "Gas Chromatography 1964", A. Goldup, Ed., 1965, p.94.

71. G.W. A. Rijnders, "Advances in Chromatography Vol.3", Marcel Dekker, Ed., New York, 1966, p.215.

72. K.P. Hupe, U. Busch and K. Winde, J. Chromatogr. Sci., 7, 1 (1969).

73. S.A. Volkov, V. Yu, Zel'venskii, K.I. Sakodynskii and F. Ya. Frolov, J. Chromatogr., 77, 97 (1973).

74. A.B. Littlewood, Anal. Chem., 38, 2 (1966).

75. S.T. Sie and G.W.A. Rijinders, Anal. Chem. Acta., 38, 3 (1967).

76. V. Pretorius and K. de Clerk, "Preparative Gas Chromatography," A. Zlatkis and V. Pretorius, Eds., Wiley-Interscience, London, 1971, p.1.

77. S.F. Spencer and P. Kucharski, Facts and Methods, 7 (4), 8 (1966).

78. J.H. Knox, "Advances in Gas Chromatography", A. Zlatkis and L. Ettre, Eds., Preston Technical Abstracts Co. Illinois, 1966.

79. J.H. Knox and J.F. Parcher, Anal. Chem., 41, 1599 (1959).

80. M. Dixmier, B. Roz, and G. Guiochon, Anal. Chim. Acta., 38, 73 (1967).

81. J. Peters and C.B. Euston, Anal. Chem., 37, 657 (1965).

82. A. Rose, D.J. Royer and R.S. Henly, Separation Sci., 2, 229 (1967).

83. R.P.W. Scott, Anal. Chem., 35, 481 (1963).

84. M. Verzele, J. Chromatogr., 15, 482 (1964).

85. M. Verzele, Planta. Medica. Suppl. 38 (1967).

86. F. Helfferich, J. Chem. Educ., 41, 410 (1964).

87. G.L. Hargrove and D.T. Sawyer, Anal. Chem., 38, 1634 (1966).

88. C.L. Guillemin, J. Chromatogr., 12, 163 (1963).

89. C.L. Guillemin, J. Chromatogr., 30, 222 (1967).

90. C.L. Guillemin. J. Gas Chromatogr., 4, 104 (1966).

91. J. Albrecht and M. Verzele, J. Chromatogr., Sci., 8, 586 (1970).

92. C.E. Reese and E. Grushka, Chromatographia., 8 (2), 85 (1975).

93. M. Verzele, J. Gas Chromatogr., 4, 180 (1966).

94. E.M. Taft, Aerograph. Tech. Bull. W116, Varian Aerograph, Walnut Creek, California, 1964.

95. J.C. Giddings, Anal. Chem., 34, 37 (1962).

96. K. Kishimoto and Y. Yasumori, Japan Analyst., 12, 125 (1963).

97. B.M. Mitzner and W.V. Jones, J. Gas Chromatogr., 3, 294 (1965).

98. "Carlo Erba Short Notes", Scientific Instruments Division, Carlo Erba, Milan, Italy, p.2.

99. J.L. Wright, J. Gas Chromatogr., 1 (11), 10 (1963).

100. R. W. Reiser, J. Gas Chromatogr. , 4, 390 (1966).

101. A. Rose, D.J. Royer and R.S. Henly, Separation Sci., 2,211 (1967)

102. J.Q. Walker, Anal. Chem., 40, 226 (1968).

103. I. Pirogova, M. Ya. Shtaerman and D.A. Vyakhirev, J. Chromatogr., 58, 107 (1971).

104. T. Johns, M.R.Burnett and D.W. Clarke, "Gas Chromatography", H.J. Noebels R.F. Wall and N. Brenner, Eds., Academic Press, New York, 1961, p.207.

105. J.D. McCallum, "Progress in Industrial Gas Chromatography Vol. 1, H.A. Szymanski, Ed., Plenum Press, 1961, p.125.

106. W.N. Musser and R.E. Sparks, J. Chromatogr. Sci., 9, 116 (1971).

107. J. Albrecht and M. Verzele, J. Chromatogr. Sci., 9, 745 (1971).

108. A.B. Carel and G. Perkins, Anal. Chim. Acta, 34, 83 (1966).

109. A.B. Carel and G. Perkins, J. Chromatogr. Sci., 7, 218 (1969).

110. F.J. Debbrecht, R.H. Kolloff, L. Mikkelsen, A.J. Martin, G.R. Umbreit and C.E. Bennett, F. and M. Technical Paper 33, 1965.

111. F.J. Debbrecht, Hewlett-Packard, Tech. Paper 28, Hewlett-Packard, Avondale, Pennsylvania, 1965.

112. M. Verzele, Univ. of Ghent, Belgium, personal communication to R.E. Pescar, 1967.

113. R.E. Pescar, "Preparative Gas Chromatography", A. Zlatkis and V. Pretorious, Eds., Wiley-Interscience, London, 1971, p.73.

114. L. Mir, J. Chromatogr. Sci., 9, 436 (1971).

115. M. Verzele, J. Chromatogr., 9, 116 (1962).

116. S.M. Gordon, G.J. Kringe and V. Pretorius, J. Gas Chromatogr., 2, 241 (1964).

117. " " " " "
2,246 (1964)

118. " " " " "
2,285 (1964)

119. " " " " "
3, 87 (1965)

120. P.C. Haarhoff, P.C. van Berge and V. Pretorius, Trans. Faraday Soc., 57, 1838 (1961).

121. J.R. Condor and M.K. Shingari, J. Chromatogr. Sci., 11, 525 (1973).

122. J.R. Condor, paper presented at the Symposium on Less Common Means of Separation, Inst. Chem. Eng., London, 1972.

123. C.A. Sakodynsky, "Gas Chromatography", M. van Swaay, Ed., Butterworths, London, 1962.

124. J.A. Perry, Chem. and Ind., 21, 576 (1966).

125. D.T. Sawyer and J.H. Purnell, Anal. Chem., 36, 457 (1964).

126. D.A. Craven, J. Chromatogr. Sci., 8, 540 (1970).

127. K.P. Hupe, J. Chromatog. Sci., 9, 11 (1971).

128. J.R. Condor, "New Developments in Gas Chromatography", J.H. Purnell, Ed., Wiley-Interscience, New York and London, 1973, p.137.

129. J.R. Condor, Chromatographia, 8 (2), 60 (1975).

130. J.M. Ryan and G.L. Dienes, Drug and Cosmetic, Ind., 99, 60 (1966).

131. J.M. Ryan and G.L. Dienes, Chem. Eng., February 14th (1968).

132. J.R. Condor, Chem. Eng. Sci., 28, 173 (1973).

133. B. Roz., R. Bonmati, G. Hagenbach, P. Valentin and G. Guiochon, J. Chromatogr., Sci., 14, 367 (1976).

134. B.J. Bradley and P.F. Tiley, Chem. Ind. (London), 18, 743 (1963).

135. G.R. Fitch, M.E. Probert, and P.F. Tiley, J. Chem. Soc., 4875 (1962).

136. D.W. Pritchard, M.E. Probert and P.F. Tiley, Chem. Eng. Sci., 26, 2063 (1971).

137. W. Kuhn, E. Narten and M. Thurkauf, 5th World Petroleum Congress, 1958, Section V, Paper 5, p.45.

138. W. Kuhn, E. Narten and M. Thurkauf, Helv. Chim. Acta., 41, 2135 (1958).

139. S. Turina, V. Krajovan and T. Kostomaj, Z. Anal. Chem., 189, 100 (1962)

140. R. H. Wilhelm, A.W. Rice and A.R. Bendelius, Ind. Eng. Chem. Fund., 5, 141 (1966).

141. R.H. Wilhelm, and N.M. Sweed, Science., 159, 522 (1968).

142. R.H. Wilhelm, A.W. Rice, R.K. Wolke and N.W. Sweed, Ind. Eng. Chem. Fund., 7, 337 (1968).

143. N.M. Sweed, "Progress in Sep. and Purification No.4", E.S. Perry and C.J. van Oss, Eds., John Wiley and Sons, New York, 1971, p.171.

144. R.L. Pigford, B. Baker and D.E. Blum, Ind. Eng. Chem. Fund., 8, 144 (1969).

145. R.L. Pigford, B. Baker and D.E. Blum, Ind. Eng. Chem., Fund., 8, 848 (1969).

146. E.J. Tuthill, J. Chromatogr., Sci., 8, 285 (1970).

147. D.W. Thompson, Trans. Inst. Chem. Engrs., 39, 19 (1961).

148. U.S. Patent, 3,136,616 (1964).

149. P.C. Wankat, Separation Sci., 9, 85 (1974).

150. P.C. Wankat, Ind. Eng. Chem. Fund. 14 (2), 96 (1975).

151. A.J.P. Martin, Discussions. Faraday Soc., 7, 332 (1949).

152. D. Dinelli, S. Polezzo and M. Taramasso, J. Chromatogr., 7, 447 (1962).

153. U.S. Patent, 3,187,486 (1965).

154. S. Polezzo and M. Taramasso, J. Chromatogr., 11, 19 (1963).

155. M. Taramasso and D. Dinelli, J. Gas Chromatogr., 2, 150 (1962).

156. M. Taramasso, F. Sallusto and A. Guerra, J. Chromatogr., 20, 226 (1965).

157. M. Taramasso, J. Chromatogr., 49, 27 (1970).

158. U.S. Patent, 3,078,647 (1963).

159. R. Hybarger, C.W. Tobias and T. Vermenlen., Ind. Eng. Chem., Process.Des. & Dev., 2, 65 (1963).

160. Z. Pucar, Chromatogr. Review, 3, 38 (1961).

161. M.V. Sussman and C.C. Huang, Science, 156, 974 (1967).

162. U.S. Patent, 3,503,712 (1970).

163. M.V. Sussman, K.N. Astill, R. Rombach, A. Cerrulo and S.S. Chen, Ind. Eng. Chem., Fund., 11, 181 (1972).

164. M.V. Sussman, K.N. Astill and R.N.S. Rathore, J. Chromatogr. Sci., 12, 91 (1974).

165. R.P.W. Scott, "Gas Chromatography 1958", D.H. Desty, Ed., Butterworths, London, 1958, p.189.

166. H. Schultz, "Gas Chromatography 1962", M. van Swaay, Ed., Butterworths, London, 1963, p.225.

167. A. Clayer, L. Agneray, G. Vandenbussche, and P. Petel, Z. Anal. Chem., 236, 240 (1968).

168. A. Clayer, L. Agneray, G. Vandenbussche and M. Bruni, Z. Anal. Chem., 236, 250 (1968).

169. U.S. Patent, 2,869,672 (1958).

170. W.L. Nelson, "Petroleum Refinery Eng.," McGraw-Hill, New York, 1958.

171. H. Pichler and H. Schultz, Brennstoff Chem., 39 48 (1958)

172. U.S. Patent, 2,893,955 (1959).

173. U.S. Patent, 3,016,107 (1962).

174. D. Glasser, "Gas Chromatography 1966", A.B. Littlewood, Ed., Inst. of Petroleum, London, 1967, p.119.

175. L. Szepesy, Sz. Sebestyen, I. Feher and Z. Nagy, J. Chromatog., 108, 285 (1975).

176. D.B. Broughton, Chem. Eng. Prog., 64 (8), 60 (1968).

177. D.B. Broughton, R.W. Neuzil, J.M. Pharis and C.S. Brearley, Chem. Eng. Prog., 66 (9), 70 (1970).

178. Gow-Mac Bulletin 5B-13, Gow-Mac, Shannon Airport, Eire.

179. Instruction manual for Perkin-Elmer F11 Gas Chromatograph. Perkin-Elmer Ltd., Beaconsfield, Bucks.

180. K. Denbigh, "The Principles of Chemical Equilibrium" Cambridge University Press, 1964, p.276.

181. "Chemical Engineers Handbook", J.H. Perry, Ed., McGraw-Hill, New York, 1963.

182. "Handbook of Chemistry and Physics", R.C. Weart, Ed., Chemical Rubber Co., 1972.

183. V.P. Chizhkov. G.A. Yushina, L.A. Sinitzina and B.A. Rudenko, J. Chromatogr., 120, 35 (1976).

184. P.E. Barker, Trans. Inst. Chem. Engnrs., 40, (4), 221 (1962).

185. M.S. Lynham, unpublished work, University of Aston in Birmingham, 1974.

186. J.H. Knox and L. Mclaren, Anal. Chem., 36, 1477 (1964).

187. J.O. Hirschfelder, R.B. Bird, S. Spotz, Trans. Am. Soc., Mech. Engnrs., 71, 921 (1949).

188. C.R. Wilke, P. Chang, Am. Inst. Chem. Engnrs., 1, 264 (1955).

189. S. Glasstone, K.J. Laidler and H. Eyring, "The Theory of Rate Processes", McGraw-Hill, New York, 1941.

190. C.T. Sciance and O.K. Crosser, A.I. Ch.E. Journal, 12 (1), 100 (1966).

191. P. Rony, Separat. Sci., 3, 239 (1968).

192. P. Rony, Separat. Sci., 3, 357 (1968).

193. P. Rony, Separat. Sci., 5, 121 (1970).

194. L. Alders, "Liquid Liquid Extraction", Elsevier, Amsterdam, 1959 (2nd edition).

195. P. Tiley, J. Appl. Chem., 17 (5), 131 (1967).

196. G.J. Arkenbout and W.M. Smit, Separat.Sci. 2, 575 (1967).

197. R.E. Rubac. R.McDaniel, C.D. Holland, A.I.Ch.E. Journal, 15, 568 (1969).

198. K.I. Sakodynskii, L.V. Streltzov, V. Yu. Zelvenskii, S.A. Volkov, I.N. Rozhenko, Anal. Chem., 45, 1557 (1973).

199. I.N. Rozhenko, V. Yu Zelvenskii, S.A. Volkov and K.I. Sakodynskii, Theor. Osn. Khim. Tekhnol., 9, 3 (1975).

200. I.N. Rozhenko, A.G. Zyskin, V. Yu Zelvenskii, K.I. Sakodynskii, Chromatographia, 10, (1), 25 (1977).

201. S. Ergun, Chem, Eng. Prog., 48 (2), 89 (1952).

202. J. Kozeny, Sitzber. Akad. Wiss. Wien. Math-Naturw Klasse., 136, 271 (1927).

203. N.I. Sax, "Dangerous Properties of Industrial Materials," van Nostrand Rheinhold, London, 1968.

204. J.P. Fletcher, private communication

205. G.N. Lance, "Numerical Methods for High Speed Computers", London 1960.